E_20_642

Final Technical Report

on

AFOSR Grant 84-0020

Studies on Control, Nonlinear Dynamics and Modeling Problems in Large Space Structures

Submitted to

Dr. Spencer Wu
Air Force Office of Scientific Research
Building 410
Bolling Air Force Base
District of Columbia 20332

by

Satya N. Atluri
Regents' Professor & Director
Computational Mechanics Center
Georgia Institute of Technology
Atlanta, GA 30332-0356

The research performed under this grant has been documented in the following archival literature. One copy of each of the papers is being forwarded to AFOSR.

S.N. Atluri and A.K. Amos (Eds), *Large Space Structures: Dynamics & Control*, Springer-Verlag, 470 pp., 1988.

"Static & Dynamic Analysis of Space Frames with Non-linear Flexible Connections", *Int. Jrl. Num. Meth. Engg.* Vol. 28, 1989, pp. 2635-2650, (with G. Shi).

"Active Control of Nonlinear Dynamic Response of Space-Frames Using Piezo-Electric Actuators", *Computers & Structures* Vol. 34, No. 4, 1990, pp. 549-564, (with G. Shi).

"Effects of a Piezo-Actuator on a Finitely Deformed Beam Subjected to General Loading", *AIAA Journal*, Vol. 27, No. 12, pp. 1801-1807, 1989, (with S. Im).

"Space-Time Finite Element Analysis of Traveling Waves in Rod and Beam Structures", *Computers & Structures*, (to appear), 1989, (with M. Iura and M. Borri).

"Variational Approaches for Dynamics and Time - Finite - Elements: Numerical Studies", *Computational Mechanics*, (to appear), 1989, (with M. Borri and F. Mello).

"Time Finite Element Methods for Large Rotational Dynamics of Multibody Systems", *Computers & Structures* Vol. 37, No. 2, pp. 231-240, 1990 (with M. Borri and F. Mello).

"Primal and Mixed Forms of Hamilton's Principle for Constrained Rigid Body Systems: Numerical Studies", *Computational Mechanics*, (to appear), 1989, (with M. Borri and F. Mello).

"Nonlinear Dynamic Response of Space-Frames with Hysteritic Damping at the Joints", *Computers & Structures*, (to appear), 1989, (with G. Shi).

"On a Consistent Theory, and Variational Formulation, of Finitely Stretched and Rotated 3-D Space-Curved Beams", *Computational Mechanics*, Vol. 4, No. 1, 1989, pp. 73-88, (with M. Iura).

"Dynamic Analysis of Finitely Stretched and Rotated 3-D Space Curved Beams", *Computers & Structures*, Vol. 29, No. 5, pp. 875-889, 1988, (with M. Iura).

"Multi-Body Dynamics by the Finite Element Method in Time Domain" in *Computational Mechanics '88: Theory and Application* (Eds: S.N. Atluri and G. Yagawa), Springer, 1988, paper 64.ii (with M. Borri).

"Analysis of Traveling Wave Responses of Structures" in *Computational Mechanics '88: Theory and Application* (Eds: S.N. Atluri and G. Yagawa), Springer, 1988, paper 44.v, (with M. Iura and M. Borri).

"Dynamic Analysis of Finitely Stretched and Rotated 3-D Space-Curved Beams" in *Computational Mechanics '88: Theory and Application* (Eds: S.N. Atluri and G. Yagawa), Springer, 1988, paper 40.ii, (with M. Iura).

"Large Deformation, Post-Buckling Analyses of Large Space Frame Structure, Using Explicitly Derived Tangent Stiffness Matrices" in *Computational Mechanics '88: Theory and Application*

(Eds: S.N. Atluri and G. Yagawa), Springer, 1988, paper 28.iii, (with K. Kondoh and M. Hangai).

"Time-Finite Element Method for the Constrained Dynamics of a Rigid Body" in *Computational Mechanics '88: Theory and Application* (Eds: S.N. Atluri and G. Yagawa), Springer, 1988, paper 41.i, (with M. Borri).

"Nonlinearities in Dynamics & Control of Space Structures: Some Issues for Computational Mechanics" in *Large Space Structures: Dynamics and Control* (Eds: S.N. Atluri and A.K. Amos), Springer-Verlag, Berlin, 1988, Chapter 3 (with M. Iura).

"Elasto-Plastic Large Deformation Analysis of Space Frames: A Plastic-Hinge and Stress-Based Explicit Derivation of Tangent Stiffnesses" *Int Jrl for Num Meth in Engg* Vol 26, pp 586-615, 1988 (with G. Shi)

"Post-Buckling Analysis of Shallow Shells by the Field-Boundary-Element Method", *Int. Jrl. Numerical Methods in Engineering*, Vol. 26, pp. 571-587, 1988, (with J.D. Zhang).

"Dynamics of 3-D Space-Curved Beams, Undergoing Finite Rotations and Finite Strains: A Variational Theory and Numerical Studies", *ESP 24.87036, Society of Engineering Science*, 12 pages, 1987.

"Field/Boundary Element Approach to the Large Deflections of Thin Plates", *Computers & Structures*, Vol. 27, No. 3, pp. 427-436, 1987, (with P.E. O'Donoghue).

"Large-Deformation Elasto-Plastic Analysis of Frames Under Non-Conservative Loading, Using Explicitly derived Tangent Stiffnesses Based on Assumed Stresses", *Computational Mechanics*, Vol. 2, No. 1, pp. 1-25, 1987, (with K. Kondoh).

"Analysis of Control of Finite Deformations of Plates and Shells", *Chapter 6 in Finite Element Methods for Plates and Shell Structures*, (Eds: T.J.R. Hughes and E. Hinton), Pineridge Press, Swansea, pp. 127-153, 1986, (with J.D. Zhang and P.E. O'Donoghue).

Nonlinear Analysis of Shallow Shells: Interior/Boundary Element Algorithms in *Boundary Elements* (Ed: Q. Du), Pergamon Press, Oxford, pp. 87-110, 1986 (with J.D. Zhang).

"An Explicit Expression for the Tangent-Stiffness of a Finitely Deformed 3-D Beam and Its Use in the Analysis of Space Frames", *Computers & Structures*, Vol. 24, No. 2, pp. 253-272, 1986 (with K. Kondoh and K. Tanaka).

"A Boundary/Interior Element Method for Quasi-Static and Transient Response Analyses of Shallow Shells", *Computers & Structures*, Vol. 24, No. 2, pp. 213-224, 1986, (with J.D. Zhang).

"Control of Dynamic Response of a Continuum Model of a Large Space Structure", *Computers & Structures*, Vol. 23, No. 2, pp. 199-210, 1986, (with F.W. Brust).

"A Singular-Solution Approach for Controlling the Nonlinear Response of a Continuum Model of a Large Space Structure", *Proc. 27th Structures, Structural Dynamics, and Materials Conf*, Part 2, pp. 25-42, 1986, (with P.E. O'Donoghue).

"Instability Analysis of Space Trusses Using Exact Tangent-Stiffness Matrices", *Finite Elements in Analysis & Design*, Vol. 2, No. 4, pp. 291-311, 1985, (with K. Tanaka and K. Kondoh).

"A Simplified Finite Element Method for Large Deformation, Post-Buckling Analysis of Large Frame Structures, Using Explicitly Derived Tangent Stiffness Matrices", *International Journal of Numerical Methods in Engineering*, Vol. 23, No. 1, pp. 69-90, 1985, (with K. Kondoh).

"Influence of Local Buckling on Global Instability: Simplified Large Deformation, Post-Buckling Analysis of Plane Trusses", *Computers and Structures*, Vol. 24, No. 4, pp. 613-626, 1985, (with K. Kondoh).

"Control of Transient Dynamic Response of Structures", *Numerical Methods in Engineering: Theory and Applications*, Pine Ridge Press, Swansea, United Kingdom, January 1985, (with P.E. O'Donoghue).

"Servo-Elastic Oscillations: Control of Transient Dynamic Motion of a Plate", in *Advances in Aerospace Sciences and Engg* (Eds: U. Yuceglu, R. Hesser) ASME NY, ASME-AD-08, pp 139-149, 1984 (with P.E. O'Donoghue).

INTERNATIONAL JOURNAL FOR NUMERICAL METHODS IN ENGINEERING, VOL. 28, 0000–0000 (1989)

STATIC AND DYNAMIC ANALYSIS OF SPACE FRAMES WITH NON-LINEAR FLEXIBLE CONNECTIONS

G. SHI AND S. N. ATLURI

Computational Mechanics Center, Georgia Institute of Technology, Atlanta, GA 30332-0356, U.S.A.

SUMMARY

This paper deals with the effect of non-linearly flexible hysteritic joints on the static and dynamic response of space frames. It is shown that a complementary energy approach based on a weak form of the compatibility condition as a whole of a frame member, and of the joint equilibrium conditions for the frame, is best suited for the analysis of flexibly jointed frames. The present methodology represents an extension of the authors' earlier work[14] on rigidly connected frames. In the present case also, an explicit expression for the tangent stiffness matrix is given when (i) each frame member, along with the flexible connections at its ends, is represented by a single finite element, (ii) each member can undergo arbitrarily large rigid rotations and only moderate relative rotations and (iii) the non-linear bending–stretching coupling is accounted for in each member. Several examples, with both quasi-static and dynamic loading, are included, to illustrate the accuracy and efficiency of the developed methodology.

INTRODUCTION

In the analysis and design of frame-type space structures, the traditional methods are based on the simple assumptions that the joints are completely either pinned or rigid. However, the experimental investigations of actual joint behaviour have clearly demonstrated that the so-called 'pinned' connections do possess a certain amount of rotational rigidity, while the 'rigid' connections exhibit some degree of flexibility. Thus, in practice, all types of connections of frame structures are *semi-rigid* or *flexible*. The experimental study has also shown that the flexible connections behave non-linearly because of the local distortions, yielding and buckling, etc. in the connections. The flexible connections affect significantly the performance of the structures, such as deformations, stress distributions and dynamic responses. Also, joint flexibility and hysterisis is considered to be a significant source of passive damping of vibration in low-mass structures to be deployed in outer space.

In order to account for the effects of flexible connections on the behaviour of the structures, the modelling of the flexible connections is an essential step. The behaviour of flexible connections is usually described by the moment–rotation curves of the connection in which the slope of the curve corresponds to the rotational rigidity of the connections. A lot of experimental data for various types of connections has been obtained in the past five decades[1–3] and many models have been proposed to represent the behaviour of the connections. For simplicity, the *linear semi-rigid* model has been widely used, with concepts such as effective length,[4] rigidity factors[5] and linear rotational springs.[6–8] However, the approximation of a linear semi-rigid connection is good only when the force at the connection is quite small. When the moment acting at the connection is not small, the rigidity of the connection may change dramatically compared with the initial rigidity,

0029–5981/89/000000–00$05.00

Received 23 January 1989
Revised 3 April 1989

and the structure becomes more flexible. Especially under dynamic loading, the non-linear flexible connections will lead to hysteresis loops in the moment–rotation curve, and some energy will be dissipated in the connections. So for both static and dynamic problems, the non-linearity of the connections should be considered.

The non-linear behaviour of the flexible connections can be approximated by bilinear or trilinear functions, or expressed by some types of functions, for example, polynomial, exponential[9] and Ramberg–Osgood[8, 10] functions. The bilinear and trilinear models are simple and present no problems in determining the rigidity of the connections, but they are not accurate enough. Also, the non-smoothness of the curve may cause more numerical difficulties. For the models expressed by the non-linear functions, determining the instantaneous rigidity is very important for the efficiency and accuracy of the analysis. The Ramberg–Osgood function for the moment–rotation relations used by Ang and Morris[8] is a good function to describe the non-linear behaviour of the flexible connections. A scheme for determining the instantaneous rigidity of the connection described by the Ramberg–Osgood function is presented here, which is convenient and accurate for both static and dynamic problems.

Recently, Shi *et al.*[11] and Chen and Lui[9] used non-linear rotational springs to model the non-linear flexible connections for static problems. In the former paper, the rotational spring was modelled by a connecting element, and treated as an independent element. The 'connecting element' approach could easily handle the non-linear flexible connection, but results in an increase in the number of degrees of freedom. In the latter paper, the rotational spring had been treated as an element first, then the element was condensed statically, leading to a more complicated formulation. One purpose of the present paper is to present a very simple and natural approach to account for the behaviour of non-linear flexible connections, without an increase in the number of degrees of freedom. Furthermore, it is demonstrated in this paper that the *complementary energy approach*, involving the weak form of the *compatibility* of member deformations, is the simplest way to account for the additional deformation caused by flexible joints.

When the space frame (with non-linearly flexible joints) is subjected to a dynamic load, the non-linearity of the connections will lead to hysteresis loops in the moment–rotation curves and some energy will be dissipated in the connections. Popov and co-workers[12, 13] demonstrated by experiments that the hysteresis loops under repeated and reversed loading are very stable, so, the moment–rotation curves obtained by static experiments can be extended to the dynamic analysis of flexibly connected frames. Up to now, except for a few experimental works, the influence of non-linear flexible connection on the dynamic behaviour of structures was studied analytically in few papers. In the paper by Kawashima and Fujimotgo about vibration analysis,[6] they just calculated the frequencies of the structures with linear semi-rigid connections. The effect of hysteritic damping resulting from the non-linear flexible connection on the dynamic response of the frame will be studied in this paper.

MODELLING OF NON-LINEAR FLEXIBLE CONNECTIONS

In general, the behaviour of flexible connections is expressed by its moment–rotation curves. Because of the complexity, the moment–rotation relation is usually determined by experiments. By curve fitting the experimental data, many types of functions were generated to approximate the non-linear behaviour of the flexible connections. Because the behaviour of non-linear flexible connections is actually represented, in a computational model, by the instantaneous rotational stiffness of the connection, i.e. the slope of the moment–rotation curve, the property of the function used for the moment–rotation curve is very important for the numerical analysis of

flexibly jointed frame structures. The polynomial function has a considerable accuracy for the moment–rotation relation, but it may give undesirable negative 'connection-stiffness' since the nature of a polynomial is to peak and trough within a certain region. The exponential function used by Chen and Lui[9] can always give a positive derivative, but its stiffness expression is not convenient to be implemented for programming, especially for dynamic problems. The standardized Ramberg–Osgood function for the moment–rotation relation proposed by Ang and Morris[8] has many advantages. It not only can describe the non-linear behaviour very well just by three parameters, and guarantee a positive derivative, but also can take into account of the additional moment at the connection due to the P-Δ effect,[8] and give a convenient expression for the

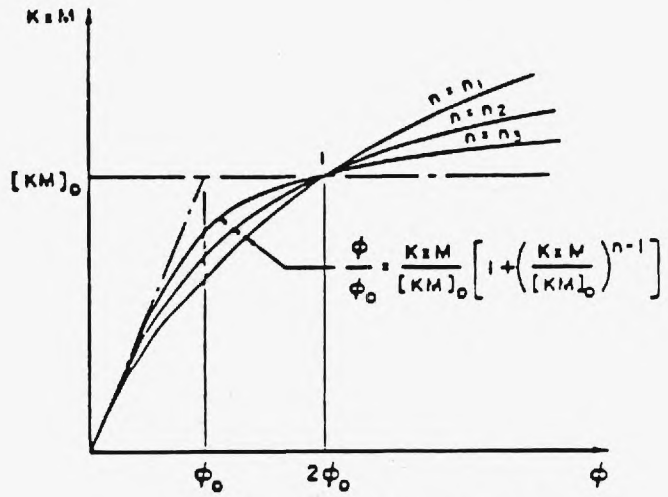

Figure 1(a). The Ramberg–Osgood function

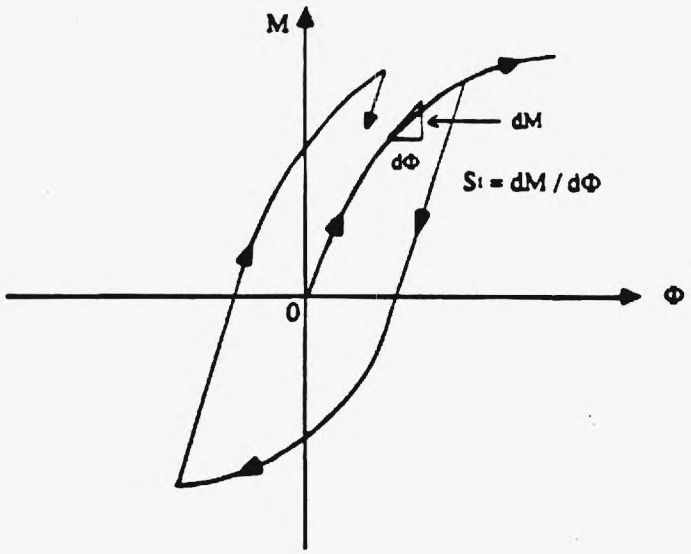

Figure 1(b). Behaviour of non-linear flexible connection and the rotational rigidity of the connection

instantaneous rotational rigidity of a non-linear flexible connection, as will be demonstrated later on in this paper.

The standardized moment–rotation behaviour is expressed by the Ramberg–Osgood function as

$$\frac{\phi}{\phi_0} = \frac{K \cdot M}{(KM)_0}\left[1 + \left(\frac{KM}{(KM)_0}\right)^{n-1}\right] \tag{1}$$

where ϕ is the relative rotation at the connection, M is its corresponding bending moment, ϕ_0, $(KM)_0$ and n are parameters in which n is a positive real number. As illustrated in Figure 1(a), the three parameters control the shape of the moment–rotation curve. The parameters can be easily determined for a given type of connection. The standardized Ramberg–Osgood functions of moment–rotation relations for five typical connections were given in Ang and Morris' paper.[8]

Differentiating equation (1) with respect to M gives

$$\frac{1}{\phi_0}\frac{\mathrm{d}\phi}{\mathrm{d}M} = \frac{K}{(KM)_0}\left[1 + n\left(\frac{KM}{(KM)_0}\right)^{n-1}\right] \tag{2}$$

Then the instantaneous rotational rigidity of the non-linear flexible connection, i.e. the slope of the moment–rotation curve, denoted by S^t, is given by

$$S^t = \frac{\mathrm{d}M}{\mathrm{d}\phi} = \frac{(KM)_0}{\phi_0 K\left[1 + n\left(\frac{KM}{(KM)_0}\right)^{n-1}\right]} \qquad M > 0 \tag{3}$$

and the initial rigidity S^0 is

$$S^0 = \left.\frac{\mathrm{d}M}{\mathrm{d}\phi}\right|_{m=0} = \frac{(KM)_0}{\phi_0 K} \tag{4}$$

Considering that the moment M at the connection can be positive or negative, the general form of equation (3) corresponding to loading or reloading, i.e. the case when $M\,\mathrm{d}M > 0$, can be written as

$$S^t = \frac{S^0}{1 + n\left[\frac{K|M|}{(KM)_0}\right]^{n-1}} \tag{5}$$

and the initial rigidity S^0 is used for the case of unloading in which $M\,\mathrm{d}M < 0$.

The instantaneous rigidity of the non-linear connection, S^t, in equation (5) is a function of the moment at the connection. Such an expression for S^t has some advantages. Because the moment acting on the connection is the same as that at the connecting end of the structural member, the connection moment can be very easily evaluated. Therefore equation (5) is very suitable for a computational model.

The non-linear equation of moment–rotation relation can be solved by its incremental form. Supposing M_i and ϕ_i were known, then

$$M_{i+1} = M_i + \Delta M \tag{6}$$

Corresponding to the increment ΔM, the increment of ϕ can be approximated as

$$\Delta\phi = \Delta M / S^t \tag{7}$$

and

$$\phi_{i+1} = \phi_i + \Delta\phi \tag{8}$$

The difference between $\phi = \phi(M_{i+1})$ defined in equation (1) and ϕ_{i+1} approximated in equation (8) can be corrected by some iterative scheme, and equations (6) and (8) become

$$M_{i+1} = M_i + \sum_k \Delta M^{(k)} \tag{6a}$$

$$\phi_{i+1} = \phi_i + \sum_k \Delta M^{(k)}/S^{\mathrm{I}} \tag{8a}$$

in which the superscript k indicates the iteration.

TANGENT STIFFNESS OF A FLEXIBLY CONNECTED BEAM COLUMN: AN EXPLICIT EXPRESSION

The behaviour of a non-linear flexible connection can be represented by a non-linear rotational spring in which the rotational rigidity of the spring corresponds to the slope of the moment–rotation curve. The flexibly jointed frame is modelled as a collection of beam-columns with rotational springs at the ends of each beam-column. Unlike the model used in the authors' previous paper,[11] the beam together with the springs is considered as a single element in the present study.

A procedure for the elasto-plastic large deformation analysis of rigidly jointed space frames was presented by Shi and Atluri,[14] which was based on the weak forms of governing equations, assumed stress fields and the incremental forms for the non-linear equations. When the beam-column is connected by rotational springs at its ends, the compatibility conditions for the beam as a whole will be different from those in Reference 14. We examine the new compatibility conditions here.

A typical beam element with rotational springs at its ends is illustrated in Figure 2 in which $\mathbf{X}$ is the global reference system, $\mathbf{X}'$ and $\hat{\mathbf{X}}$ are the co-ordinates in undeformed and deformed configurations respectively. It was assumed that the element has a constant cross-section with two perpendicular principal axes. Therefore, the governing equations of an element can be established in the principal axes of the element.

Because of the non-linearity of the connection, the compatibility conditions will be written in the incremental form.

As illustrated in Figures 2 and 3, in the presence of rotational springs at the ends of the beam-column, the incremental nodal rotations measured in the 'co-rotational' local basis $\hat{\mathbf{e}}_i$, denoted by $\Delta^{\alpha}\theta_i^*$ $(i = 2, 3, \alpha = 1, 2)$, are composed of two parts: $\Delta^{\alpha}\theta_i^{**}$ and $\Delta^{\alpha}\phi_i$, where $\Delta^{\alpha}\theta_i^{**}$ is the part resulting from the elastic beam and $\Delta^{\alpha}\phi_i$ is the contribution of the rotational spring. ${}^{\alpha}S_i^{\mathrm{I}}$ is the instantaneous rigidity of the spring about axis x_i and at node α.

Using the nomenclature of deformations as defined in Figure 2, the incremental curvatures in the local co-ordinates of the deformed element are given by

$$\begin{aligned} \Delta k_1 &= \Delta\theta^*_{1,1} \\ \Delta k_2 &= -\Delta\theta^*_{2,1} \\ \Delta k_3 &= \Delta\theta^*_{3,1} \end{aligned} \tag{9}$$

Let $\Delta N, \Delta M_i\,(i = 1, 2, 3)$ be the increments of the Cauchy stress resultant and stress couples in the

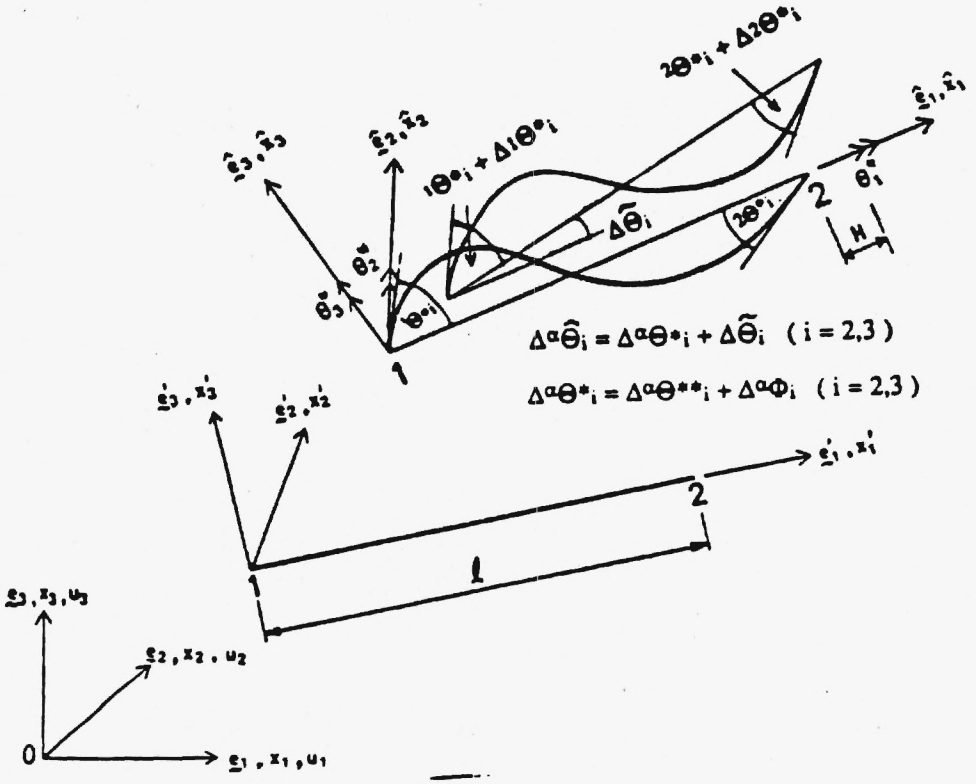

Figure 2. Increments of element local rotations

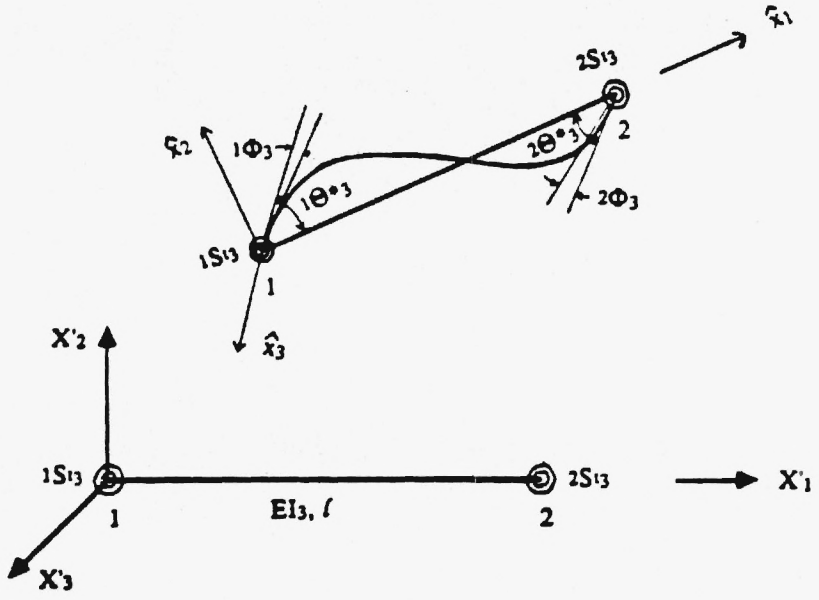

Figure 3. A typical beam-column with rotational springs at the ends in $\hat{x}_1$–$\hat{x}_2$ plane

convected element co-ordinates, then, as shown by Shi and Atluri,[14] the trial stress fields obtained from the linear and angular momentum balance relations are

$$\begin{aligned} \Delta N &= \Delta n \\ \Delta M_1 &= \Delta m_1 \\ \Delta M_2 &= (1-\hat{x}_1/l)\Delta^1 m_2 + (\hat{x}_1/l)\Delta^2 m_2 \\ \Delta M_3 &= (1-\hat{x}_1/l)\Delta^1 m_3 + (\hat{x}_1/l)\Delta^3 m_3 \end{aligned} \tag{10}$$

where ${}^{\alpha}m_i$ ($\alpha = 1,2$; $i = 2,3$) are the moments at the element ends, α refers to the node and i refers to the direction. Corresponding to the incremental stress resultant and stress couples, the increment ΔW_c of the complementary energy density will be

$$\Delta W_c = \frac{1}{2}\left[\frac{(\Delta N)^2}{EA} + \frac{(\Delta M_1)^2}{EI_1} + \frac{(\Delta M_2)^2}{EI_2} + \frac{(\Delta M_3)^2}{EI_3}\right] \tag{11}$$

where EA is the tensile stiffness of the element and EI_i ($i = 1,2,3$) is the flexural rigidity of the element about axis $\hat{x}_i$.

The stress–strain relations between the conjugate pairs of the mechanical and kinematic variables are of the form

$$\begin{aligned} \frac{\partial \Delta W_c}{\partial(\Delta N)} &= \Delta h \\ \frac{\partial \Delta W_c}{\partial(\Delta M_1)} &= \Delta k_1 \\ \frac{\partial \Delta W_c}{\partial(\Delta M_2)} + \delta(\hat{x}_1)\Delta^1\phi_2 + \delta(\hat{x}_1 - l)\Delta^2\phi_2 &= -\Delta k_2 \\ \frac{\partial \Delta W_c}{\partial(\Delta M_3)} + \delta(\hat{x}_1)\Delta^1\phi_3 + \delta(\hat{x}_1 - l)\Delta^2\phi_3 &= \Delta k_3 \end{aligned} \tag{12}$$

in which Δh is the incremental stretch in $\hat{x}_i$ direction, δ is the Dirac delta function and $\delta(\hat{x}_1 - x_0)\Delta\phi$ represents the effects of the rotational springs at the ends of the element. For a small strain problem we have

$$\Delta h = \Delta u^*_{1,1} \tag{13}$$

Rather than considering the point-wise compatibility conditions, the weak form of the compatibility conditions is written for the element *as a whole*. Let Δv be the test function corresponding to ΔN, $\Delta\mu_i$ ($i = 1,2,3$) are the test functions corresponding to ΔM_i, then the weak forms of the compatibility conditions are

$$\begin{aligned} \int_0^l \frac{\partial \Delta W_c}{\partial(\Delta N)}\Delta v\, d\hat{x}_1 &= \int_0^l \Delta h \Delta v\, d\hat{x}_1 \\ &= \Delta v \int_0^l \Delta u^*_{1,1}\, d\hat{x}_1 = \Delta v(\Delta u^*_{1,1})|_0^l = \Delta v \Delta H \end{aligned} \tag{14}$$

$$\int_0^l \frac{\partial W_c}{\partial(\Delta M_1)}\Delta\mu_1\, d\hat{x}_1 = \int_0^l \Delta\theta^*_{1,1}\Delta\mu_1\, d\hat{x}_1 = (\Delta^2\theta^*_1 - \Delta^1\theta^*_1)\Delta\mu_1 \tag{15}$$

$$\int_0^l \left[\frac{\partial \Delta W_c}{\partial (\Delta M_2)} + \delta(\hat{x}_1)\Delta^1\phi_2 + \delta(\hat{x}_1 - l)\Delta^2\phi_2 \right] \Delta\mu_2 \, d\hat{x}_1$$

$$= \int_0^l \frac{\partial \Delta W_c}{\partial (\Delta M_2)} \Delta\mu_2 \, d\hat{x}_1 + \Delta^1\phi_2\Delta^1\mu_2 + \Delta^2\phi_2\Delta^2\mu_2 = \Delta^2\theta_2^*\Delta^2\mu_2 - \Delta^1\theta_2^*\Delta^1\mu_2 \tag{16}$$

$$\int_0^l \left[\frac{\partial \Delta W_c}{\partial (\Delta M_3)} + \delta(\hat{x}_1)\Delta^1\phi_3 + \delta(\hat{x}_1 - l)\Delta^2\phi_3 \right] \Delta\mu_3 \, d\hat{x}_1$$

$$= \int_0^l \frac{\partial \Delta W_c}{\partial (\Delta M_3)} \Delta\mu_3 \, d\hat{x}_1 + \Delta^1\phi_3\Delta^1\mu_3 + \Delta^2\phi_3\Delta^2\mu_3 = \Delta^2\theta_3^*\Delta^2\mu_3 - \Delta^1\theta_3^*\Delta^1\mu_3 \tag{17}$$

In equations (16) and (17), on the right hand side, the identities $\int_0^l \theta_2^* \, d\hat{x}_1 = 0$ and $\int_0^l \theta_3^* \, d\hat{x}_1 = 0$ are used. The increments of the spring rotations can be expressed as

$$\Delta^\alpha\phi_i = (-1)^\alpha \frac{\Delta^\alpha M_i}{{}^\alpha S_i^t} \qquad \text{for each } i = 2, 3; \text{ and } \alpha = 1, 2 \tag{18}$$

where S^t is the instantaneous rigidity of the spring as defined in equation (5). Substituting equations (10), (11) and (18) into equations (16) and (17), and recalling $\Delta\mu_i$ is the variation of ΔM_i, one has

$$(\Delta\mu_i)^T \frac{l}{6EI_i} \begin{bmatrix} 2 + a_i & 1 \\ 1 & 2 + b_i \end{bmatrix} \Delta\mathbf{M}_i = (\Delta\mu_i)^T \Delta\theta_i \qquad \text{no sum on } i; \text{ for } i = 2, 3 \tag{19}$$

in which EI_i and l are the flexural rigidity and length of the element respectively, and the following notations are used:

$$\begin{aligned} \Delta\mu_i &= \{\Delta^1\mu_i \quad \Delta^2\mu_i\}^T \\ \Delta\theta_i &= \{-\Delta^1\theta_i^* \quad \Delta^2\theta_i^*\}^T \\ \Delta M_i &= \{\Delta^1 M_i \quad \Delta^2 M_i\}^T \\ a_i &= \frac{6EI_i}{{}^1S_i^t l}, \qquad b_i = \frac{6EI_i}{{}^2S_i^t l} \end{aligned} \tag{20}$$

Equation (19) can also be rewritten as

$$\Delta\mathbf{M}_i = \frac{6EI_i}{l} \frac{1}{(2 + a_i)(2 + b_i) - 1} \begin{bmatrix} 2 + b_i & -1 \\ -1 & 2 + a_i \end{bmatrix} \Delta\theta_i$$

$$= (\hat{\mathbf{A}}_{\sigma\sigma}^{-1})_i \Delta\theta_i \qquad \text{(no sum on } i, \text{ for } i = 2, 3) \tag{21}$$

In equation (17), a_i and b_i are the modifying terms resulting from the rotational springs at the element ends. It is evident that equation (19) goes back to the rigid connection when ${}^1S \to \infty$, ${}^2S \to \infty$, and to the pinned connection when ${}^1S \to 0$, ${}^2S \to 0$. Therefore, equations (19) and (20) are valid for all kinds of connections.

By letting

$$\Delta\sigma = \{\Delta n, \Delta m_1, \Delta^1 m_2, \Delta^2 m_2, \Delta^1 m_3, \Delta^2 m_3\}^T \tag{22}$$

$$\Delta d = \{\Delta H, (\Delta^2\theta_1^* - \Delta^2\theta_1^*), -\Delta^1\theta_2^*, \Delta^2\theta_2^*, -\Delta^1\theta_3^*, \Delta^2\theta_3^*\}^T \tag{23}$$

$$\hat{A}_{\sigma\sigma}^{-1} = \begin{bmatrix} EA/l & & & & & 0 \\ & EI_1/l & & & & \\ & & (\hat{A}_{\sigma\sigma}^{-1})_2 & & & \\ & & & & & \\ 0 & & & & & (\hat{A}_{\sigma\sigma}^{-1})_3 \end{bmatrix} \tag{24}$$

Equations (14)–(17) can be written in a matrix form

$$\Delta\sigma = \hat{A}_{\sigma\sigma}^{-1}\,\Delta d \tag{25}$$

For the small deformation problem, $\hat{A}_{\sigma\sigma}^{-1}$ is the element stiffness matrix in the local co-ordinates ($\hat{\mathbf{e}}_i$). $\hat{A}_{\sigma\sigma}^{-1}$ can be transformed into the global co-ordinates in the usual manner. It should be pointed out that the element stiffness matrix for the large deformation problem is the combination of the transformations of $\hat{A}_{\sigma\sigma}^{-1}$ with a deformation dependent matrix, as explained in Shi and Atluri's paper.[14] *It should be noted that the derivation* of the *explicit expression for the tangent stiffness matrix for the finitely deformed beam* follows the same lines as in Reference 14, except for the modifications in equations (14)–(25) above.

Referring to the complementary energy analysis of finitely deformed, *rigidly jointed* frames as discussed in Shi and Atluri,[14] the only difference in the analysis due to the presently considered non-linear, hysteritic joint flexibility is the following: the incremental compatibility conditions in the presence of flexible joints, i.e. equations (14)–(17) above, contain additional terms as compared to the incremental counterparts of the compatibility conditions, equations (41)–(44) in Reference 14, for rigidly connected frames. Following the details given in equations (41)–(78) as well as the Appendix of Reference 14, it is seen that the matrix $A_{\sigma\sigma}$ of equations (A21)–(A24) of Reference 14 must now be replaced by the matrix $\hat{A}_{\sigma\sigma}$ given in equation (24) above. Thus, the explicit expression for the tangent stiffness matrix of a *flexibly connected, finitely deformed* space frame is given by

$$K = A_{\sigma d0}^{\mathrm{t}}\,\hat{A}_{\sigma\sigma}^{-1}\,A_{\sigma d} + A_{dd} \tag{26}$$

wherein the expressions for $A_{\sigma d0}$, $A_{\sigma d}$, A_{dd} are given in the Appendix of Reference 14. It should be noted that $\hat{A}_{\sigma\sigma}^{-1}$ is explicitly given in equation (24), and the explicit expressions (without involving element integrations) for $A_{\sigma d}$, A_{dd} and $A_{\sigma d0}$ are given in Reference 14. It may be seen that $\hat{A}_{\sigma\sigma}^{-1}$ is the so-called 'linear' stiffness matrix in the local co-ordinates $\hat{\mathbf{e}}_i$ of the deformed beam-member, $A_{\sigma d}$ and $A_{\sigma d0}$ are deformation-dependent transformations; and A_{dd} is the additional deformation-dependent stiffness.

The analysis of the frame with non-linear flexible connections is a kind of materially non-linear analysis. The system non-linear equations are approximated by the incremental tangent stiffness matrix equations, and a modified arc-length method[15] is employed to solve the system equations.

HYSTERETIC DAMPING RESULTING FROM THE NON-LINEAR FLEXIBLE CONNECTION

Under the dynamic loading, the non-linearity of the flexible connection will result in the hysteretic loop in the moment–rotation curve from the cyclic displacement at the connection. The area enclosed by the loop corresponds to the energy dissipated in a cycle of the oscillation. Such hysteretic damping plays a very important role for the dynamic behaviour of the structure. Because the hysteretic loop of the non-linear flexible connection is very highly reproducible, even in the presence of the pronounced local buckling at the connection,[12,13] as illustrated in Figure 4, the moment–rotation curve obtained by static experiments can be extended to dynamic analysis. So, the Ramberg–Osgood function used for the static problem is employed here again. In this case, the hysteretic loop is determined by the Ramberg–Osgood function, the unloading criterion and the initial rigidity of the connection. The unloading criterion is

$$M\Delta M < 0 \tag{27}$$

where M is the total moment at the connection and ΔM is its increment and the unloading

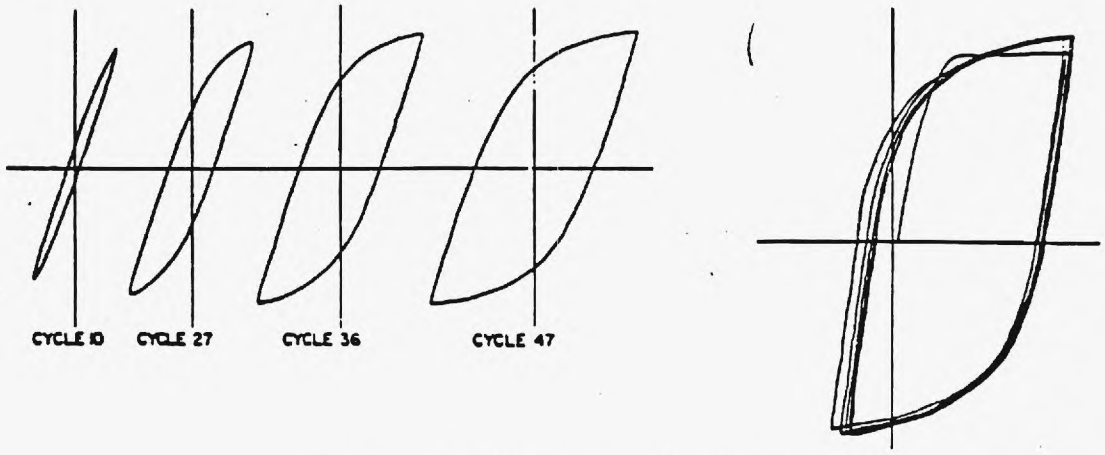

Figure 4. Hysteretic loops are very highly reproducible

criterion is checked in each time step for all rotational springs. Corresponding to the loading and unloading, the instantaneous rigidity of the spring for the dynamic problem S_d will take, respectively, the value

$$S_d = S^t \quad \text{for loading} \tag{28}$$

$$S_d = S^0 \quad \text{for unloading} \tag{29}$$

Similarly, the element stiffness matrix $\hat{A}_{\alpha\alpha}^{-1}$ in the local co-ordinates will be

$$\hat{A}_{\alpha\alpha}^{-1} = \hat{A}_{\alpha\alpha}^{-1}(S^t) \quad \text{for loading} \tag{30}$$

$$\hat{A}_{\alpha\alpha}^{-1} = \hat{A}_{\alpha\alpha}^{-1}(S^0) \quad \text{for unloading} \tag{31}$$

in which S^t was defined in equation (5), S^0 in equation (4) and in equation (24). The tangent stiffness matrix of element in the global co-ordinates can be built up by the local tangent element stiffness matrix $\hat{A}_{\alpha\alpha}^{-1}$ in the same way as in the static problem, but takes different rigidities for the spring according to loading and unloading to represent the hysteretic loop of the moment–rotation curve. Let $\mathbf{K}^t = \sum_{\text{elem}} \mathbf{K}_e^t$ be the system tangent stiffness matrix, $\mathbf{M}$ the system mass matrix, $\mathbf{C}$ the damping coefficient matrix ($\mathbf{M}$ and $\mathbf{C}$ can be established in the usual way), then the equations of motion of a non-linear system can be written in the incremental form

$$\mathbf{M}\Delta\ddot{\boldsymbol{u}} + \mathbf{C}\Delta\dot{\boldsymbol{u}} + \mathbf{K}^t\Delta\boldsymbol{u} = \Delta\boldsymbol{P} \tag{32}$$

where $\Delta\boldsymbol{u}$, $\Delta\dot{\boldsymbol{u}}$, $\Delta\ddot{\boldsymbol{u}}$ and $\Delta\boldsymbol{P}$ are increments of displacement, velocity, acceleration and external loading vectors. After establishing $\mathbf{K}^t$ by equations (30) and (31), equation (32) can be solved by any time integration scheme.[16]

NUMERICAL EXAMPLES

The efficiency and accuracy of the present approach are demonstrated by the following numerical examples. In order to compare the present results with others, three examples which were solved by other researchers are analysed here again.

Example 1

The three storey single bay frame shown in Figure 5(a) is taken from Arbabi's paper[7] and the linear semi-rigid connection was used there. However, the Young's modulus was not given there. The lateral displacements corresponding to rigid and semi-rigid connection are shown in Figures 5(b) and (c) respectively. While the two sets of results are close for the case of a rigid connection, present results for the flexible connection are different from those in Reference 7, but close to those of the three storey three bay frame in the same paper. A possible reason for the difference is that the single bay frame was reduced to a cantilevered beam by some assumption in Reference 7.

Example 2

This example concerns a T-shaped frame with a non-linear flexible connection. The geometry and load conditions are shown in Figure 6 and the behaviour of the connection is given by the

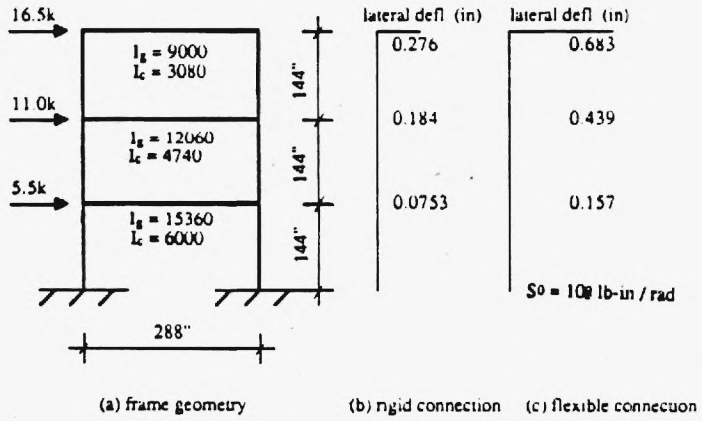

Figure 5. Three storey single bay frame

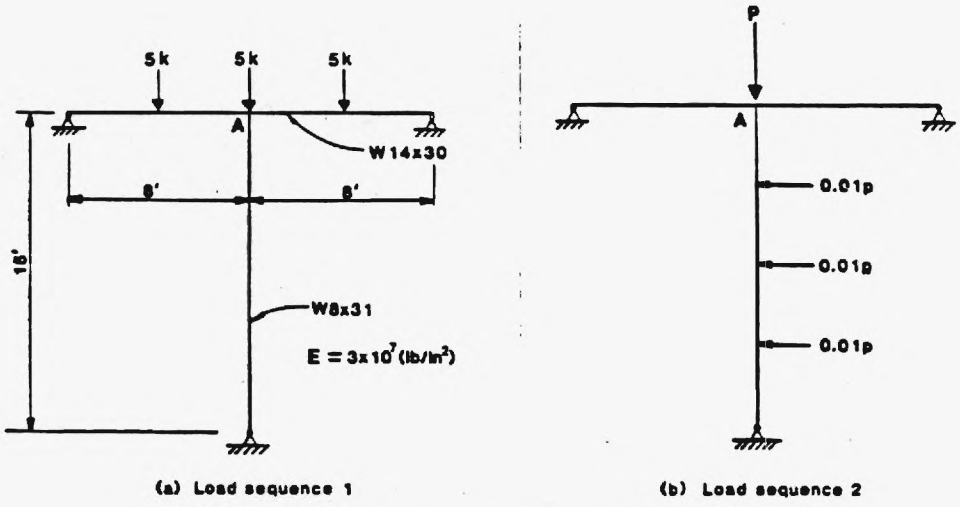

Figure 6. Geometry and loading conditions

moment–rotation curve, as illustrated in Figure 7. Because only the slope of the curve is used in the modelling of the connection, it is better to interpolate the derivative of the curve directly rather than to fit the curve. The ratios of the rotation/translation at point A for both the rigid and flexible connections are plotted in Figure 8. The results agree quite well with those given by Lui.[17] Some similar results can be found in Chen and Lui's paper.[9]

Example 3

The geometric and material data of a simple three-dimensional frame are given in Figure 9. The non-linear moment–rotation behaviour of the connection that Lui used for a similar plane toggle[17] is illustrated in Figure 10. The deflections for both cases of rigid supports and flexible supports for the 3-D case of Figure 9 are shown in Figure 11.

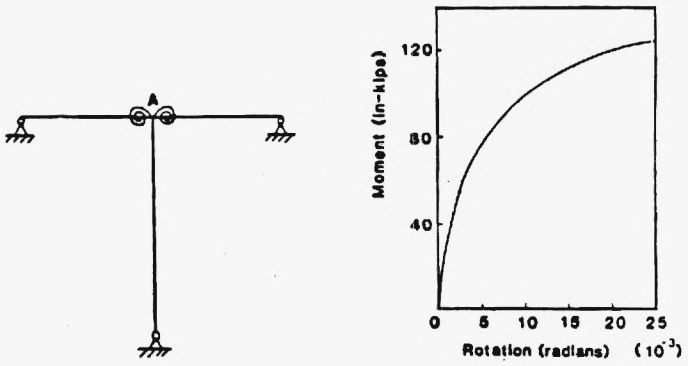

Figure 7. The flexible connection and its moment–rotation behaviour

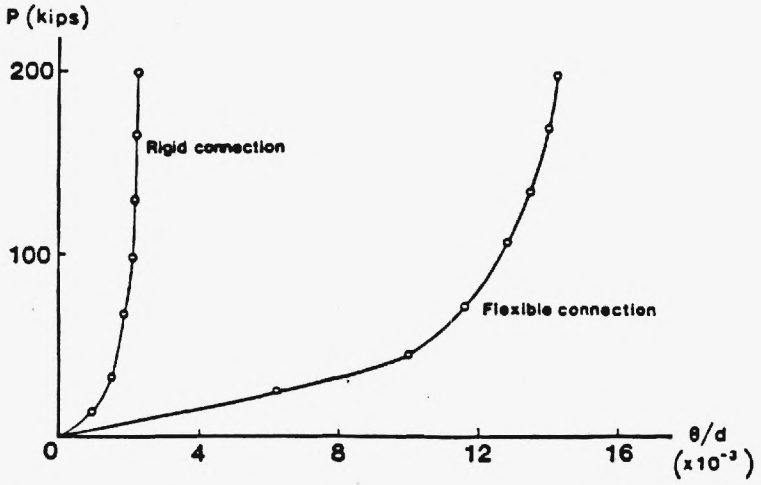

Figure 8. The ratio of rotation/translation at point A

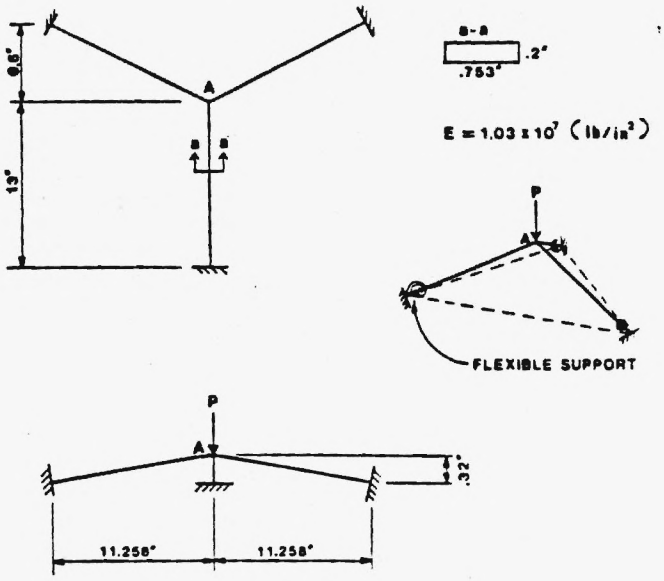

Figure 9. The geometry and support condition of the 3-D toggle

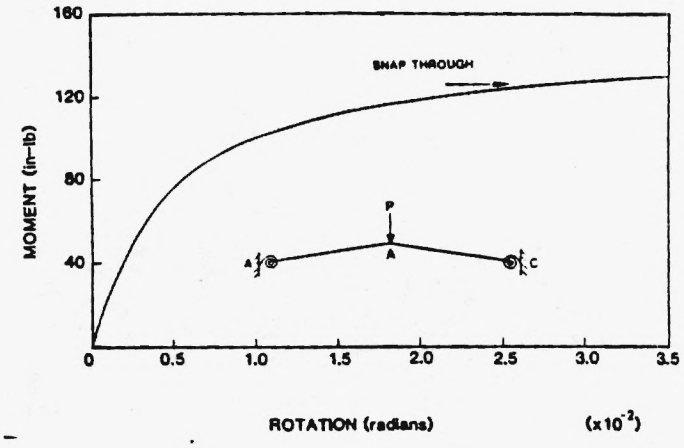

Figure 10. Connection moment–rotation behaviour used for the toggle

Example 4

Now we study two dynamic problems. Kawashima and Fujimotgo[6] gave the analytical and experimental natural frequencies of the L-type frame with a linear semi-rigid connection, as indicated in Figure 12, and material property $EI = 4230\ \text{kg cm}^2$, $\nu = 0{\cdot}47$. The present results are also shown in the figure. It can be seen that the present results are very good.

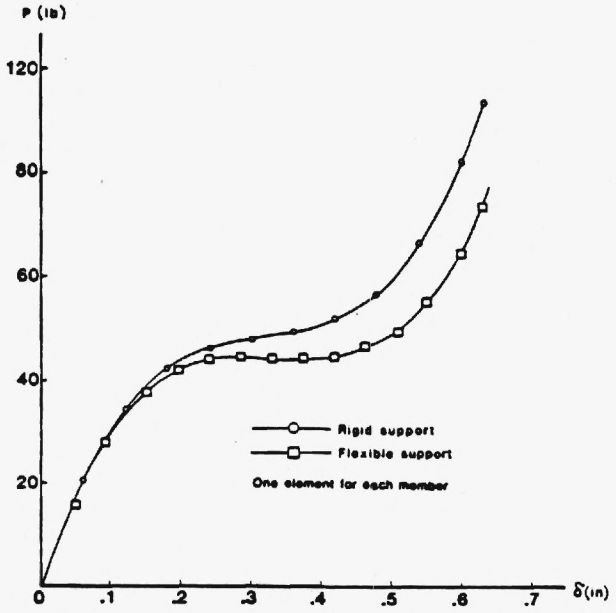

Figure 11. The load–deflection curve at point A

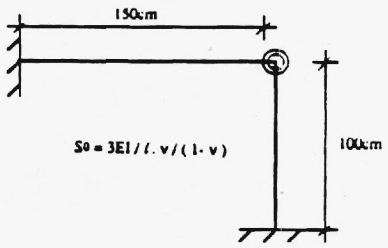

	rigid connection		semi-rigid connection		
mode	cal.	cal. Ref. 6	cal.	cal. Ref. 6	exp. Ref. 6
1	15.87	16.3	14.75	14.9	15.5
2	35.3	35.9	32.06	33.0	30.8

Figure 12. Geometry and natural frequencies of L-frame with rigid connection and semi-rigid connection

Example 5

Kawashima and Fujimotgo considered only the influence of a linear flexible connection on the frequencies. Here we will consider the effects of a non-linear flexible connection on the dynamic response. A header plate connection with the instantaneous rigidity

$$S^t = \frac{1400}{1 + 4{\cdot}32|0{\cdot}1184M|^{3{\cdot}32}}$$

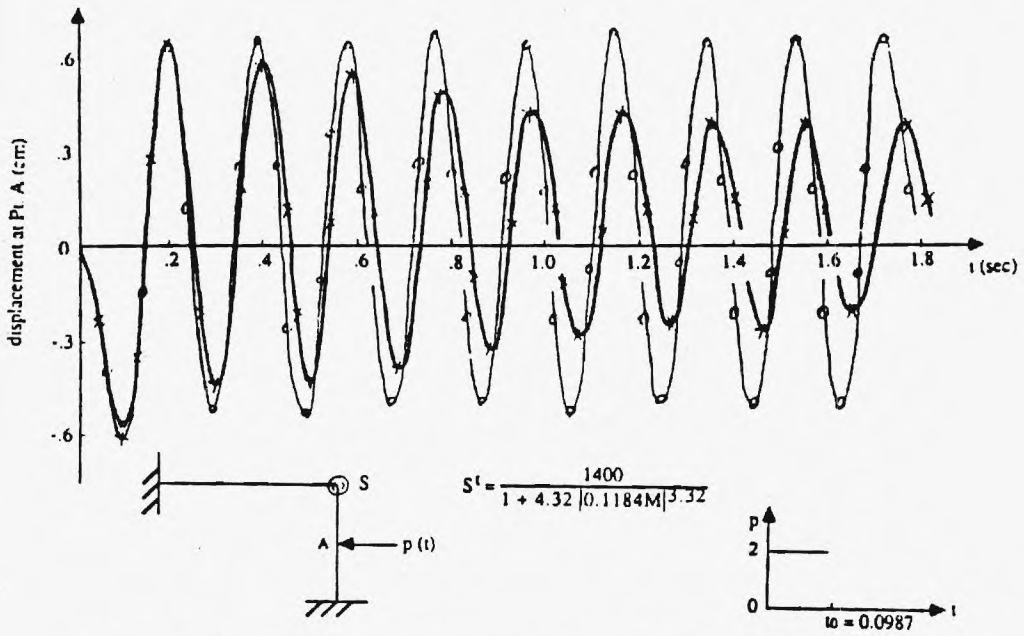

Figure 13. Dynamic responses at point A for linear and non-linear flexible connection

is used for the non-linear connection. The responses of the structure with a linear or non-linear connection are illustrated in Figure 13. The response corresponding to a non-linear connection, indicated by the curve with crosses, shows that the hysteretic damping resulted from the non-linearity of the connection really affects the response considerably.

CLOSURE

The weak form of the incremental governing equations in the *complementary energy approach* provides a simple way to handle the non-linear behaviour of flexible connections. By the present approach, there is no difference in the treatment for a flexibly jointed plane frame and a flexible jointed space frame, and there is no difficulty in handling a flexible torsional connection if such data are available. The Ramberg–Osgood function not only can represent the non-linear behaviour well, but also has some advantage for computational modelling. In order to consider the structural response of lattice structures more accurately, non-linear flexible connections should be used for both static and dynamic problems. The numerical examples demonstrate that the approaches presented in this paper are very efficient and accurate for both static and dynamic analysis of flexibly jointed space structures.

ACKNOWLEDGEMENTS

This work was supported by AFOSR, with Dr A. K. Amos as the program official. The assistance of Ms. Deanna Winkler is sincerely appreciated.

REFERENCES

1. S. W. Jones, *et al.*, 'Effect of semi-rigid connection on steel column strength', *J. Construct. Steel Res.*, **1**, 38–46 (1980).
2. B. Kato, 'Beam-column connection research in Japan', *J. Struct. Div ASCE*, **108**, 343–359 (1982).
3. M. J. Frye and G. A. Morris, 'Analysis of flexibly connected steel frames', *Can. J. Civil Eng.*, **2**, 280–291 (1975).
4. S. W. Jones, *et al.*, 'Column with semi-rigid joints', *J. Struct. Div. ASCE*, **108**, 361–372 (1982).
5. E. Lightfoot and A. P. Messurier, 'Elastic analysis of frame-works with elastic connection', *J. Struct. Div. ASCE*, **100**, 1297–1309 (1979).
6. S. Kawashima and T. Fujimotgo, 'Vibration analysis of frames with semi-rigid connections', *Comp. Struct.*, **19**, 85–92 (1984).
7. F. Arbabi, 'Drift of flexible connection frames', *Comp. Struct.*, **15**, 103–108 (1982).
8. K. M. Ang and G. A. Morris, 'Analysis of three-dimensional frame with flexible beam-column connection', *Can. J. Civil Eng.*, **11**, 241–254 (1984).
9. W.-F. Chen and E. M. Lui, 'Effect of joint flexibity on the behavior of steel frames', *Comp. Struct.*, **26**, 719–732 (1987).
10. W. Ramberg and W. R. Osgood, 'Description of stress–strain curves by three parameters', *NACA Technical Report No. 902*, 1943.
11. G. Shi, C. T. Yang and S. N. Atluri, 'Plastic-hinge analysis of flexible-jointed frames using explicit derived tangent stiffness matrices', *Proc. 6th OMAE, Vol. 3*, Houston, Texas, 1987, pp. 393–401.
12. E. P. Popov and R. B. Pinkney, 'Cyclic yield reversal in steel building connections', *J. Struct. Div. ASCE*, **95**, 327–353 (1969).
13. V. T. Bedero and E. P. Popov, 'Beam-column subassemblages under repeated loading', *J. Struct. Div. ASCE*, **98**, 1137–1159 (1972).
14. G. Shi and S. N. Atluri, 'Elasto-plastic large deformation analysis of space-frames: A plastic-hinge and stress-based explicit derivation of tangent stiffnesses', *Int. j. numer. methods eng.*, **26**, 589–615 (1988).
15. K. Kondoh and S. N. Atluri, 'A simplified finite element method for large deformation, post-buckling analysis of large frame structures, using explicitly derived tangent stiffness matrices', *Int. j. numer. methods eng.*, **23**, 69–90 (1986).
16. K.-J. Bathe, *Finite Element Procedures in Engineering Analysis*, Prentice-Hall, Englewood, Cliffs, N.J., 1982.
17. E. M. Lui, 'Effect of connection flexibility and planal zone deformation on the behavior of plane steel frames', *Ph.D Thesis*, Purdue University, 1985.

Computers & Structures Vol. 34, No. 4, pp. 549–564, 1990
Printed in Great Britain.

0045-7949/90 $3.00 + 0.00

ACTIVE CONTROL OF NONLINEAR DYNAMIC RESPONSE OF SPACE-FRAMES USING PIEZO-ELECTRIC ACTUATORS

G. SHI and S. N. ATLURI
Computational Mechanics Center, Georgia Institute of Technology, Atlanta, GA 30332-0356, U.S.A.

(*Received* 24 *January* 1989)

Abstract—A scheme for active control of nonlinear vibration of space-structures, wherein each member is modeled as a beam-column, is presented. The expressions for shear stresses transmitted to the structural member by the distributed segmented piezo-electric actuators, which are bonded on the surfaces of the member, are derived in the general case in which the structural member is subjected to moments, transverse shear forces and an axial force. Based on the weak form of the governing equations, and a complementary energy approach based on assumed stress fields, the viability of active control of nonlinear dynamic response of lattice-type space structures, using piezo actuators, is studied. Four examples are given to demonstrate the feasibility of the approaches presented in this paper.

1. INTRODUCTION

The active control of vibration of large flexible space structures is a topic of current interest. A distributed actuator network is a good means to actively control any possible disturbance to the structures. Recently, Crawley and de Luis [1] proposed to use segmented piezo-electric materials bonded on the surfaces of structural members as actuators for large space structures. Such piezo-electric materials exhibit mechanical deformations when an electric field is applied to them and will not extensively modify the passive mechanical and dynamic properties of the system. But Crawley and Luis analysed the shear stresses transmitted to the structural member by a piezo actuator for a very simple case when the member itself is subjected only to pure bending. Consequently, the results for the shear stresses exerted by the actuator are functions of only the applied voltages and the bending moment in the beam. In order to implement piezo-electric actuators in space structures, wherein each member may be modeled, in general, as a beam column, the shear stresses exerted by the piezo actuators must be analysed for the case when the structural member is subjected to not only pure bending moments, but also transverse shear and axial forces. The shear stresses induced by the piezo actuators would be, in general, functions of the applied voltages to the actuators, and the internal bending moments, transverse shear forces and axial forces in the structural member. Having obtained the expressions for shear stresses exerted by the actuators, the computational model for nonlinear active control through piezo actuators has to be established. The questions to be answered concern: (i) the number and placement of the actuators; and (ii) the voltages that are to be applied to each actuator. The purpose of the present paper is to investigate these questions, and to present numerical examples to establish the viability of the developed procedures.

2. ACTIVE CONTROL OF NONLINEAR VIBRATION

The equations of motion of a discretized nonlinear system with control force $\mathbf{F}_c = \mathbf{b}\mathbf{f}_c$ can be written in an incremental form as

$$\mathbf{M}\Delta\ddot{\mathbf{u}} + \mathbf{C}\Delta\dot{\mathbf{u}} + \mathbf{K}\Delta\mathbf{u} = \Delta\mathbf{P} + \mathbf{b}\Delta\mathbf{f}_c \tag{1}$$

where $\mathbf{M}$, $\mathbf{C}$, and $\mathbf{K}$ are the tangent mass, damping and stiffness matrices, and $\Delta\ddot{\mathbf{u}}$, $\Delta\dot{\mathbf{u}}$, $\Delta\mathbf{u}$, $\Delta\mathbf{P}$ and $\mathbf{b}\Delta\mathbf{f}_c$ are the increments of acceleration $\ddot{\mathbf{u}}$, velocity $\dot{\mathbf{u}}$, displacement $\mathbf{u}$, external loading $\mathbf{P}$ and control force $\mathbf{F}_c$, respectively. In general, eqn (1) has the initial conditions:

$$\mathbf{u}(o) = \mathbf{u}_o \quad \dot{\mathbf{u}}(o) = \dot{\mathbf{u}}_o. \tag{2}$$

As a prelude to the proposed simple algorithm for nonlinear control, we first consider the linear optimal control. The equations of motion of a linear system are of the form

$$\mathbf{M}_o\ddot{\mathbf{u}}(t) + \mathbf{C}_o\dot{\mathbf{u}}(t) + \mathbf{K}_o\mathbf{u}(t) = \mathbf{P}(t) + \mathbf{b}\mathbf{f}_c(t) \tag{3}$$

wherein the subscript o implies the initial values of the respective quantity, i.e. we are dealing with the linearized system. Let $\mathbf{S}$ denote the state variable vector, i.e.

$$\mathbf{S} = \begin{Bmatrix}\mathbf{u}\\ \dot{\mathbf{u}}\end{Bmatrix}, \qquad \mathbf{S}_o = \begin{Bmatrix}\mathbf{u}_o\\ \dot{\mathbf{u}}_o\end{Bmatrix}. \tag{4}$$

Omitting the external load at this stage, eqn (3) can be written as:

$$\dot{\mathbf{S}} = \mathbf{A}\mathbf{S} + \mathbf{B}\mathbf{f}_c \tag{5}$$

where

$$\mathbf{A}=\begin{bmatrix}\mathbf{0} & \mathbf{I}\\ -\mathbf{M}_o^{-1}\mathbf{K}_o & -\mathbf{M}_o^{-1}\mathbf{C}_o\end{bmatrix} \tag{6}$$

$$\mathbf{B}=\begin{bmatrix}\mathbf{0}\\ \mathbf{M}_o^{-1}\mathbf{b}\end{bmatrix}. \tag{7}$$

For a linear regulator problem, a typical quadratic performance index may be defined as:

$$J=\tfrac{1}{2}\mathbf{S}^{\mathrm{T}}(t_f)\mathbf{T}\mathbf{S}(t_f)+\frac{1}{2}\int_{t_o}^{t_f}(\mathbf{S}^{T}\mathbf{Q}\mathbf{S}+\mathbf{f}_c^{\mathrm{T}}\mathbf{R}\mathbf{f}_c)\,\mathrm{d}t \tag{8}$$

in which t_o is the initial time, t_f is the final time, and **T**, **Q** and **R** are constant positive definite weighing matrices which determine the magnitudes of the control forces and the quantitative decay of the vibration amplitude. If the structure comes to rest at its initial configuration at the terminal time t_f, i.e. $\mathbf{S}(t_f)=\mathbf{0}$, the first term in eqn (8) can be neglected. Minimizing eqn (8) subject to the constraint equations (eqn 5), gives (see Ref. [9])

$$f_c=-\mathbf{R}^{-1}\mathbf{B}^{\mathrm{T}}\mathbf{G}\mathbf{S} \tag{9}$$

where **G** is the feedback gain matrix and is the solution of the Riccati differential equation:

$$\dot{\mathbf{G}}=-\mathbf{G}\mathbf{A}-\mathbf{A}^{\mathrm{T}}\mathbf{G}+\mathbf{G}\mathbf{B}\mathbf{R}^{-1}\mathbf{B}^{\mathrm{T}}\mathbf{G}-\mathbf{Q}.\quad \mathbf{G}(t_f)=0. \tag{10}$$

Thus, the linear optimal control problem just depends on the solution of the Riccati equation. A common way is to solve the steady state Riccati equation, i.e. $\dot{\mathbf{G}}=\mathbf{0}$, is by the Schur vector approach [2]. Here we introduce another approach to solve the Riccati equation as proposed by Davison and Maki [3].

By letting

$$\mathbf{X}=\mathbf{G}\mathbf{S} \tag{11}$$

and using eqns (5), (6), (9) and (10), (11) yields:

$$\begin{bmatrix}\dot{\mathbf{S}}\\ \dot{\mathbf{X}}\end{bmatrix}=\begin{bmatrix}\mathbf{A} & -\mathbf{B}\mathbf{R}^{-1}\mathbf{B}^{\mathrm{T}}\\ -\mathbf{Q} & -\mathbf{A}^{\mathrm{T}}\end{bmatrix}\begin{bmatrix}\mathbf{S}\\ \mathbf{X}\end{bmatrix}=\mathbf{H}\begin{bmatrix}\mathbf{S}\\ \mathbf{X}\end{bmatrix} \tag{12}$$

and

$$\mathbf{X}(t_f)=\mathbf{0},\quad \mathbf{S}(o)=S_o. \tag{13}$$

Integrating eqn (12) and applying the terminal conditions in eqn (13) results in

$$\mathbf{G}(t)=[\phi_{21}(t)+\phi_{22}(t)\mathbf{G}(o)][\phi_{11}(t)+\phi_{12}(t)\mathbf{G}(o)]^{-1},\quad 0\leqslant t\leqslant t_f \tag{14}$$

where

$$G(o)=-\phi_{22}^{-1}(t_f)\phi_{21}(t_f) \tag{15}$$

and

$$\exp(\mathbf{H}t)=\begin{bmatrix}\phi_{11}(t) & \phi_{12}(t)\\ \phi_{21}(t) & \phi_{22}(t)\end{bmatrix}. \tag{16}$$

A simple scheme for evaluating $\exp(\mathbf{H}h)$ in which h is the time step can be found in Davison and Maki's paper [3]. It can be seen from eqn (14) that $\mathbf{G}(t)$ is time dependent and an inversion is involved in each time step. If the total degrees of freedom of the system are n, then G will be of the dimension $2n\times 2n$. So the inversion involved in evaluating $\mathbf{G}(t)$ will be very time consuming. By the property of G as shown in Fig. 1, $\mathbf{G}(t)$ can be approximated by

$$\mathbf{G}(t)=\alpha(t)\mathbf{G}(o) \tag{17}$$

where $\alpha(t)$ is a decay function used to represent the decay characteristic. A linear function will be good enough for $\alpha(t)$.

For a nonlinear system, **M**, **C** and **K** will depend on the history of the displacement, and it is not easy to determine the optimal control forces. An economic and feasible approximation is to use the feedback gain matrix of the linear system with operator

$$\mathbf{A}=\begin{bmatrix}\mathbf{0} & \mathbf{I}\\ -\mathbf{M}_o^{-1}\mathbf{K}_o & -\mathbf{M}_o^{-1}\mathbf{C}_o\end{bmatrix} \tag{18}$$

for the nonlinear system. In eqn (18), $\mathbf{M}_o$, $\mathbf{C}_o$ and $\mathbf{K}_o$ are the initial mass, damping and stiffness matrices of the nonlinear system.

By splitting $\mathbf{G}(t)$ into portions relating to $\mathbf{u}(t)$ and $\dot{\mathbf{u}}(t)$ as

$$\mathbf{G}(t)=\alpha(t)\begin{bmatrix}\mathbf{G}_{11}(o) & \mathbf{G}_{12}(o)\\ \mathbf{G}_{21}(o) & \mathbf{G}_{22}(o)\end{bmatrix} \tag{19}$$

the incremental control forces for the nonlinear system will be

$$\Delta\mathbf{F}_c=-\mathbf{b}\mathbf{R}^{-1}\mathbf{b}^{\mathrm{T}}\mathbf{M}^{-1}\alpha(t)[\mathbf{G}_{21}\,\Delta\mathbf{u}+\mathbf{G}_{22}\,\Delta\dot{\mathbf{u}}]$$
$$=-\alpha(t)\mathbf{E}[\mathbf{G}_{21}\,\Delta\mathbf{u}+\mathbf{G}_{22}\,\Delta\dot{\mathbf{u}}]. \tag{20}$$

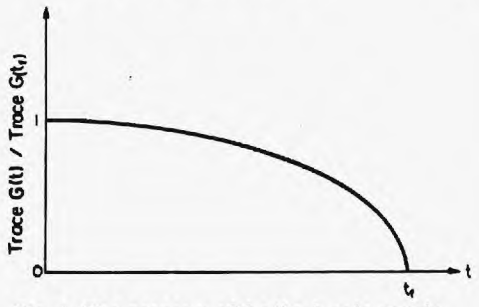

Fig. 1. The property of feedback gain matrix.

So eqn (1) becomes

$$\mathbf{M}\Delta\ddot{\mathbf{u}} + [\mathbf{C} + \alpha(t)\mathbf{E}\mathbf{G}_{22}]\,\Delta\dot{\mathbf{u}} + [\mathbf{K} + \alpha(t)\mathbf{E}\mathbf{G}_{21}]\Delta\mathbf{u} = \Delta\mathbf{P}. \quad (21)$$

It can be seen from the above equation that the system with operators **M**, **C** and **K** becomes a new system with opertors **M**, **C*** and **K***, in which **C*** and **K*** are the terms relating to $\Delta\dot{\mathbf{u}}$ and $\Delta\mathbf{u}$ in eqn (21), respectively. Equation (21) is just a common initial value problem and can be solved very easily.

3. SHEAR STRESSES TRANSMITTED TO THE STRUCTURAL MEMBER BY A PAIR OF PIEZO-ELECTRIC ACTUATORS

The piezo actuators exhibit mechanical deformations when an electric field is applied to them. The deformations of the actuators which are bonded to the underlying structure produce some localized strains and stresses which provide the control forces required to damp out the vibration of the structure. Therefore, in order to determine the active control forces induced by piezo actuators, the effects of the actuators on the underlying structure should be studied first.

For the purpose of exerting control forces efficiently, short segmented-actuators are preferred rather than long continuous ones, and the actuators bonded on the surfaces of a structural member are to be symmetric in the cross-section of the member. For the distributed segmented actuator model, the length of actuator segments is much less than that of the structural member itself. So it can be assumed that the flexural deformation of the segment is decoupled with its axial deformation, and that the effect of the axial force in the beam upon the flexural deformation is negligible. A typical differential element of the structural member with piezo-electric materials on its upper and lower surfaces is indicated in Fig. 2. The piezo-electric layers are bonded to the surfaces by very thin layers of adhesive. In order that the actuators do not extensively modify the mechanical properties of the system, the thickness t_c of piezo actuators will be much less than the thickness t_b of the member, and the thickness t_s of the adhesive will be less than t_c. It is thus feasible to assume that the bonding layer carries shear stress only, and the piezo material carries normal stress only.

Under the above assumptions, the static linear and angular momentum balance equations for the piezo materials and the sub-structure are, respectively:

$$\frac{d\sigma_c'}{dx} - \frac{\tau'}{t_c} = 0 \quad (22)$$

$$\frac{d\sigma_c''}{dx} - \frac{\tau''}{t_c} = 0 \quad (23)$$

$$\frac{dN}{dx} + (\tau'' - \tau')b = 0 \quad (24)$$

$$\frac{dM}{dx} + \frac{t_b}{2}b(\tau' + \tau'') + Q = 0 \quad (25)$$

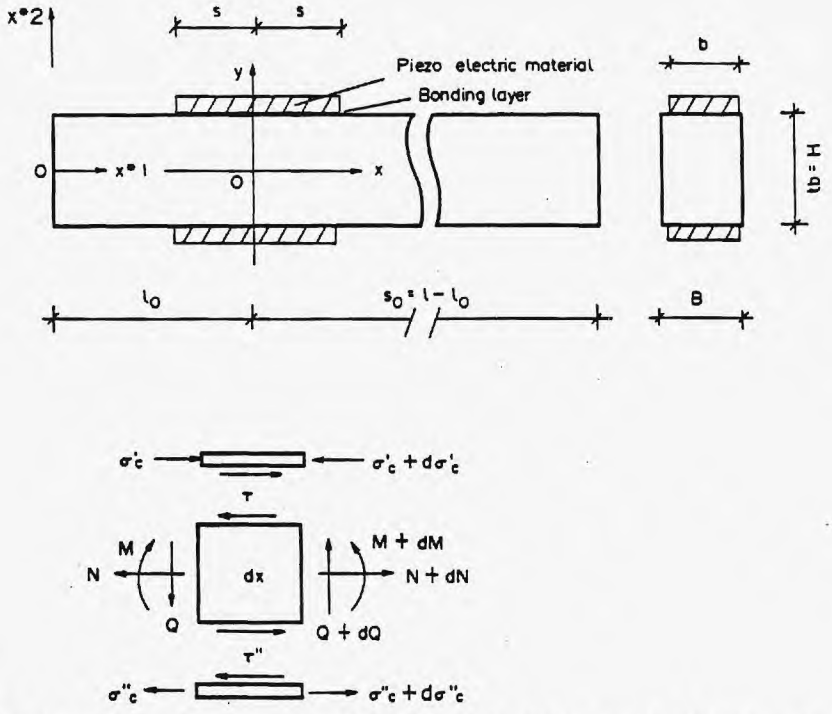

Fig. 2. A structural member bonded by a pair of piezo-electric actuators and the differential elements.

where σ_c' and σ_c'' are the normal stresses in the upper and lower piezo material layers, respectively, τ' and τ'' are the shear stresses in the upper and lower bonding layers, respectively. N, M, Q and b are the axial force, bending moment, transverse shear force, and the width of the actuators, respectively.

On the other hand, the stress–strain and strain–displacement relations are given by:

$$\frac{du_b'}{dx} = \frac{N}{EA} - \frac{t_b}{2}\frac{M}{EI} \tag{26}$$

$$\frac{du_b''}{dx} = \frac{N}{EA} + \frac{t_b}{2}\frac{M}{EI} \tag{27}$$

$$\frac{du_c'}{dx} = -\frac{\sigma_c'}{E_c} + \frac{d_{31}V'}{t_c} \tag{28}$$

$$\frac{du_c''}{dx} - = \frac{\sigma_c''}{E_c} + \frac{d_{31}V''}{t_c} \tag{29}$$

$$\tau' = G_s\frac{u_b' - u_c'}{t_s} \tag{30}$$

$$\tau'' = G_s\frac{u_c'' - u_b''}{t_s} \tag{31}$$

in which V' and V'' are the voltages applied to the upper and lower piezo materials, respectively, the term d_{31} is the piezo-electric material constant relating the voltage applied to the material to the mechanical strain produced; u_b' and u_b'' are the displacements on the upper and lower surfaces of the member respectively, u_c' and u_c'' are the displacements of the upper and lower actuators; E_c is the Young's modulus of the piezo-electric material, G_s the shear modulus of the bounding layer, and EA and EI are the axial and flexural ridigities of the structural member, respectively.

Differentiating eqns (30), (31) and substituting eqns (26)–(29) into them, gives

$$\frac{d\tau'}{dx} = \frac{G_s}{t_s}\left(\frac{\sigma_c'}{E_c} - \Lambda' + \frac{N}{EA} - \frac{t_b}{2}\frac{M}{EI}\right) \tag{32}$$

$$\frac{d\tau''}{dx} = \frac{G_s}{t_s}\left(\frac{\sigma_c''}{E_c} + \Lambda'' - \frac{N}{EA} - \frac{t_b}{2}\frac{M}{EI}\right) \tag{33}$$

in which

$$\Lambda' = \frac{d_{31}V'}{t_c}, \quad \Lambda'' = \frac{d_{31}V''}{t_c}. \tag{34}$$

By letting

$$\tau_1 = \tau' + \tau'' \tag{35}$$

$$\tau_2 = \tau' - \tau'' \tag{36}$$

$$\sigma_1 = \sigma_c' + \sigma_c'' \tag{37}$$

$$\sigma_2 = \sigma_c' - \sigma_c'' \tag{38}$$

$$\Lambda_1 = -\Lambda' + \Lambda'' \tag{39}$$

$$\Lambda_2 = -\Lambda' - \Lambda'' \tag{40}$$

eqns (22)–(24) and (32)–(33) become

$$\frac{d\sigma_1}{dx} - \frac{\tau_1}{t_c} = 0 \tag{41}$$

$$\frac{d\sigma_2}{dx} - \frac{\tau_2}{t_c} = 0 \tag{42}$$

$$\frac{dN}{dx} - b\tau_2 = 0 \tag{43}$$

$$\frac{dM}{dx} - \frac{t_b}{2}b\tau_1 + Q = 0 \tag{44}$$

$$\frac{d\tau_1}{dx} = \frac{G_s}{t_s}\left(\frac{\sigma_1}{E_c} + \Lambda_1 - t_b\frac{M}{EI}\right) \tag{45}$$

$$\frac{d\tau_2}{dx} = \frac{G_s}{t_s}\left(\frac{\sigma_2}{E_c} + \Lambda_2 + \frac{2N}{EA}\right). \tag{46}$$

Integrating eqns (43)–(44), and using eqns (41)–(42) and the boundary conditions $N = N_1$, $M = M_1$ and $Q = Q_1$ at $x = -s$ yields

$$N = N_1 + bt_c\sigma_2 \tag{47}$$

$$M = M_1 - \frac{t_c t_b}{2}b\sigma_1 - Q_1(x + s). \tag{48}$$

Substituting eqns (41)–(42) and (47)–(48) into eqns (45)–(46), we finally have

$$\frac{d^2\sigma_1}{dx^2} - \alpha^2\sigma_1 = a_1\left\{\Lambda_1 - \frac{t_b}{EI}[M_1 - Q_1(x + s)]\right\} \tag{49}$$

$$\frac{d^2\sigma_2}{dx^2} - \gamma^2\sigma_2 = a_1\left\{\Lambda_2 + \frac{2}{EA}N_1\right\} \tag{50}$$

in which

$$a_1 = \frac{G_s}{t_c t_s} \tag{51}$$

$$\alpha^2 = a_1\left(\frac{1}{E_c} + \frac{t_c t_b^2 b}{2EI}\right) \tag{52}$$

$$\gamma^2 = a_1\left(\frac{1}{E_c} + \frac{2bt_c}{EA}\right). \tag{53}$$

The solutions of eqns (49) and (50) are

$$\sigma_1 = A\sinh\alpha x + B\cosh\alpha x - \frac{a_1}{\alpha^2}\left\{\Lambda_1 - \frac{t_b}{EI}[M_1 - Q_1(x + s)]\right\} \tag{54}$$

$$\sigma_2 = C \sinh \gamma x + D \cosh \gamma x - \frac{a_1}{\alpha^2}\left\{\Lambda_2 + \frac{2}{EA} N_1\right\}. \quad (55)$$

From the boundary conditions

$$\sigma' = \sigma'' = 0 \quad \text{at } x = -s$$

$$\sigma' = \sigma'' = 0 \quad \text{at } x = s$$

$$M = M_2 \quad \text{at } x = s$$

the constants of integration in eqns (54) and (55) are

$$A = \frac{a_1}{\alpha^2} \frac{1}{2 \sinh \alpha s} \frac{t_b}{EI} (M_1 - M_2) \quad (56)$$

$$B = \frac{a_1}{\alpha^2} \frac{1}{2 \cosh \alpha s} \left[2\Lambda_1 - \frac{t_b}{EI}(M_1 + M_2)\right] \quad (57)$$

$$C = 0 \quad (58)$$

$$D = \frac{a_1}{\gamma^2} \frac{1}{\cosh \gamma s} \left[\Lambda_2 + \frac{2}{EA} N_1\right]. \quad (59)$$

Equations (41) and (42) give

$$\tau_1 = \frac{t_c a_1}{\alpha} \left\{\frac{\sinh \alpha x}{\cosh \alpha s} \Lambda_1 + \frac{t_b}{2EI}\left[(M_1 - M_2) \frac{\cosh \alpha x}{\sinh \alpha s} - (M_1 + M_2) \frac{\sinh \alpha x}{\cosh \alpha s} - \frac{2}{\alpha} Q_1\right]\right\} = \tau_{1V} + \tau_{1M} \quad (60)$$

$$\tau_2 = \frac{t_c a_1}{\gamma} \left\{\frac{\sinh \gamma x}{\cosh \gamma s} \Lambda_2 + \frac{2}{EA} \frac{\sinh \gamma x}{\cosh \gamma s} N_1\right\} = \tau_{2V} + \tau_{2N}. \quad (61)$$

In eqns (60) and (61), τ_{1V} and τ_{2V} are parts of the stresses τ_1 and τ_2 related to the applied voltages, τ_{1M} is the part related to the internal forces M and Q of the member, and τ_{2N} is that relating to axial force N.

It can be seen from the above derivations that the piezo actuators affect the structural member only through localized shear stresses, and that the shear stresses are functions of not only the applied voltage, but also of the moment, shear force, and axial force in the member. Having obtained the shear stress sum τ_1 and the stress difference τ_2 transmitted to the member by the pair of piezo actuators, the shear stress τ' and τ'' acting on the upper and lower layers, respectively, can be obtained from eqns (35) and (36). However, as a matter of fact, it is just that the τ_1 and τ_2 contribute to the momentum balances as indicated in eqns (24) and (25). So τ_1 and τ_2 will be used rather than τ' and τ''.

In eqns (60) and (61), both τ_1 and τ_2 are decomposed into two parts, one is related to the voltage applied to the actuators, and the other is related to the internal forces of the member. The parts of the τ_1 and τ_2 related to the voltage will provide the required control forces, and the other parts will contribute to the stiffness matrix of the member. The distributions of τ_{1V} and τ_{1M} are illustrated in Figs 3 and 4. The distributions of τ_{2V} and τ_{2N} are similar to τ_{1V}. The value τ_{1V} is the "simpler case" called by Crawley and Luis [1]. In fact, τ_{1V} is only one part of the shear stress. Crawley and Luis did not consider the effect of the transverse force Q and axial force N on the shear forces induced by the actuators. The Q and N have a considerable influence to the τ_1 and τ_2, for example, in the presence of N, τ_2 will not be zero even when the voltage is applied in the manner $\Lambda_2 = 0$.

The total axial force N_V^* and the total moments M_V^* induced by the voltages applied to a pair of piezo actuators are, respectively,

$$N_V^* = \int_{-s}^{s} b\tau_{2V}\, dx = \frac{a_1 t_c b \Lambda_2}{\gamma \cosh \gamma s} \int_{-s}^{s} \sinh \gamma x\, dx = 0 \quad (62)$$

$$M_V^* = \int_{-s}^{s} \frac{t_b}{2} b\tau_{1V}\, dx = 0. \quad (63)$$

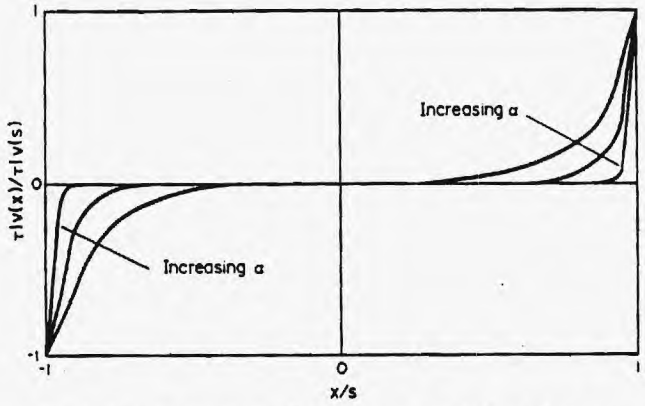

Fig. 3. The distributions of shear stress $\tau_{1v}(x)$ for various α.

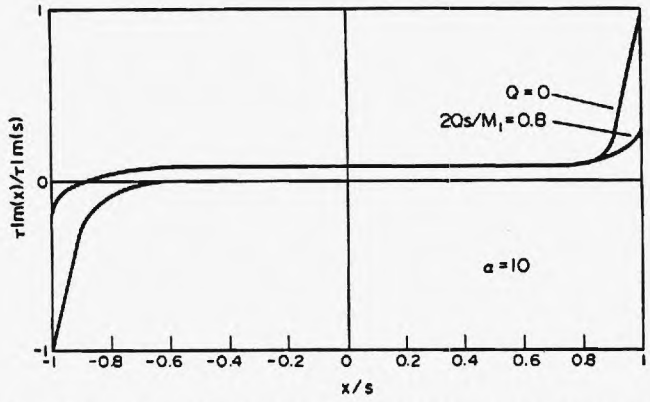

Fig. 4. The distributions of shear stress τ_{1m} for $Q = 0$ and $2Qs/M_1 = 0.8$.

Thus τ_{1V} and τ_{2V} provide only the localized axial force and moment to the structural member. It is useful to keep this in mind when deciding an efficient placement of the actuators.

4. THE CONTRIBUTIONS OF PIEZO ACTUATORS TO THE MOMENTUM BALANCE EQUATIONS OF THE STRUCTURE

Having solved for the shear stresses transmitted to the member by a pair of piezo actuators, we are able to establish an appropriate computational model for active control.

It is assumed that the member of the frame can undergo arbitrary large rigid translations and rotations but only moderate relative rotations. Further, for simplicity, it is assumed that the principal axes of the cross-section of the member are perpendicular to each other. So the governing equations of the element will be established in the element local coordinates composed of the element axis and the cross-section principal axes. Based on the weak form of governing equations, assumed stress fields and plastic hinge method, Shi and Atluri [4] presented an approach for elasto-plastic large deformation analysis of space frames. Similar weak forms of governing equations, and an assumed stress approach, will be employed here again.

The nomenclature of the kinematics and generalized nodal forces for a space frame member are demonstrated in Figs 5 and 6, respectively. e_i ($i = 1, 2, 3$) denote a fixed global Cartesian reference structure; e_i' ($i = 1, 2, 3$) denote the reference frame attached to an undeformed member of the frame; $\hat{e}_i$ denote the vectors attached to a member that has undergone large rigid rotations; and e_i^* are base vectors attached to a member that has undergone

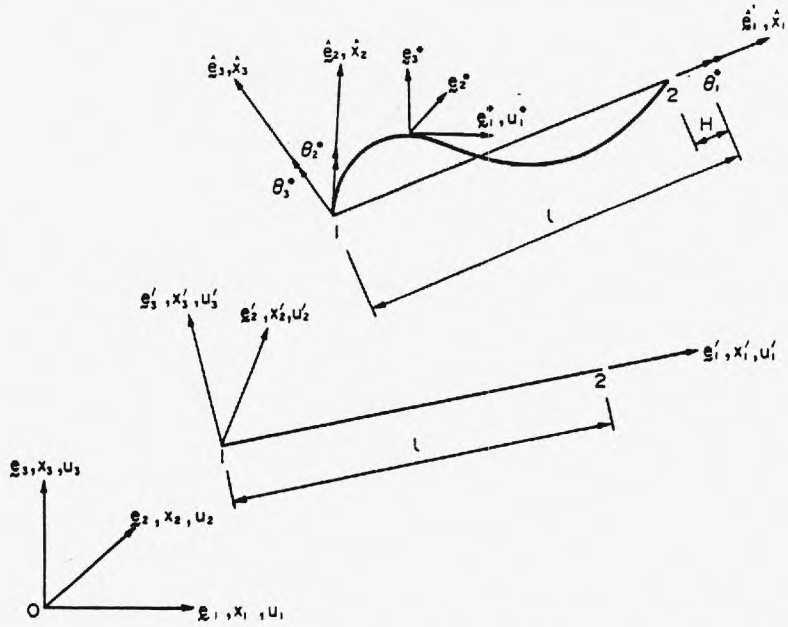

Fig. 5. Nomenclature for kinematics of deformation of a space-frame member.

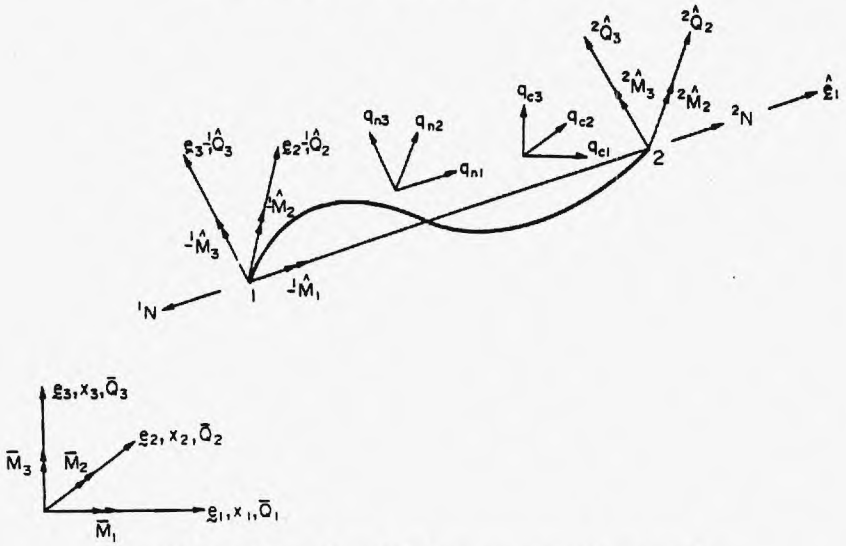

Fig. 6. Nomenclature for nodal forces on a space-frame member.

moderate local elastic deformation in addition to a large overall rigid rotation. The consistent forms of linear and angular momentum balance equations for the Jaumann stress resultants N, $\hat{Q}_2$ and $\hat{Q}_3$ and stress couples $\hat{M}_1$, $\hat{M}_2$ and $\hat{M}_3$ are of the form [5]

$$\frac{\partial N}{\partial \hat{x}_1} + \hat{q}_1 = 0$$

$$\frac{\partial \hat{M}_1}{\partial \hat{x}_1} + \hat{m}_1 = 0$$

$$\frac{\partial \hat{Q}_2}{\partial \hat{x}_1} + \hat{q}_2 = 0$$

$$\frac{\partial \hat{Q}_3}{\partial \hat{x}_1} + \hat{q}_3 = 0$$

$$\frac{\partial \hat{M}_2}{\partial \hat{x}_1} - \hat{Q}_3 + N\theta_2^* + \hat{m}_2 = 0$$

$$\frac{\partial \hat{M}_3}{\partial \hat{x}_1} - \hat{Q}_2 + N\theta_3^* + \hat{m}_3 = 0 \tag{64}$$

where $\hat{q}_i$ is the distributed load density along $\hat{e}_i$ direction, and $\hat{m}_i$ is the distributed moment density about $\hat{e}_i$ axis. The trial functions for N, $\hat{M}_2$ and $\hat{M}_3$ corresponding to arbitrary $\hat{q}_1$, $\hat{q}_2$ and $\hat{q}_3$ were given in Shi and Atluri's paper [4]. For simplicity, we will only concentrate our attention on the distributed forces induced by the actuators. A rectangular cross-section of the beam, with height H and width B, is assumed. In this case, we have

$$\hat{q}_1 = -b_{ul}\tau_{2ul} - b_{lr}\tau_{2lr} \tag{65}$$

in the region bonded by the actuators, and $\hat{q}_1 = 0$ elsewhere,

$$\hat{m}_2 = \begin{cases} \dfrac{B}{2} b_{lr}\tau_{1lr} & \text{in the region of actuators;} \\ 0 & \text{elsewhere} \end{cases} \tag{66}$$

$$\hat{m}_3 = \begin{cases} \dfrac{H}{2} b_{ul}\tau_{1ul} & \text{in the region of actuators;} \\ 0 & \text{elsewhere} \end{cases} \tag{67}$$

and $\hat{q}_2 = \hat{q}_3 = \hat{m}_1 = 0$ where the subscripts 'ul' and 'lr' denote the upper and lower surfaces and the left and right surfaces, respectively, of the cross-section. Since the total length of the actuators along a surface is shorter than that of the beam, it is feasible to assume that the trial functions which satisfy only the linear parts of the momentum balance equations are

$$\begin{Bmatrix} N \\ \hat{M}_1 \\ \hat{M}_2 \\ \hat{M}_3 \end{Bmatrix} = \begin{bmatrix} 1 & 0 & 0 & 0 & 0 & 0 \\ 0 & 1 & 0 & 0 & 0 & 0 \\ 0 & 0 & 1-\hat{x}_1/l & \hat{x}_1/l & 0 & 0 \\ 0 & 0 & 0 & 0 & 1-\hat{x}_1/l & \hat{x}_1/l \end{bmatrix} \begin{Bmatrix} n \\ m_1 \\ {}^1m_2 \\ {}^2m_2 \\ {}^1m_3 \\ {}^2m_3 \end{Bmatrix} = \mathbf{F}\sigma \tag{68}$$

in which l is the element length and

$$\sigma = \{n\ m_1\ {}^1m_2\ {}^2m_2\ {}^1m_3\ {}^2m_3\}^{\mathrm{T}} \tag{69}$$

is the element nodal force vector in the local coordinates. Because the trial functions for $\hat{M}_2$ and $\hat{M}_3$ satisfy the linear parts of the balance equations, the

following relations hold:

$$\hat{Q}_2 = -\frac{\partial \hat{M}_3}{\partial \hat{x}_1}$$

$$\hat{Q}_3 = \frac{\partial \hat{M}_2}{\partial \hat{x}_1}. \tag{70}$$

From the above discussion, the weak form of the remainder of the balance equations may be written as

$$\int_0^l \left[\frac{\partial N}{\partial \hat{x}_1} + \hat{q}_1\right] v^* \, d\hat{x}_1 = 0 \tag{71}$$

$$\int_0^l \left[\frac{\partial \hat{M}_2}{\partial \hat{x}_1} - \hat{Q}_3 + N\theta_2^* + \hat{m}_2\right] \beta_2^* \, d\hat{x}_1 = 0 \tag{72}$$

$$\int_0^l \left[\frac{\partial \hat{M}_3}{\partial \hat{x}_1} + \hat{Q}_2 + N\theta_3^* + \hat{m}_3\right] \beta_3^* \, d\hat{x}_1 = 0 \tag{73}$$

where v^*, β_2^* and β_3^* are the test functions corresponding to N, $\hat{M}_2$ and $\hat{M}_3$.

As derived in detail by Shi and Atluri [4], the weak form of compatibility conditions for an elastic element, as a whole, is

$$-\mathbf{D}^T \delta\sigma + \int_0^l \mathbf{W}^T \cdot \mathbf{F} \delta\sigma \, d\hat{x}_1 = 0 \tag{74}$$

in which $\boldsymbol{D}^T$ is the element displacement vector in the local coordinate system $\hat{e}_i$. The vector $\mathbf{D}^T$ and $\mathbf{W}^T$ are defined, respectively, as:

$$\mathbf{D}^T = [\mathbf{H}, ({}^2\theta_1^* - {}^1\theta_1^*), -{}^1\theta_2^*, {}^2\theta_2^*, -{}^1\theta_3^*, {}^2\theta_3^*] \tag{75}$$

$$\mathbf{W}^T = \left[\frac{\partial W_c}{\partial N}, \frac{\partial W_c}{\partial \hat{M}_1}, \frac{\partial W_c}{\partial \hat{M}_2}, \frac{\partial W_c}{\partial \hat{M}_3}\right]. \tag{76}$$

The element displacements are shown in Fig. 5, W_c is the complementary energy density, $\mathbf{F}$ is the interpolation matrix as defined in eqn (68).

Let $\mathbf{Q}_e$ denote the internal nodal force vector of an element

$$\mathbf{Q}_e = \{N_1, {}^1Q_2, {}^1Q_3, {}^1\hat{M}_1, {}^1\hat{M}_2, {}^1\hat{M}_3, N_2, \times {}^2Q_2, {}^2Q_3, {}^2\hat{M}_1, {}^2\hat{M}_2, {}^2\hat{M}_3\}, \tag{77}$$

$\bar{\mathbf{f}}$ represent the external nodal force vector at the ends of the element in the global coordinates, and let $\mathbf{R}^*$ be the transformation matrix which transforms the element local vector to the global coordinates, then the weak form of the joint equilibrium can be written as (see Ref. [4]):

$$\sum_{\text{elem}} [\delta \mathbf{d}^T \mathbf{R}^* \mathbf{Q}_e - \delta \mathbf{d}^T \bar{\mathbf{f}}] = 0 \tag{78}$$

in which $\delta\mathbf{d}$ is the variation of the element nodal displacement vector $\mathbf{d}$ in the global coordinates, and $\mathbf{d}$ is of the form

$$\mathbf{d}^T = \{{}^1u_1, {}^1u_2, {}^1u_3, {}^1\theta_1, {}^1\theta_2, {}^1\theta_3, \times {}^2u_1, {}^2u_2, {}^2\theta_3, {}^2\theta_1, {}^2\theta_2, {}^2\theta_3\}. \tag{79}$$

Recalling eqn (70), the combined weak form of the governing equations is

$$\sum_{\text{elem}} \left\{-\mathbf{D}^T \delta\sigma + \int_0^l \mathbf{W}^T \mathbf{F} \delta\sigma \, d\hat{x}_1 + \delta \mathbf{d}^T \mathbf{R}^* \mathbf{Q}_e - \delta \mathbf{d}^T \bar{\mathbf{f}} + \int_0^l N\theta_2^* \beta_2^* \, d\hat{x}_1 + \int_0^l N\theta_3^* \beta_3^* \, d\hat{x}_1 + \int_0^l \hat{q}_1 v^* \, d\hat{x}_1 + \int_0^l [\hat{m}_2 \beta_2^* + \hat{m}_3 \beta_3^*] \, d\hat{x}_1 \right\} = 0. \tag{80}$$

It was shown by Atluri [6] that the terms involving $N\theta_i^* \beta_i^*$ $(i = 2, 3)$ contribute to the so-called "initial stress" stiffness correction to the tangent stiffness matrix, and neglecting the terms in the formulation, while resulting in a slightly incorrect tangent stiffness matrix, is entirely consistent in the context of an iterative solution of a nonlinear problem. Therefore, the terms $N\theta_i^* \beta_i^*$ in eqn (80) will be omitted. Then eqn (80) becomes

$$\sum_{\text{elem}} \left\{-\mathbf{D}^T \delta\sigma + \int_0^l \mathbf{W}^T \mathbf{F} \delta\sigma \, d\hat{x}_1 + \delta \mathbf{d}^T \mathbf{R}^* \mathbf{Q}_e - \delta \mathbf{d}^T \bar{\mathbf{f}} + \int_0^l \hat{q}_1 v^* \, d\hat{x}_1 + \int_0^l [\hat{m}_2 \beta_2^* + \hat{m}_3 \beta_3^*] \, d\hat{x}_1 \right\} = 0. \tag{80}$$

The last two integrals are induced by the piezo actuators. Let us consider their effects on the system equations. We first consider a simple case: only one pair of actuators in $\hat{x}_1$–$\hat{x}_2$ plane. If the center of the actuator located at $\hat{x}_1 = l_o$ and the length of the actuators is $2s$ then

$$\int_0^l \hat{q}_1 v^* \, d\hat{x}_1 = -\int_{-s}^{s} b\tau_2 v^* \, dx = -\int_{-s}^{s} b(\tau_{2V} + \tau_{2N}) v^* \, dx \tag{81}$$

$$\int_0^l \hat{m}_3 \beta_3^* \, d\hat{x}_1 = \int_{-s}^{s} \frac{bH}{2} \tau_1 \beta_3^* \, dx = \frac{bH}{2} \int_{-s}^{s} (\tau_{1V} + \tau_{1M}) \beta_3^* \, dx \tag{82}$$

in which x is the local coordinate of the actuators, and $x = \hat{x}_1 - l_o$. Recalling that v^* and β_3^* are the variations of the element local displacement u_1^* and θ_3^*, respectively, v^* and θ_3^* can be interpolated as

$$v^* = \frac{1}{l} \{s_o - x; \quad l_o + x\} \begin{Bmatrix} \delta {}^1u_1^* \\ \delta {}^2u_1^* \end{Bmatrix} \tag{83}$$

$$\beta_3^* = \frac{1}{l}\{s_o - x; \quad l_o + x\}\begin{Bmatrix}\delta^1\theta_3^* \\ \delta^2\theta_3^*\end{Bmatrix} \tag{84}$$

where $s_o = l - l_o$.

By substituting eqns (60), (61), (83) and (84) into them, the integrations in eqns (81) and (82) can be very easily carried out, and these integrations convert the distributed shear stresses into the equivalent nodal forces in the sense of the weak form. Since τ_{1V} and τ_{2V} will provide the required control forces and play an important role in the present study, it will be helpful to seek a more efficient way to evaluate the equivalent nodal control forces.

The values τ_{1V} and τ_{2V} are distributed in the region of the member bonded by the actuators. Instead of considering the distributed stresses, a pair of equivalent concentrated axial forces and moments can be used. The equivalent moments M_V and axial forces N_V are

$$M_V = \frac{a_1 t_b t_c b}{\alpha \cosh \alpha s} \Lambda_1 \int_0^s \sinh \alpha x \, dx \tag{85}$$

$$N_V = \frac{a_1 t_c}{\gamma \cosh \gamma s} \Lambda_2 \int_0^s \sinh \gamma x \, dx \tag{86}$$

and M_V and $-N_V$ are located at $x = r$, $-M_V$ and N_V located at $-r$ where r is given by

$$r \int_0^s \sinh \alpha x \, dx = \int_0^s x \sinh \alpha x \, dx. \tag{87}$$

Having determined M_V, N_V and r, the corresponding equivalent nodal forces $\mathbf{p}_V$ in the local coordinates can be very easily calculated, and $\mathbf{p}_V$ is of the form

$$\mathbf{p}_V = \mathbf{T}_e \begin{Bmatrix}\Lambda_1 \\ \Lambda_2\end{Bmatrix} \tag{88}$$

where $\mathbf{T}_e$ is a 12×2 matrix.

From eqns (61) and (83) we have

$$b \int_{-s}^{s} \tau_{2N} v^* \, dx = \frac{bt_c a_1}{\gamma \cosh \gamma s} \frac{2N_1}{eAl} \times \int_{-s}^{s} \sinh \gamma x [s_o - x, x + l_0] \, dx \begin{Bmatrix}\delta^1 u_1^* \\ \delta^2 u_1^*\end{Bmatrix} = \{\delta^1 u_1^*, \delta^2 u_1^*\}\begin{bmatrix}-1 \\ 1\end{bmatrix} \beta_1 N_1 \tag{89}$$

in which

$$\beta_1 = -\frac{4bt_c a_1}{\gamma^2 EAl}\left(s - \frac{\sinh \gamma s}{\gamma \cosh \gamma s}\right). \tag{90}$$

Similarly, by eqns (60), (84) and (70), we get

$$\frac{Hb}{2}\int_{-s}^{s} \tau_{1M} \beta_3^* \, dx = \{\delta^1\theta_3^* \quad \delta^2\theta_3^*\} \times \begin{bmatrix} s_o & l_o \\ -s_o & -l_o \end{bmatrix} \beta_2 \begin{Bmatrix} \hat{M}_3|_{s_1 = l_o - s} \\ \hat{M}_3|_{s_1 = l_o + s} \end{Bmatrix} \tag{91}$$

where

$$\beta_2 = \frac{H^2 t_c b a_1}{\alpha^2 EIl}\left(s - \frac{\sinh \alpha s}{\alpha \cosh \alpha s}\right). \tag{92}$$

For a member of a space frame with N_{up} pair of actuators on the "upper and lower" surfaces of the member and N_{LR} pairs on the "left and right" surfaces, the last two integrations W_{pz} in eqn (80) will be

$$\begin{aligned} W_{pz} &= \int_0^l \hat{q}_1 v^* \, d\hat{x}_1 + \int_0^l [\hat{m}_2 \beta_2^* + \hat{m}_3 \beta_3^*] \, d\hat{x}_1 \\ &= \sum_{i=1}^{N_{uL}} \left\{ \int_{-s_i}^{s_i} \left[-b_i \tau_{2N_i} v^* + \frac{Hb_i}{2} \tau_{1M_i} \right] dx + \delta \hat{\mathbf{a}}^T \mathbf{R}^* \mathbf{p}_{V_i} \right\} \\ &\quad + \sum_{j=1}^{N_{LR}} \left\{ \int_{-s_j}^{s_j} \left[-b_j \tau_{2N_j} v^* + \frac{Bb_j}{2} \tau_{1M_j} \right] dx + \delta \mathbf{d}^T \mathbf{R}^* \mathbf{p}_{V_j} \right\} \end{aligned} \tag{93}$$

in which $\delta \mathbf{d}^T$ and $\mathbf{R}^*$ are the same as those in eqn (78). By letting

$$\delta \mathbf{d}^* = \delta\{{}^1u_1^*, {}^2u_1^*, {}^1\theta_2^*, {}^2\theta_2^*, {}^1\theta_3^*, {}^2\theta_3^*\}^T \tag{94}$$

$$M^* = \{N_{l_o - s}, M_1, \hat{M}_2|_{l_o - s}, \hat{M}_2|_{l_o + s}, \times \hat{M}_3|_{l_o - s}, \hat{M}_3|_{l_o + s}\}^T \tag{95}$$

and using the results of eqns (89) and (91), eqn (93) can be written as the following matrix form

$$\begin{aligned} W_{pz} &= (\delta \mathbf{d}^*)^T \left[\sum_{i=1}^{N_{uL}} (\mathbf{PP}_1 \cdot \mathbf{M}^*) + \sum_{j=1}^{N_{LR}} (\mathbf{PP}_2 \cdot \mathbf{M}^*) \right] \\ &\quad + \delta \mathbf{d}^T \mathbf{R}^* \left[\sum_{i=1}^{N_{uL}} \mathbf{p}_{V_i} + \sum_{j=1}^{N_{LR}} \mathbf{p}_{V_j} \right] \\ &= \delta \mathbf{d}^T \cdot \mathbf{TR} \cdot \mathbf{PP} \cdot \mathbf{M}^* + \delta \mathbf{d}^T \cdot \mathbf{R}^* \cdot \mathbf{T} \cdot \Lambda \\ &= \delta \mathbf{d}^T [\mathbf{TR} \cdot \mathbf{PP} \cdot \mathbf{TM} \cdot \sigma + \mathbf{R}^* \cdot \mathbf{T} \cdot \Lambda] \end{aligned} \tag{96}$$

in which $\mathbf{TR}$ is the transformation matrix for $\mathbf{d}^* = \mathbf{TRd}$, $\mathbf{TM}$ is the transformation matrix for $\mathbf{M}^* = \mathbf{TM}\sigma$, and $\mathbf{d}$ and σ are defined as in eqns (79) and (69), respectively.

Substituting eqn (96) into eqn (80a) yields

$$\sum_{\text{elem}}\left\{-\mathbf{D}^{\mathrm{T}}\delta\boldsymbol{\sigma}+\int_0^l \mathbf{W}^{\mathrm{T}}\mathbf{F}\delta\boldsymbol{\sigma}\,\mathrm{d}\hat{x}_1+\delta\mathbf{d}^{\mathrm{T}}\mathbf{R}^*\mathbf{Q}_e-\delta\mathbf{d}^{\mathrm{T}}\bar{\mathbf{f}}\right.$$

$$\left.+\delta\mathbf{d}^{\mathrm{T}}[\mathbf{TR}\cdot\mathbf{PP}\cdot\mathbf{TM}\cdot\boldsymbol{\sigma}+\mathbf{R}^*\cdot\mathbf{T}\cdot\boldsymbol{\Lambda}]\right\}=0. \quad (97)$$

Corresponding to eqn (97), the weak form of the incremental governing equations is

$$\sum_{\text{elem}}\{\delta\Delta\mathbf{d}^{\mathrm{T}}[\mathbf{R}^*\mathbf{Q}_e+\mathbf{TR}\cdot\mathbf{PP}\cdot\mathbf{TM}\cdot\boldsymbol{\sigma}+\mathbf{R}^*\mathbf{T}\boldsymbol{\Lambda}-\bar{\mathbf{f}}]$$

$$+\delta\Delta\mathbf{d}^{\mathrm{T}}[\Delta\mathbf{R}^*\mathbf{Q}_e+\mathbf{R}^*\Delta\mathbf{Q}_e+\mathbf{TR}\cdot\mathbf{PP}\cdot\mathbf{TM}\cdot\boldsymbol{\sigma}$$

$$+\mathbf{TR}\cdot\mathbf{PP}\cdot\mathbf{TM}\cdot\Delta\boldsymbol{\sigma}+\Delta\mathbf{R}^*\mathbf{T}\boldsymbol{\Lambda}-\mathbf{R}^*\mathbf{T}\Delta\boldsymbol{\Lambda}-\Delta\bar{\mathbf{f}}]$$

$$+\Delta\delta\boldsymbol{\sigma}^{\mathrm{T}}\left[-\mathbf{D}+\int_0^l \mathbf{F}^{\mathrm{T}}\mathbf{W}\,\mathrm{d}\hat{x}_1\right]$$

$$+\Delta\delta\boldsymbol{\sigma}^{\mathrm{T}}\left[-\Delta\mathbf{D}+\int_0^l \mathbf{F}^{\mathrm{T}}\Delta\mathbf{W}\,\mathrm{d}\hat{x}_1\right]\Big\}=0. \quad (98)$$

By letting

$$\mathbf{R}^*(\mathbf{Q}_e+\mathbf{T}\boldsymbol{\Lambda})+\mathbf{TR}\cdot\mathbf{PP}\cdot\mathbf{TM}\cdot\boldsymbol{\sigma}=\mathbf{R}_d$$

$$\mathbf{TR}\cdot\mathbf{PP}\cdot\mathbf{TM}=\mathbf{A}_{\sigma dV}^{T}$$

$$\mathbf{R}^*\mathbf{T}=\mathbf{RP}$$

$$\sum_{\text{elem}}\bar{\mathbf{f}}=\mathbf{P}$$

$$\Delta\mathbf{R}^*\mathbf{Q}_e=\mathbf{A}_{ddo}\Delta\mathbf{d}$$

$$\mathbf{R}^*\Delta\mathbf{Q}_e=\mathbf{A}_{\sigma do}\Delta\boldsymbol{\sigma}$$

$$\Delta\mathbf{TR}\cdot\mathbf{PP}\cdot\mathbf{TM}\cdot\boldsymbol{\sigma}=\mathbf{A}_{ddn}\Delta\mathbf{d}$$

$$\Delta\mathbf{R}^*\mathbf{T}\boldsymbol{\Lambda}=\mathbf{A}_{ddV}\Delta\mathbf{d}$$

$$\sum\Delta\bar{\mathbf{f}}=\Delta\mathbf{P}$$

$$-\mathbf{D}+\int_0^l \mathbf{F}^{\mathrm{T}}\mathbf{W}\,\mathrm{d}\hat{x}_1=\mathbf{R}_\sigma$$

$$\Delta\mathbf{D}=\mathbf{A}_{\sigma do}^{\mathrm{T}}\Delta\mathbf{d}$$

$$\int_0^l \mathbf{F}\Delta\mathbf{W}\,\mathrm{d}\hat{x}_1=\mathbf{A}_{\sigma\sigma}\Delta\boldsymbol{\sigma}$$

eqn (98) becomes

$$\sum_{\text{elem}}\{\delta\Delta\mathbf{d}^{\mathrm{T}}[(\mathbf{A}_{ddo}+\mathbf{A}_{ddn}+\mathbf{A}_{ddV})\Delta\mathbf{d}$$

$$+(\mathbf{A}_{\sigma do}+\mathbf{A}_{\sigma dV})\Delta\boldsymbol{\sigma}+\mathbf{PR}\Delta\boldsymbol{\Lambda}-\Delta\bar{\mathbf{f}}$$

$$+\mathbf{R}_d-\bar{\mathbf{f}}]+\delta\Delta\boldsymbol{\sigma}^{T}[\mathbf{A}_{\sigma\sigma}\Delta\boldsymbol{\sigma}-\mathbf{A}_{\sigma do}^{\mathrm{T}}\Delta\mathbf{d}$$

$$+\mathbf{R}\sigma]\}=0. \quad (99)$$

Since the parameters $\delta\Delta\boldsymbol{\sigma}^{\mathrm{T}}$ are independent and arbitrary in each element, the above equation gives

$$\Delta\boldsymbol{\sigma}=\mathbf{A}_{\sigma\sigma}^{-1}(\mathbf{A}_{\sigma do}^{\mathrm{T}}\Delta\mathbf{d}-\mathbf{R}_\sigma). \quad (100)$$

Because the parameters $\delta\Delta\mathbf{d}^{\mathrm{T}}$ are arbitrary, eqn (99) gives

$$\sum_{\text{elem}}[\mathbf{A}_{ddo}+\mathbf{A}_{ddo}+\mathbf{A}_{ddV}$$

$$+(\mathbf{A}_{\sigma do}+\mathbf{A}_{\sigma dV})\mathbf{A}_{\sigma\sigma}^{-1}\mathbf{A}_{\sigma do}^{\mathrm{T}}]\Delta\mathbf{u}$$

$$=\sum_{\text{elem}}[\Delta\bar{\mathbf{f}}-\mathbf{PR}\cdot\Delta\boldsymbol{\Lambda}+\bar{\mathbf{f}}-\mathbf{R}_d$$

$$+(\mathbf{A}_{\sigma do}+\mathbf{A}_{\sigma dV})\mathbf{A}_{\sigma\sigma}^{-1}\mathbf{R}_\sigma] \quad (101)$$

or

$$\mathbf{K}\Delta\mathbf{u}=\Delta\mathbf{P}+\mathbf{PZ}\cdot\Delta\mathbf{V}+\mathbf{P}-\mathbf{R} \quad (102)$$

in which $\mathbf{K}$ is the tangent stiffness matrix of the system, $\Delta\mathbf{u}$ is the increment of the system displacement vector, $\Delta\mathbf{P}$ is the increment of the external loading, $(\mathbf{P}-\mathbf{R})$ is the unbalanced nodal force vector, $\mathbf{PZ}\cdot\Delta\mathbf{V}$ is the increment of control force vector induced by the piezo actuator excited by the voltage ΔV and is of the form

$$\Delta\mathbf{F}_p=\mathbf{PZ}\cdot\Delta\mathbf{V}=\sum_{\text{elem}}-\mathbf{PZ}\cdot\Delta\mathbf{V} \quad (103)$$

in which $\mathbf{V}$ is the voltage vector applied to the actuators. It can be seen from eqn (101) that the stiffness matrix is unsymmetric since the shear stresses exerted by the actuators are a kind of non-conservative loading.

If $\mathbf{M}$ and $\mathbf{C}$ denote the "tangent" mass and damping coefficient matrices, respectively, for dynamic problems, $\mathbf{R}'$ denotes the total "internal" nodal force vector resulting from the previous displacements of displacement $\mathbf{u}$, acceleration $\ddot{\mathbf{u}}$ and velocity $\dot{\mathbf{u}}$, then the equations of motion corresponding to eqn (102) is

$$\mathbf{M}\Delta\ddot{\mathbf{u}}+\mathbf{C}\Delta\dot{\mathbf{u}}+\mathbf{K}\Delta\mathbf{u}=\Delta\mathbf{P}+\mathbf{PZ}\Delta\mathbf{V}+\mathbf{P}-\mathbf{R}'. \quad (104)$$

The difference between eqn (104) and eqn (1) is that the unbalanced forces resulting from the linear approximation in each time step and iteration is considered in eqn (104).

5. DETERMINATION OF VOLTAGE APPLIED TO THE PIEZO ACTUATORS

The nodal control forces $\Delta\mathbf{F}_c$ given by eqn (20) are obtained from the optimal control theory. Since the piezo actuators are distributed along the structural members, it is difficult to place them appropriately, in order to provide the equivalent nodal control forces exactly as required by the control law. For the fixed

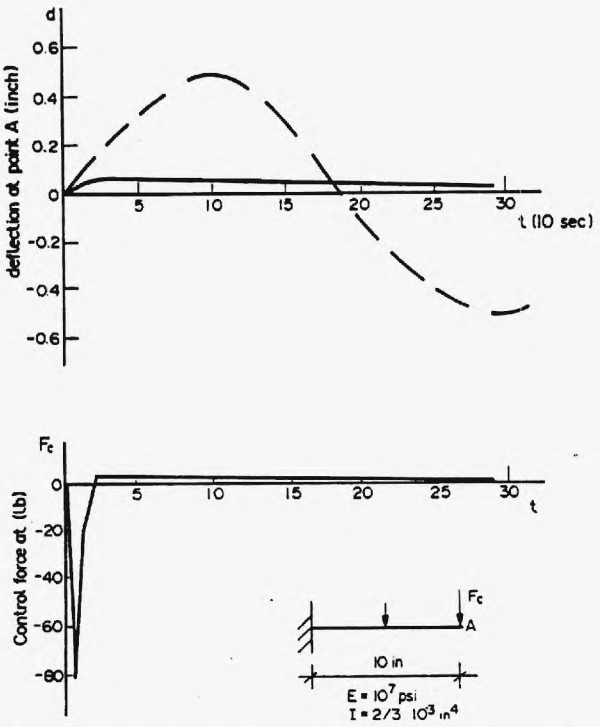

Fig. 7. Response and control force at point A by linear optimal control.

geometry of the actuators, the nodal control forces (equivalent nodal force vector) exerted by the piezo actuators would be functions of the applied voltages. Then the control algorithm has to be used to determine the appropriate voltages to be applied to the actuators, i.e. voltage vector ΔV in eqn (102) according to the control forces obtained by the control law.

From eqn (20), the increment of the control forces is

$$\Delta \mathbf{F}_c = -\mathbf{b}\mathbf{R}^{-1}\mathbf{b}^T\mathbf{M}^{-1}\alpha(t)\mathbf{G}\Delta\mathbf{S} = \mathbf{G}^*\Delta\mathbf{S}. \quad (105)$$

Therefore our objective is to determine ΔV from the given $\mathbf{G}^*\Delta\mathbf{S}$.

There are many possible ways to determine the

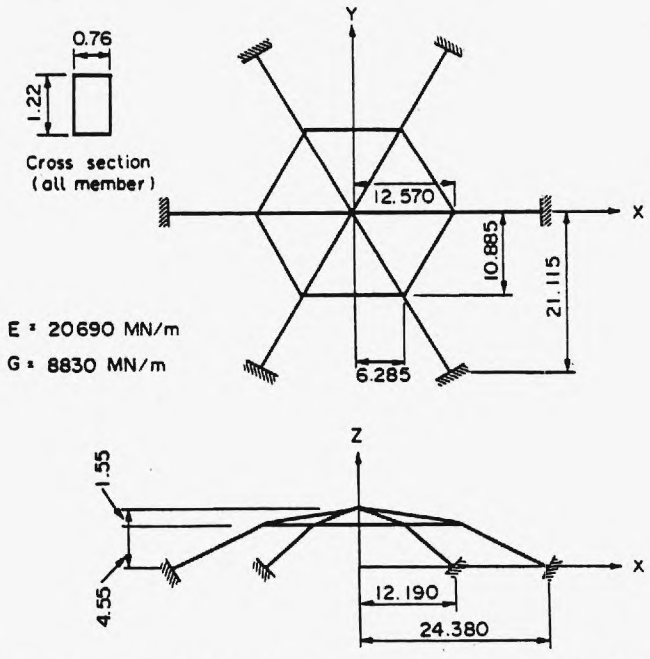

Fig. 8. Geometric and material data for framed dome. (The unit of length is meters.)

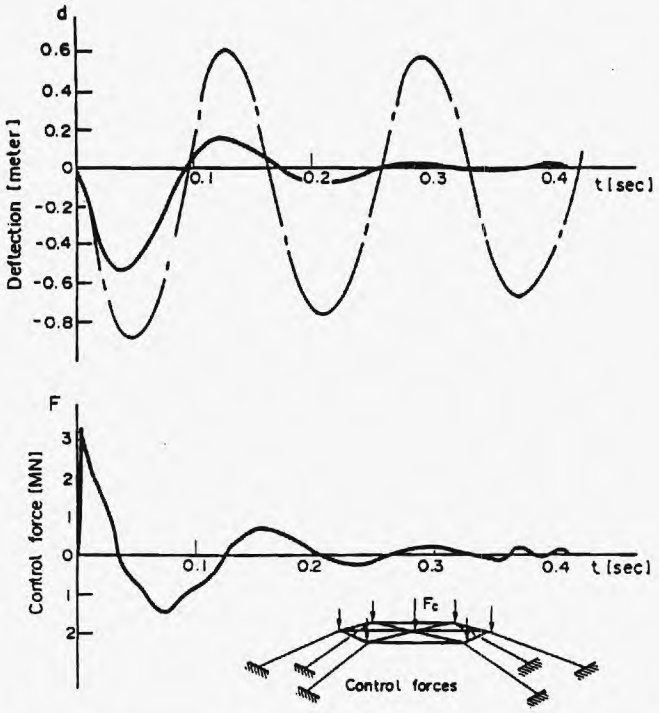

Fig. 9. Controlled response, free vibration and control force at the crown point.

appropriate voltage ΔV. If $PZ\delta d$ are the arbitrary "virtual displacements", ΔF_p in eqn (12) can be equivalent to ΔF_c in eqn (105), in the sense of "virtual work", as given by:

$$\delta \mathbf{d}^T \cdot \mathbf{PZ}^T \cdot \mathbf{PZ} \cdot \Delta V = \delta \mathbf{d}^T \cdot \mathbf{PZ}^T \cdot \mathbf{G}^* \Delta \mathbf{S} \quad (106)$$

when $(\mathbf{PZ}^T \cdot \mathbf{PZ})$ is invertible, we have

$$\Delta V = (\mathbf{PZ}^T \cdot \mathbf{PZ})^{-1} \mathbf{PZ}^T \cdot \mathbf{G}^* \Delta \mathbf{S} = \mathbf{G}^{**} \Delta \mathbf{S}. \quad (107)$$

So the increment of the appropriate voltages is determined by the increment of the state variable vector $\Delta \mathbf{S}$.

The dimension of $\mathbf{PZ}$ is $n \times q$ in which n is the number of total degrees of freedom of the system, q is the number of kinds of voltages applied to actuators. So the necessary condition that $\mathbf{PZ}$ is invertible is $q \leqslant n$. When only few different voltages are applied to the actuators on a member, and only few members are jointed at each structural joint, the condition $q \leqslant n$ will be satisfied without much difficulty. When $q > n$, ΔV can be determined by other equivalent criteria that are yet to be explored.

6. NUMERICAL EXAMPLES

Two examples of implementing nonlinear active control algorithm of Sec. 2, and two examples of the application of piezo actuators for active control, are presented in this section. In all the examples, the weighting matrices $\mathbf{R}$ and $\mathbf{Q}$ in eqn (8) are taken as identity matrices.

Example 1

The first example concerns the nonlinear active control algorithm of Sec. 2. For the fixed-fixed beam shown in Fig. 7, the static deflection–load curve demonstrates that the beam behaves nonlinearly when the mid-span deflection is larger than 0.1 in. [4]. The half span of the beam is modeled by two elements. Corresponding to an initial velocity $v_o = 400$ in/sec at the mid-span, the dynamic response without control is shown in Fig. 7 by broken line, and the response under active control is depicted in the same figure by solid line. The control force vs time is plotted there too. The figure shows that the vibration is damped out by the control forces very rapidly. Recall that the computed control force is, at this point, simply a mathematical result, and the physical means of inducing this actuator force is not addressed yet.

Example 2

This example considers the nonlinear active control of a space dome. The geometry of the dome is given in Fig. 8. The nonlinear static and dynamic analyses of the dome were studied by Remseth [7] and Shi and Atluri [4]. Here each member of the dome is modeled by a single element again as in the authors' previous paper [4]. Under the disturbance, an initial velocity $v_o = 30$ m/sec at the crown point, the free vibration, the controlled vibration and the control force at the crown point are illustrated in Fig. 9.

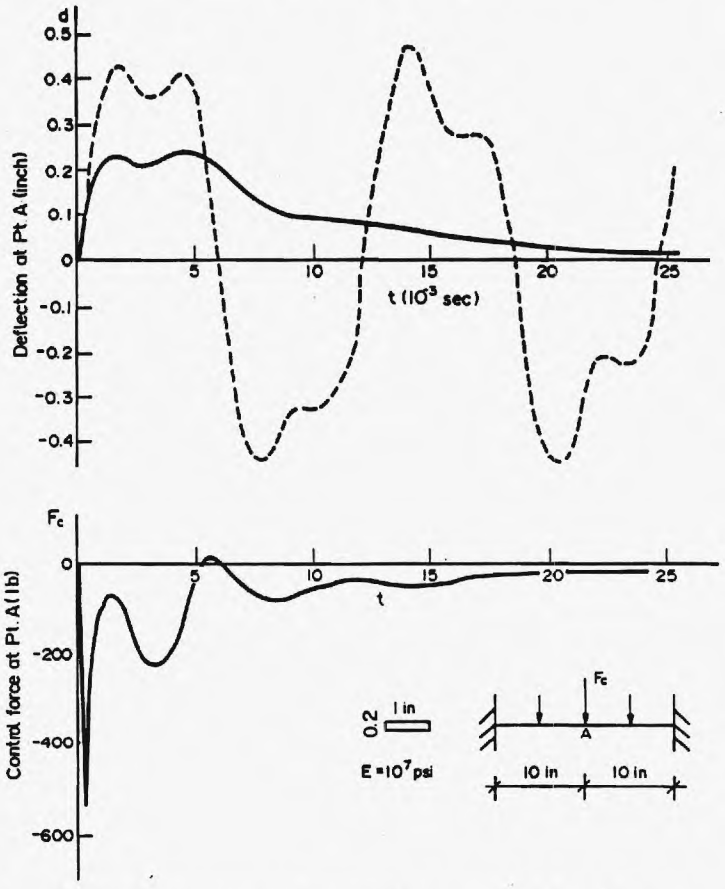

Fig. 10. Nonlinear response and control force at point A by optimal control.

Example 3

Now let us turn to the concept of active control using piezo actuators. Crawley and Luis [1] studied a cantilevered beam by experiment, but they did not give data of the bonding layers. For the assumed data of the layer, our computational model gives a similar result.

Let us consider another cantilevered beam shown in Fig. 11 in detail here. Corresponding to an initial velocity $v_o = 100$ in/sec applied at the free end of the beam, the response with the control forces obtained by optimal control theory and the control force at the free end are shown in Fig. 12. The placement of the piezo actuators and their data are given in Fig. 11. For simplicity, the same magnitude of voltage is applied to all actuators and in the manner $V' = -V''$ for the upper and lower surfaces. The response under the control by the piezo actuators and the corresponding control moment at the free end are shown in Fig. 12. Because only one amplitude for voltage is used, it is no problem to calculate the inverse in eqn (107), and the required voltage can be very easily calculated.

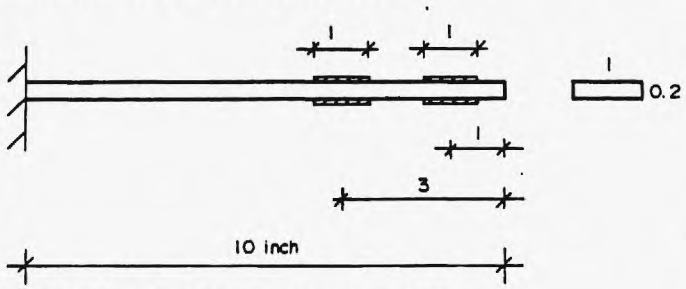

$E = 10^7$ psi, $t_b = 0.2$ in, $b = 1$ in, $s = 0.5$ in
$E = 10^7$ psi, $G = 2.5^* 10^5$ psi,
$t_c = 0.015$ in, $t_s = 0.003$ in, $d_{31} = 2.7^* 10^{-10}$

Fig. 11. The placement and data of piezo actuators.

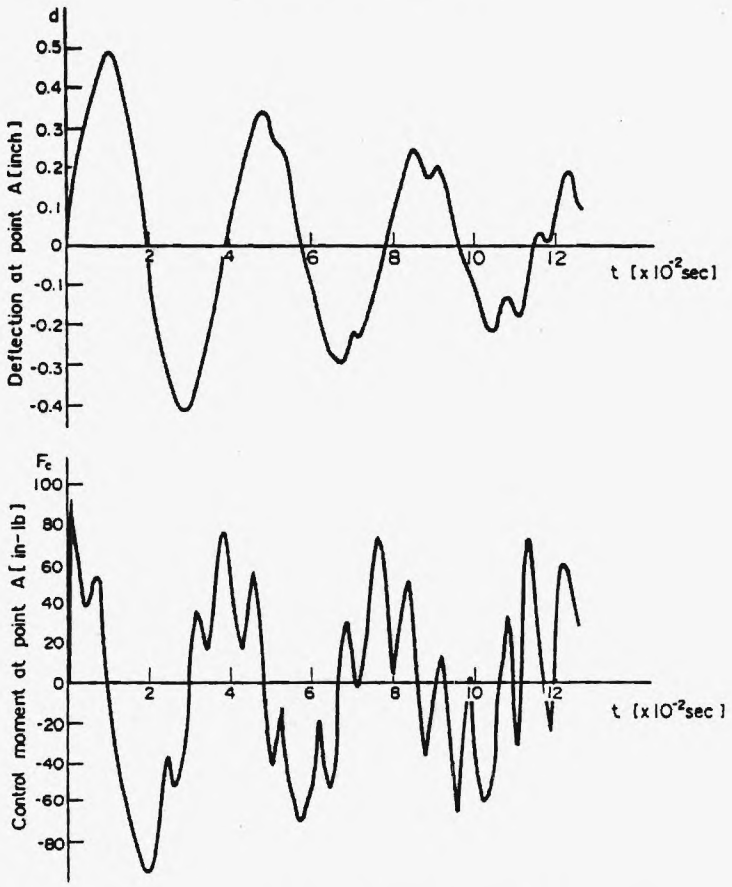

Fig. 12. Controlled response and control moment at point A by piezo actuators.

Example 4

The last example concerns a plane frame and its geometry and the placement of the piezo actuators are given in Fig. 13. The actuators are only placed on the columns in order to achieve an efficient control for the lateral displacements. An initial velocity as a disturbance is used again as shown in Fig. 13. The response and control force at point A corresponding to the optimal control are shown in Fig. 14. The response and control moment at point A by using piezo actuators are illustrated in Fig. 15. Here the voltage is applied in the same manner as in Example 3.

The last two examples clearly demonstrate that the vibrations are indeed damped out by the piezo actuators, or in other words, the piezo actuators can provide some control for vibration although they cannot provide the control forces as required by the optimal control law. The two examples also show that responses controlled by piezo actuators decay

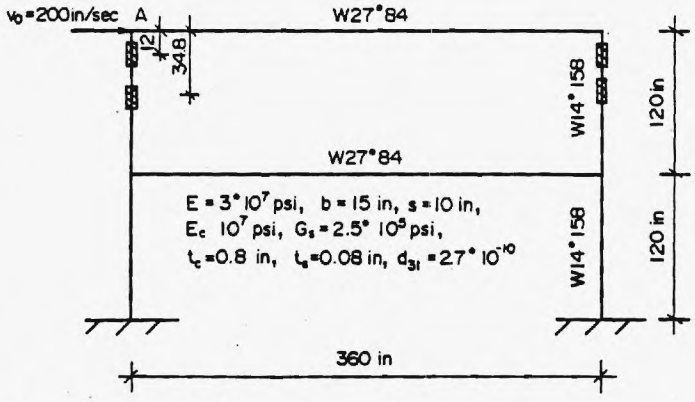

Fig. 13. Geometry of the structure and placement of piezo actuators.

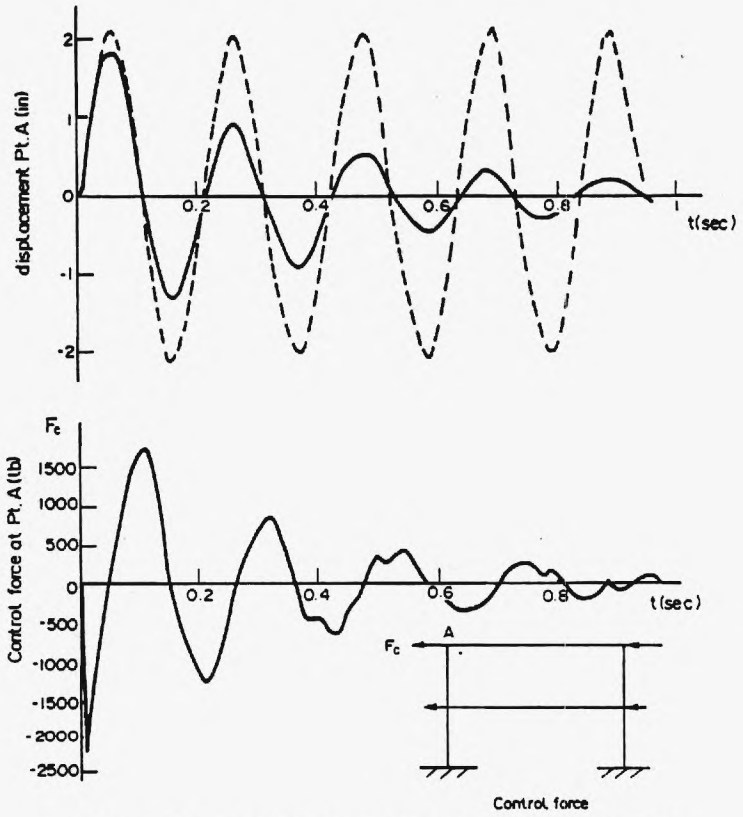

Fig. 14. Active control of vibration by linear optimal control.

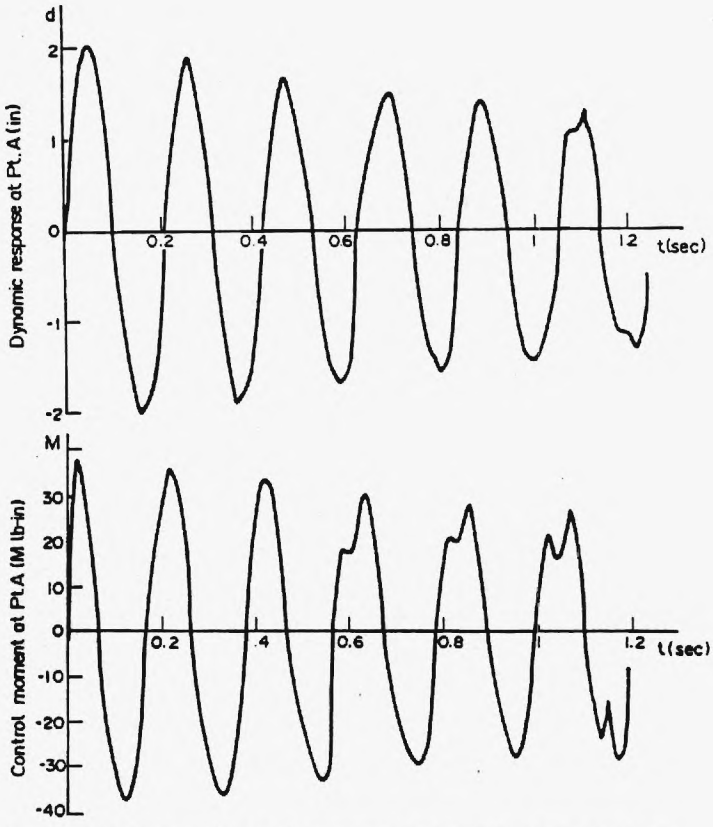

Fig. 15. Response and control moment at point A by piezo actuators.

quite smoothly, but the corresponding control forces are not smooth enough. This is natural because the displacements are minimized in the performance index eqn (8), however the real control force $\mathbf{F}_p$ is not directly determined by the optimal control law.

7. CONCLUSIONS

(1) The approximations involved in using the solution of Riccati equations of a linear system, for a nonlinear system, and using $\alpha(t)G(o)$ for $G(t)$, are indeed efficient schemes for the active control of nonlinear vibration.

(2) The shear stresses induced by the piezo actuators can be divided into two parts: the stress difference τ_2 which contributes to the linear momentum balance of the structural member, and the stress sum τ_1 which contributes to the angular momentum balance. Furthermore, τ_1 and τ_2 can be decomposed into two parts too, one part is related to the internal forces of the structural member and contributes to the element stiffness matrix; and the other is a function of the voltages applied to the actuators and provides the required control forces.

(3) The control moments induced by a pair of piezo actuators are "self-balanced". So actuators should have a suitable length and be placed in segments at appropriate locations to provide control forces efficiently.

(4) Since the piezo actuators cannot exactly provide the control forces required by the optimal control law, there are many possible ways to determine the voltages for the actuators to yield an approximate control effect. A scheme which provides equivalent control forces in the sense of "equal virtual work" is proposed here. However determining the voltage for each actuator is still an interesting question when each member of structure is bonded by many actuators and each actuator is excited with a different voltage.

Acknowledgements—This work was supported by AFOSR. The encouragement of Dr A. K. Amos is appreciated. The assistance of Ms Deanna Winkler is acknowledged with thanks.

REFERENCES

1. E. F. Crawley and J. de Luis, Use of piezo-ceramic as distributed actuators in large space structures. 26th Structures, Structural Dynamics and Materials Conference, Orlando, Florida (April 1985).
2. P. E. O'Donoghue and S. N. Atluri, Control of dynamic response of a continuum model of a large space structure. *Comput. Struct.* **23**, 199–211 (1986).
3. E. J. Davison and M. C. Maki, The numerical solution of the matrix Riccati differential equation, IEEE Trans. on Automatic Control, Vol. Ac-18, No. 1, pp. 71–73 (1973).
4. G. Shi and S. N. Atluri, Elasto-plastic large deformation analysis of space-frames: a plastic hinge and stress based explicit derivation of tangent stiffnesses. *Int. J. Numer. Meth. Engng* **26**, 589–615 (1988).
5. S. N. Atluri, Alternate stress and conjugate strain measures and mixed variational formulations involving rigid rotation, for computational analyses of finitely deformed solids with application to plates and shells—I. Theory. *Comput. Struct.* **18**, 93–106 (1983).
6. S. N. Atluri, On some new general complementary energy theorems for the rate problems in finite strain, classical elastoplasticity. *J. Struct. Mech.* 3(1), 61–92 (1980).
7. S. N. Remseth, Nonlinear static and dynamic analysis of framed structures. *Comput. Struct.* **10**, 879–897 (1979).
8. A. E. Bryson, Jr and Y.-C. Ho, *Applied Optimal Control.* Hemisphere Publishing Corporation, New York (1975).

Effects of a Piezo-Actuator on a Finitely Deformed Beam Subjected to General Loading

Seyoung Im*
Korea Advanced Institute of Science and Technology, Seoul, South Korea
and
S. N. Atluri†
Georgia Institute of Technology, Atlanta, Georgia 20332-0356

The deformation of a beam-column, the upper and lower surfaces of which are bonded in segments with piezo-ceramic liners, is studied for the purpose of obtaining appropriate expressions for the force transferred to the structural member by the piezo-actuator. This concept may be employed for the control of large dynamic deformations of a lattice-type flexible space-structure. The present model, which is based upon a static analysis, accounts for the effects of transverse shear and axial forces in addition to a bending moment on the beam in formulating the governing equilibrium equations. The present model provides more complete expressions for the force transmitted to the structural member than a model reported earlier in literature, in which the shear and axial forces are neglected.

Nomenclature

t_a = thickness of adhesive
t_p = thickness of piezo-actuator
t = thickness of beam column
L = Length of the segment of the beam column which is lined with a piezo-actuator (Fig. 1)
l = shortest distance from one end of the deformed beam-column segment to the other (Fig. 2)
G_a = shear modulus of adhesive
E_p = Young's modulus of piezo-electric material
E = Young's modulus of beam column
τ', τ'' = shear stresses on the upper and lower interfaces (Fig. 3)
N_p', N_p'' = Axial forces upon the cross sections of the upper and lower piezo-actuator (Fig. 3)
S_p', S_p'' = shear forces upon the cross section of the upper and lower piezo-actuator (Fig. 3)
σ', σ'' = normal stresses on the upper and lower interfaces (Fig. 3)
M_p', M_p'' = moment upon the cross section of the upper and lower piezo-actuator (Fig. 3)
N, S, M = axial force, shear force, and moment upon the cross section of the beam column (Fig. 3)
H, V = horizontal and vertical forces upon the cross section of the beam column (Fig. 2)
$\bar{x}$ = x/L
m = LM/EI
h = G_aL^2/tt_aE
h_p = $G_aL^2/t_at_pE_p$
α = $(6h + h_p)^{1/2}$
β = $(2h + h_p)^{1/2}$

Received Oct. 31, 1988; revision received April 24, 1989.

*Assistant Professor, Mechanical Engineering.
†Regents' Professor and Director, Center for the Advancement of Computational Mechanics. Member AIAA.

I. Introduction

THE control of large dynamic motions of space structures is a subject of considerable importance in connection with the deployment of large structures in outer space for various missions. The space structures are very flexible in most cases, and therefore necessitate the control of elastic deformations in addition to rigid motions for proper performance. Piezo-electric materials, which exhibit mechanical deformations when an electric field is applied, have recently received attention because of their potential application to the control of the flexible structure.[1,2] These materials, bonded to the surface of a structural element, transfer forces to the structural member according to the magnitude of exitation voltage applied to them. These forces exerted by the piezo-electric actuators may be employed to actively control the deformations of the structure. Recently Crawly and de Luis proposed a static model of the mechanical coupling of such "segmented piezo-actuators" bonded to a beam element with the dynamic deformation of the beam. No structural forces other than a pure bending moment upon the cross section of beam was considered in their model. Thus, the model in Ref. 2 does not account for the effects of the transverse shear and axial forces in the beam on the magnitudes of shear stresses τ' and τ'', which are exerted on the beam by the piezo-actuator. The purpose of the present work is to propose a refined model which takes into account the axial force as well as the transverse shear force in the structural member (beam column) in formulating the governing equations for the shear stresses transferred to the structural member by a piezo-electric actuator bonded to the structure.

These control forces can be included as external forces acting on the space-truss/frame, in the nonlinear dynamic analysis models developed by Kondoh and Atluri,[3,5] Tanka, et al.[4] and Shi and Atluri.[6,7] In these works, explicit expressions for the tangent stiffness matrices of each beam column in a three-dimensional lattice structure undergoing large deformations, incorporating exactly the effects of nonlinear bending-stretching coupling, have been derived. In as much as the control forces exerted by the piezo-actuators are functions of the applied voltages in each actuator segment, the "equivalent nodal force" would also be a function of the applied voltages.

It is the object of the control algorithm, then, to determine the appropriate voltages to be applied to the actuators in order to damp out the nonlinear dynamic deformations of the lattice-type structure.

In Sec. II, we first consider the exact equilibrium equation for a segment of a beam column to the upper and lower surfaces of which, piezo-electric liners are bonded. We neglect the inertia forces and use a static analysis in formulating the equilibrium equations of this beam-column segment. Under the assumption that the piezo-electric liner is very thin, we manipulate the integral form of equilibrium equations together with the compatability relations and the stress-strain relations in order to obtain a differential form of governing equations for the forces and moments acting on the cross section of the beam column and the shear stresses τ' and τ'' transferred to it by the piezo-actuator. These governing equations, together with appropriate end conditions, will determine the desired expression for the shear stresses transferred to the beam column in terms of the geometry of the beam column and the end forces and moments.

In Sec. III, we consider segmented piezo-actuators which are distributed along the length of the beam column to obtain the expression for the shear stresses τ' and τ''. The beam-column segment, formed by cutting at both ends of the piezo-actuator, is assumed to be sufficiently short so that its buckling load is very large compared with the axial force applied upon it. It is seen that the end conditions of Crawly and de Luis,[2] in which they prescribed two different bending strains at the ends of the beam segment, are not compatible with the moment equilibrium of their model. The result of the present work, as opposed to that of Crawly and de Luis,[2] accurately reflects the effect of the axial force as well as the transverse shear force upon the shear stresses τ' and τ'' transmitted by a segmented piezo-actuator. The influences of these forces are demonstrated through numerical examples, and this is followed by some discussion of the numerical results. A brief synopsis of the present work, which was completed in 1987, has been included in the survey article by Atluri and Iura.[8]

II. Governing Equations of a Beam Column Lined with Piezo-Actuators and Undergoing Large Deflections

A piezo-electric material, bonded to the upper and lower surfaces of a beam column, transfers forces to the structural element according to the magnitude of exitation voltage applied to it. Such actuator force fields may be used to control the dynamic deformations of a space frame, each member of which is modeled as a beam column. For such control applications, the expressions of the forces transferred to the structural element are required in terms of the excitation voltage. In this section, we examine the deformations of a beam column, lined with piezo-actuators on its upper and lower surfaces, to establish the governing equations for the forces and moments transferred to the beam column. The assumptions of small strains and linear elastic material behavior are made, but we do not place any restrictions upon the magnitude of deflections and rotations in formulating the governing equations. We restrict our attention in formulating the governing equations in this paper only to the case of planar motions of the beam column.

Consider a segment of the beam column of length L, along which the piezo-electric actuator is lined (see Figs. 1, 2). The thickness and length of the upper and lower piezo-actuators are assumed to be the same, and we take the width of the beam column and the actuator to be unified for convenience. The piezo-actuators are assumed to be bonded to the surfaces of the beam column by very thin layers of adhesive.

The kinematic assumptions in the present analysis are summarized as follows:

a) The length of the piezo-actuator segment L (see Fig. 1) is assumed to be much smaller than the total length of the beam column itself. Thus, along a single beam column there may be several piezo-actuators.

b) The total beam column may undergo large deformations with arbitrarily large rotations but small strains.

c) The segment of the beam column along which a piezo-actuator is bonded may also undergo large rotations from the undeformed configuration. If, in the deformed configuration, the ends of the beam-column segment (along which a piezo-actuator is bonded) are joined by a straight line, it is assumed that a) this straight line may be oriented at an arbitrary angle to the undeformed axes of the beam; however b) the local elastic rotations of the differential elements of the beam with respect to this straight line, in the deformed configuration are assumed to be small.

In the undeformed configuration, we employ a rectangular Cartesian coordinate system with origin at the left end and take the x-axis to be along the line of centroids and the z-axis to be downward. In the deformed configuration, a rigid rotation is imposed upon the deformed segment of the beam column so that the line connecting the two centroids at both ends is considered to be horizontal (see Fig. 2). Then we take the y_1-axis to be along that horizontal line and the y_3-axis to be downward.

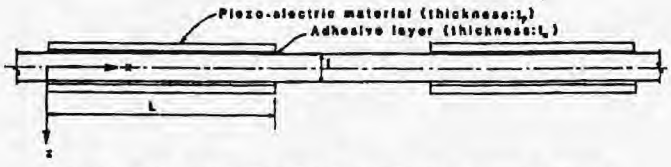

Fig. 1 Beam column bonded with a piezo-electric material.

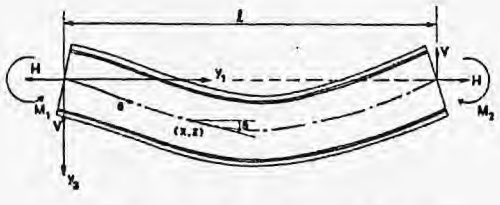

Fig. 2. Deformed beam-column segment.

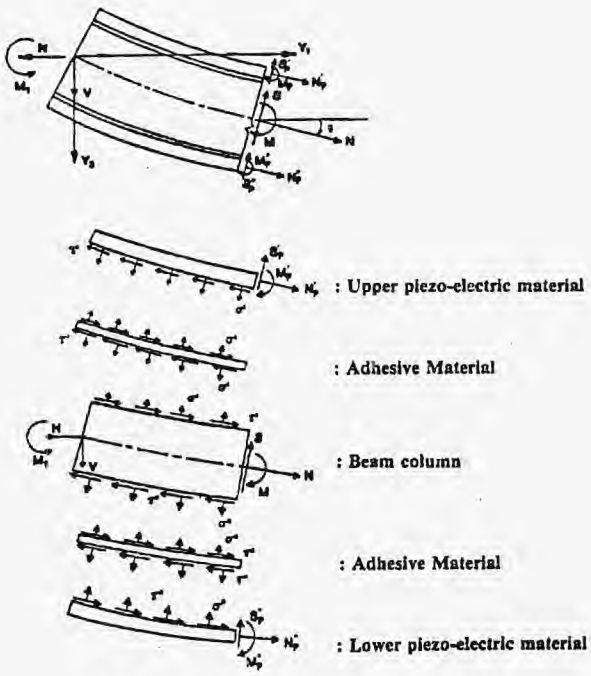

Fig. 3. Free-body diagram of each layer.

We denote by θ the angle between the tangent to the deformed centroidal axis and the y_1 axis. The coordinates of the deformed centroidal axis of the beam column in the y_1-y_3 coordinate frame are denoted by (X, Z). We then have

$$\frac{dX}{ds} = \frac{1}{(1+e)}\frac{dX}{dx} = \cos\theta, \qquad \frac{dZ}{ds} = \frac{1}{(1+e)}\frac{dZ}{dx} = \sin\theta \quad (1)$$

where s is a coordinate along the deformed centroidal axis and e is the extensional strain along the centroidal axis.

We first consider the balance equations for forces and moments for each slice of the beam column between $s = 0$ and an arbitrary value of s. After differentiation and appropriate manipulation of these balance equations, we can obtain the differential form of equilibrium equations. From Fig. 3, we have the following.

A. Upper Piezo-actuator

$$N_p' \cos\theta + S_p' \sin\theta - \int_0^s \tau' \cos\bar{\theta}\, d\bar{s} - \int_0^s \sigma' \sin\bar{\theta}\, d\bar{s} = 0 \quad (2)$$

$$-N_p' \sin\theta + S_p' \cos\theta + \int_0^s \tau' \sin\bar{\theta}\, d\bar{s} - \int_0^s \sigma' \cos\bar{\theta}\, d\bar{s} = 0 \quad (3)$$

$$M_p' - \int_0^s \tau' \cos\bar{\theta}\left(Z - \bar{Z} - \frac{t_p}{2}\cos\bar{\theta}\right)d\bar{s} + \int_0^s \tau' \sin\bar{\theta}\left(X - \bar{X} - \frac{t_p}{2}\sin\bar{\theta}\right)d\bar{s} - \int_0^s \sigma' \cos\bar{\theta}\left(X - \bar{X} - \frac{t_p}{2}\sin\bar{\theta}\right)d\bar{s} - \int_0^s \sigma' \sin\bar{\theta}\left(Z - \bar{Z} - \frac{t_p}{2}\cos\bar{\theta}\right)d\bar{s} \quad (4)$$

B. Lower Piezo-actuator

$$N_p^* \cos\theta + S_p^* \sin\theta + \int_0^s \tau'' \cos\bar{\theta}\, d\bar{s} + \int_0^s \sigma'' \sin\bar{\theta}\, d\bar{s} = 0 \quad (5)$$

$$-N_p^* \sin\theta + S_p^* \cos\theta - \int_0^s \tau'' \sin\bar{\theta}\, d\bar{s} + \int_0^s \sigma'' \cos\bar{\theta}\, d\bar{s} = 0 \quad (6)$$

$$M_p^* + \int_0^s \tau'' \cos\bar{\theta}\left(Z - \bar{Z} + \frac{t_p}{2}\cos\bar{\theta}\right)d\bar{s} - \int_0^s \tau'' \sin\bar{\theta}\left(X - \bar{X} - \frac{t_p}{2}\cos\bar{\theta}\right)d\bar{s} + \int_0^s \sigma'' \cos\bar{\theta}\left(X - \bar{X} - \frac{t_p}{2}\sin\bar{\theta}\right)d\bar{s} + \int_0^s \sigma'' \sin\bar{\theta}\left(Z - Z + \frac{t_p}{2}\cos\bar{\theta}\right)d\bar{s} = 0 \quad (7)$$

C. Beam column

$$\mathrm{N}\cos\theta - H + S\sin\theta + \int_0^s \tau' \cos\bar{\theta}\, d\bar{s} - \int_0^s \tau'' \cos\bar{\theta}\, d\bar{s} + \int_0^s \sigma' \sin\bar{\theta}\, d\bar{s} - \int_0^s \sigma'' \sin\bar{\theta}\, d\bar{s} = 0 \quad (8)$$

$$-N\sin\theta - V + S\cos\theta - \int_0^s \tau' \sin\bar{\theta}\, d\bar{s} + \int_0^s \tau'' \sin\bar{\theta}\, d\bar{s} + \int_0^s \sigma' \cos\bar{\theta}\, d\bar{s} - \int_0^s \sigma'' \cos\bar{\theta}\, d\bar{s} = 0 \quad (9)$$

and

$$M - M_1 - XS\cos\theta - ZS\sin\theta - ZN\cos\theta + XN\sin\theta + \int_0^s \tau' \cos\bar{\theta}\left(\frac{t}{2}\cos\bar{\theta} - \bar{Z}\right)d\bar{s} + \int_0^s \tau' \sin\bar{\theta}\left(\frac{t}{2}\sin\bar{\theta} + \bar{X}\right)d\bar{s} + \int_0^s \tau'' \cos\bar{\theta}\left(\frac{t}{2}\cos\bar{\theta} + \bar{Z}\right)d\bar{s} - \int_0^s \tau'' \sin\bar{\theta}\left(\bar{X} - \frac{X}{2}\sin\bar{\theta}\right)d\bar{s} - \int_0^s (\sigma' - \sigma'')\cos\bar{\theta}\bar{X}ds - \int_0^s (\sigma' - \sigma'')\sin\bar{\theta}\bar{Z}d\bar{s} = 0 \quad (10)$$

Here a superposed bar " − " indicates a dummy variable, for example, $\bar{\theta} = \theta(\bar{s})$.

Differentiating Eqs. (2) through (10) with respect to the length variable s, and using Eq. (1) while invoking the assumption that θ is small (which renders $\cos\theta \approx 1$ and $\sin\theta \approx \theta$), we have

$$\frac{dN_p'}{ds} - \tau' + S_p'\frac{d\theta}{ds} = 0, \qquad \frac{dS_p'}{ds} - \tau' - N_p'\frac{d\theta}{ds} = 0 \quad (11a)$$

$$\frac{dM_p'}{ds} - S_p'\frac{\tau' t_p}{2} = 0 \quad (11b)$$

$$\frac{dN_p^*}{ds} + \tau'' + S_p^*\frac{d\theta}{ds} = 0, \qquad \frac{dS_p^*}{ds} + \sigma'' - N_p^*\frac{d\theta}{ds} = 0 \quad (12a)$$

$$\frac{dM_p^*}{ds} - S_p^* + \frac{\tau'' t_p}{2} = 0 \quad (12b)$$

$$\frac{dN}{ds} + \left(\tau' - \tau''\right) + S\frac{d\theta}{ds} = 0, \qquad \frac{dS}{ds} + \left(\sigma' - \sigma''\right) - N\frac{d\theta}{ds} = 0, \quad (13a)$$

$$\frac{dM}{ds} - S + \frac{t}{2}\left(\tau' + \tau''\right) = 0 \quad (13b)$$

Since the extensional strain of the centroidal axis is assumed to be small, for our present purpose, we can replace (ds) by (dx) in the preceding equations.

From the overall equilibrium (See Fig. 2 and Fig. 3), we obtain the following relations

$$V = (M_2 - M_1)/l \quad (14a)$$

$$S = V\cos\theta + H\sin\theta - (S_p' + S_p^*) \quad (14b)$$

$$N = H\cos\theta - V\sin\theta - (N_p' + N_p^*) \quad (14c)$$

$$M = M_1 + HZ + VX + \frac{t + t_p}{2}(N_p^* - N_p') - M_p^* - M_p' \quad (14d)$$

The above equilibrium equations, except Eq. (14d), are completely compatible with the differential forms of equilibrium Eq. (11) through (13). Equation (14d) has a minor discrepancy with these equations when S_p' and S_p'' are not equal to each other. In most cases, the piezo-actuators are sufficiently thin $(t_p/t \ll 1)$ so that we can neglect the normal stress components (σ', σ''), the transverse shear forces (S_p', S_p''), and the moments (M_p', M_p''). Under these conditions the moment balance

equations, Eqs. (11b) and (12b) can be neglected, and we obtain the following simplified equations

$$\frac{dN_p'}{dx} - \tau' = 0, \qquad \frac{dN_p''}{ds} + \tau'' = 0 \tag{15}$$

$$\frac{dN}{dx} + \left(\tau' - \tau''\right) + S\frac{dQ}{dx} = 0, \tag{16a}$$

$$\frac{dS}{dx} - N\frac{d\theta}{dx} = 0 \tag{16b}$$

$$\frac{dM}{dx} - S + \frac{t}{2}\left(\tau' + \tau''\right) = 0 \tag{16c}$$

In the above five equations, we have eight unknowns N_p', N_p'', τ', τ'', N, S, M, θ, and, thus, three more equations are required to form a complete set of governing equations. These three equations are obtained from the stress-strain relations and the compatibility equation. The moment curvature and the axial force-extension relations are given by

$$M = \frac{E}{12}t^3\frac{d\theta}{dx} \tag{17}$$

and

$$N = E \cdot (\text{et}) \tag{18}$$

Assuming that the adhesive layers are perfectly bonded to the surfaces of the piezo-actuator and the beam column, we write the transferred shear stresses as

$$\tau' = G_a\gamma' = G_a(u_p' - u_f')/t_a$$
$$\tau'' = G_a\gamma'' = G_a(u_f'' - u_p'')/t_a \tag{19}$$

where u_p' and u_p'' are the tangential displacement of the piezo-actuator, u_f' and u_f'' are the tangential displacements at the upper and lower fibers of the beam-column. The compatibility relations at the upper and lower surfaces of the beam-column can be written as

$$\frac{du_f'}{dx} = e + \frac{t}{2}\frac{d\theta}{dx} \qquad \frac{du_f''}{dx} = e - \frac{t}{2}\frac{d\theta}{dx} \tag{20}$$

Denoting by V' and V'', the excitation voltages applied to the upper and lower piezo-actuators, we write the axial force-extension relations for the piezo-electric material as

$$N_p' = E_pt_p\left(\frac{du_p'}{dx} - \frac{cV'}{t_p}\right) = E_pt_p\left(\frac{du_p'}{dx} - \Lambda'\right) \tag{21}$$

and

$$N_p'' = E_pt_p\left(\frac{du_p''}{dx} - \frac{cV''}{t_p}\right) = E_pt_p\left(\frac{du_p''}{dx} - \Lambda''\right) \tag{22}$$

where c is the piezo-electric constant relating the voltages to the mechanical strains Λ' and Λ'' induced by the voltages.

Now manipulating the preceding Eqs. (17)–(22), we can eliminate the displacements u_p', u_p'', u_f', u_f'', and obtain the two equations

$$\frac{d\tau'}{dx} = \frac{G_a}{t_a}\left(\frac{N_p'}{E_pt_p} + \Lambda' - \frac{N}{Et} - \frac{6M}{Et^2}\right) \tag{23a}$$

$$\frac{d\tau''}{dx} = \frac{G_a}{t_a}\left(-\frac{N_p''}{E_pt_p} - \Lambda'' + \frac{N}{Et} - \frac{6M}{Et^2}\right) \tag{23b}$$

The complete set of eight governing equations are now given by Eqs. (15), (16), (17), and (23). As seen from these equations, the shear stresses τ' and τ'', transmitted by the piezo-actuators to the beam column, are dependent upon the force (N) and moment (M) as well as the mechanical strains Λ' and Λ'' induced by the excitation voltages.

The boundary conditions for the aforementioned governing equations are given as

$$N_p' = 0 \qquad N_p'' = 0, \qquad \text{at } x = 0, L \tag{24}$$

$$M = M_1 \qquad \text{at } x = 0, \qquad M = M_2 \qquad \text{at } x = L \tag{25}$$

$$\theta = \theta_1 \qquad \text{at } x = 0, \qquad \theta = \theta_2, \qquad \text{at } x = L \tag{26}$$

Thus, we have established the complete set of governing equations and the associated boundary conditions.

III. Forces Transmitted to the Beam Column by the Piezo-actuator

The shear stresses τ' and τ'', transmitted by the piezo-actuator to the beam column, depend upon the excitation voltages applied to the actuators as well as on the forces and moment acting upon the cross section of the beam column. These actuator forces are used to control the overall deformations of the structure. The axial force (N) and the bending moment (M) in each beam column are quantities that depend upon the external loading on the structure. In order to predict the response of the structure for a given set of excitation voltages, we need to express the shear stresses τ' and τ'' in terms of the strains Λ' and Λ'' induced by the applied voltages and the loading parameters, N and M.

For the purpose of control, it is desirable to have segments of actuators distributed along the structure because this enables us to vary the input exitation voltage along the length of the structure.[2] Moreover, most of the transfer of actuator shear forces to the beam column occurs near the ends of the actuator segment.[2] It is therefore more effective to have many short segments of actuators, rather than one long piezo-actuator. Thus, we assume that the length of the piezo-actuator (and thus the beam column segment which is lined with the piezo-actuator) is not long so that the following approximations can be made

$$\cos\theta \approx 1, \qquad \sin\theta \approx \theta, \qquad l \approx L \tag{27}$$

In order to obtain the governing equation for θ, we first manipulate Eqs. (15) and (23) to obtain

$$\frac{d^2(\tau' + \tau'')}{dx^2} - \frac{G_a}{t_at_pE_p}\left(\tau' + \tau''\right) = -\frac{12G_a}{Et^2t_a}\frac{dM}{dx} \tag{28}$$

Substituting Eq. (16c) into the above equation and using Eqs. (27) and (17), we obtain the following nondimensional equation.

$$\frac{d^4\theta}{d\bar{x}^4} - L^2\left(\frac{6G_a}{t_atE} + \frac{G_a}{t_at_pE_p} + \frac{12H}{Et^3}\right)\frac{d^2\theta}{d\bar{x}^2} + \frac{12HG_aL^4}{t_at_pE_pEt^3}\theta$$
$$= -\frac{12G_a(M_2 - M_1)L^3}{t_at_pt^3E_pE} \tag{29}$$

where $\bar{x} = x/L$ and higher order nonlinear terms such as $(d\theta/dx)^2$; $\theta\,(d^2\theta/dx^2)$; and $\theta\,(d\theta/dx^2)$ have been neglected consistent with the approximation of Eq. (27).

The term $12H/Et^3$ is negligible compared with the other two terms multiplied by $d^2\theta/dx^2$ because $|H/t| \ll G_at/t_a$, and $|H/t| \ll G_a(t/t_a)(t/t_p)\,(E/E_p)$. The last term on the left side of Eq. 29 represents the contribution of the horizontal axial force to the flexural deformation. It is negligible if θ is very small and if the axial force is small compared with the buckling load of the beam-column segment. This will be the case because the

beam-column segment is short; even when H is close to the critical load of the beam column itself, it will be much smaller than the critical load of the beam-column segment, which is very short compared with the whole beam column. With this approximation, we can thus obtain accurate solutions in most of the practically important cases.

Introducing the nondimensional variables

$$m = LM/EI = \frac{d\theta}{d\bar{x}}, \qquad h = \frac{G_a L^2}{t_a t E}, \qquad h_p = \frac{G_a L^2}{t_a t_p E_p} \tag{30}$$

The nondimensional parameter h characterizes the ratio of the shear rigidity of the adhesive material to the stiffness of beam; whereas the parameter h_p characterizes the ratio of the shear rigidity of the adhesive material to the stiffness of the piezo-actuator material. We rewrite the governing Eq. (29) with the aforementioned terms being neglected as

$$\frac{d^3m}{d\bar{x}^3} - \left(6h + h_p\right)\frac{dm}{d\bar{x}} = -h_p\left(m_2 - m_1\right) \tag{31}$$

We consider the boundary conditions for the above governing equations. Two conditions are provided by Eq. (25), which are rewritten using the nondimensional variables, as

$$m = m_1 \quad \text{at } \bar{x} = 0 \quad m = m_2 \quad \text{at } \bar{x} = 1 \tag{32}$$

Another condition is obtained from Eq. (24), which is written as

$$N_p' - N_p^* = 0 \qquad \text{at } \bar{x} = 0 \qquad \text{and } \bar{x} = 1 \tag{33a}$$

$$N_p' + N_p^* = 0 \qquad \text{at } \bar{x} = 0 \qquad \text{and } \bar{x} = 1 \tag{33b}$$

Adding Eqs. (23a and b) and using Eqs. (33) and (16b) and (16c), we obtain

$$\frac{d^2m}{d\bar{x}^2} - 6hm = -6h\xi\left(\Lambda' - \Lambda''\right) \quad \text{at } \bar{x} = 0 \quad \text{and } \bar{x} = 1 \tag{34}$$

where $\xi = L/t$. Consistent with the approximation taken in Eq. (31), we have neglected a term involving the horizontal axial force H. As will be shown later, only three of the four boundary conditions of Eqs. (32) and (34) are independent of one another. The general solution to Eq. (31) is given as

$$m = c_1 \cosh\left(\alpha\bar{x}\right) + c_2 \sinh\left(\alpha\bar{x}\right) + c_3 + \frac{h_p(m_2 - m_1)}{a_2}\bar{x}_1 \tag{35}$$

where $\alpha = (6h + h_p)^{1/2}$.

Applying the boundary conditions of Eqs. (32) and (34), we determine the constants c_1, c_2, c_3 as

$$c_1 = 6h\left[m_1 - \xi(\Lambda' - \Lambda'')\right]/\alpha^2 \tag{36a}$$

$$c_2 = 6h\left[(m_2 - m_1\cosh\alpha) - \xi(\Lambda' - \Lambda'')(1 - \cosh\alpha)\right]/\alpha^2 \sinh\alpha \tag{36b}$$

$$c_3 = \left[h_p m_1 + 6h\xi(\Lambda' - \Lambda'')\right]/\alpha^2 \tag{36c}$$

As a consequence of the assumption that the beam-column segment lined with a piezo-actuator is short, the flexural deformation is decoupled from the axial deformation, and the axial force does not appear in the above solution for the flexural deformation. The effect of the axial force upon the flexural deformation is not negligible when the magnitude of the axial force is of the order of the critical load of the beam-column segment. However, we exclude such an extreme case from the present consideration.

As solutions for the shear stresses transmitted to the beam-column, we obtain the expressions for p^+ and p^-, which are defined as

$$p+ = (\tau' + \tau'')/E_p, \qquad p- = (\tau' - \tau'')/E_p \tag{37}$$

With the aid of Eqs. (16b) and (35), we then obtain

$$p^+ = \eta\bar{G}\left[\frac{m_2 - m_1}{\alpha^2} - \frac{\left[m_1 - \xi(\Lambda' - \Lambda'')\right]\sinh\alpha\bar{x}}{\alpha} - \frac{\left[m_2 - m_1\cosh\alpha - \xi(\Lambda' - \Lambda'')(1 - \cosh\alpha)\right]\cosh\alpha\bar{x}}{\alpha\sinh\alpha}\right] \tag{38}$$

where $\eta = t/t_a$, $\bar{G} = G_a/E_p$. Noting that the last term in Eq. (16a) is negligible within the accuracy of the present model for a short beam-column segment. By combining this equation with Eqs. (15) and (23), we obtain the differential equation for $p-$, as

$$\frac{d^2p^-}{d\bar{x}^2} - \beta^2 p^- = 0 \tag{39}$$

where $\beta = (2h + h_p)^{1/2}$. The boundary conditions for this equation are obtained by combining Eq. (23) with Eq. (33b) (which has not been used yet) as

$$\frac{dp^-}{d\bar{x}} = \eta\xi\bar{G}\left(\Lambda' - \Lambda'' - \frac{2N}{Et}\right) \approx \eta\xi\bar{G}\left(\Lambda' - \Lambda'' - 2e_0\right)$$

$$\text{at } \bar{x} = 0 \text{ and } \bar{x} = 1 \tag{40}$$

where the extension of the beam-column segment at both ends is given by $e_0 = N/Et$ within the present approximation. The conditions of Eq. (40) are associated with the axial deformation of the beam-column segment, which is decoupled with the flexural deformations when the axial force is very small compared with the critical load of the beam-column segment. The axial strain may have the same order of magnitude as the strains induced in the piezo-actuator, Λ' and Λ'', but N is small compared with the critical load of the beam-column segment, which is assumed to be short.

The solution to Eq. (39) under the conditions of Eq. (40) is obtained as

$$p- = \frac{\xi\eta\bar{G}(\Lambda' + \Lambda'' - 2e_0)}{\beta}\left\{\frac{1 - \cosh\mathrm{B}}{\sinh\beta}\cosh\beta\bar{x} + \sinh\beta\bar{x}\right\} \tag{41}$$

In order to compare with the solution of Crawley and de Luis,[2] we assume $\Lambda' = -\Lambda''$ and the axial forces at both ends are zero. Then $p^- = 0$ and $\tau'/E_p = \tau''/E_p = p^+/2$. After accounting for the difference between the coordinate system in the present study and that in Crawley and de Luis,[2] we find that the expressions for the shear stress agree with each other only for the case of pure bending (also see Fig. 4). This is due to the fact that the effect of the transverse shear force has been taken into account in the present mode; whereas such an effect was neglected in Crawley and de Luis.[2] Different bending strains at the ends of the beam segments are apparently not allowed in their model, and, therefore, the boundary conditions in which they prescribed two different strain values at the ends of the segment are not compatible with the overall moment equilibrium of their model. To illustrate the shear transmitted by the piezo-actuators, we consider the following material and geometrical data and the boundary condition at $x = 0$.

$$\xi = \frac{L}{t} = 10, \qquad \eta = \frac{t}{t_a} = 40$$

$$\bar{G} = \frac{Ga}{E_p} = 1/63, \quad h = G_a L^2/t_a t E = 57, \quad h_p = \frac{G_a L^2}{t_a t_p E_p} = 423$$

$$\Lambda' = -\Lambda'' = 10^{-3}, \qquad m_1 = 10^{-3}$$

The above material data corresponds approximately to that of an aluminum beam column, epoxy adhesive, and ceramic piezo-actuator. We first plot the shear-stress distribution in Fig. 4 when there is no axial force in the beam column. We have a similar trend for other values of transverse shear force in the beam column, and, therefore, only one case with a nonzero transverse shear force is shown. When the transverse shear force in the beam is zero, i.e., $(VL/M_1) = 0$, the present results agree with those of Crawley and de Luis.[2] On the other hand, a nonzero transverse shear force (see the case of $VL/M_1 = 0.8$ in Fig. 4) in the beam contributes to a significant change in the distribution of the shear stress exerted by the actuator as shown in Fig. 4. Also, as seen from Fig. 4, the degree of localization in the transmitted shear stress at the two ends of the actuator segment may be very different depending on the magnitude of the transverse shear force in the beam. It should be noted, on the other hand, that the Crawley-de Luis[2] solution is not applicable in the case when $(VL/M_1) \neq 0$.

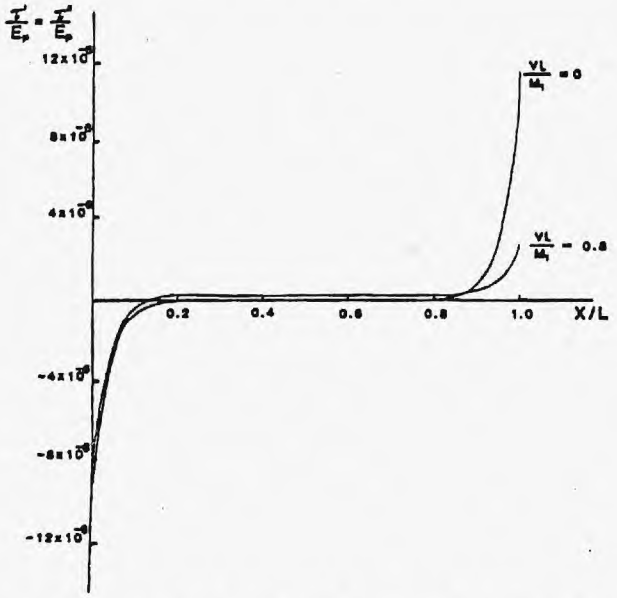

Fig. 4 Effect of shear force in the beam upon the distribution of shear stress exerted by the piezo-actuator when there is not axial force.

Because of the assumption that the piezo-actuator segment is short, the flexural deformation of the piezo-actuator segment is decoupled with its axial deformation, and the effect of the axial force in the beam upon its flexural deformation is negligible. However, the axial force in the beam has a significant effect on the shear stress transmitted by the piezo-actuator to the beam column because the axial force transferred to the piezo-actuator changes the response of the piezo-actuator by inducing deformation in it. For numerical illustration, the distribution of the shear stress exerted by the actuator is plotted in Fig. 5, for a case when there is no transverse shear force in the beam, but there exists a nonzero axial force in the beam. Due to the axial force in the beam, the shear stress exerted by the upper actuator has a totally different distribution as compared to the shear stress exerted by the lower actuator.

As another example, we consider both the transverse shear and axial forces in the beam to be nonzero and plot the distributions of the transmitted shear stresses in Fig. 6. Compared with the preceding two cases, the distribution of the transmitted shear stress may be more complex; however, we still observe the trend of stress localization around the ends of the segment.

Finally, it is recalled that in the present study only the rotation of one end of the beam-column segment relative to the other is assumed to be small because the beam-column segment is short. Further, we imposed an appropriate rigid rotation, which can be finite, to bring the deformed beam-column segment to the configuration in Fig. 2 so that the line connecting

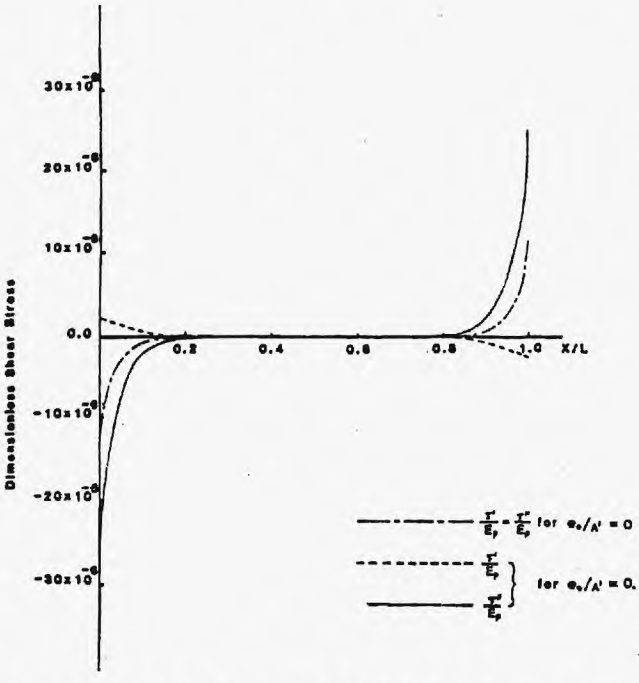

Fig. 5 Effect of axial force upon the shear stress distribution when there is not sheer force.

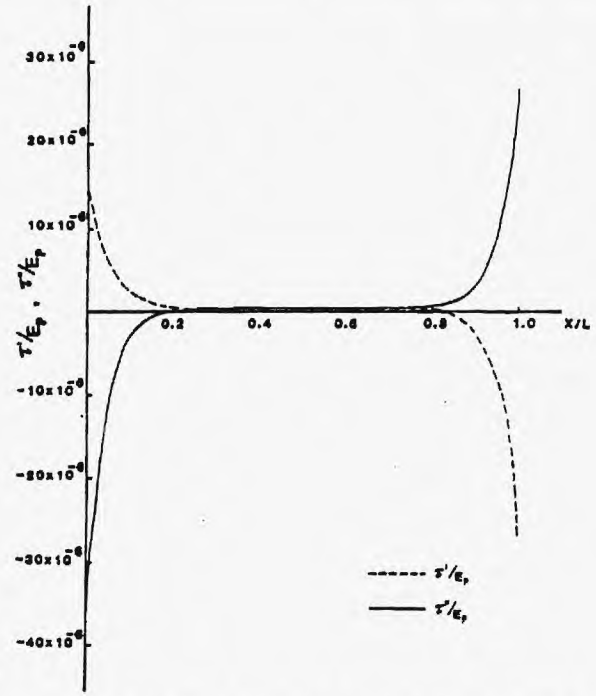

Fig. 6 Shear stress distribution for nonzero shear and axial forces $\frac{VL}{M_1} = 1 e_0/\Lambda' = 1.$

the two ends is horizontal. Therefore, the present result is applicable to the case of the slender flexible structures undergoing large deflections and rotations if it is combined with the special finite element method as given by Kondoh and Atluri.[3,5]

The use of the present analysis in implementing an active control of nonlinear dynamic response of three-dimensional, lattice-type structures, wherein each member carries axial loads, transverse shear loads, and moments, is discussed in detail in a recent report.[7]

Acknowledgments

This work was supported by the U. S. Air Force Office of Scientific Research. The authors thank Dr. A. K. Amos for his suggestions.

References

[1]Bailey, T. L. and Hubbard, J. E., "Distributed-Parameter Vibrator Control of a Cantilevered Beam Using a Distributed-Parameter Actuator," S M Thesis, Massachusetts Institute of Technology, 1984.

[2]Crawley, E. G. and de Luis, J., "Use of Piezo-Ceramics as Distributed Actuators in Large Space Structures," *AIAA Journal*, Vol. 25, No. 10, 1987, pp. 1373–1385.

[3]Kondoh, D. and Atluri, S. N., "A Simplified Finite Element Method for Large Deformation, Post-Buckling Analysis of Large Frame Structures, Using Explicitly Derived Tangent Stiffness Matrices," *International Journal of Numerical Methods in Engineering*, Vol. 23, 1986, pp. 69–90.

[4]Tanka, K., Kondoh, K., and Atluri, S. N., "Instability Analysis of Space Trusses Using Exact Tangent–Stiffness Matrices," *Finite Elements in Analysis and Design*, Vol. 1, 1985, pp. 291–311.

[5]Kondoh, K. and Atluri, S. N., "Large-Deformation Elasto-Plastic Analysis of Frames Under Non-Conservative Loading, Using Explicitly Derived Tangent Stiffness Based on Assumed Stresses," *Computational Mechanics*, Vol. 2, No. 1, 1987, pp. 1–25.

[6]Shi, G. and Atluri, S. N., "Elasto-Plastic Large Deformation Analysis of Space Frames: A Plastic-Hinge and Stress-Based Explicit Derivation of Tangent Stiffness," *International Journal of Numerical Methods in Engineering*, Vol. 26, No. 3, 1989, pp. 571–588.

[7]Shi, G. and Atluri, S. N., "Active Control of Nonlinear Dynamic Response of Space-Frames Using Piezo-Electric Actuators," *Computers & Structures* (to be published).

[8]Atluri, S. N. and Iura, M., "Nonlinearities in the Dynamics & Control of Space Structures: Some Issues for Computational Mechanics," *Large Space Structures: Dynamics & Control*, edited by S. N. Atluri and A. K. Amos, Editors, Springer-Verlag, New York, 1988, pp. 35–70.

#2

Space-Time Finite Element Analysis of Traveling Wave of Rod and Beam Structures

M. Iura, M. Borri and S. N. Atluri
Center for the Advancement of Computational Mechanics
Georgia Institute of Technology, Atlanta, GA 30332

1 Introduction

The prediction of transient response of structures, in the form of traveling waves, is very important for controlling the dynamic behavior of structures. It is well known that the standard semi-discrete form of the finite element method is not suitable for predicting the wave propagation, due to the inherent dispersion involved. In this paper, an application of space-time finite element method to the wave propagation problem is discussed.

On the basis of Hamilton's principle, Argyris and Scharpf (1969), Fried (1969) and Oden (1969) have developed the space-time finite element method. Hamilton's principle and the associated variational principle for dynamic problems state that the variation of displacement at the initial and final times should vanish (Washizu 1982). The abandonment of this assumption leads to Hamilton's Law of varying action (Bailey 1975, 1987, Leipholz 1987, Baruch and Riff 1982, and Simikins 1981). When an initial condition is given at the initial time, the displacement at the final time is, in general, unknown. This fact plays an important role in the direct application of Hamilton's Law of varying action.

When we solve an initial value problem of second-order ordinary differential equation, we have two initial conditions. In order to satisfy these initial conditions, the use of finite elements based on Hamilton's principle or Hamilton's Law of varying action requires, at least, a quadratic function for trial one. Borri et al. (1985), using a linear trial function, have succeeded in satisfying the initial conditions on the basis of a weak Hamilton's principle. The main idea is that the variation at the initial and final times

uate the momentum accurately. Hughes and Hulbert (1988) have used independent displacement and velocity interpolations on the basis of the discontinuous finite element method. In their approach, continuity of displacement and velocity between space-time slabs is enforced weakly. In this paper, a mixed finite element formulation is developed to improve the accuracy of velocity and strain. In the case of shock wave propagation problems, we have to note that the derivatives of displacement with respect to space and time may be discontinuous, while the displacement itself remain continuous. This fact motivates us to introduce the strain and the velocity as independent values which are discontinuous across elements, and which can be eliminated at element level. As a result, the size of matrix is the same as that derived from a displacement approach.

A simple example for an initial problem is used in Section 2 to show the difference between the present formulation and the existing ones. Even though the present trial functions are linear, exact solutions for displacement and momentum at the final time are obtained in this example. In Section 3, we discuss the weak form for continuous solids in which ther jump condition is enforced in a weak sense. Finite element implementation for rod and beam elements, based on a linear theory, is given in Section 4. Several numerical results for rod and beam structures are presented in Section 5. The problems for rods with discontinuous velocity and strain are solved. In these simple examples the present method predict accurately the discontinuities in the solutions without any significant wiggles that are typical, however, of the usual semidiscrete approaches.

2 Preliminaries

In order to show the basic features of the present method, we consider the following second-order ordinary differential equation:

$$\ddot{x} - F(t) = 0, \qquad (\dot{\ }) = \frac{\mathrm{d}(\ )}{\mathrm{d}t}, \qquad 0 \le t \le 1 \tag{1}$$

Depending on the problem, without loss of generality, two of the following conditions are specified so that a unique solution exists:

$$x(0) = \bar{x}_o, \quad \dot{x}(0) = \bar{v}_o, \quad x(1) = \bar{x}_1, \quad \dot{x}(1) = \bar{v}_1 \tag{2}$$

Some numerical examples will be helpful to understand the difference among the formulations cited before. While there are different choices for the trial and test functions, for sake of simplicity we will discuss here the Galerkin approach for the initial value problem. As trial functions, we consider the simplest piece-wise linear functions. When Hamilton's principle or Hamilton's Law of varying action are used, the two coefficients in the trial function are determined uniquely from the initial conditions without using Eq. (6) or Eq. (7). Simikins (1981)[1], therefore, has introduced a special technique in which the displacements at the initial and second steps are prescribed. Since the displacement at the second step is, in general, unknown, this technique seems to have some limitations. The use of Hamilton's principle or Hamilton's Law of varying action require, at least, a quadratic trial function (Argyris and Scharpf 1969).

In the present approach, based on Eq. (4), the linear trial function takes the form

$$x_h = x_o(1-t) + x_1 t \tag{8}$$

Substituting Eq. (8) into Eq. (4) yields

$$x_o - x_1 + \bar{v}_o + f_o = 0 \tag{9a}$$

$$-x_o + x_1 - \bar{v}_1 + f_1 = 0 \tag{9b}$$

where

$$f_o = \int_0^1 (1-t)F\,\mathrm{d}t, \qquad f_1 = \int_0^1 tF\,\mathrm{d}t \tag{10}$$

As pointed out by Borri, et al. (1985), Eq. (9) gives the exact values for momenta at $t = 0$ and $t = 1$; moreover adding Eq. (9a) and (9b) we have the exact relation: $\bar{v}_1 - \bar{v}_o = \int_0^1 F\,\mathrm{d}t$. We will show here that Eq. (9) gives also the exact values for displacements at $t = 0$ and $t = 1$. In fact, from the definition of f_o and f_1, substituting the relation $F = \ddot{x}$ into Eq. (10) and integrating by part twice lead to

$$\begin{aligned} f_o &= -\dot{x}|_{t=0} + x|_{t=1} - x|_{t=0} \\ f_1 &= \dot{x}|_{t=1} - x|_{t=1} + x|_{t=0} \end{aligned} \tag{11}$$

In the case of initial conditions we have

$$x_o = x|_{t=0} \qquad \bar{v}_o = \dot{x}|_{t=0}, \tag{12}$$

[1]There are some errors in the exact solutions of Table 3 (Simikins 1981). The corrections have been given by Borri, et al. (1985).

problems are expressed as (Eringen, 1980)

$$
\begin{array}{lll}
\frac{\partial A}{\partial \mathbf{F}} - \mathbf{P} = 0: & \text{Constitutive Equation} & \text{in } \Omega \\
\nabla(\boldsymbol{X} + \boldsymbol{U}) - \mathbf{F} = 0: & \text{Strain} - \text{Displacement Relation} & \text{in } \Omega \\
\text{DIV}\,\mathbf{P} - \rho_o \dot{\boldsymbol{V}} + \rho_o \boldsymbol{B} = 0: & \text{LMB Condition} & \text{in } \Omega - \Sigma \\
\boldsymbol{V} - \dot{\boldsymbol{U}} = 0: & \text{Definition of Velocity} & \text{in } \Omega \\
\mathbf{P} \cdot \boldsymbol{N} - \bar{\boldsymbol{T}} = 0: & \text{Mechanical Boundary Condition} & \text{at } S_\sigma \\
\boldsymbol{U} - \bar{\boldsymbol{U}} = 0: & \text{Geometrical Boundary Condition} & \text{at } S_u \\
\rho \boldsymbol{V} - \bar{\boldsymbol{M}} = 0: & \text{Initial Condition} & \text{at } t = t_o \\
\|\rho_o \boldsymbol{V}\| V_N + \|\mathbf{P}\| \cdot \boldsymbol{N} = 0: & \text{Jump Condition} & \text{at } \Sigma
\end{array}
\tag{17}
$$

where A is a strain energy function, $\mathbf{F}$ a deformation gradient tensor, $\mathbf{P}$ a first Piola-Kirchhoff stress tensor, $\boldsymbol{X}$ a position vector in the reference configuration, $\boldsymbol{U}$ a displacement vector, $\boldsymbol{V}$ a velocity, ρ_o a density in the reference configuration and $\boldsymbol{B}$ a body force; $\boldsymbol{N}$ denotes the unit normal vector at the boundary, V_N the normal velocity at the discontinuous surface Σ, Ω the domain of solids, and S_σ and S_u denote the boundaries on which mechanical and geometrical boundary conditions, respectively, are prescribed. The notation $\| \cdot \|$ denotes the jump at the discontinous surface: $\| \cdot \| = (\cdot)^+ - (\cdot)^-$.

For later convenience, the boundary and initial conditions are changed into the form

$$
\mathbf{P} \cdot \boldsymbol{N} - \bar{\boldsymbol{T}} = 0; \quad \boldsymbol{U} - \bar{\boldsymbol{U}} = 0 \quad \text{at } S = S_\sigma + S_u \tag{18a}
$$

$$
\rho_o \boldsymbol{V} - \bar{\boldsymbol{M}} = 0 \qquad \text{at } t = t_i \text{ and } t = t_f \tag{18b}
$$

Note that some of $\bar{\boldsymbol{T}}$, $\bar{\boldsymbol{U}}$, and $\bar{\boldsymbol{M}}$ are prescribed and the rest of them are unknown.

The weak form for this problem is written as

$$
\begin{aligned}
&\int_{t_i}^{t_f} \Big[\int \Big\{ \Big(\frac{\partial A}{\partial \mathbf{F}} - \mathbf{P} \Big) : \hat{\mathbf{F}} + \hat{\mathbf{P}} : \langle \nabla(\boldsymbol{X} + \boldsymbol{U}) - \mathbf{F} \rangle \\
&- (\text{DIV}\,\mathbf{P} - \rho_o \dot{\boldsymbol{V}} + \rho_o \boldsymbol{B}) \cdot \hat{\boldsymbol{U}} + (\boldsymbol{V} - \dot{\boldsymbol{U}}) \cdot \rho_o \hat{\boldsymbol{V}} \Big\} \mathrm{d}\Omega \\
&+ \int \{ (\mathbf{P} \cdot \boldsymbol{N} - \bar{\boldsymbol{T}}) \cdot \hat{\boldsymbol{U}} + (\bar{\boldsymbol{U}} - \boldsymbol{U}) \cdot \hat{\mathbf{p}} \cdot \boldsymbol{N} \} \mathrm{d}S \\
&- \int \{ \|\rho_o \boldsymbol{V}\| V_N + \|\mathbf{P}\| \cdot \mathbf{N} \} \cdot \hat{\boldsymbol{U}} \, \mathrm{d}\Sigma \Big] \mathrm{d}t \\
&- \int (\rho_o \boldsymbol{V} - \bar{\boldsymbol{M}}) \cdot \hat{\boldsymbol{U}} \, \mathrm{d}S \, \Big|_{t=t_i}^{t=t_f} = 0
\end{aligned}
\tag{19}
$$

v and the strain ε appear only in the domain integral. Therefore these values may be chosen to be discontinuous across elements. This choice is advantageous for an analysis of shock wave problems. It is easily shown from Eq. (22) that the velocity and the strain are expressed in terms of the displacements since the matrices associated with v and ε are positive definite. As a result, the size of matrix in this formulation is the same as that derived from the standard displacement based formulation.

3.3 Mixed Weak Form of Transverse Wave Propagation in a Timoshenko Beam

Consider a straight and uniform Timoshenko beam consisting of homogeneous and isotropic materials. A rectangular domain is introduced for a space-time finite element. Let G be the shearing modulus, μ a shear correction factor, I the moment of inertia, w the transverse displacement, α the cross-section rotation, f a distributed load, and g a distributed moment. We assume that the geometrical boundary conditions are satisfied a priori. Then, using Eq. (21), we have the weak form for beam elements

$$\begin{aligned}
&\int_{t_i}^{t_f}[\int\{GA\mu\gamma\hat{w}_{,x} - \rho Av\dot{\hat{w}} - f\hat{w} + EI\kappa\hat{\alpha}_{,x} + GA\mu\gamma\hat{\alpha} \\
&-\rho IS\dot{\hat{\alpha}} - g\hat{\alpha} - \rho A(\dot{w} - v)\hat{v} - \rho I(\dot{\alpha} - S)\hat{S} \\
&+EI(\alpha_{,x} - \kappa)\hat{\kappa} + GA\mu\{(\alpha + w_{,x}) - \gamma\}\hat{\gamma}\}dx \\
&-[\bar{m}\hat{\alpha} + \bar{Q}\hat{w}]_{x_i}^{x_f}]dt + \int_{x_i}^{x_f}(\bar{M}\hat{w} + \hat{R}\hat{\alpha})dx\,|_{t_i}^{t_f} = 0
\end{aligned} \tag{23}$$

where

$$\begin{aligned}
\kappa = \alpha_{,x}, \quad \gamma = \alpha + w_{,x}, \quad v = \dot{w}, \quad S = \dot{\alpha} \\
\bar{m} = EI\kappa, \quad \bar{Q} = GA\mu\gamma, \quad \bar{M} = \rho Av, \quad \bar{R} = \rho IS
\end{aligned} \tag{24}$$

These relations, expressed by Eq. (24), are enforced weakly in Eq. (23).

4 Space-Time Finite Elements

4.1 Rod Elements

We discuss, at first, an implementation of space-time finite element method for rods. From the requirement of the order of trial and test functions, the

$$v_o = (-u_1 + u_2 - u_3 + u_4)/(2\Delta t) \tag{29}$$

It should be noted that the strain ε_o and the velocity ν_o are the average values over the element so that they might be interpreted as the values at the center point.

Let us explain the procedure for solving Eq. (28) by using a simple example. We consider a cantilevered rod subjected to an axial load at the tip, as shown in Fig. 2. The number of elements in the space direction is assumed to be n, while one element is used in the time direction (Fig. 3). The initial condition for $\bar{P}$ is introduced in Eq. (28) to calculate $\bar{P}_1, \bar{P}_3, \ldots, \bar{P}_{2n+1}$. The boundary condition for $\bar{N}$ is substituted in Eq. (28) for calculating $\bar{N}_1$ and $\bar{N}_2$. As trial functions for unknown values $\bar{P}$ and $\bar{N}$, a delta function is employed. It follows, then, from the boundary condition that $\bar{P}_{2(n+1)} = 0$. After the strains and the velocities are eliminated, the number of equation is $2(n+1)$. The unknown values are n displacements, n velocity and two tractions. Figure 3 indicates the unknown values (denoted by $\Longrightarrow$) and the prescribed ones (denoted by $\longrightarrow$) in this example. It should be noted that the components associated with the interelement forces $\bar{N}$ are equal to zero since there exist no external load at the interelement nodes. After prescribing the initial and boundary conditions, we can write the global equation in the form

$$\begin{bmatrix} A_{11} & A_{12} \\ A_{21} & A_{22} \end{bmatrix} \begin{Bmatrix} X \\ \bar{X} \end{Bmatrix} = \begin{bmatrix} B_{11} & B_{12} \\ B_{21} & B_{22} \end{bmatrix} \begin{Bmatrix} Y \\ \bar{Y} \end{Bmatrix} \tag{30}$$

where $\bar{\ }$ denotes the prescribed values. In order to solve Eq. (30), we must rewrite it in the form

$$\begin{bmatrix} A_{11} & -B_{11} \\ A_{21} & -B_{21} \end{bmatrix} \begin{Bmatrix} X \\ Y \end{Bmatrix} = \begin{bmatrix} -A_{12} & B_{12} \\ -A_{22} & B_{22} \end{bmatrix} \begin{Bmatrix} \bar{X} \\ \bar{Y} \end{Bmatrix} \tag{31}$$

The standard solver is now available for solving Eq. (31).

4.2 Beam Elements

The simplest trial functions for beam elements are expressed as

$$\begin{aligned} w &= w_1(1-\bar{x})(1-\bar{t}) + w_2(1-\bar{x})\bar{t} + w_3\bar{x}(1-\bar{t}) + w_4\bar{x}\bar{t} \\ \alpha &= \alpha_1(1-\bar{x})(1-\bar{t}) + \alpha_2(1-\bar{x})\bar{t} + \alpha_3\bar{x}(1-\bar{t}) + \alpha_4\bar{x}\bar{t} \\ S &= S_o, \quad v = v_o, \quad \kappa = \kappa_o, \quad \gamma = \gamma_o \end{aligned} \tag{32}$$

numerical results would be obtained for the stresses which are calculated from the obtained displacements. The present results, shown in Fig. 7, however, indicate an excellent agreement with exact solutions even for the discontinuous stresses.

These two examples show that the present finite elements are potentially able to predict the mean value of jump at the discontinuous points. The wiggles, appeared in the existing shock capturing finite element method [17], do not exist in the present numerical results.

5.2 Transverse Wave Propagation of Beams

We have confirmed in [11] that no shear locking has been observed in static problems by using the present elements. To investigate the effects of the ratio $\Delta x/\Delta t$ on the responses of beams, we analyze a cantilevered beam subjected to the step load at the tip, as shown in Fig. 8. The dynamic responses of the beam are shown in Fig. 9. It is shown that the ratio $\Delta x/\Delta t$ does not affect substantially the present numerical results unlike the case of longitudinal wave propagation (Riff and Baruch, 1984 and Bajer, 1986). The numerical results in the case of $\Delta t = 0.3$, however, show the small vibration in the range of $x > 8$. This fact shows that, by contrast with the semi-discrete method, the use of small time increment does not always give a good numerical result in the case of the space-time finite element method.

For a comparison of numerical results obtained from the present method and the semi-discrete method, we consider a fixed-fixed beam subjected to the concentrated load at the midpoint of beam, as shown in Fig. 10. Since the structure is symmetric, the half of structure is solved by using the same conditions as those given by Fig. 8. The results for the semi-discrete method are obtained through the use of Newmark's β method ($\beta = 1/4, \gamma = 1/2$). Figure 11 compares the numerical results. It is shown that the wavefront is captured by the present method and also by the semi-discrete method with lumped mass. The use of consistent mass, however, produces the wiggles especially around the wavefront. Figure 10 indicates also that the numerical results obtained from the semi-discrete method with lumped mass are vibrating along $2 < x < 4$. The CPU time of the present method is about $1.2 \sim 1.3$ time more than that of the semi-discrete method. In spite of this deficiency, the worthwhile aspects of using the present space-time finite element method are its accuracy and simple implementation.

7. Cella, A., Lucchesi, M., and Pasquinelli, G. (1980): Space-Time Elements for the Shock Wave Propagation Problem, *Int. J. Num. Meth. Eng. 15*, pp. 1475-1488.

8. Eringen, A. C. (1980): *Mechanics of Continua*, 2nd Ed., R. Z. Krieger Publishers, New York.

9. Fried, I. (1969): Finite Element Analysis of Time-dependent Phenomena, *AIAA Journal 7*, pp. 1170-1173.

10. Hughes, T. J. R. and Hulbert, G. H. (1988): Space-time Finite Element Methods for Elastodynamics: Formulations and Error Estimates, *Comp. Meth. Appl. Mech. Eng. 56*, pp. 339-363.

11. Iura, M., Borri, M., and Atluri, S. N. (1988): Analysis of Traveling Wave Responses of Structures, *Proc. Int. Conf. on Comp. Eng. Sci.*,, 10-14 April 1988, Atlanta, GA.

12. Lasaint, P. and Raviart, P. A. (1974): On a Finite Element Method for Solving the Neutron Transport Equations, *Proc. Symp. Math. Aspects of Finite Elements in Partial Differential Equations, Madison, WI (Academic Press, New York).*

13. Leipholz, H. H. E. (1987): On Some Development in Direct Methods of the Calculus of Variations, *Appl. Mech. Rev. 40*, No. 10, pp. 1379-1392.

14. Oden, J. T. (1969): A General Theory of Finite Elements II. Applications, *Int. J. Num. Methods Eng. 1*, pp. 247-259.

15. Peters, D. A. and Izadpanah, A. P. (1988): hp-version Finite Elements for the Space-time Domain, *Computational Mechanics 3*, pp. 73-88.

16. Reed, W. H. and Hill, T. R. (1973): Triangular Mesh Methods for the Neutron Transport Equation, LA-UR-73-479, Los Alamos Scientific Laboratory.

17. Riff, R. and Baruch, M. (1984): Wave Propagation Problems by Time-Space Finite Elements, *Israel J. of Technology, 22*, pp. 45-57.

18. Rizzi, A., and Engquist, B. (1987): Selected Topics in the Theory and Practice of Computational Fluid Dynamics, *J. Comp. Physics, 72*, pp. 1-69.

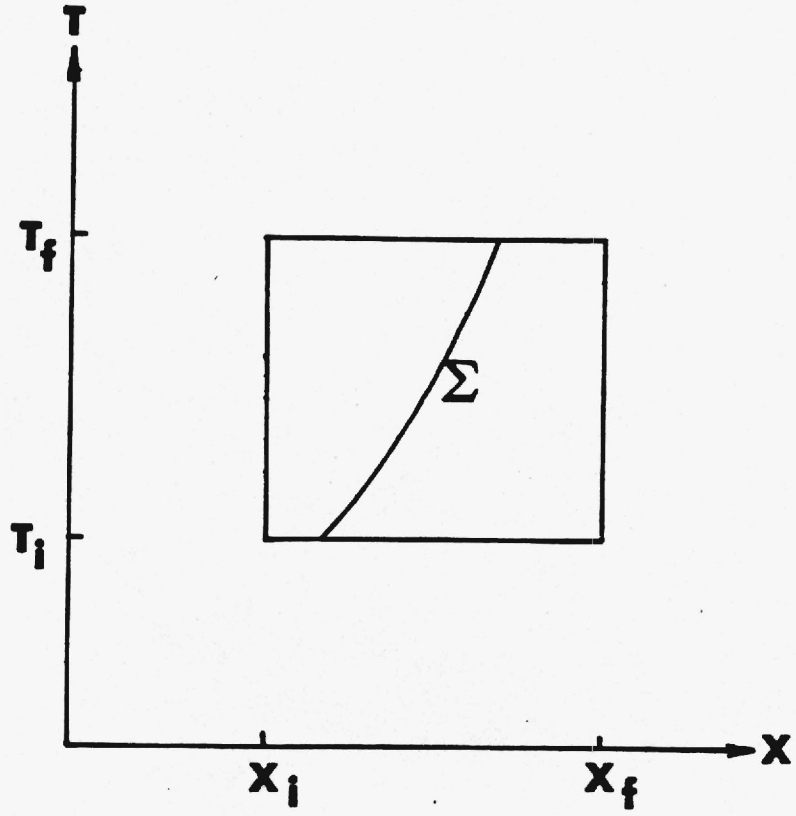
T
T_f
T_i
Σ
X
X_i
X_f

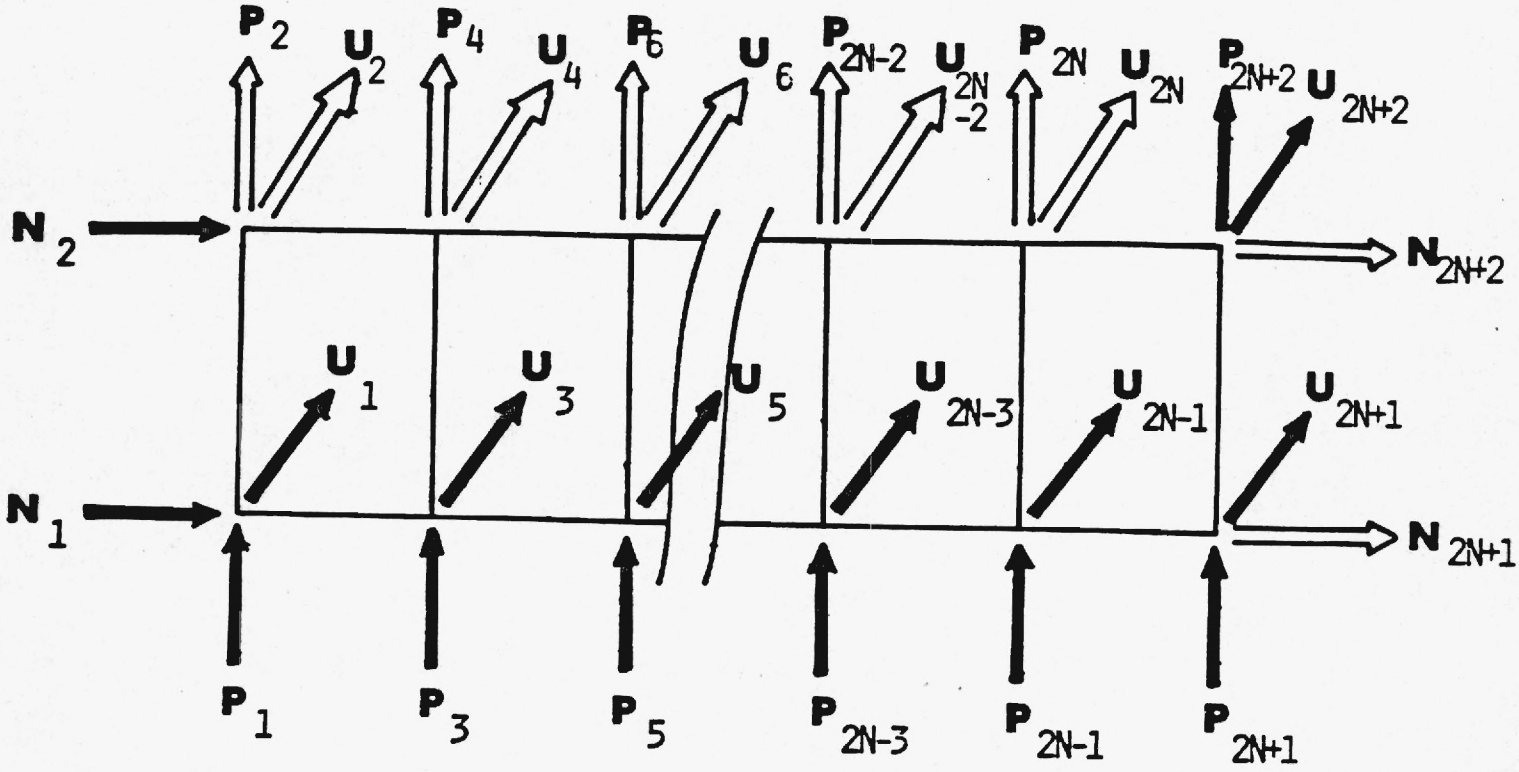
P 2
U 2
P 4
U 4
P 6
U 6
P 2N-2
U 2N -2
P 2N
U 2N
P 2N+2
U 2N+2
N 2
N 2N+2
U 1
U 3
U 5
U 2N-3
U 2N-1
U 2N+1
N 1
N 2N+1
P 1
P 3
P 5
P 2N-3
P 2N-1
P 2N+1

Fig. 3

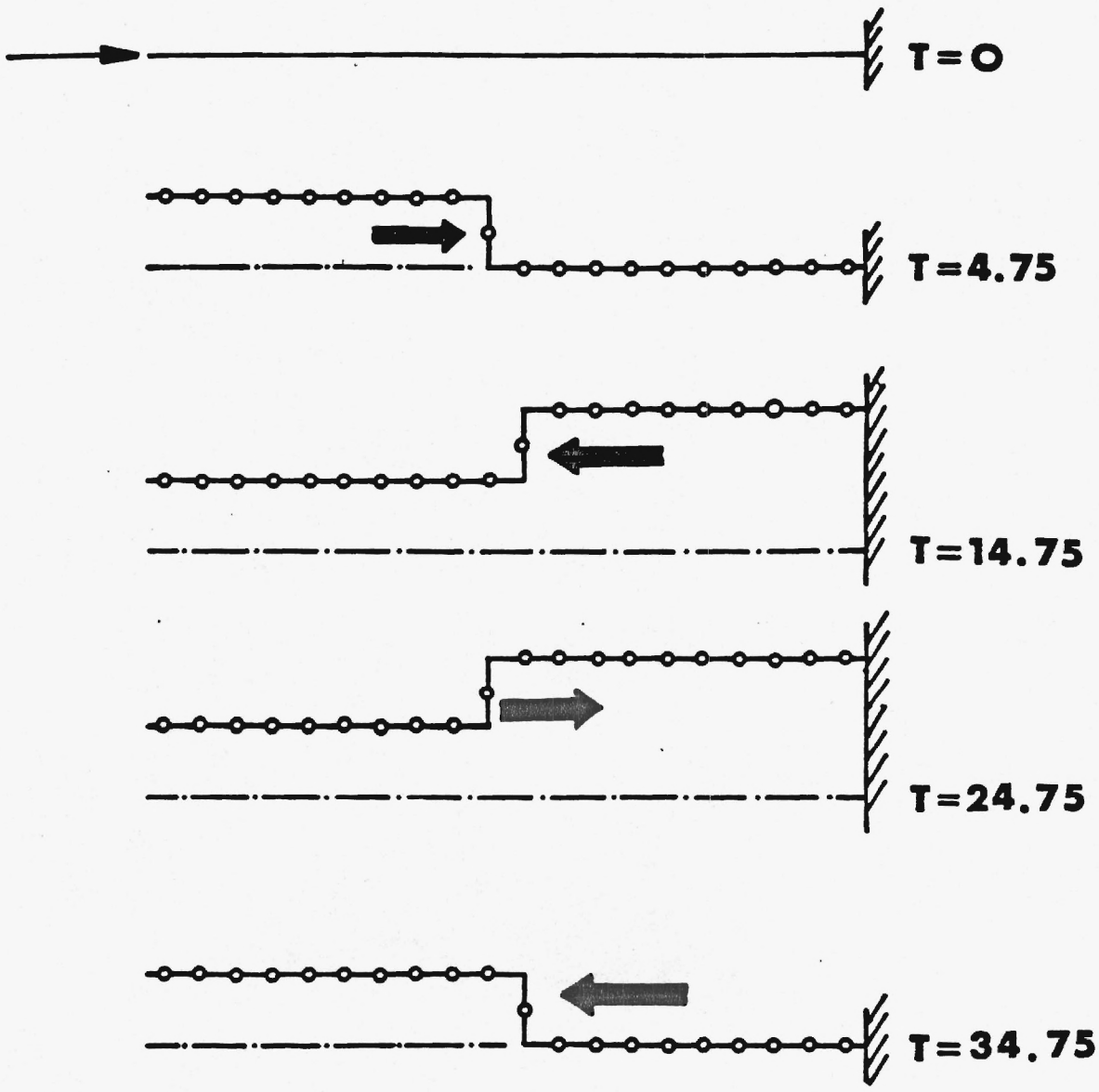

Fig. 5

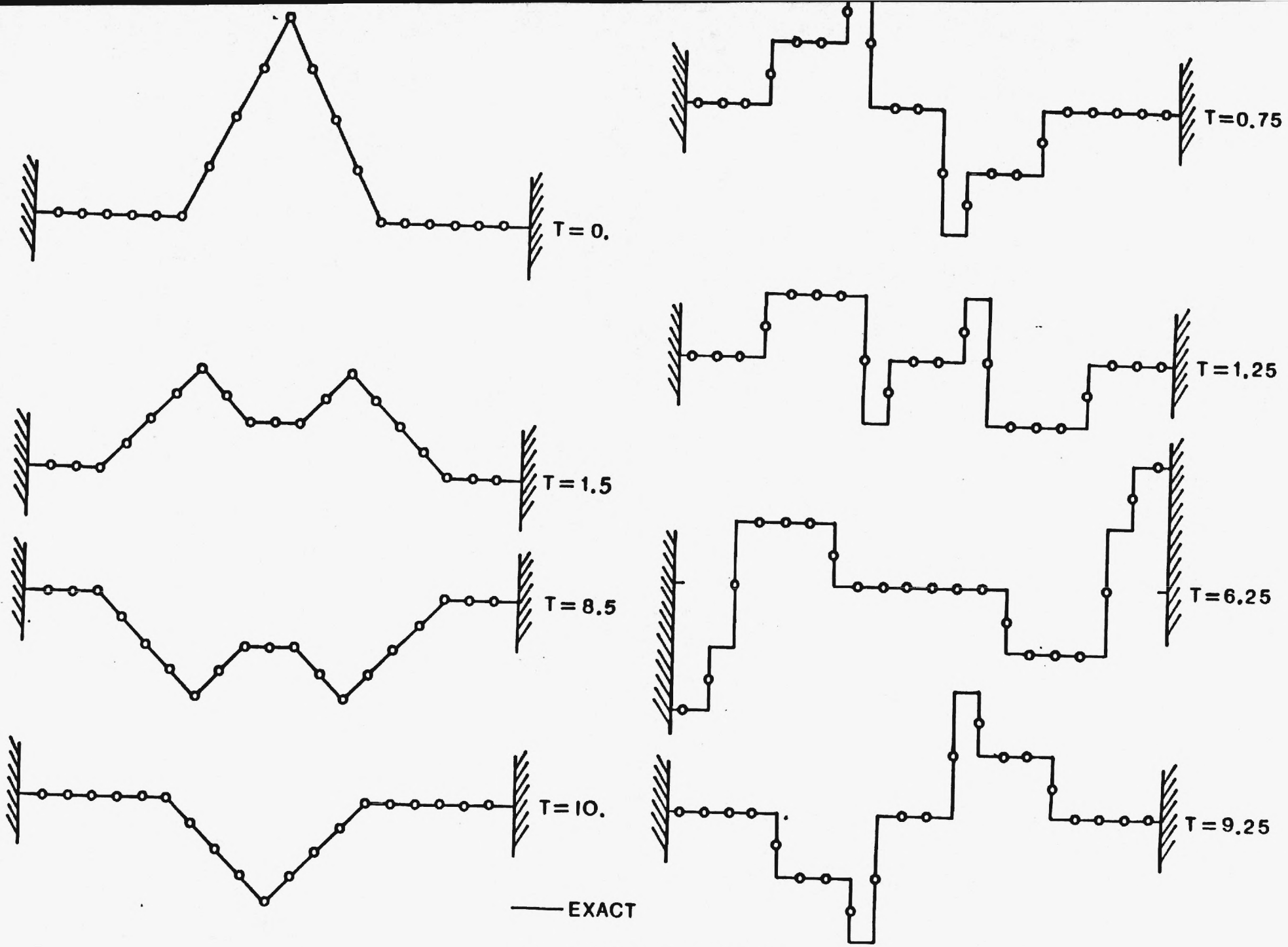

Propagation of Displacement

Propagation of Stress

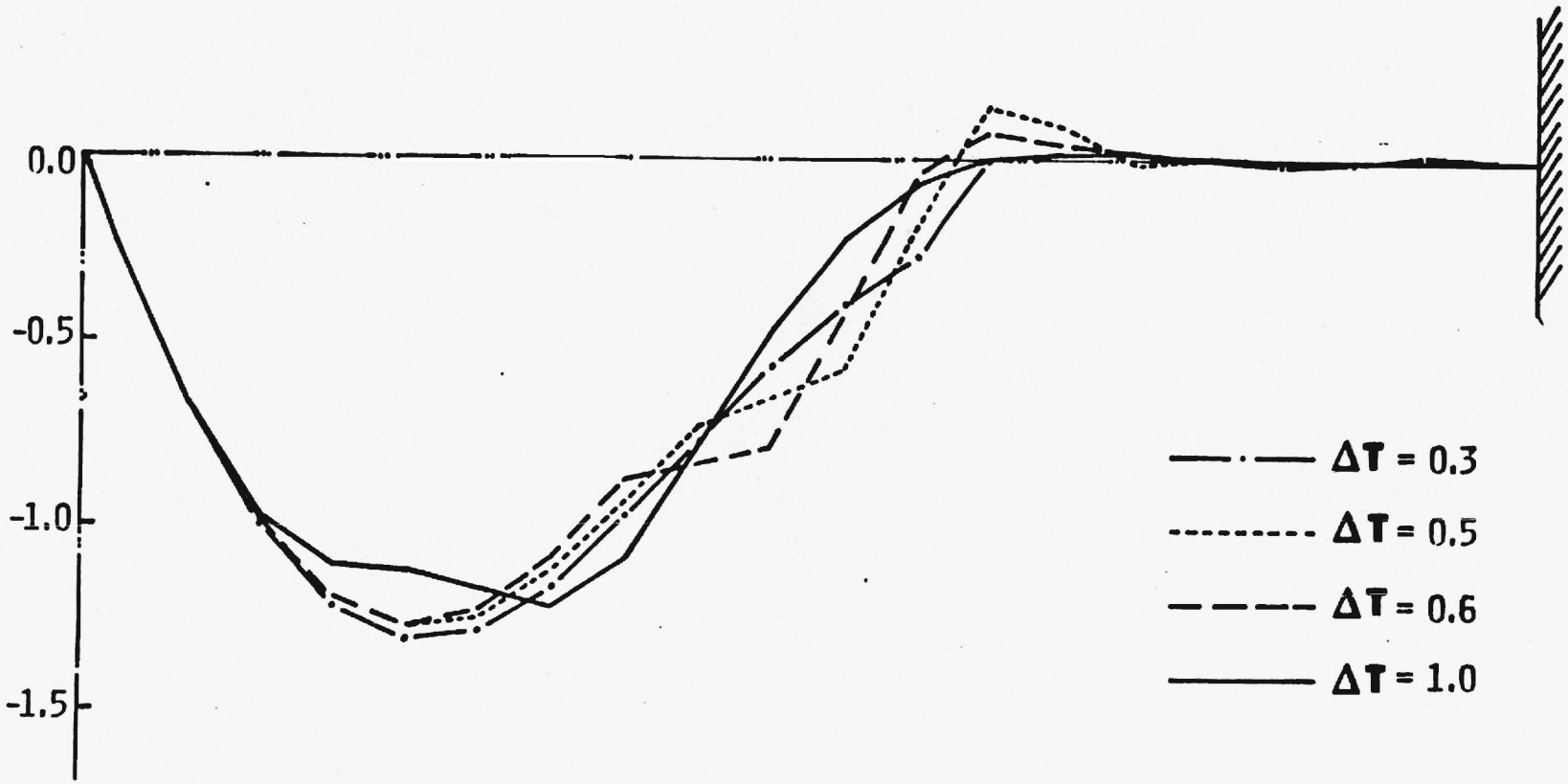
0.0
-0.5
-1.0
-1.5
ΔT = 0.3
ΔT = 0.5
ΔT = 0.6
ΔT = 1.0

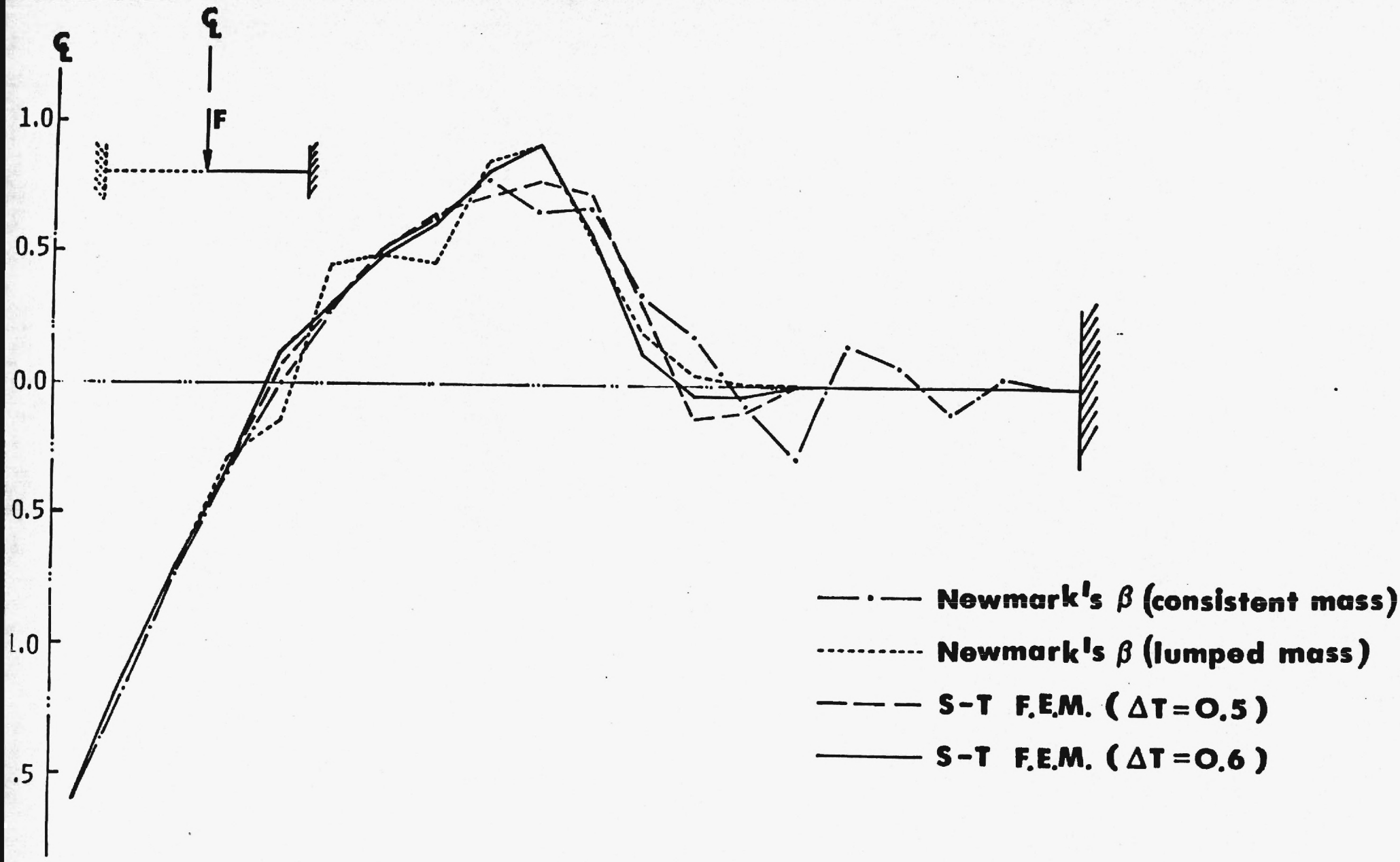
℄
℄
F
1.0
0.5
0.0
0.5
1.0
.5
Newmark's β (consistent mass)
Newmark's β (lumped mass)
S-T F.E.M. (ΔT=0.5)
S-T F.E.M. (ΔT=0.6)

Variational Approaches for Dynamics and Time - Finite - Elements: Numerical Studies

M. Borri [1] F. Mello and S. N. Atluri
Center for Computational Mechanics
Georgia Institute of Technology, Atlanta, GA. 30332-0356, USA.

Abstract

This paper presents general variational formulations for dynamical problems, which are easily implemented numerically. The development presents the relationship between the very general weak formulation arising from linear and angular momentum balance considerations, and well known variational principles. Two and three field mixed forms are developed from the general weak form. The variational principles governing large rotational motions are linearized and implemented in a time finite element framework, with appropriate expressions for the relevant "tangent" operators being derived. In order to demonstrate the validity of the various formulations, the special case of free rigid body motion is considered. The primal formulation is shown to have unstable numerical behavior, while the mixed formulation exhibits physically stable behavior. The formulations presented in this paper form the basis for continuing investigations into constrained dynamical systems and multi-rigid-body systems, which will be reported in subsequent papers.

1 Introduction

Recently there has been a renewed interest in the study of multibody dynamics and its application to a wide variety of engineering problems. Research is very active in the areas of vehicle dynamics (e.g. Agrawal and Shabana (1986), Kim and Shabana (1984) and McCullough and Haug (1986)), spacecraft dynamics and attitude control (e.g. Hughes (1986), Kane and Levinson (1980) and Kane, Likins and Levinson (1983)), large space stuctures (e.g. Meirovitch and Quinn (1987), Modi and Ibrahim (1987), Shi (1988) and Amos and Atluri (1987)) and machine dynamics (e.g. Haug, Wu and Yang (1986), Haug and McCullough (1986) and Khulief and Shabana (1986)). One common interest in all these fields is the automated development and solution of the equations of motion. As discussed in Wittenburg (1985), symbolic manipulation programs are being applied to this task. The nonlinear equations of motion, in explicit form are quite complex due to the expression for absolute acceleration. These complexities are avoided if a weak form of the dynamical equations is employed. The priciple of virtual work, or Hamilton's principle is one such weak form (e.g. Borri, et al (1985)). There has been a great deal of discussion in the literature concerning the equivalence of different formulations (e.g. Desloge (1987) and

[1] Permanent affiliation - Politecnico di Milano, Dept. of Aerospace Engineering, Milano, Italy

Banerjee (1987)) and the use of Hamilton's principle as a starting point for the numerical solution of dynamics problems (e.g. Bailey (1975) and Baruch and Riff (1982)). Some of this discussion involves the conditions under which Hamilton's principle may be stated as the stationarity condition of a scalar functional (e.g. Smith and Smith (1974)). Due to the unsymmetric character of initial value problems, the governing equations are not expressible as such a condition. This fact in no way diminishes the usefulness of variational approaches for initial value problems. In fact, drawing on the mature literature concerning variational methods in the mechanics of deformable bodies, very general weak forms can be developed for dynamical systems, the most general being analogous to a Hu - Washizu type formulation. The principle of virtual work is obtainable from the general weak form by satisfying displacement compatibility (the definition of velocity) and the displacement boundary conditions *a priori*. A Hamiltonian or complementary energy approach is obtained by satisfying the constitutive relations between momentum and velocity *a priori*.

In order to establish the methodology and assess the performance of the different weak formulations, the dynamics of a single rigid body is considered. Even in its simplicity, from a theoretical viewpoint, the dynamics of a single rigid body, with its high degree of nonlinearity, constitutes a significant test for numerical procedures.

When dealing with rigid body dynamics, the choice of coordinates for finite rotation greatly influences the character of the resulting numerical procedures. As a result, many representations of finite rotation have been adopted in the literature, including: Euler angles, quaternions, Rodigues' parameters, and various rotation vectors (e.g. Geradin and Cardona (1989), Iura and Atluri (1989) and Pietraszkiewicz and Badur (1983)). It is difficult to establish one set of coordinates as the best choice for all problems. For the purposes of the present development, the finite rotation vector is chosen as the Lagrangian coordinate for the angular motion. This coordinate choice preserves the vectorial character of the formulae and results in a minimum number of independent variables. However, since any three parameter representation of rotation cannot be both global and non-singular, an incremental approach is required to obtain a solution. The incremental displacement and rotation are measured from a reference configuration, which in general depends on time. For different choices of the reference configuration, different incremental approaches are obtained.

Moreover, depending on the form chosen for the virtual rotations (or test functions for rotational variables), different but equivalent forms of the linear and angular momentum balance conditions arise. One choice leads to a symmetric variational statement, while the other does not.

In this paper, several formulations for the dynamics of a rigid body are discussed, with the objective of developing a system of equations which may be directly implemented in the framework of time finite elements. This approach leads to a set of nonlinear equations, which are solved using Newton's method. The merits of this strategy, as related to the dynamics of constrained rigid body systems, will be discussed in a subsequent paper.

The simple example of a free tumbling rigid body is presented, and the accuracy and numerical stability of the various approaches are discussed.

The remainder of this paper is organized as follows; Section 2 deals with geometry and coordinate selection; Section 3 with the formulation of the variational principles; Section 4, the linearization of the resulting equations; Section 5, with finite element approximation;

Section 6 deals with linearized stability analysis; Section 7, with numerical stability; and Section 8, with numerical results and Section 9 lists the cited references. Appendix A contains relevant formulas for rotation while the full expressions for the tangent matrices and residual vectors are presented in Appendix B.

Throughout this paper, lowercase bold roman characters will indicate a vector, while uppercase bold roman characters will indicate a tensor.

2 Coordinate Selection and Kinematics of a Rigid Body

In order to avoid redundant degrees of freedom, the finite rotation vector is chosen as rotational coordinates, which is a three parameter representation. Finite rotation vectors have also been used by Iura and Atluri (1989), Kane, Likins and Levinson (1983) and others. As pointed out by Struelpnagel (1964), a three parameter representation can not be both global and nonsingular. In order to overcome this, many investigators have adopted Euler parameters to uniquely describe finite rotations. However, this results in five degrees of freedom being associated with the rotation, if the constraint of unit magnitude for the Euler parameters is included through a Lagrange multiplier. Geradin and Cardona (1989) use the conformal rotation vector as a set of three rotation parameters in a global algorithm, which avoids the singularities as the rotation crosses integer multiples of π. Similarly, it is shown in Appendix A, that the finite rotation vector may be used in a similar approach if the rotation is rescaled as it passes through multiples of 2π. However, for this numerical implementation, an incremental approach is adopted, to avoid the singularities.

In order to specify the configuration of a rigid body, two orthogonal frames of reference are defined, namely $(\mathrm{O},\ \boldsymbol{e}_i)$ and $(\mathrm{O}',\ \boldsymbol{e}'_i)$. The first frame is fixed, while the second is embedded in the body. At any given time t the embedded frame is completely identified by the position vector $\boldsymbol{x}(t) = \mathrm{O}' - \mathrm{O}$, and by the rotation vector $\boldsymbol{r}(t)$, such that $\boldsymbol{e}'_i = \boldsymbol{R}(\boldsymbol{r}) \cdot \boldsymbol{e}_i$, where $\boldsymbol{R}(\boldsymbol{r})$ denotes the rotation tensor corresponding to $\boldsymbol{r}$. The spin of the embedded frame relative to the fixed frame may be expressed by the angular velocity vector $\boldsymbol{\omega}$, such that $\boldsymbol{\omega} \times \boldsymbol{I} = \dot{\boldsymbol{R}} \cdot \boldsymbol{R}^t$ which depends linearly on $\dot{\boldsymbol{r}}$.

One common representation of the rotation vector is $\boldsymbol{r} = \phi \boldsymbol{e}$, where ϕ is the magnitude of rotation and $\boldsymbol{e}$ is the rotation axis, i.e. $\boldsymbol{R} \cdot \boldsymbol{e} = \boldsymbol{e}$. In terms of $\boldsymbol{r}$, the rotation tensor $\boldsymbol{R}$ may be conveniently expressed through the exponential map, which is the form that will be adopted here, as;

$$\boldsymbol{R}(\boldsymbol{r}) = \exp(\boldsymbol{r}(t) \times \boldsymbol{I}) \tag{2.1}$$

In Appendix A, several common rotation vectors are shown to be easily expressed in this form.

The reference configuration and incremental coordinates are now defined in the following way. Assuming that the state of the rigid body is known at some initial time t_1, the reference trajectory for the body can be defined. This reference configuration can be specified in many ways. For example, the reference could be a time varying configuration, compatible with some specified external forces and moment resultant, or the configuration corresponding to a constant linear and angular velocity, or simply held constant. Since Newton's method is used to iteratively solve the nonlinear system of equations, the reference configuration must be a reasonably good estimate of the true configuration, in order for the method to converge

rapidly. At any point in time, the reference configuration is described by a position vector $x_o(t)$, and a rotation $R_o(t)$. The true solution will in general follow another path, with any point on the true configuration being described by a position vector $x(t)$ and the rotation $R(t)$. Since the reference configuration is prescribed, the true path may also be represented by the position vector $x_\star(t)$, given by $x_\star(t) = x(t) - x_o(t)$, and the rotation $R_\star(t)$, where $R_\star(t) = R(t) \cdot R_o^t(t)$. The incremental coordinates are now defined as $(x_\star, r_\star)$, where $r_\star$ is the rotation vector such that $R_\star = R(r_\star) = \exp(r_\star \times I)$.

Henceforth, all quantities associated with the reference configuration will be designated by a subscript o and a subscript $\star$ will indicate a quantity associated with the current configuration, but referred to the reference configuration. For example, v_o and ω_o represent the linear and angular velocity of the reference configuration, and are defined as:

$$v_o = \dot{x}_o \tag{2.2}$$

$$\omega_o \times I = \dot{R}_o \cdot R_o^t \tag{2.3}$$

Similarly, $v_\star$ and $\omega_\star$ are the linear and angular velocity of the true configuration with respect to the reference, and are defined in a consistent way:

$$v_\star = \dot{x}_\star \tag{2.4}$$

$$\omega_\star \times I = \dot{R}_\star \cdot R_\star^t \tag{2.5}$$

The linear and angular velocities of the true configuration with respect to the fixed frame can now be expressed as:

$$v = v_\star + v_o \tag{2.6}$$

$$\omega = \omega_\star + R_\star \cdot \omega_o \tag{2.7}$$

Clearly, the angular velocity of the incremental motion, $\omega_\star$ is not the same as the relative velocity from the reference configuration, $\omega - \omega_o$. Having defined the angular velocity $\omega_\star$, and the rotation coordinates $r_\star$, the relationship between $\omega_\star$ and $r_\star$ may be established. Substitution of $R_\star = \exp(r_\star \times I)$ into the definition for $\omega_\star$ yields:

$$\omega_\star = \Gamma(r_\star) \cdot \dot{r}_\star \tag{2.8}$$

where:

$$\Gamma(r_\star) = I + \frac{1 - \cos\phi_\star}{\phi_\star^2}(r_\star \times I) + \frac{1}{\phi_\star^2}\left(1 - \frac{\sin\phi_\star}{\phi_\star}\right)(r_\star \times I)^2 \tag{2.9}$$

and $\phi_\star$ is the magnitude of $r_\star$. The details of this derivation are presented in Appendix A. Clearly, the operator Γ also relates ω and ω_o to $\dot{r}$ and $\dot{r}_o$ respectively, i.e. $\omega = \Gamma(r) \cdot \dot{r}$ and $\omega_o = \Gamma(r_o) \cdot \dot{r}_o$.

This section concludes with some comments on the virtual displacement and rotation fields. The virtual displacement of the point O′ can be defined as the variation of its

position $\delta x(t) = \delta x_\star(t)$. However, the virtual change in the orientation of the rigid body can be represented either by the variation of the rotation vector $\delta r_\star$ or by means of a virtual rotation $\theta_{\star\delta}$ defined by:

$$\theta_{\star\delta} \times I = \delta R_\star \cdot R_\star^t \tag{2.10}$$

Due to the orthogonality of the rotation tensor, $\delta R_\star \cdot R_\star^t$ is skew symmetric and its correspondence with $\theta_{\star\delta} \times I$ is always possible. Substituting for $R_\star$ in terms of R and R_o, demonstrates that the total virtual rotation θ_δ coincides with the incremental virtual rotation $\theta_{\star\delta}$, since the reference configuration is prescribed, i.e. $\delta R_o \equiv 0$. In fact:

$$\begin{aligned} \theta_{\star\delta} \times I &= \delta R_\star \cdot R_\star^t = \delta(R \cdot R_o^t) \cdot (R \cdot R_o^t)^t \\ &= \delta R \cdot R^t = \theta_\delta \times I \end{aligned} \tag{2.11}$$

The notation of subscript δ indicates that θ_δ and $\theta_{\star\delta}$ are not variations of true coordinates. Consequently θ are commonly refered to as quasicoordinates. Since θ does not exist, solution procedures cannot involve quasicoordinates exclusively.

Moreover, the virtual rotation θ_δ is related to the virtual change of the incremental rotation vector through the same relationship that exists between the angular velocity ω and $\dot{r}$ i.e.:

$$\theta_\delta = \Gamma(r_\star) \cdot \delta r_\star \tag{2.12}$$

3 Weak Forms for Rigid Body Dynamics

Let b and m denote respectively the external force and moment resultants and let l and h be the linear and angular momenta, respectively, of the rigid body, with respect to the point O′. Since the body is rigid, the velocity of any point $\tilde{v}$, may be expressed in terms of the linear velocity of the point O′ and the angular velocity of the body about point O′. Thus,

$$\tilde{v} = v - y \times \omega \tag{3.1}$$

where y is the position of the point relative to O′. The linear and angular momenta with respect to O′ are, respectively,

$$\begin{aligned} l &= \int_B \rho \tilde{v} \mathrm{d}B \\ &= v \int_B \rho \mathrm{d}B - \omega \int_B \rho y \times I \mathrm{d}B \end{aligned} \tag{3.2}$$

$$h = v \int_B \rho y \times I \mathrm{d}B - \omega \int_B \rho y \times y \times I \mathrm{d}B$$

The dynamical equations, viz., the equations of linear and angular momentum balance, are written as:

$$\begin{aligned} \dot{\boldsymbol{l}} &= \boldsymbol{b} \\ \dot{\boldsymbol{h}} + \boldsymbol{v} \times \boldsymbol{l} &= \boldsymbol{m} \end{aligned} \tag{3.3}$$

The weak forms of these equations along with the weak forms of the natural boundary conditions can be written as:

$$\int_{t_1}^{t_2} [\boldsymbol{d}_1(t) \cdot (\dot{\boldsymbol{l}} - \boldsymbol{b}) + \boldsymbol{d}_2(t) \cdot (\dot{\boldsymbol{h}} + \boldsymbol{v} \times \boldsymbol{l} - \boldsymbol{m})] \mathrm{d}t = 0 \tag{3.4}$$

$$\boldsymbol{b}_1(t_k) \cdot (\boldsymbol{l}_{bk} - \boldsymbol{l}(t_k)) = 0, \qquad \boldsymbol{b}_2(t_k) \cdot (\boldsymbol{h}_{bk} - \boldsymbol{h}(t_k)) = 0 \quad (k = 1, 2) \tag{3.5}$$

where $\boldsymbol{d}_1, \boldsymbol{d}_2, \boldsymbol{b}_1, \boldsymbol{b}_2$ are respectively, domain and boundary test functions. The subscript b indicates boundary quantities.

Since the expressions for $\boldsymbol{l}$ and $\boldsymbol{h}$ contain $\boldsymbol{v}$ and $\boldsymbol{\omega}$, which in turn depend on the time derivatives of the generalized coordinates $\boldsymbol{x}_\star, \boldsymbol{r}_\star$, the implementation of this weak form would require trial functions which are at least twice differentiable on (t_1, t_2), while the test functions $\boldsymbol{d}_1$ and $\boldsymbol{d}_2$ have no continuity restrictions. In order to avoid higher order trial functions, the terms in Eq.(3.4) containing time derivatives are integrated by parts and combined with the boundary terms, Eq.(3.5), obtaining:

$$\begin{aligned} &\int_{t_1}^{t_2} \left[(\dot{\boldsymbol{d}}_1 + \boldsymbol{v} \times \boldsymbol{d}_2) \cdot \boldsymbol{l} + \dot{\boldsymbol{d}}_2 \cdot \boldsymbol{h} + \boldsymbol{d}_1 \cdot \boldsymbol{b} + \boldsymbol{d}_2 \cdot \boldsymbol{m} \right] \mathrm{d}t \\ &= [\boldsymbol{b}_1 \cdot \boldsymbol{l}_b + (\boldsymbol{d}_1 - \boldsymbol{b}_1) \cdot \boldsymbol{l} + \boldsymbol{b}_2 \cdot \boldsymbol{h}_b + (\boldsymbol{d}_2 - \boldsymbol{b}_2) \cdot \boldsymbol{h}]|_{t_1}^{t_2} \end{aligned} \tag{3.6}$$

For simplicity, let the boundary test functions $(\boldsymbol{b}_1, \boldsymbol{b}_2)$ be chosen such that they are equal to the domain test functions $(\boldsymbol{d}_1, \boldsymbol{d}_2)$ evaluated at the boundary, thus eliminating the terms in $(\boldsymbol{d}_1 - \boldsymbol{b}_1)$ and $(\boldsymbol{d}_2 - \boldsymbol{b}_2)$. Moreover, for particular choices of test functions, some of the terms in Eq.(3.6) can be made to correspond to the variation of kinetic energy (or the variation of the Lagrangian, if the conservative part of the applied loads is grouped with the kinetic energy).

In fact the kinetic energy of the rigid body may be expressed as:

$$T = \tfrac{1}{2} \boldsymbol{v} \cdot \boldsymbol{l} + \tfrac{1}{2} \boldsymbol{\omega} \cdot \boldsymbol{h} \tag{3.7}$$

where the linear and angular momenta are related to the linear and angular velocities through the "constitutive" equations:

$$\begin{aligned} \boldsymbol{l} &= \boldsymbol{M} \cdot \boldsymbol{v} + \boldsymbol{S}^T \cdot \boldsymbol{\omega} \\ \boldsymbol{h} &= \boldsymbol{S} \cdot \boldsymbol{v} + \boldsymbol{J} \cdot \boldsymbol{\omega} \end{aligned} \tag{3.8}$$

Here, $\boldsymbol{M}$ is the mass, and $\boldsymbol{S}$ and $\boldsymbol{J}$ are the first and second moments of inertia, respectively, about point O′. The definitions of $\boldsymbol{S}$ and $\boldsymbol{J}$ are clear by comparison to Eq.(3.2). In the following discussion, use will be made of the fact that the moments of inertia in the embedded frame are constant. That is to say:

$$\boldsymbol{R}^t \cdot \boldsymbol{M} \cdot \boldsymbol{R} = \bar{\boldsymbol{M}} = \text{constant}$$

$$\boldsymbol{R}^t \cdot \boldsymbol{S} \cdot \boldsymbol{R} = \bar{\boldsymbol{S}} = \text{constant} \tag{3.9}$$

$$\boldsymbol{R}^t \cdot \boldsymbol{J} \cdot \boldsymbol{R} = \bar{\boldsymbol{J}} = \text{constant}$$

We define the corotational variations of $\boldsymbol{v}$ and $\boldsymbol{\omega}$ to be:

$$\begin{aligned} \delta^o \boldsymbol{v} &\stackrel{\text{def}}{=} \boldsymbol{R} \cdot \delta(\boldsymbol{R}^t \cdot \boldsymbol{v}) = \delta \boldsymbol{v} + \boldsymbol{v} \times \boldsymbol{\theta}_\delta = \delta \dot{\boldsymbol{x}} + \dot{\boldsymbol{x}} \times \boldsymbol{\theta}_\delta \\ \delta^o \boldsymbol{\omega} &\stackrel{\text{def}}{=} \boldsymbol{R} \cdot \delta(\boldsymbol{R}^t \cdot \boldsymbol{\omega}) = \delta \boldsymbol{\omega} + \boldsymbol{\omega} \times \boldsymbol{\theta}_\delta = \dot{\boldsymbol{\theta}}_\delta \end{aligned} \tag{3.10}$$

These are discussed further in Appendix A. With this notation in place, the variation of kinetic energy is carried out as follows:

$$\delta T = \tfrac{1}{2}(\boldsymbol{l} \cdot \delta \boldsymbol{v} + \delta \boldsymbol{l} \cdot \boldsymbol{v}) + \tfrac{1}{2}(\boldsymbol{h} \cdot \delta \boldsymbol{\omega} + \delta \boldsymbol{h} \cdot \boldsymbol{\omega}) \tag{3.11}$$

Considering the constitutive equations, and retaining the terms involving the variation of the mass (which of course is zero), $\delta \boldsymbol{l}$ and $\delta \boldsymbol{h}$ may be expressed as:

$$\begin{aligned} \delta \boldsymbol{l} \quad &= (\delta \boldsymbol{R} \cdot \bar{\boldsymbol{M}} \cdot \boldsymbol{R}^t + \boldsymbol{R} \cdot \bar{\boldsymbol{M}} \cdot \delta \boldsymbol{R}^t) \cdot \boldsymbol{v} + \boldsymbol{M} \cdot \delta \boldsymbol{v} \\ &\quad + (\delta \boldsymbol{R} \cdot \bar{\boldsymbol{S}}^T \cdot \boldsymbol{R}^t + \boldsymbol{R} \cdot \bar{\boldsymbol{S}}^T \cdot \delta \boldsymbol{R}^t) \cdot \boldsymbol{\omega} + \boldsymbol{S}^T \cdot \delta \boldsymbol{\omega} \\ \delta \boldsymbol{h} \quad &= (\delta \boldsymbol{R} \cdot \bar{\boldsymbol{S}} \cdot \boldsymbol{R}^t + \boldsymbol{R} \cdot \bar{\boldsymbol{S}} \cdot \delta \boldsymbol{R}^t) \cdot \boldsymbol{v} + \boldsymbol{S} \cdot \delta \boldsymbol{v} \\ &\quad + (\delta \boldsymbol{R} \cdot \bar{\boldsymbol{J}} \cdot \boldsymbol{R}^t + \boldsymbol{R} \cdot \bar{\boldsymbol{J}} \cdot \delta \boldsymbol{R}^t) \cdot \boldsymbol{\omega} + \boldsymbol{J} \cdot \delta \boldsymbol{\omega} \end{aligned} \tag{3.12}$$

From the definition of $\boldsymbol{\theta}_\delta$ it is known that $\delta \boldsymbol{R} = (\boldsymbol{\theta}_\delta \times \boldsymbol{I}) \cdot \boldsymbol{R}$ and $\delta \boldsymbol{R}^t = \boldsymbol{R}^t \cdot (\boldsymbol{\theta}_\delta \times \boldsymbol{I})$. Using these relations in Eq.(3.12) leads to:

$$\delta T = \boldsymbol{l} \cdot (\delta \boldsymbol{v} + \boldsymbol{v} \times \boldsymbol{\theta}_\delta) + \boldsymbol{h} \cdot (\delta \boldsymbol{\omega} + \boldsymbol{\omega} \times \boldsymbol{\theta}_\delta) \tag{3.13}$$

In terms of the corotational variations of $\boldsymbol{v}$ and $\boldsymbol{w}$, as defined above, the variation of kinetic engergy may be written concisely as:

$$\delta T = \delta^o \boldsymbol{v} \cdot \boldsymbol{l} + \delta^o \boldsymbol{\omega} \cdot \boldsymbol{h} \tag{3.14}$$

This result is useful in selecting meaningful test functions for the linear and angular momentum balance conditions. If the test functions $(\boldsymbol{d}_1, \boldsymbol{d}_2)$ in Eq.(3.6) are taken to be $\delta \boldsymbol{x}$ and $\boldsymbol{\theta}_\delta$ respectively, the first two terms in the integrand correspond exactly with the variation of kinetic energy. Then denoting the virtual work of the external force and moment resultants by $L_\delta = \delta \boldsymbol{x} \cdot \boldsymbol{b} + \boldsymbol{\theta}_\delta \cdot \boldsymbol{m}$, Eq.(3.6) can be rewritten as:

$$\int_{t_1}^{t_2} (\delta T + L_\delta) \mathrm{d}t = \delta \boldsymbol{x} \cdot \boldsymbol{l}_b + \boldsymbol{\theta}_\delta \cdot \boldsymbol{h}_b \Big|_{t_1}^{t_2} \tag{3.15}$$

This combined weak form requires trial functions which are only once differentiable, at the expense of requiring differentiability of the test functions. The kinematic relations between $x_\star, r_\star$ and v, ω as well as the boundary conditions on $x_\star, r_\star$ are satisfied *a priori*. If the test functions in Eq.(3.15) are chosen so as to vanish at the boundaries, then this reduces to the classical Hamilton's principle. Eq.(3.15) will be used, in its complete form, as the basis for the numerical methods presented in the following sections.

In the interest of brevity, the following notation is introduced:

$$\begin{aligned}
&q = (x_\star, r_\star) \\
&\dot{q} = (\dot{x}_\star, \dot{r}_\star) && w = (\dot{x}, \omega) \\
&\delta q = (\delta x_\star, \delta r_\star) && \delta\hat{q} = (\delta x_\star, \theta_\delta) \\
&p = (l, \Gamma^t(r_\star) \cdot h) && \hat{p} = (l, h) \\
&f = (b, \Gamma^t(r_\star) \cdot m) && \hat{f} = (b, m)
\end{aligned} \tag{3.16}$$

It may be seen that the following relations hold:

$$\delta q = \mathbf{X}^{-1} \cdot \delta\hat{q} \qquad p = \mathbf{X}^T \cdot \hat{p} \qquad f = \mathbf{X}^T \cdot \hat{f} \tag{3.17}$$

where:

$$\mathbf{X} = \begin{bmatrix} I & 0 \\ 0 & \Gamma(r_\star) \end{bmatrix} \tag{3.18}$$

The constitutive equation is then rewritten as:

$$\hat{p} = M_6 \cdot w \tag{3.19}$$

where $M_6 = \begin{bmatrix} M & S^T \\ S & J \end{bmatrix}$ is the generalized mass tensor. Similarly, the virtual work of the external force is rewritten as $L_\delta = \delta\hat{q} \cdot \hat{f} = \delta q \cdot f$.

The kinematical equations then become:

$$w = \mathbf{X} \cdot \dot{q} + w_n \tag{3.20}$$

where:

$$w_n = (v_o, R_\star \cdot \omega_o) \tag{3.21}$$

Finally the corotational virtual change of the generalized velocity is written as:

$$\delta^o w = \tfrac{\mathrm{d}}{\mathrm{dt}} \delta\hat{q} - S_1^t(w) \cdot \delta\hat{q} \qquad S_1(w) = \begin{bmatrix} 0 & 0 \\ v \times I & 0 \end{bmatrix} \tag{3.22}$$

where $\delta^o w = (\delta^o v, \delta^o \omega)$. Eq.(3.15) may now be written as:

$$\int_{t_1}^{t_2} (\delta^o \boldsymbol{w} \cdot \hat{\boldsymbol{p}} + \delta\hat{\boldsymbol{q}} \cdot \hat{\boldsymbol{f}}) \mathrm{d}t = \delta\hat{\boldsymbol{q}} \cdot \hat{\boldsymbol{p}}_b|_{t_1}^{t_2} \tag{3.23}$$

where Eq.(3.19) and Eq.(3.22) are understood.

From this variational form, two numerical approaches can be developed using the finite element method in the time domain. In the first, $\delta\hat{\boldsymbol{q}}$ is treated as an independent variation. Since the linearization process must be performed in terms of the true coordinates $\boldsymbol{q}$, the resulting tangent matrix is unsymmetric. The second approach makes use of Eq.(3.20) to express $\delta\hat{\boldsymbol{q}}$ in terms of the coordinates $\boldsymbol{q}$, and a symmetric tangent matrix results. The latter approach requires that the variation of kinetic energy be expressed in terms of $\dot{\boldsymbol{q}}$ and $\boldsymbol{q}$, and that the external force and moment resultant be expressed in a form conjugate to $\delta\boldsymbol{q}$.

$$\int_{t_1}^{t_2} (\delta T(\dot{\boldsymbol{q}}, \boldsymbol{q}, t) + \delta\boldsymbol{q} \cdot \boldsymbol{f}) \mathrm{d}t = \delta\boldsymbol{q} \cdot \boldsymbol{p}_b|_{t_1}^{t_2} \tag{3.24}$$

where $\boldsymbol{p}_b$ denotes the generalized momentum at the boundary of the time interval. Eq.(3.23) and Eq.(3.24) are the primal or kinematic forms of Hamilton's law for rigid body dynamics.

In general, the primal forms are conditionally stable and may require a small step size for accurate results. Again, this behavior is the dynamical counterpart to the locking phenomenon, which is well known in elasto-statics. As with locking, the restriction on the step size can be avoided, either through selective reduced integration or by utilizing a mixed formulation (e.g. Belytschko and Hughes (1981), Kardestuncer (1987), Malkus and Hughes (1978) and Zienkiewicz, Taylor and Too (1971)).

By means of a Legendre transformation, the mixed form of Hamilton's law for rigid body dynamics is obtained in the following way. Let $\hat{T} = \hat{T}(\boldsymbol{w}, \boldsymbol{q}, t)$ be the kinetic energy expressed as a function of $\boldsymbol{w}$ and $\boldsymbol{q}$. The complementary Hamiltonian is defined as:

$$\hat{H}(\hat{\boldsymbol{p}}, \boldsymbol{q}, t) = \hat{\boldsymbol{p}} \cdot \boldsymbol{w}(\hat{\boldsymbol{p}}, \boldsymbol{q}, t) - \hat{T}(\boldsymbol{w}(\hat{\boldsymbol{p}}, \boldsymbol{q}, t), \boldsymbol{q}, t) = \tfrac{1}{2}\hat{\boldsymbol{p}} \cdot \boldsymbol{M}_6^{-1} \cdot \hat{\boldsymbol{p}} \tag{3.25}$$

Then, the variational statement Eq.(3.15) may be expressed as:

$$\int_{t_1}^{t_2} (\delta(\hat{\boldsymbol{p}} \cdot \boldsymbol{w} - \hat{H}) + \delta\hat{\boldsymbol{q}} \cdot \hat{\boldsymbol{f}}) \mathrm{d}t = \delta\hat{\boldsymbol{q}} \cdot \hat{\boldsymbol{p}}_b|_{t_1}^{t_2} \tag{3.26}$$

Moreover, letting $\delta^* \boldsymbol{p} = \mathbf{X}^T \cdot (\delta\boldsymbol{l}, \delta^o\boldsymbol{h})$, and enforcing the displacement continuity *a posteriori*, Eq.(3.26) may be expressed as:

$$\begin{aligned} \int_{t_1}^{t_2} \frac{\mathrm{d}}{\mathrm{d}t}\delta\hat{\boldsymbol{q}} \cdot \hat{\boldsymbol{p}} + \delta^*\boldsymbol{p} \cdot [\dot{\boldsymbol{q}}^{\bullet} + \mathbf{X}^{-1} \cdot (\boldsymbol{w}_n - \hat{\boldsymbol{w}})] + \delta\hat{\boldsymbol{q}} \cdot (\hat{\boldsymbol{f}} + \mathbf{S}_1(\hat{\boldsymbol{p}}) \cdot \hat{\boldsymbol{w}}) \mathrm{d}t \\ = [\delta\hat{\boldsymbol{q}} \cdot \hat{\boldsymbol{p}}_b - \delta^*\boldsymbol{p}(\boldsymbol{q}_b - \boldsymbol{q})]|_{t_1}^{t_2} \end{aligned} \tag{3.27}$$

where: $\hat{\boldsymbol{v}} \stackrel{\text{def}}{=} \boldsymbol{M}_6^{-1} \cdot \hat{\boldsymbol{p}}$ and $\boldsymbol{q}_b$ denotes the coordinates at the boundary of the time domain. Finally, integrating the term in $\dot{\boldsymbol{q}}$ by parts, leads to the following:

$$\int_{t_1}^{t_2} \frac{\mathrm{d}}{\mathrm{dt}}\delta\hat{q}\cdot\hat{p} - \frac{\mathrm{d}}{\mathrm{dt}}\delta^{*}p\cdot q - \delta^{*}p\cdot\mathbf{X}^{-1}\cdot(\hat{w}-w_n) + \delta\hat{q}\cdot(\hat{f}+\mathbf{S}_1(\hat{p})\cdot\hat{w})\mathrm{dt}$$
$$= (\delta\hat{q}\cdot\hat{p}_b - \delta^{*}p\cdot q_b)\Big|_{t_1}^{t_2} \tag{3.28}$$

A similar procedure applied to Eq.(3.24), using the transformation:

$$H(p,q,t) = p\cdot\overset{\bullet}{q}(p,q,t) - T(p,q,t) \tag{3.29}$$

yields:

$$\int_{t_1}^{t_2} (\delta\overset{\bullet}{q}\cdot p - \delta\overset{\bullet}{p}\cdot q - \delta H + \delta q\cdot f)\mathrm{dt}$$
$$= (\delta q\cdot p_b - \delta p\cdot q_b)\Big|_{t_1}^{t_2} \tag{3.30}$$

Eq.(3.28) and Eq.(3.30) are "two-field" forms, wherein the trial functions may be discontinuous.

Relaxing the kinematic relations and considering the velocity w as an independent variable, Eq.(3.20) may be enforced in a weak sense. This leads to the most general three field form.

Modifying the Lagrangian by the weak form of the kinematic relations weighted with the momentum $\hat{p}$, a three field variational statement can be formulated in the following way:

$$\int_{t_1}^{t_2} (\delta\bar{\mathcal{L}} + \delta q\cdot\hat{f})\mathrm{dt} = \delta\hat{q}\cdot\hat{p} \tag{3.31}$$

where:

$$\bar{\mathcal{L}} = \hat{\mathcal{L}}(w,q) - \hat{p}\cdot(w - w_n - \mathbf{X}\cdot\overset{\bullet}{q}) \tag{3.32}$$

It is clear that the momentum $\hat{p}$ plays the role of Lagrange multiplier. In carrying out the variation of $\bar{\mathcal{L}}$, note that:

$$\delta\hat{\mathcal{L}} = \delta w\cdot\frac{\delta\hat{\mathcal{L}}}{\delta w} + \theta_\delta\cdot\left(v\times\frac{\delta\hat{\mathcal{L}}}{\delta v} + w\times\frac{\delta\hat{\mathcal{L}}}{\delta w}\right) \tag{3.33}$$

and, $\delta\omega_n = \theta_\delta\times\omega_n$. Then using the fundamental relation, $\delta\theta_\mathrm{d} - \mathrm{d}\theta_\delta = \theta_\delta\times\theta_\mathrm{d}$, which is established in Appendix A, and defining $\delta^{*}w = (\delta v, \delta^{o}\omega)$, Eq.(3.33) may be rearranged in the following way:

$$\int_{t_1}^{t_2} [\delta\hat{q}\cdot\left(\hat{f} - S_1(w)\cdot\frac{\delta\hat{\mathcal{L}}}{\delta w}\right) - \delta^{*}w\cdot\left(\hat{p} - \frac{\delta\hat{\mathcal{L}}}{\delta w}\right) - \delta^{*}\hat{p}\cdot\mathbf{X}^{-1}\cdot(w-w_n)$$
$$+\frac{\mathrm{d}}{\mathrm{dt}}(\delta\hat{q})\cdot\hat{p} - \frac{\mathrm{d}}{\mathrm{dt}}(\delta^{*}p)\cdot q]\mathrm{dt} = (\delta\hat{q}\cdot\hat{p}_b - \delta^{*}\hat{p}\cdot q_b)\Big|_{t_1}^{t_2} \tag{3.34}$$

This form is very suitable for numerical implementation, since the field variables do not need to be differentiable over the time element, and the three fields, $q, w, \hat{p}$ are completely independent. Therefore, very simple trial functions may be chosen. This feature arises from the particular chioce of the virtual velocity $\delta^* w$ and the virtual momentum $\delta^* p$. The Euler-Lagrange equations and the weak forms of the boundary conditions, corresponding to Eq.(3.34) are easily obtained, by means of integrating by parts the terms involving time derivatives of $\delta^* p$ and $\delta\hat{q}$. In this way, the following expression is obtained:

$$\int_{t_1}^{t_2} \left[\delta\hat{q} \cdot \left(\hat{f} - S_1(w) \cdot \frac{\delta\hat{\mathcal{L}}}{\delta w} - \dot{\hat{p}} \right) - \delta^* w \cdot \left(\hat{p} - \frac{\delta\hat{\mathcal{L}}}{\delta w} \right) \right.$$

$$\left. -\delta^* \hat{p} \cdot \left[\mathbf{X}^{-1} \cdot (w - w_n) - \dot{\hat{q}} \right] \mathrm{d}t = \right. \tag{3.35}$$

$$\delta\hat{q} \cdot (\hat{p}_b - \hat{p}) - \delta^* \hat{p} \cdot (\hat{q}_b - \hat{q}) \Big|_{t_1}^{t_2}$$

Due to the arbitrariness of the virtual displacements $\delta\hat{q}$, the virtual velocity $\delta^* w$, and the virtual momentum $\delta^* p$, Eq.(3.35) constitutes the weak form of the linear and angular momentum balance equations, the constitutive equations, the compatability conditions and the boundary conditions. Eq.(3.35) is analogous to the Hu-Washizu three field form (see Washizu (1980)), for rigid body dynamics. Each of the previous formulations, primal and mixed, may be obtained from this form. The primal formulation, can be obtained if the displacement field compatibility and the displacement boundary conditions are satisfied *a priori*. The mixed form arrises when the constitutive relations are satisfied *a priori*.

The drawback of this approach is that there are eighteen degrees of freedom associated with a single unconstrained rigid body. In the next section the linearization of the primal and mixed varational statements is presented.

4 Linearization

Since the variational forms developed in the previous section are nonlinear in the coordinates q, a solution scheme such as a Newton or Quasi-Newton method is needed. In order to take advantage of the quadratic convergence property of the Newton method, consistent linearized expressions for the various weak forms are required. These linearizations are also useful in evaluating the stability of the system.

To illustrate the linearization, consider Eq.(3.23), written as:

$$\int_{t_1}^{t_2} \left(\frac{\mathrm{d}}{\mathrm{d}t}\delta\hat{q}, \delta\hat{q}\right) \cdot \left(\hat{p}, \left[\hat{f} - S_1(w) \cdot \hat{p}\right]\right) \mathrm{d}t = \delta\hat{q} \cdot \hat{p}_b \Big|_{t_1}^{t_2} \tag{4.1}$$

Then, at a given state $(\dot{q}_g, q_g)$, the linearized form of Eq.(4.1) is:

$$\int_{t_1}^{t_2} \left(\frac{\mathrm{d}}{\mathrm{d}t}\delta\hat{q}, \delta\hat{q}\right) \cdot \hat{T}_p \cdot \left(\frac{\mathrm{d}}{\mathrm{d}t}\mathrm{d}q, \mathrm{d}q\right) \mathrm{d}t = \delta\hat{q} \cdot \hat{p}_b \Big|_{t_1}^{t_2} - \int_{t_1}^{t_2} \left(\frac{\mathrm{d}}{\mathrm{d}t}\delta\hat{q}, \delta\hat{q}\right) \cdot \hat{\mathcal{R}}_p \mathrm{d}t \tag{4.2}$$

Where $\hat{T}$ and $\hat{\mathcal{R}}$, are the tangent matrix and residual vector, respectively. The subscript $(\,)_p$ indicates a primal formulation and the hat indicates that $\delta\hat{q}$ is the variation used in the weak form. The residual vector and tangent matrix are formally defined as:

$$\hat{\mathcal{R}}_p = \left(\hat{p}, \left[\hat{f} - S_1(w)\cdot\hat{p}\right]\right)\Big|_{\substack{\dot{q}=\dot{q}_g \\ q=q_g}} \tag{4.3}$$

$$\hat{\mathcal{T}}_p = \left[\begin{array}{cc} \dfrac{\partial \hat{p}}{\partial \dot{q}} & \dfrac{\partial \hat{p}}{\partial q} \\ \dfrac{\partial(\hat{f} - S_1(w)\cdot\hat{p})}{\partial \dot{q}} & \dfrac{\partial(\hat{f} - S_1(w)\cdot\hat{p})}{\partial q} \end{array}\right]_{\substack{\dot{q}=\dot{q}_g \\ q=q_g}} \tag{4.4}$$

The complete expression for $\hat{\mathcal{T}}_p$ is given in Appendix B. As mentioned previously, this matrix is not symmetric, since the weak form is not expressed in terms of the variation of the rotation coordinates.

However, if the variation of kinetic energy is expressed in terms of $\delta\dot{q}$ and δq, Eq.(3.24) may be written as:

$$\int_{t_1}^{t_2} (\delta\dot{q}, \delta q)\cdot\left(\frac{\partial T}{\partial \dot{q}}, \frac{\partial T}{\partial q} + f\right) \mathrm{d}t = \delta q \cdot p_b\Big|_{t_1}^{t_2} \tag{4.5}$$

The linearization of Eq.(4.5) about the given state is then;

$$\int_{t_1}^{t_2} (\frac{\mathrm{d}}{\mathrm{d}t}\delta q, \delta q)\cdot\mathcal{T}_p\cdot(\frac{\mathrm{d}}{\mathrm{d}t}\mathrm{d}q, \mathrm{d}q)\mathrm{d}t = \delta q\cdot p_b\Big|_{t_1}^{t_2} - \int_{t_1}^{t_2}(\frac{\mathrm{d}}{\mathrm{d}t}\delta q, \delta q)\cdot\mathcal{R}_p\mathrm{d}t \tag{4.6}$$

Here, δq is the variation used in the weak form, and consequently the part of the tangent matrix associated with the kinetic energy is symmetric. The residual vector and tangent matrix are given by;

$$\mathcal{R}_p = \left(\frac{\partial T}{\partial \dot{q}}, \frac{\partial T}{\partial q} + f\right)\Big|_{\substack{\dot{q}=\dot{q}_g \\ q=q_g}} \tag{4.7}$$

$$\hat{\mathcal{T}}_p = \left[\begin{array}{cc} \dfrac{\partial^2 T}{\partial \dot{q}^2} & \dfrac{\partial^2 T}{\partial q \partial \dot{q}} \\ \dfrac{\partial^2 T}{\partial \dot{q}\,\partial q} + \dfrac{\partial f}{\partial \dot{q}} & \dfrac{\partial^2 T}{\partial q^2} + \dfrac{\partial f}{\partial q} \end{array}\right]_{\substack{\dot{q}=\dot{q}_g \\ q=q_g}} \tag{4.8}$$

Following the same procedure, the tangent matrices for the other principles are developed in Appendix B. The results for the mixed (two field) form are sketched out briefly here. Eq.(3.30) may be written as:

$$\begin{aligned} &\int_{t_1}^{t_2} (\frac{\mathrm{d}}{\mathrm{d}t}\delta p, \frac{\mathrm{d}}{\mathrm{d}t}\delta q)\cdot\mathbf{I}_S\cdot(p, q) + (\delta p, \delta q)\cdot\left(-\frac{\partial H}{\partial p}, -\frac{\partial H}{\partial q} + f\right)\mathrm{d}t \\ &\qquad = (\delta p, \delta q)\cdot\mathbf{I}_S\cdot(p_b, q_b)\Big|_{t_1}^{t_2} \end{aligned} \tag{4.9}$$

where $\mathbf{I}_S = \begin{bmatrix} 0 & -I_6 \\ I_6 & 0 \end{bmatrix}$ and I_6 is the six dimensional identity. The linearization of Eq.(4.9) leads to:

$$\int_{t_1}^{t_2} \left[(\frac{\mathrm{d}}{\mathrm{dt}}\delta p, \frac{\mathrm{d}}{\mathrm{dt}}\delta q) \cdot \mathbf{I}_S \cdot (\mathrm{d}p, \mathrm{d}q) + (\delta p, \delta q) \cdot \mathcal{T}_m \cdot (\mathrm{d}p, \mathrm{d}q) \right] \mathrm{d}t$$

$$= (\delta p, \delta q) \cdot \mathbf{I}_S \cdot (p_b, q_b)|_{t_1}^{t_2} - \int_{t_1}^{t_2} \left[(\frac{\mathrm{d}}{\mathrm{dt}}\delta p, \frac{\mathrm{d}}{\mathrm{dt}}\delta q) \cdot \mathbf{I}_S \cdot (p_g, q_g) + (\delta p, \delta q) \cdot \mathcal{R}_m \right] \mathrm{d}t \tag{4.10}$$

Here:

$$\mathcal{R}_m = \left(-\frac{\partial H}{\partial p}, -\frac{\partial H}{\partial q} + f \right)_{\substack{p = p_g \\ q = q_g}} \tag{4.11}$$

$$\mathcal{T}_m = \begin{bmatrix} -\dfrac{\partial^2 H}{\partial p^2} & -\dfrac{\partial^2 H}{\partial p \partial q} \\ \left(-\dfrac{\partial^2 H}{\partial q \partial p} + \dfrac{\partial f}{\partial p} \right) & \left(-\dfrac{\partial^2 H}{\partial q^2} + \dfrac{\partial f}{\partial q} \right) \end{bmatrix}_{\substack{p = p_g \\ q = q_g}} \tag{4.12}$$

are respectively, the residual vector and tangent matrix evaluated at the given state (p_g, q_g).

5 Finite Element Approximation

In the time finite element approximation employed in this paper, the time interval $[t_1, t_2]$ is subdivided by a number of equispaced time nodal points. The time interval $[t_1, t_2]$ may then be covered by $m < n$ consecutive non-overlapping time elements each containing two or more nodes. The shape functions used over the elements are of the piecewise Lagrange type. Once the time interval is discretized, the weak forms are applied over each element. Here only one element is considered for the primal form given in Eq.(4.1) and the mixed form given in Eq.(4.9).

Primal Form

Considering the variational form Eq.(4.1) and an n noded time element, let $U = (q_1, q_2, \cdots, q_n)$ and $V = (\delta\hat{q}_1, \delta\hat{q}_2, \cdots, \delta\hat{q}_n)$ be vectors of nodal values of the trial and test functions respectively. The parametric approximations for q and $\delta\hat{q}$ are then:

$$q = \sum_{k=1}^{n} s_k q_k = s \cdot U \qquad \delta\hat{q} = \sum_{k=1}^{n} s_k \delta\hat{q}_k = s \cdot V \tag{5.1a}$$

$$\dot{q} = \sum_{k=1}^{n} \dot{s}_k \, q_k = \dot{s} \cdot U \qquad \frac{\mathrm{d}}{\mathrm{dt}}(\delta\hat{q}) = \sum_{k=1}^{n} \dot{s}_k \, \delta\hat{q}_k = \dot{s} \cdot V \tag{5.1b}$$

Moreover, the increment δq is approximated as:

$$\delta q = \sum_{k=1}^{n} s_k \delta q_k = s \cdot \Delta U \tag{5.2}$$

where s_k are shape functions with the property $s_k(t_j) = \delta_{kj}$ and ΔU is the increment in the nodal values of the generalized coordinates. The nonlinear solution of Eq.(4.1) is performed using the linearized form Eq.(4.2) in an iterative procedure. The solution U is then the limit of the sequence $U_1, U_2, \cdots, U_m$ as the difference between successive solutions, $U_{m-1} - U_m$ approaches zero. Performing the integrations in Eq.(4.2) using standard Gauss quadrature and considering $\delta\hat{q}$ as an arbitrary variation the following is obtained, for the i^{th} solution step:

$$\mathbf{K}_i \cdot \Delta U_i = \mathbf{B} \cdot (\hat{p}_1, \hat{p}_2) - \mathbf{F}_i \qquad \text{(no sum on } i\text{)} \tag{5.3}$$

where:

$$\mathbf{K}_i = \int_{t_1}^{t_2} (\overset{\bullet}{s}, s)^t \cdot \hat{\mathcal{T}}_p(U_i) \cdot (\overset{\bullet}{s}, s) \mathrm{d}t \tag{5.4}$$

$$\mathbf{F}_i = \int_{t_1}^{t_2} (\overset{\bullet}{s}, s)^t \cdot \hat{\mathcal{R}}_p(U_i) \mathrm{d}t \tag{5.5}$$

$(\hat{p}_1, \hat{p}_2)$ are the boundary values of $\hat{p}$ at the times t_1, t_2 respectively, and the matrix $\mathbf{B}$ is give by:

$$\mathbf{B} = \begin{bmatrix} - & I_6, 0, 0, \cdots, & 0 \\ & 0, 0, 0, \cdots, & I_6 \end{bmatrix}^t \tag{5.6}$$

Further, the matrix $\mathbf{K}_i$ is the integrated tangent matrix at the i^{th} solution step and $\mathbf{F}_i$ is the integrated residual vector.

In the case of an initial value problem, q_1 and $\hat{p}_1$ are prescribed so that the components of ΔU associated with the first node are always zero. Since the equations for $\hat{p}_1$ and $\hat{p}_2$ are decoupled, the iteration scheme may be carried out considering a reduced problem. The final momentum $\hat{p}_2$ need only be calculated after the iterations have converged. This is a simple matter, since at the converged solution ΔU is zero, to within some prescribed tolerance. The final momentum is then obtained by computing the residual vector at the converged solution.

Mixed Form

For the mixed form Eq.(4.9), a different approach is required. Continuity of the coordinates (p, q) is not satisfied "a priori" over the time element, while at the boundary, continuity of $(\delta p, \delta q)$ is required. It is therefore important to understand $(\delta p, \delta q)$ to be a virtual state vector rather than a mere variation of (p, q). Since the trial and test functions may be chosen independently, they may be approximated as:

$$(p,q) = \sum_{k=1}^{n-1} s_k U_k = s_a \cdot U \qquad\qquad (\delta p, \delta q) = \sum_{k=1}^{n} s_k V_k = s_b \cdot V \tag{5.7}$$

where $U_k = (p_k, q_k)$ and $V_k = (\delta p_k, \delta q_k)$ are vectors of nodal values. The expression for $(\delta p, \delta q)$ contains one more term than that for (p,q) . Further, the values (p,q) evaluated at the boundary are not required to be equal to (p_b, q_b). The linearized form Eq.(4.10) is then:

$$\mathbf{K}_i \cdot \Delta U_i = \mathbf{B} \cdot (p_1, q_1, p_2, q_2) - \mathbf{F}_i \tag{5.8}$$

where $\mathbf{K}_i$ and $\mathbf{F}_i$ are given by:

$$\mathbf{K}_i = \int_{t_1}^{t_2} (\overset{\bullet}{s}_b^t \cdot \mathbf{I}_S \cdot s_a + s_b^t \cdot \mathcal{T}_{rm}(U_i) \cdot s_a) \mathrm{d}t \tag{5.9a}$$

$$\mathbf{F}_i = \int_{t_1}^{t_2} (\overset{\bullet}{s}_b^t \cdot \mathbf{I}_S \cdot s_a \cdot U_i + s_b^t \cdot \mathcal{R}_{rm}(U_i)) \mathrm{d}t \tag{5.9b}$$

In this case the matrix $\mathbf{B}$ is defined as:

$$\mathbf{B} = \begin{bmatrix} \mathbf{I}_S, & 0, 0, \cdots, & 0 \\ & & \\ 0, & 0, 0, \cdots, & -\mathbf{I}_S \end{bmatrix}^t \qquad\qquad \mathbf{I}_S = \begin{bmatrix} 0 & -I_6 \\ & \\ I_6 & 0 \end{bmatrix} \tag{5.10}$$

For the initial value problem (p_1, q_1) is prescribed and we can solve for ΔU_i and (p_2, q_2). In this case the increments in the variables p and q are not zero at the first time node.

6 Linearized Stability Analysis

In dynamical problems, a stability analysis, even in linearized form, is useful in evaluating the behavior of the system. Further, a stability analysis, for a problem where the solution is known in advance, is valuable in assessing the performance of the numerical approximation scheme. Rearranging Eq.(5.3) so that the boundary nodes and interior nodes are grouped together i.e. $U = (U_B, U_I)$ and performing the same partitioning on $\mathbf{K}$, $\mathbf{F}$ and $\mathbf{B}$, Eq.(5.3) becomes:

$$\begin{aligned} \mathbf{K}_{BB} \cdot \Delta U_B + \mathbf{K}_{BI} \cdot \Delta U_I &= \mathbf{B}_{BB} \cdot (\hat{p}_1, \hat{p}_2) - \mathbf{F}_B \\ \mathbf{K}_{IB} \cdot \Delta U_B + \mathbf{K}_{II} \cdot \Delta U_I &= \mathbf{B}_{IB} \cdot (\hat{p}_1, \hat{p}_2) - \mathbf{F}_I \end{aligned} \tag{6.1}$$

Since, by definition $\mathbf{B}_{IB} = 0$, this is equivalent to:

$$\tilde{\mathbf{K}}_{BB} \cdot \Delta U_B = \mathbf{B}_{BB} \cdot (p_1, p_2) - \tilde{\mathbf{F}}_B \tag{6.2}$$

where:

$$\tilde{\mathbf{K}}_{BB} = \mathbf{K}_{BB} - \mathbf{K}_{BI} \cdot \mathbf{K}_{II}^{-1} \cdot \mathbf{K}_{IB} \tag{6.3}$$

$$\tilde{\mathbf{F}}_B = \mathbf{F}_B - \mathbf{K}_{BI} \cdot \mathbf{K}_{II}^{-1} \cdot \mathbf{F}_I \tag{6.4}$$

In the case of a two noded time element there are no interior nodes, so that $\tilde{\mathbf{K}}_{BB}$ and $\tilde{\mathbf{F}}_B$ reduce to $\mathbf{K}_{BB}$ and $\mathbf{F}_B$ respectively.

Eq.(6.2) is also useful in a perturbation analysis. If we consider a perturbation of a dynamical solution, we have the following equations:

$$\begin{aligned} \tilde{\mathbf{F}}_B - \mathbf{B}_{BB} \cdot (\hat{\boldsymbol{p}}_1, \hat{\boldsymbol{p}}_2) &= 0 \\ \tilde{\mathbf{K}}_{BB} \cdot \mathrm{d}\boldsymbol{U}_B - \mathbf{B}_{BB} \cdot (\mathrm{d}\hat{\boldsymbol{p}}_1, \mathrm{d}\hat{\boldsymbol{p}}_2) &= 0 \end{aligned} \tag{6.5}$$

Since $\mathbf{B}_{BB} = \begin{bmatrix} -\boldsymbol{I}_6 & 0 \\ 0 & \boldsymbol{I}_6 \end{bmatrix}$ the second of Eq.(6.5) becomes:

$$\begin{aligned} \tilde{\mathbf{K}}_{11} \cdot \mathrm{d}\boldsymbol{q}_1 + \tilde{\mathbf{K}}_{12} \cdot \mathrm{d}\boldsymbol{q}_2 + \mathrm{d}\hat{\boldsymbol{p}}_1 &= 0 \\ \tilde{\mathbf{K}}_{21} \cdot \mathrm{d}\boldsymbol{q}_1 + \tilde{\mathbf{K}}_{22} \cdot \mathrm{d}\boldsymbol{q}_2 - \mathrm{d}\hat{\boldsymbol{p}}_2 &= 0 \end{aligned} \tag{6.6}$$

where the subscripts 1 and 2 refer to nodes at times t_1 and t_2 and the subscript $()_{BB}$ is dropped for simplicity of notation. Eq.(6.6) can be put in the form of a transition matrix, which maps the perturbation of the initial state vector $(\mathrm{d}\hat{\boldsymbol{p}}_1, \mathrm{d}\boldsymbol{q}_1)$ into the perturbation of the final state vector $(\mathrm{d}\hat{\boldsymbol{p}}_2, \mathrm{d}\boldsymbol{q}_2)$ i.e.:

$$(\mathrm{d}\hat{\boldsymbol{p}}_2, \mathrm{d}\boldsymbol{q}_2) = \mathbf{T} \cdot (\mathrm{d}\hat{\boldsymbol{p}}_1, \mathrm{d}\boldsymbol{q}_1) \tag{6.7}$$

The transition matrix $\mathbf{T}$ has the following expression:

$$\mathbf{T} = \begin{bmatrix} -\tilde{\mathbf{K}}_{22} \cdot \tilde{\mathbf{K}}_{12}^{-1} & \tilde{\mathbf{K}}_{21} - \tilde{\mathbf{K}}_{22} \cdot \tilde{\mathbf{K}}_{12}^{-1} \cdot \tilde{\mathbf{K}}_{11} \\ -\tilde{\mathbf{K}}_{12}^{-1} & -\tilde{\mathbf{K}}_{12}^{-1} \cdot \mathbf{K}_{11} \end{bmatrix} \tag{6.8}$$

It may be seen that the above transition matrix is a function of the time step $t_2 - t_1$ and is problem dependent. Here the eigenvalues of $\mathbf{T}$ are denoted by λ. If any of the eigenvalues have moduli greater than 1, the corresponding eigensolution will increase exponentially, and the solution step is not stable. If the eigenvalues of the true transition matrix are known, comparison with those of the approximated matrix will provide a measure of the accuracy of the numerical method. Some examples of this are given in the next section.

Proceding in a similar fashion for the mixed form, the linearized expression Eq.(5.8) may be partitioned such that $\boldsymbol{V} = (\boldsymbol{V}_i, \boldsymbol{V}_m, \boldsymbol{V}_f)$ where the subscripts i, m, f refer to initial, middle, and final nodes. Eq.(5.8) then takes the form:

$$\begin{aligned} \mathbf{K}_i \cdot \Delta\boldsymbol{U} &= -\mathbf{I}_S \cdot (\boldsymbol{p}_1, \boldsymbol{q}_1) - \mathbf{F}_i \\ \mathbf{K}_m \cdot \Delta\boldsymbol{U} &= -\mathbf{F}_m \\ \mathbf{K}_f \cdot \Delta\boldsymbol{U} &= \mathbf{I}_S \cdot (\boldsymbol{p}_2, \boldsymbol{q}_2) - \mathbf{F}_f \end{aligned} \tag{6.9}$$

Solving the first two expressions for $\Delta\boldsymbol{U}$, and substituting into the last expression, the transition matrix for the mixed form is calculated. In the case of a two noded element, there are no middle nodes, leading to:

$$\Delta U = -\mathbf{K}_i^{-1} \cdot (\mathbf{I}_S \cdot (p_1, q_1) + \mathbf{F}_i) \tag{6.10}$$

Recalling that $\mathbf{I}_S^{-1} = -\mathbf{I}_S$, the final state (p_2, q_2) is;

$$(p_2, q_2) = \mathbf{T} \cdot (p_1, q_1) - \tilde{\mathbf{F}}_f \tag{6.11}$$

where:

$$\begin{aligned} \mathbf{T} &= \mathbf{I}_S \cdot \mathbf{K}_f \cdot \mathbf{K}_i^{-1} \cdot \mathbf{I}_S \\ \tilde{\mathbf{F}}_f &= \mathbf{I}_S \cdot (\mathbf{F}_f + \mathbf{K}_f \cdot \mathbf{K}_i^{-1} \cdot \mathbf{F}_i) \end{aligned} \tag{6.12}$$

The perturbed state equation is then

$$(\mathrm{d}p_2, \mathrm{d}q_2) = \mathbf{T} \cdot (\mathrm{d}p_1, \mathrm{d}q_1) \tag{6.13}$$

7 Numerical Stability Considerations

In order to understand the behavior of the various approaches, the stability of a vertical spinning top is evaluated. Even though it is quite simple, this example will show the different behaviour of the primal and mixed forms. For simplicity, the development presented is for the two noded element only and the time step $t_2 - t_1$ is denoted by Δt. Numerical comparisons are given for the three and four node elements.

Let us consider the vertical spinning top rotating about the vertical axis e_3 at a constant rate Ω and acted upon by gravity. Let d be the distance from the center of gravity to the suspension point. The steady rotation about the vertical axis is taken as a reference configuration.

$$R_o = R(\Omega t e_3) \tag{7.1}$$

First consider the primal form. Eliminating the translational degrees of freedom, it is easily seen that the tangent matrices $\hat{T}$ and T, become:

$$\hat{T} = \begin{bmatrix} J & -h \times I \\ 0 & L \end{bmatrix} \qquad T = \begin{bmatrix} J & -\frac{1}{2} h \times I \\ \frac{1}{2} h \times I & L \end{bmatrix} \tag{7.2}$$

where:

$$\begin{aligned} J &= \mathcal{J}_a e_3 \cdot e_3^t + \mathcal{J}_t (I - e_3 \cdot e_3^t) \\ h &= \mathcal{J}_a \Omega e_3 \\ L &= (I - e_3 \cdot e_3^t) mgd \end{aligned} \tag{7.3}$$

$\mathcal{J}_a$ and $\mathcal{J}_t$ are respectively the axial and transverse moments of inertia referred to the suspension point, and d and g are the moduli of d and g. The vertical component of rotation is decoupled from the others. Therefore, the transverse rotation is denoted by ψ

and the stability of transverse motion only is analysed. Representing $\psi = \psi_a + i\psi_b$, where $i = \sqrt{-1}$, the reduced tangent matrices in terms of $\dot{\psi}$ and ψ, are :

$$\hat{T}_r = \begin{bmatrix} \mathcal{J}_t & -i\Omega\mathcal{J}_a \\ 0 & mgd \end{bmatrix} \qquad T_r = \begin{bmatrix} \mathcal{J}_t & -\frac{1}{2}i\Omega\mathcal{J}_a \\ \frac{1}{2}i\Omega\mathcal{J}_a & mgd \end{bmatrix} \tag{7.4}$$

Assuming linear shape functions for the virtual rotation, and the rotation itself, leads to:

$$\hat{\mathbf{K}}_{BB} = \begin{bmatrix} A & -B+iC \\ -B-iC & A \end{bmatrix} \qquad \mathbf{K}_{BB} = \begin{bmatrix} A+iC & -B+iC \\ -B-iC & A-iC \end{bmatrix} \tag{7.5}$$

where:

$$A = \frac{\mathcal{J}_t}{\Delta t} + \frac{amgd}{2}\Delta t, \quad B = \frac{\mathcal{J}_t}{\Delta t} - \frac{bmgd}{2}\Delta t, \quad C = \frac{\Omega\mathcal{J}_a}{2} \tag{7.6}$$

An exact integration of the tangent matrices leads to $a = \frac{2}{3}$, $b = \frac{1}{3}$. Reduced order integration using only one Gauss point yields $a = b = \frac{1}{2}$. The transition matrices for quasi coordinates and full Lagrange coordinates are then:

$$\hat{\mathbf{T}} = \frac{B+iC}{B^2+C^2}\left[\begin{array}{c|c} A-iC & A^2-B^2 \\ \hline 1 & A+iC \end{array}\right] \qquad \mathbf{T} = \frac{B+iC}{B^2+C^2}\left[\begin{array}{c|c} A & A^2-(B^2+C^2) \\ \hline 1 & A \end{array}\right] \tag{7.7}$$

Both of these matrices have the same eigenvalues, λ. Letting $\lambda = \dfrac{B+iC}{(B^2+C^2)^{1/2}}\mu$ the characteristic equation will be:

$$\mu^2 - \frac{2A}{(B^2+C^2)^{1/2}}\mu + 1 = 0 \tag{7.8}$$

Since λ and μ differ by a unit complex factor, they gain the same stability limits. It is interesting to note that when using a reduced order integration, the stability boundary is independent of the time step Δt, and coincides with the physical stability boundary. In fact, solving Eq.(7.8) results in:

$$\mu = \frac{1}{(B^2+C^2)^{1/2}}(A \pm D^{1/2}) \tag{7.9}$$

where:

$$\begin{aligned} D &= A^2 - B^2 - C^2 \\ &= -\frac{1}{4}\left[(\mathcal{J}_a\Omega)^2 - (2\mathcal{J}_t\omega)^2\left(1 - \frac{a^2-b^2}{4}\omega^2\Delta t^2\right)\right] \end{aligned} \tag{7.10}$$

and:

$$\omega = \left(\frac{mgd}{\mathcal{J}_t}\right)^{1/2} \tag{7.11}$$

For reduced order integration, D becomes negative when $\Omega = \Omega_c = \frac{2\mathcal{J}_t\omega}{\mathcal{J}_a}$ which is also the physical stability limit. On the other hand with exact integration, D becomes negative when $\Omega = \Omega_c\sqrt{1+\frac{(\omega\Delta t)^2}{12}}$. In this case, the stability limit is dependent on the step size and approaches the physical limit only as $\Delta t \to 0$.

8 Numerical Examples

In order to demonstrate numerical stability and to show how reduced order integration affects this behavior, the vertical spinning top is solved numerically. The problem is solved using two, three and four noded time elements. For a top spinning at its critical speed, the eigenvalues of the system are purely imaginary. The exact eigenvalues of the system considered are $\pm i\frac{5}{3}$. Table 1 summarizes the numerical results obtained at the critical speed for exact integration. The influence of time step on the real part of the eigenvalues is clear. While the effect is not as strong in the higher order elements, the trend is the same.

The results for reduced order integration are presented in Table 2. It should be noted that the real parts of the eigenvalues are essentially zero, and are insensitive to the time step. For the case of a vertical spinning top or other simple system, it is straightforward to choose the degree of reduced integration required to follow the physics of the problem. However this is not the case in general.

For the mixed form, the stability boundary obtained numerically coincides with the physical boundary, without resorting to reduced order integration.

"Torque- Free" Body"

In this section, the numerical results for a "torque-free" rigid body having one axis of symmetry are compared with the exact solution. Numerical studies of the accuracy, when using two, three and four noded elements, are summarized.

In order to compare the different formulations and check their accuracy, the very simple problem of a torque free rigid body with an axis of material symmetry is studied. This is a convenient problem for checking the methods since the closed form solution is well known. If we choose the reference point to coincide with the center of mass, the linear and angular degrees of freedom are coupled only by the external force, which in this case is zero. The exact solution of this problem is briefly summarized here.

If $\boldsymbol{a}$ denotes the axis of symmetry, the moment of inertia has the form:

$$\boldsymbol{J} = \mathcal{J}_a \boldsymbol{a}\otimes\boldsymbol{a} + \mathcal{J}_t(\boldsymbol{I} - \boldsymbol{a}\otimes\boldsymbol{a}) \tag{8.1}$$

One of the peculiarities of the symmetrical inertia is that the vectors $\boldsymbol{h}$, $\boldsymbol{\omega}$, and $\boldsymbol{a}$ are coplanar, i.e. $\boldsymbol{\omega}\cdot\boldsymbol{a}\times\boldsymbol{h} = 0$. In fact $\boldsymbol{\omega}\cdot\boldsymbol{a}\times\boldsymbol{h} = \boldsymbol{\omega}\cdot\boldsymbol{a}\times\boldsymbol{J}\cdot\boldsymbol{\omega}$ which is zero due to the skew symmetry of $\boldsymbol{a}\times\boldsymbol{J} \equiv \mathcal{J}_t\boldsymbol{a}\times\boldsymbol{I}$.

The angular momentum balance equation, referred to the center of gravity, is simply that $\dot{\boldsymbol{h}} = 0$. This leads to:

$$\frac{\mathrm{d}}{\mathrm{d}t}(\boldsymbol{h}\cdot\boldsymbol{a}) = \boldsymbol{h}\cdot\boldsymbol{\omega}\times\boldsymbol{a} \equiv 0 \tag{8.2a}$$

$$\frac{\mathrm{d}}{\mathrm{d}t}(\boldsymbol{h}\times\boldsymbol{a})=\boldsymbol{h}\times\dot{\boldsymbol{a}}=\boldsymbol{h}\times(\boldsymbol{\omega}\times\boldsymbol{a})=\frac{\boldsymbol{h}}{\mathcal{J}_t}\times(\boldsymbol{h}\times\boldsymbol{a}) \tag{8.2b}$$

where the fact that $\dot{\boldsymbol{a}}=\boldsymbol{\omega}\times\boldsymbol{a}$ and $\boldsymbol{\omega}\times\boldsymbol{a}=\frac{\boldsymbol{h}}{\mathcal{J}_t}\times\boldsymbol{a}$ are used. The ratio $\frac{\boldsymbol{h}}{\mathcal{J}_t}=\boldsymbol{\omega}_p$, called the precession angular velocity, represents the angular velocity of the plane containing $\boldsymbol{a}$, $\boldsymbol{h}$, and $\boldsymbol{\omega}$. If $\boldsymbol{n}$ is the normal to this plane, then:

$$\dot{\boldsymbol{n}}=\boldsymbol{\omega}_p\times\boldsymbol{n} \tag{8.3}$$

The corotational time derivative of $\boldsymbol{n}$ is:

$$\frac{\mathrm{d}^o}{\mathrm{d}t}\boldsymbol{n}=-\boldsymbol{\omega}_r\times\boldsymbol{n} \tag{8.4}$$

where:

$$\boldsymbol{\omega}_r=\boldsymbol{\omega}-\boldsymbol{\omega}_p=\frac{\mathcal{J}_t-\mathcal{J}_a}{\mathcal{J}_t\mathcal{J}_a}(\boldsymbol{h}\cdot\boldsymbol{a})\boldsymbol{a} \tag{8.5}$$

which is called the relative spin. The vector $\boldsymbol{\omega}_p$ is constant while $\boldsymbol{\omega}_r$ is time-variant, with:

$$\dot{\boldsymbol{\omega}}_r=\frac{\mathcal{J}_t-\mathcal{J}_a}{\mathcal{J}_t\mathcal{J}_a}(\boldsymbol{h}\cdot\boldsymbol{a})\,\dot{\boldsymbol{a}}=\boldsymbol{\omega}_p\times\boldsymbol{\omega}_r \tag{8.6}$$

Denoting the value of $\boldsymbol{\omega}_r$ at time t_o by $\boldsymbol{\omega}_{r_o}$ results in:

$$\boldsymbol{\omega}_r=\exp((t-t_o)\boldsymbol{\omega}_p\times\boldsymbol{I})\cdot\boldsymbol{\omega}_{r_o} \tag{8.7}$$

If $\boldsymbol{R}(t_o)$ is the rotation from some fixed reference to the orientation at time t_o, then the rotation at any later time is:

$$\boldsymbol{R}(t)=\exp((t-t_o)\boldsymbol{\omega}_p\times\boldsymbol{I})\cdot\exp((t-t_o)\boldsymbol{\omega}_r(t_o)\times\boldsymbol{I})\cdot\boldsymbol{R}(t_o) \tag{8.8}$$

Since $\boldsymbol{\omega}=\boldsymbol{\omega}_p+\boldsymbol{\omega}_r$, Eq.(8.7) and Eq.(8.8) constitute the integral of the motion.

The numerical solution has been computed using two, three, and four noded time finite elements, for both primal and mixed forms. Several nodal spacings are investigated, for a body with a ratio of transverse to axial inertia of 1.875. The initial conditions are, angular velocity of $15\frac{\text{rad}}{\text{sec}}$ about the axis of symmetry and $10\frac{\text{rad}}{\text{sec}}$ about one transverse axis. The results are shown in Figures 1 through 5. The total rotation of the body after 6 seconds is roughly 100 radians. The errors plotted in Figures are absolute errors. That is to say, the error is the magnitude, in radians, of the difference in rotation between the calculated solution and the exact solution. Figure 1 compares the error of the two noded primal and mixed elements. The time between nodes is .015 seconds. Figure 2 shows the three noded elements with the same time between the nodes, which means that the time elements in this case are .030 seconds long. Figure 3 compares results for the four noded elements. Again, the same time (.015 seconds) between nodes is used, so the four noded element is .045 seconds in length. Figures 4 and 5 compare the four noded elements at different time steps. Figure 4 contains plots of the error for a time between nodes of .030 seconds, while Figure 5 shows the results for a time of .045 seconds between nodes. Therefore, the elements

for Figures 4 and 5 are, .090 seconds long and .135 seconds long, respectively. The bahavior of the error in the mixed form is clearly more stable than the primal form. Comparing the primal curves in Figures 1 and 5, shows that the use of a four noded element with a total length of .135 seconds results in about the same error as the two noded element of length .015 seconds. However the mixed four noded element has an order of magnitude improvement in error. It is interesting to note that the maximum error in all of the test cases is less that .2 radians out of about 100 radians total rotation. It is difficult to generalize based on this simple, yet numerically significant, test case; but the behavior of the mixed formulation is very encouraging.

Acknowledgements

The authors thankfully acknowledge the support of the AFOSR and the SDIO/IST.

9 References

Agrawal, O.P.; Shabana, A.A. (1986): Automated Visco-Elastic Analysis of Large Scale Inertia-Variant Spacial Vehicles. Computers and Structures Vol. 22 No. 2, 165-178

Amos, A.K.; Atluri S.N. (1987): Large Space Structures: Dynamics and Control. Springer-Verlag

Bailey, C.D. (1975): Application of Hamilton's Law of Varying Action. AIAA Journal Vol. 13 No. 9,1154-1157

Banerjee, A.K. (1987): Comment on "Relationship Between Kane's Equations and the Gibbs-Appell Equations". Journal of Guidance Vol. 10 No. 6, 596

Baruch, M.; Riff, R. (1982): Hamilton's Principle, Hamilton's Law - 6^n Correct Formulations. AIAA Journal Vol. 20 No. 5, 687-692

Belytschko, T.; Hughes, T.J.R. (1981): editors, Computational Methods in Transient Analysis. North - Holland Publishing Co., Amsterdam

Borri, M.; et al (1985): Dynamic Response of Mechanical Systems by a Weak Hamiltonian Formulation. Computers and Structures Vol. 20 No. 1, 495-508

Desloge, E.A. (1987): Relationship Between Kane's Equations and the Gibbs-Appell Equations. Journal of Guidance Vol. 10 No. 1, 120-122

Geradin, M.; Cardona, A. (1989): Kinematics and Dynamics of Rigid and Flexible Mechanisms Using Finite Elements and Quaternion Algebra. Computational Mechanics Vol. 4, 115-135

Haug, E.J.; Wu, S.C.; Yang, S.M. (1986): Dynamics of Mechanical Systems with Coulomb Friction, Stiction, Impact and Constraint Addition - Deletion - I Theory. Mechanism and Machine Theory Vol. 21 No. 5, 401-406

Haug, E.J.; McCullough, M.K. (1986): A Variational - Vector Calculus Approach to Machine Dynamics. Journal of Mechanisms, Transmissions, and Automation in Design Vol. 108, 25-30

Hughes, P.C. (1986): Spacecraft Attitude Dynamics. Wiley and Sons

Iura, M.; Atluri, S.N. (1989): On a Consistent Theory and Variational Formulation of Finitely Stretched and Rotated 3-D Space-Curved Beams. Computational Mechanics Vol. 4, 73-88

Kane, T.R.; Levinson, D.A. (1980): Formulation of Equations of Motion for Complex Spacecraft. Journal of Guidance and Control Vol. 3 No. 2, 99-112

Kane, T.R.; Likins, P.W.; Levinson, D.A. (1983): Spacecraft Dynamics. McGrawHill

Kardestuncer, H. (1987): editor in chief, Finite Element Handbook. McGraw-Hill Inc.

Khulief, Y.A.; Shabana, A.A. (1986): Dyanmics of Multibody Systems with Variable Kinematic Structure. Journal of Mechanisms, Transmissions, and Automation in Design Vol. 108, 167-175

Kim, S.S.; Shabana, A.A; Haug, E.J. (1984): Automated Vehicle Dynamic Analysis with Flexible Components. Journal of Mechanisms, Transmissions, and Automation in Design Vol. 106,126-132

Malkus, D.S.; Hughes, T.J.R. (1978): Mixed Finite Element Methods - Reduced and Selective Integration Techniques: A Unification of Concepts. Computer Methods in Applied Mechanics and Engineering Vol. 15 No. 1, 63-81

McCullough, M.K.; Haug, E.J. (1986): Dyanmics of High Mobility Track Vehicles. Journal of Mechanisms, Transmissions, and Automation in Design Vol. 108,189-196

Meirovitch, L.; Quinn, R.D. (1987): Equations of Motion for Maneuvering Flexible Spacecraft. Journal of Guidance Vol. 10 No. 5, 453-465

Modi,V.J.; Ibrahim, A.M. (1987): On the Transient Dynamic Analysis of Flexible Orbiting Structures. Large Space Structures: Dynamics and Control. Springer - Verlag

Pietraszkiewicz, W.; Badur, J. (1983): Finite Rotations in the Description of Continuum Deformation. International Journal of Engineering Science Vol. 21 No. 9,1097-1115

Shi, G. (1988): Nonlinear Static and Dynamic Analyses of Large-Scale Lattice-Type Structures and Nonlinear Active Control by Piezo Actuators. Ph.D. Thesis, Georgia Institute of Technology

Smith, D.R.; Smith, C.V. (1974): When is Hamilton's Principle an Extremum Principle? AIAA Journal, Nov., 1573-1576

Struelpnagel, J. (1964): On the Parametrization of the Three - Dimensional Rotation Group. SIAM Review Vol. 6 No. 4, 422-430

Washizu, K. (1980): Variational Methods in Elasticity and Plasticity. third edition, Pergamon

Wittenburg, J.; Wolz, U. (1985): MESA VERDE: A Symbolic Program for Nonlinear Articulated Rigid Body Dynamics. ASME 85-DET-151

Zienkiewicz, O.C.; Taylor, R.L.; Too, J.M. (1971): Reduced Integration Technique in General Analysis of Plates and Shells. International Journal for Numerical Methods in Engineering Vol. 3, 275-290

Eow

Communicated by G. Yagawa, 1 oct 1989.

Appendix A - Relevant Formulas for Rotation

This appendix reports some fundamental formulas related to the three dimensional parametrization of the finite rotation tensor.

Exponential Representation and its Tangent Map

Let $\boldsymbol{a}$ be an arbitrary vector undergoing a rotation to a new orientation $\hat{\boldsymbol{a}}$. This proper rotation may be expressed as $\boldsymbol{r} = \phi \boldsymbol{e}$, where ϕ is the magnitude of rotation and $\boldsymbol{e}$ defines the rotation axis. This constitutes a three dimensional parametrization of the rotation and is therefore not unique. Expressing $\hat{\boldsymbol{a}}$ in terms of its components in the basis $\boldsymbol{e}, \boldsymbol{t}, \boldsymbol{s}$, respectively defined as $\boldsymbol{e}, \boldsymbol{e} \times \boldsymbol{a}, \boldsymbol{e} \times (\boldsymbol{e} \times \boldsymbol{a})$, leads to:

$$\hat{\boldsymbol{a}} = [\boldsymbol{I} \cos\phi + (\boldsymbol{e} \times \boldsymbol{I}) \sin\phi + (1 - \cos\phi)\boldsymbol{e} \cdot \boldsymbol{e}^t] \cdot \boldsymbol{a} \tag{A.1}$$

The term in brackets is the familiar form of the rotation tensor $\boldsymbol{R}$. Making use of the fact that $\boldsymbol{e} \cdot \boldsymbol{e}^t = \boldsymbol{e} \times (\boldsymbol{e} \times \boldsymbol{I}) + \boldsymbol{I}$, the rotation tensor may be written as:

$$\boldsymbol{R} = \boldsymbol{I} + \sin\phi(\boldsymbol{e} \times \boldsymbol{I}) + (1 - \cos\phi)\boldsymbol{e} \times (\boldsymbol{e} \times \boldsymbol{I}) \tag{A.2}$$

or in terms of $\boldsymbol{r}$ as:

$$\boldsymbol{R} = \boldsymbol{I} + \frac{\sin\phi}{\phi}(\boldsymbol{r} \times \boldsymbol{I}) + \frac{(1 - \cos\phi)}{\phi^2}\boldsymbol{r} \times (\boldsymbol{r} \times \boldsymbol{I}) \tag{A.3}$$

Expanding $\sin\phi$ and $\cos\phi$ in power series and substituting in the above expression, leads to:

$$\begin{aligned} \boldsymbol{R} = \boldsymbol{I} &+ \left[\phi - \frac{\phi^3}{3!} + \frac{\phi^5}{5!} - \frac{\phi^7}{7!} + \cdots\right](\boldsymbol{e} \times \boldsymbol{I}) \\ &+ \left[\frac{\phi^2}{2!} - \frac{\phi^4}{4!} + \frac{\phi^6}{6!} - \frac{\phi^8}{8!}\right]\boldsymbol{e} \times (\boldsymbol{e} \times \boldsymbol{I}) \end{aligned} \tag{A.4}$$

Making use of the fact that $\boldsymbol{e} \times \boldsymbol{e} \times \boldsymbol{e} \times \boldsymbol{I} = -\boldsymbol{e} \times \boldsymbol{I}$ and $\boldsymbol{r} = \phi \boldsymbol{e}$ we may rewrite this expression in the following form:

$$\boldsymbol{R} = \boldsymbol{I} + (\boldsymbol{r} \times \boldsymbol{I}) + \frac{1}{2!}\boldsymbol{r} \times (\boldsymbol{r} \times \boldsymbol{I}) + \frac{1}{3!}\boldsymbol{r} \times [\boldsymbol{r} \times (\boldsymbol{r} \times \boldsymbol{I})] + \cdots \text{h.o.t.} \tag{A.5}$$

This has the form of an exponential in $\boldsymbol{r} \times \boldsymbol{I}$, so the rotation tensor may be written concisely as:

$$\boldsymbol{R} = \exp(\boldsymbol{r} \times \boldsymbol{I}) \tag{A.6}$$

Other common rotation vectors such as $r_s = \sin\phi e$ and $r_t = 2\tan(\phi/2)e$ give rise to completely equivalent representations for R. In the former case, substituting $r_s = \sin\phi e$ into Eq.(A.3) and using the trigonometric half angle relations results in an expression for R of the form:

$$R = I + r_s \times I + \frac{1}{2\cos\frac{\phi}{2}} r_s \times r_s \times I \tag{A.7}$$

Substitution of $r_t = 2\tan(\phi/2)e$ into Eq.(A.3) and again using the half angle relations yield an expression for R which is:

$$R = I + \frac{1}{1 + \frac{1}{4} r_t \cdot r_t} r_t \times \left(I + \frac{1}{2} r_t \times I \right) \tag{A.8}$$

These two forms and the form of Eq.(A.3) are the most common finite rotation vectors. The following properties of the rotation tensor are well known and easily verified.

$$\begin{gathered} R^t \cdot R = R \cdot R^t = I \\ \det R = 1, \\ \det(R - I) = 0 \end{gathered} \tag{A.9}$$

The last of these properties shows that the rotation tensor has one real unit eigenvalue, where the corresponding eigenvector is the axis of rotation. Differentiation of Eq.(A.9) with respect to time yields:

$$\dot{R} \cdot R^t = -R \cdot \dot{R}^t \tag{A.10}$$

This skew symmetric tensor may be represented by a spin vector ω defined by:

$$\omega \times I = \dot{R} \cdot R^t \tag{A.11}$$

The spin, or angular velocity, vector ω is not the rate of the rotation vector $\dot{r}$, but is related to $\dot{r}$ through the tensor Γ, which itself depends on r, i.e. $\omega = \Gamma(r)\,\dot{r}$. Since this relationship is essential for constructing the tangent matrices in Appendix B, its derivation is briefly sketched out here. From Eq.(A.2) it is clear that R^t is:

$$R^t = I - \sin\phi(e \times I) + (1 - \cos\phi) e \times e \times I \tag{A.12}$$

and that $\dot{R}$ may be written as:

$$\dot{R}= \cos\phi\ \dot{\phi}\ (e \times I) + \sin\phi(\dot{e} \times I) + \sin\phi\ \dot{\phi}\ (e \times e \times I)$$
$$+(1-\cos\phi)(\dot{e} \times e \times I + e \times \dot{e} \times I) \tag{A.13}$$

Substituting Eq.(A.12) and Eq.(A.13) into Eq.(A.11) and making use of the fact that $\dot{e} \cdot e = 0$, and $e \times \dot{e} \times e \times I = 0$, results in:

$$\omega \times I = \dot{\phi}\ (e \times I) + \sin\phi(\dot{e} \times I) + (1-\cos\phi)(e \times \dot{e} \times I) \tag{A.14}$$

With the use of the definition of r, this expression may be written as:

$$\omega \times I = \left[\dot{r} + \frac{1-\cos\phi}{\phi^2}(r \times \dot{r}) + \frac{1}{\phi^2}\left(1 - \frac{\sin\phi}{\phi}\right)(r \times r \times \dot{r})\right] \times I \tag{A.15}$$

Then:

$$\omega = \left[I + \frac{1-\cos\phi}{\phi^2}(r \times I) + \frac{1}{\phi^2}\left(1 - \frac{\sin\phi}{\phi}\right)(r \times r \times I)\right] \cdot \dot{r} \tag{A.16}$$

This leads directly to the definition of Γ.

$$\Gamma(r) = \left[I + \frac{1-\cos\phi}{\phi^2}(r \times I) + \frac{1}{\phi^2}\left(1 - \frac{\sin\phi}{\phi}\right)(r \times r \times I)\right]$$
$$= I + \sum_{k=1}^{\infty} \frac{(r \times I)^k}{(k+1)!} \tag{A.17}$$

Clearly the above arguments, which establish the relationship between ω and $\dot{r}$, are equally valid for the virtual rotations θ_δ and δr, where:

$$\theta_\delta \times I = \delta R \cdot R^t \tag{A.18}$$

and we may write:

$$\theta_\delta = \Gamma(r) \cdot \delta r \tag{A.19}$$

Starting with the expression for Γ in Eq.(A.17) it is straightforward to verify that:

$$\Gamma^t = I - a_1(r \times I) + b_1(r \times r \times I) \tag{A.20}$$

$$\Gamma^{-1} = I - \frac{1}{2}(r \times I) + \frac{1}{\phi^2}\left(1 - \frac{a_o}{2b_1}\right)(r \times r \times I) \tag{A.21}$$

$$\boldsymbol{\Gamma}^{-t} = \boldsymbol{I} + \frac{1}{2}(\boldsymbol{r} \times \boldsymbol{I}) + \frac{1}{\phi^2}\left(1 - \frac{a_o}{2b_1}\right)(\boldsymbol{r} \times \boldsymbol{r} \times \boldsymbol{I}) \tag{A.22}$$

where:

$$a_o = \frac{\sin\phi}{\phi} \qquad a_1 = \frac{1-\cos\phi}{\phi^2} \qquad b_1 = \frac{1}{\phi^2}(1 - a_o) \tag{A.23}$$

Further, the tensors $\boldsymbol{\Gamma}$ and $\boldsymbol{R}$ are related by:

$$\boldsymbol{R} = \boldsymbol{\Gamma}^{-t} \cdot \boldsymbol{\Gamma} = \boldsymbol{\Gamma} \cdot \boldsymbol{\Gamma}^{-t} \tag{A.24}$$

and:

$$\boldsymbol{\Gamma}^{-t} - \boldsymbol{\Gamma}^{-1} = \boldsymbol{r} \times \boldsymbol{I} \tag{A.25}$$

Then multiplying Eq.(A.25) by $\boldsymbol{\Gamma}$ and taking Eq.(A.24) into account leads to:

$$\boldsymbol{R} = \boldsymbol{I} + \boldsymbol{\Gamma} \cdot \boldsymbol{r} \times \boldsymbol{I} = \boldsymbol{I} + \boldsymbol{r} \times \boldsymbol{\Gamma} \tag{A.26}$$

It is important to recognize that $\boldsymbol{\Gamma}$ is singular for certain values of ϕ. From the general expression for the determinant of a 3×3 matrix it is seen that:

$$\det \boldsymbol{\Gamma} = \tfrac{1}{3}\operatorname{tr}\boldsymbol{\Gamma}^3 - \tfrac{1}{2}\operatorname{tr}\boldsymbol{\Gamma}^2 \cdot \operatorname{tr}\boldsymbol{\Gamma} - \tfrac{1}{6}(\operatorname{tr}\boldsymbol{\Gamma})^3 \tag{A.27}$$

Then, considering Eq.(A.17), the determinant is:

$$\det \boldsymbol{\Gamma}(\boldsymbol{r}) \;=\; \frac{2(1-\cos\phi)}{\phi^2} \tag{A.28}$$

Clearly, $\boldsymbol{\Gamma}$ is singular when $\phi = 2n\pi$ $n = 1, 2, 3\ldots$, but is not singular for $\phi = 0$. In order to avoid this problem of singularity an incremental approach is adopted. A more general rescaling process may also be used to avoid this singularity and it is briefly shown here; see also Geradin and Cardona [27].
Let:

$$\boldsymbol{r}_p = \boldsymbol{r} - 2n\pi\boldsymbol{e} \qquad n = int\left(\frac{\phi}{2\pi}\right) \tag{A.29}$$

and

$$\phi_p = \boldsymbol{e} \cdot \boldsymbol{r}_p = \phi - 2n\pi \tag{A.30}$$

Then from Eq.(A.19):

$$\boldsymbol{\theta}_\delta = \boldsymbol{\Gamma}(\boldsymbol{r}) \cdot \delta\boldsymbol{r} = \boldsymbol{\Gamma}(\boldsymbol{r}_p) \cdot \delta\boldsymbol{r}_p \tag{A.31}$$

This equation and the Eq.(A.29) constitute the rescaling process. Proving Eq.(A.31) is easy since from Eq.(A.29):

$$\delta\boldsymbol{r}_p = \delta\boldsymbol{r} - 2n\pi\delta\boldsymbol{e} \tag{A.32}$$

and since $\boldsymbol{e} = \boldsymbol{r}/\phi$:

$$\delta\boldsymbol{e} = \frac{\boldsymbol{I} - \boldsymbol{e}\cdot\boldsymbol{e}^t}{\phi}\delta\boldsymbol{r} = -\frac{\boldsymbol{e}\times\boldsymbol{e}\times\delta\boldsymbol{r}}{\phi} \tag{A.33}$$

Substituting back into Eq.(A.32) yields:

$$\delta\boldsymbol{r}_p = \left[\boldsymbol{I} + \frac{2n\pi}{\phi}(\boldsymbol{e}\times\boldsymbol{I})\cdot(\boldsymbol{e}\times\boldsymbol{I})\right]\cdot\delta\boldsymbol{r} \tag{A.34}$$

Further, since:

$$\boldsymbol{\Gamma}(\boldsymbol{r}_p)\cdot\left[\boldsymbol{I} + \frac{2n\pi}{\phi}(\boldsymbol{e}\times\boldsymbol{I})\cdot(\boldsymbol{e}\times\boldsymbol{I})\right] = \boldsymbol{\Gamma}(\boldsymbol{r}) \tag{A.35}$$

from Eq.(A.34) and Eq.(A.35) it is seen that:

$$\boldsymbol{\Gamma}(\boldsymbol{r}_p)\cdot\delta\boldsymbol{r}_p = \boldsymbol{\Gamma}(\boldsymbol{r})\cdot\delta\boldsymbol{r} \tag{A.36}$$

which proves Eq.(A.31).

Properties of the Tangent Map

In this section, some identitities associated with the tangent map of rotation are presented. These will be necessary in the development of expressions for the tangent matrices in Appendix B.

In the space of the rotations $\boldsymbol{r}$, consider two arbitrary infinitesimal variations $\delta\boldsymbol{r}$ and $\mathrm{d}\boldsymbol{r}$ and let $\delta\boldsymbol{R}$ and $\mathrm{d}\boldsymbol{R}$ be the associated variations on $\boldsymbol{R}$. The corresponding virtual rotation vectors $\boldsymbol{\theta}_\delta$ and $\boldsymbol{\theta}_\mathrm{d}$ are, respectively defined through:

$$\boldsymbol{\theta}_\delta \times \boldsymbol{I} = \delta\boldsymbol{R}\cdot\boldsymbol{R}^t \quad \text{and} \quad \boldsymbol{\theta}_\mathrm{d}\times\boldsymbol{I} = \mathrm{d}\boldsymbol{R}\cdot\boldsymbol{R}^t \tag{A.37}$$

As shown in the preceding section, $\boldsymbol{\theta}_\delta$ and $\boldsymbol{\theta}_\mathrm{d}$ are related to $\delta\boldsymbol{r}$ and $\mathrm{d}\boldsymbol{r}$ by:

$$\boldsymbol{\theta}_\delta = \boldsymbol{\Gamma}(\boldsymbol{r})\cdot\delta\boldsymbol{r} \qquad \boldsymbol{\theta}_\mathrm{d} = \boldsymbol{\Gamma}(\boldsymbol{r})\cdot\mathrm{d}\boldsymbol{r} \tag{A.38}$$

Using the fact that $\mathrm{d}\delta\boldsymbol{R} = \delta\mathrm{d}\boldsymbol{R}$ and considering Eq.(A.37) leads to:

$$\begin{aligned} \mathrm{d}\delta\boldsymbol{R} &= \mathrm{d}\boldsymbol{\theta}_\delta \times \boldsymbol{R} + \boldsymbol{\theta}_\delta \times \boldsymbol{\theta}_\mathrm{d} \times \boldsymbol{R} \\ \delta\mathrm{d}\boldsymbol{R} &= \delta\boldsymbol{\theta}_\mathrm{d} \times \boldsymbol{R} + \boldsymbol{\theta}_\mathrm{d} \times \boldsymbol{\theta}_\delta \times \boldsymbol{R} \end{aligned} \tag{A.39}$$

Post-multiplication of Eq.(A.39) by $\boldsymbol{R}^t$ yields:

$$\mathrm{d}\boldsymbol{\theta}_\delta \times \boldsymbol{I} - \delta\boldsymbol{\theta}_\mathrm{d} \times \boldsymbol{I} + \boldsymbol{\theta}_\delta \times \boldsymbol{\theta}_\mathrm{d} \times \boldsymbol{I} - \boldsymbol{\theta}_\mathrm{d} \times \boldsymbol{\theta}_\delta \times \boldsymbol{I} = 0 \tag{A.40}$$

from which:

$$\mathrm{d}\boldsymbol{\theta}_\delta = \delta\boldsymbol{\theta}_\mathrm{d} + \boldsymbol{\theta}_\mathrm{d} \times \boldsymbol{\theta}_\delta \tag{A.41}$$

This result indicates that, in general $\mathrm{d}\boldsymbol{\theta}_\delta \neq \delta\boldsymbol{\theta}_\mathrm{d}$ (i.e. when $\boldsymbol{\theta}_\mathrm{d}$ and $\boldsymbol{\theta}_\delta$ are not parallel), which is a direct consequence of the noncommutative nature of sequential rotations.

In order to better understand implications of this result consider the vectors:

$$\boldsymbol{h}_k = \boldsymbol{\Gamma}(\boldsymbol{r}) \cdot \boldsymbol{e}_k \tag{A.42}$$

Since in general $\det \boldsymbol{\Gamma}(\boldsymbol{r}) \neq 1$, the three vectors $\boldsymbol{h}_k$ are not orthogonal. Now representing $\boldsymbol{r} = r^k \boldsymbol{e}_k$, from Eq.(A.41) :

$$\frac{\partial \boldsymbol{h}_k}{\partial r^i} - \frac{\partial \boldsymbol{h}_i}{\partial r^k} = \boldsymbol{h}_i \times \boldsymbol{h}_k \tag{A.43}$$

This clearly shows that the matrix $\boldsymbol{\Gamma}$ cannot be understood as a deformation gradient or as the Jacobian of any coordinate transformation. Therefore the virtual rotation $\boldsymbol{\theta}_\delta$ can not be expressed as a variation of any coordinate, i.e. it is not an exact differential. In the same way, the integral of the angular velocity is path dependent.

Eq.(A.41) is very general, in fact if $\boldsymbol{\theta}_\mathrm{d}$ is just the inifitesimal rotation associated with the angular velocity $\boldsymbol{\omega}$ acting over the time interval $\mathrm{d}t$, then $\boldsymbol{\theta}_\mathrm{d} = \boldsymbol{\omega}\mathrm{d}t$, and:

$$\frac{\mathrm{d}\boldsymbol{\theta}_\delta}{\mathrm{d}t} = \delta\boldsymbol{\omega} + \boldsymbol{\omega} \times \boldsymbol{\theta}_\delta = \delta\boldsymbol{\omega} - \boldsymbol{\theta}_\delta \times \boldsymbol{\omega} = \delta^\circ\boldsymbol{\omega} \tag{A.44}$$

which shows that the absolute time derivative of the virtual rotation coincides with the corotational variation of the angular velocity. In the same way if the cross product term in Eq.(A.44) is moved to the left hand side, it is recognized that the corotational time derivative of the virtual rotation coincides with the absolute variation of the angular velocity, i.e.:

$$\frac{\mathrm{d}^\circ\boldsymbol{\theta}_\delta}{\mathrm{d}t} = \frac{\mathrm{d}\boldsymbol{\theta}_\delta}{\mathrm{d}t} - \boldsymbol{\omega} \times \boldsymbol{\theta}_\delta = \delta\boldsymbol{\omega} \tag{A.45}$$

In order to cast this result in a form which will be usefull in Appendix B, consider the application of $\mathrm{d}\boldsymbol{\theta}_\delta$ to an arbitrary vector $\boldsymbol{b}$.

$$\mathrm{d}\boldsymbol{\theta}_\delta \cdot \boldsymbol{b} = \delta\boldsymbol{r} \cdot \mathrm{d}\boldsymbol{\Gamma}^t(\boldsymbol{r}) \cdot \boldsymbol{b} = \delta\boldsymbol{r} \cdot \mathbf{H}(\boldsymbol{r}, \boldsymbol{b}) \cdot \mathrm{d}\boldsymbol{r} \tag{A.46}$$

where $\mathbf{H}(\boldsymbol{r}, \boldsymbol{b})$ depends linearly on $\boldsymbol{b}$ and is obtained by taking a variation of $\boldsymbol{\Gamma}^t$. The development of this expression is straightforward and it may be verified that:

$$\begin{aligned}\mathbf{H}(\boldsymbol{r}, \boldsymbol{b}) = &-a_1 \boldsymbol{b} \times \boldsymbol{I} + b_1[(\boldsymbol{b} \times \boldsymbol{r}) \times \boldsymbol{I} + \boldsymbol{b} \times \boldsymbol{r} \times \boldsymbol{I}] \\ &+c_1 \boldsymbol{b} \times \boldsymbol{r} \cdot \boldsymbol{r}^t - d_1 (\boldsymbol{b} \times \boldsymbol{r}) \times \boldsymbol{r} \cdot \boldsymbol{r}^t\end{aligned} \tag{A.47}$$

The constants, a_1 and b_1 are defined in the preceding section, and are repeated here along with there variations c_1 and d_1, respectively:

$$\begin{aligned} a_1 &= \frac{1-\cos\phi}{\phi^2} & c_1 &= \frac{1}{\phi^2}\left(\frac{\sin\phi}{\phi} - \frac{2(1-\cos\phi)}{\phi^2}\right) \\ b_1 &= \frac{1}{\phi^2}\left(1 - \frac{\sin\phi}{\phi}\right) & d_1 &= \frac{1}{\phi^2}\left[\frac{1-\cos\phi}{\phi^2} - \frac{3}{\phi^2}\left(1 - \frac{\sin\phi}{\phi}\right)\right] \end{aligned} \tag{A.48}$$

As a consequence of Eq.(A.41), $\mathbf{H}$ is not symmetric.

$$\mathbf{H}(\boldsymbol{r}, \boldsymbol{b}) = \mathbf{H}^t(\boldsymbol{r}, \boldsymbol{b}) + \boldsymbol{\Gamma}^t(\boldsymbol{r}) \cdot \boldsymbol{b} \tilde{\times} \boldsymbol{\Gamma}(\boldsymbol{r}) \tag{A.49}$$

Moreover, since $\boldsymbol{\Gamma}^t(\boldsymbol{r}) \cdot \boldsymbol{b} \times \boldsymbol{\Gamma}(\boldsymbol{r}) = \det \boldsymbol{\Gamma}(\boldsymbol{r}) \cdot (\boldsymbol{\Gamma}^{-1}(\boldsymbol{r}) \cdot \boldsymbol{b}) \times \boldsymbol{I}$ it is easily seen that $\mathbf{H}(\boldsymbol{r}, \boldsymbol{b})$ will not be symmetric for any choice of rotation parameters.

The corotational increment of the virtual rotation follows from Eq.(A.45), multiplying by the time increment $\mathrm{d}t$:

$$\mathrm{d}^\circ\boldsymbol{\theta}_\delta = \mathrm{d}\boldsymbol{\theta}_\delta - \boldsymbol{\theta}_\mathrm{d} \times \boldsymbol{\theta}_\delta = \delta\boldsymbol{\theta}_\mathrm{d} \tag{A.50}$$

From this equation and Eq.(A.46) it follows that:

$$\mathrm{d}^\circ\boldsymbol{\theta}_\delta \cdot \boldsymbol{b} = \delta\boldsymbol{r} \cdot \mathbf{H}^t(\boldsymbol{r}, \boldsymbol{b}) \cdot \mathrm{d}\boldsymbol{r} \tag{A.51}$$

As will be shown later, the development of the tangent matrix for the symmetric primal form, requires an expression for $\frac{\mathrm{d}}{\mathrm{d}t}\mathbf{H}(\boldsymbol{r}, \boldsymbol{b})$. Similarly in developing the tangent matrix for the symmetric mixed form, expressions for $\delta\boldsymbol{\Gamma}^{-1}$ and $\mathrm{d}\delta\boldsymbol{\Gamma}^{-1}$ are needed. Two other

expressions which will also be needed are, $\dot{\Gamma}$ and $\dot{\Gamma^{-1}}$. These can be easily computed recognizing that:

$$\begin{aligned} \dot{a}_1 &= c_1\phi\,\dot{\phi} \qquad & \dot{b}_1 &= d_1\phi\,\dot{\phi} \\ \dot{c}_1 &= \tfrac{1}{\phi}(b_1 - a_1 - 4c_1)\,\dot{\phi} \qquad & \dot{d}_1 &= \tfrac{1}{\phi}(c_1 - 5d_1)\,\dot{\phi} \end{aligned} \tag{A.52}$$

and $\phi\,\dot{\phi} = \boldsymbol{r}\cdot\dot{\boldsymbol{r}}$. Then the time derivative of Γ is:

$$\dot{\Gamma} = \dot{a}_1\,(\boldsymbol{r}\times I) + \dot{b}_1\,(\boldsymbol{r}\times\boldsymbol{r}\times I) + a_1(\dot{\boldsymbol{r}}\times I) + b_1(\dot{\boldsymbol{r}}\times\boldsymbol{r}\times I + \boldsymbol{r}\times\dot{\boldsymbol{r}}\times I) \tag{A.53}$$

The expression for $\dot{\Gamma^{-1}}$ is then:

$$\begin{aligned} \dot{\Gamma^{-1}} = \frac{1-2a_1}{\phi^3(2a_1)}\,\dot{\phi}\;(\boldsymbol{r}\times I)\cdot(\boldsymbol{r}\times I) - \frac{1}{2}(\dot{\boldsymbol{r}}\times I) \\ + \frac{1}{\phi^2}\left(1 - \frac{a_o}{2b_1}\right)(\dot{\boldsymbol{r}}\times\boldsymbol{r}\times I + \boldsymbol{r}\times\dot{\boldsymbol{r}}\times I) \end{aligned} \tag{A.54}$$

Since in each of Eq.(A.53) and Eq.(A.54) the time derivatives may be replaced by variations, $\delta\Gamma^{-1}$ operating on an arbitrary vector $\boldsymbol{b}$ may be written as:

$$\delta\Gamma^{-1}\cdot\boldsymbol{b} = \mathbf{K}(\boldsymbol{r},\boldsymbol{b})\cdot\delta\boldsymbol{r} \tag{A.55}$$

where:

$$\begin{aligned} \mathbf{K}(\boldsymbol{r},\boldsymbol{b}) \;=\; & \tfrac{1}{2}\boldsymbol{b}\times I + a_2[(\boldsymbol{b}\times\boldsymbol{r})\times I - \boldsymbol{r}\times\boldsymbol{b}\times I] \\ & + b_2(\boldsymbol{r}\times\boldsymbol{b}\times\boldsymbol{r})\cdot\boldsymbol{r}^t \end{aligned} \tag{A.56}$$

where ϕ is the magnitude of $\boldsymbol{r}$, and:

$$\begin{aligned} a_2 &= \frac{1}{\phi^2}\left(1 - \frac{\dfrac{\sin\phi}{\phi}}{\dfrac{2(1-\cos\phi)}{\phi^2}}\right) = \frac{1}{\phi^2}\left(1 - \frac{a_o}{2b_o}\right) \\ b_2 &= \frac{1}{\phi^4}\left(2 - \frac{1+a_o}{2b_o}\right) \end{aligned} \tag{A.57}$$

Finally, taking the variation of Eq.(A.54) we can write the expression for $\mathrm{d}\delta\Gamma^{-1}$ acting on two arbitrary vectors $\boldsymbol{b}$ and $\boldsymbol{c}$ as:

$$\boldsymbol{c}\cdot \mathrm{d}\delta\boldsymbol{\Gamma}^{-1}\cdot\boldsymbol{b}=\mathrm{d}\boldsymbol{r}\cdot\mathbf{L}(\boldsymbol{c},\boldsymbol{r},\boldsymbol{b})\cdot\delta\boldsymbol{r} \tag{A.58}$$

where:

$$\mathbf{L}(\boldsymbol{c},\boldsymbol{r},\boldsymbol{b}) \;=\; a_2\mathbf{L}_a+b_2\mathbf{L}_b+c_2\mathbf{L}_c \tag{A.59}$$

and

$$\begin{aligned} c_2 &= \left(6-\frac{1+a_o}{b_o}-\frac{a_o}{2b_o^2}\right)\\ \mathbf{L}_a &= \boldsymbol{c}\times\boldsymbol{b}\times\boldsymbol{I}+\boldsymbol{b}\times\boldsymbol{c}\times\boldsymbol{I}\\ \mathbf{L}_b &= \mathbf{L}_a\cdot\boldsymbol{r}\cdot\boldsymbol{r}^t+\boldsymbol{r}\cdot\boldsymbol{r}^t\cdot\mathbf{L}_a^t+\frac{\boldsymbol{r}\cdot\mathbf{L}_a\cdot\boldsymbol{r}}{\phi^2}\cdot(\boldsymbol{r}\times\boldsymbol{r}\times\boldsymbol{I})\\ \mathbf{L}_c &= (\boldsymbol{r}\cdot\mathbf{L}_a\cdot\boldsymbol{r})\cdot\boldsymbol{r}\cdot\boldsymbol{r}^t \end{aligned} \tag{A.60}$$

The complexity of these relations increases the computations required to calculate symmetric tangent matrices, to no apparent advantage for initial value problems. However, if the symmetry of the tangent matrices can be exploited, the effort required to calculate $\mathbf{H}$ and $\mathbf{J}$ or $\mathbf{K}$ and $\mathbf{L}$ may lead to significant savings in the solution process.

Appendix B - Tangent Matrices

In this appendix the expressions for the tangent maps of the various variational principles are obtained. In the following paragraphs several notations are introduced, involving very sparse matrices. While the notation makes the discussion simpler, this sparsity must be recognized and taken into account in the programming of the residual vectors and tangent matrices.

Primal Form - Unsymmetric Approach

The first form considered is the unsymmetric, primal formulation. In this case the variational statement is given by Eq.(3.48), which is repeated here for convenience:

$$\int_{t_1}^{t_2}(\frac{\mathrm{d}}{\mathrm{d}t}\delta\hat{\boldsymbol{q}},\delta\hat{\boldsymbol{q}})\cdot(\hat{\boldsymbol{p}},(\hat{\boldsymbol{f}}-\boldsymbol{S}_1(\boldsymbol{w})\cdot\hat{\boldsymbol{p}}))\mathrm{d}t=\delta\hat{\boldsymbol{q}}\cdot\hat{\boldsymbol{p}}_b|_{t_1}^{t_2} \tag{B.1}$$

where $\hat{\boldsymbol{p}}=\boldsymbol{M}_6\cdot\boldsymbol{w}$. The linearized form reads:

$$\int_{t_1}^{t_2}(\frac{\mathrm{d}}{\mathrm{d}t}\delta\hat{\boldsymbol{q}},\delta\hat{\boldsymbol{q}})\cdot\hat{\boldsymbol{T}}_p\cdot(\frac{\mathrm{d}}{\mathrm{d}t}\mathrm{d}\boldsymbol{q},\mathrm{d}\boldsymbol{q})\mathrm{d}t=\delta\hat{\boldsymbol{q}}\cdot\hat{\boldsymbol{p}}_b|_{t_1}^{t_2}-\int_{t_1}^{t_2}(\frac{\mathrm{d}}{\mathrm{d}t}\delta\hat{\boldsymbol{q}},\delta\hat{\boldsymbol{q}})\cdot\hat{\mathcal{R}}_p\mathrm{d}t \tag{B.2}$$

where $\hat{\mathcal{T}}_p$ and $\hat{\mathcal{R}}_p$ are respectively the tangent matrix and the residual vector for the unsymmetric primal approach. The hat indicates that the variational statement employs the test functions $\frac{\mathrm{d}}{\mathrm{dt}}\delta\hat{q}$ and $\delta\hat{q}$, and the subscript p indicates a primal formulation. Then, directly:

$$\hat{\mathcal{R}}_p = (\hat{p}, \hat{f} - S_1(w)\cdot\hat{p}) \tag{B.3}$$

Separating the contributions due to kinetic energy and external loads, leads to, $\hat{\mathcal{R}}_{pk} = (\hat{p}, -S_1(w)\cdot\hat{p})$ and $\hat{\mathcal{R}}_{pe} = (0, \hat{f})$. Similarly, let $\hat{\mathcal{T}}_p = \hat{\mathcal{T}}_{pk} + \hat{\mathcal{T}}_{pe}$. The derivation of the tangent matrix is considerably simplified if use is made of the relation, $(\frac{\mathrm{d}}{\mathrm{dt}}\mathrm{d}\hat{q}, \mathrm{d}\hat{q}) = \mathbf{Y}\cdot(\frac{\mathrm{d}}{\mathrm{dt}}\mathrm{d}q, \mathrm{d}q)$, where $\mathbf{Y}$ is:

$$\mathbf{Y} = \begin{bmatrix} \mathbf{X} & \dot{\mathbf{X}} \\ 0 & \mathbf{X} \end{bmatrix} \qquad \mathbf{X} = \begin{bmatrix} I & 0 \\ 0 & \Gamma \end{bmatrix} \tag{B.4}$$

Then, $\hat{\mathcal{T}}_{pk} = \tilde{\mathcal{T}}_{pk}\cdot\mathbf{Y}$, and:

$$\tilde{\mathcal{T}}_{pk} = \begin{bmatrix} M_6 & (S_2(\hat{p}) - S_1(w)\cdot M_6)^t \\ S_1(\hat{p}) - S_1(w)\cdot M_6 & -S_1(w)\cdot(S_2(\hat{p}) - S_1(w)\cdot M_6)^t \end{bmatrix} \tag{B.5}$$

$$\hat{\mathcal{T}}_{pe} = \begin{bmatrix} 0 & 0 \\ \frac{\partial\hat{f}}{\partial\dot{q}} & \frac{\partial\hat{f}}{\partial q} \end{bmatrix} \tag{B.6}$$

where:

$$S_1(\hat{p}) = \begin{bmatrix} 0 & 0 \\ l\times I & 0 \end{bmatrix} \qquad S_2(\hat{p}) = \begin{bmatrix} 0 & 0 \\ l\times I & h\times I \end{bmatrix} \tag{B.7}$$

For a general six dimensional vector $z = (z_L, z_A)$ the linear operators $S_1(z)$ and $S_2(z)$ are defined as:

$$S_1(z) = \begin{bmatrix} 0 & 0 \\ z_L\times I & 0 \end{bmatrix} \qquad S_2(z) = \begin{bmatrix} 0 & 0 \\ z_L\times I & z_A\times I \end{bmatrix} \tag{B.8}$$

For the following discussion it is useful to also define S_3 as: $S_3(\cdot) = S_2(\cdot) - S_1(\cdot)$.

By inspection of Eq.(B.5) it is clear that when referring to the center of gravity the tangent matrix is greatly simplified, since M_6 is block diagonal and $S_1(p) - S_1(w)\cdot M_6 = 0$. Even with this simplification, however, the tangent matrix is not symmetric.

Primal Form - Symmetric Approach

Next, consider the symmetric primal form,

$$\int_{t_1}^{t_2} \left[\delta T(\dot{q}, q, t) + \delta q \cdot f\right] \mathrm{d}t = \delta q \cdot p_b|_{t_1}^{t_2} \tag{B.9}$$

Which in linearized form may be written as:

$$\int_{t_1}^{t_2} (\frac{\mathrm{d}}{\mathrm{d}t}\delta q, \delta q) \cdot \mathcal{T}_p \cdot (\frac{\mathrm{d}}{\mathrm{d}t}\mathrm{d}q, \mathrm{d}q)\mathrm{d}t = \delta q \cdot p_b|_{t_1}^{t_2} - \int_{t_1}^{t_2} (\frac{\mathrm{d}}{\mathrm{d}t}\delta q, \delta q) \cdot \mathcal{R}_p \, \mathrm{d}t \tag{B.10}$$

Again the residual vector and the tangent matrix may be thought of as begin composed of contributions from the kinetic energy and external forces.

$$\mathcal{R}_p = \mathcal{R}_{pk} + \mathcal{R}_{pe} \qquad \mathcal{T}_p = \mathcal{T}_{pk} + \mathcal{T}_{pe} \tag{B.11}$$

Obviously $\mathcal{R}_{pk} = \left(\frac{\partial T}{\partial \dot{q}}, \frac{\partial T}{\partial q}\right)$, $\mathcal{R}_{pe} = (0, f)$ and:

$$\mathcal{T}_{pk} = \begin{bmatrix} \frac{\partial^2 T}{\partial \dot{q}^2} & \frac{\partial^2 T}{\partial \dot{q} \, \partial q} \\ \frac{\partial^2 T}{\partial \dot{q} \, \partial q} & \frac{\partial^2 T}{\partial q^2} \end{bmatrix} \tag{B.12}$$

$$\mathcal{T}_{pe} = \begin{bmatrix} 0 & 0 \\ \frac{\partial f}{\partial \dot{q}} & \frac{\partial f}{\partial q} \end{bmatrix} \tag{B.13}$$

Working in this way, $\mathcal{T}_{pk}$ is found to be symmetric.

Performing these derivatives is not a simple matter. However, the expression for $\mathcal{T}_{pk}$ may be obtained form $\tilde{\mathcal{T}}_{pk}$ and $\hat{\mathcal{R}}_{pk}$ which have already been presented. In fact:

$$\mathrm{d}\delta T = (\frac{\mathrm{d}}{\mathrm{d}t}\delta q, \delta q) \cdot \mathcal{T}_{pk} \cdot (\frac{\mathrm{d}}{\mathrm{d}t}\mathrm{d}q, \mathrm{d}q) \tag{B.14}$$

which must also be given by:

$$\mathrm{d}\delta T = (\frac{\mathrm{d}}{\mathrm{d}t}\delta \hat{q}, \delta \hat{q}) \cdot \tilde{\mathcal{T}}_{pk} \cdot (\frac{\mathrm{d}}{\mathrm{d}t}\mathrm{d}\hat{q}, \mathrm{d}\hat{q}) + \mathrm{d}(\frac{\mathrm{d}}{\mathrm{d}t}\delta \hat{q}, \delta \hat{q}) \cdot \hat{\mathcal{R}}_{pk} \tag{B.15}$$

Comparison of the last two expressions leads to:

$$\mathcal{T}_{pk} = \mathbf{Y}^t \cdot \tilde{\mathcal{T}}_{pk} \cdot \mathbf{Y} + \left(\frac{\partial(\mathbf{Y}^t \cdot \hat{\mathcal{R}}_{pk})}{\partial \dot{q}}, \frac{\partial(\mathbf{Y}^t \cdot \hat{\mathcal{R}}_{pk})}{\partial q} \right) \tag{B.16}$$

where $\hat{\mathcal{R}}_{pk}$ is held constant and is equal to the value corresponding to the given state.

Recalling the definition of the map $\mathbf{H}(r, b) = \dfrac{\partial \Gamma^t \cdot b}{\partial r}$ for an arbitrary constant vector b and defining, $\mathbf{J}(\dot{r}, r, b) = \dfrac{\partial \dot{\Gamma}^t \cdot b}{\partial r}$, the last term in Eq.(B.16) may be expressed as:

$$\left(\frac{\partial(\mathbf{Y}^t \cdot \hat{\mathcal{R}}_{pk})}{\partial \dot{q}}, \frac{\partial(\mathbf{Y}^t \cdot \hat{\mathcal{R}}_{pk})}{\partial q} \right) = \begin{bmatrix} 0 & \mathbf{H}_6(q, \hat{p}) \\ \mathbf{H}_6(q, \hat{p}) & \mathbf{J}_6(\dot{q}, q, \hat{p}) + \mathbf{H}_6(q, -S_1(w) \cdot \hat{p}) \end{bmatrix} \tag{B.17}$$

Where the operators $\mathbf{H}_6$ and $\mathbf{J}_6$ applied to a general six component vector $z = (z_L, z_A)$ are defined as:

$$\mathbf{H}_6(q, z) = \begin{bmatrix} 0 & 0 \\ 0 & \mathbf{H}(r, z_A) \end{bmatrix} \qquad \mathbf{J}_6(\dot{q}, q, z) = \begin{bmatrix} 0 & 0 \\ 0 & \mathbf{J}(\dot{r}, r, z_A) \end{bmatrix} \tag{B.18}$$

The map $\mathbf{J}(\dot{r}, r, b)$ is obtained by taking the time derivative of $\mathbf{H}(r, b)$, while considering b constant. Making use of Eq.(A.48) leads to:

$$\mathbf{J}(\dot{r}, r, b) = \mathbf{J}^t(\dot{r}, r, b) + \Gamma^t \cdot b \times \dot{\Gamma} + \dot{\Gamma}^t \cdot b \times \Gamma \tag{B.19}$$

Taking these properties into account, the symmetry of $\mathcal{T}_{pk}$ can be easily demonstrated.

Mixed Form - Unsymmetric Approach

In linearizing the unsymmetric mixed formultaion, it is convenient to rewrite Eq.(3.40) as:

$$\begin{aligned} &\int_{t_1}^{t_2} \left[\frac{\mathrm{d}}{\mathrm{dt}} (\delta^* p, \delta\hat{q}) \cdot \mathbf{I}_S \cdot (\hat{p}, q) + (\delta^* p, \delta\hat{q}) \cdot \left(\mathbf{X}^{-1} \cdot (w_n - \hat{w}), \hat{f} + S_1(\hat{p}) \cdot \hat{w} \right) \right] \mathrm{dt} \\ &\qquad = (\delta^* p, \delta\hat{q}) \cdot \mathbf{I}_S \cdot (p_b, q_b)|_{t_1}^{t_2} \end{aligned} \tag{B.20}$$

where $\hat{w} = M_6^{-1} \cdot \hat{p}$. The linearization of Eq.(B.20) leads to:

$$\int_{t_1}^{t_2} \left[\frac{\mathrm{d}}{\mathrm{dt}}(\delta^* \boldsymbol{p}, \delta\hat{\boldsymbol{q}}) \cdot \mathbf{I}_S \cdot (\mathrm{d}\hat{\boldsymbol{p}}, \mathrm{d}\boldsymbol{q}) + (\delta^* \boldsymbol{p}, \delta\hat{\boldsymbol{q}}) \cdot \hat{\mathcal{T}}_m \cdot (\mathrm{d}\hat{\boldsymbol{p}}, \mathrm{d}\hat{\boldsymbol{q}})\right] \mathrm{d}t$$

$$= (\delta^* \boldsymbol{p}, \delta\hat{\boldsymbol{q}}) \cdot \mathbf{I}_S \cdot (\hat{\boldsymbol{p}}_b, \boldsymbol{q}_b)|_{t_1}^{t_2} - \int_{t_1}^{t_2} \left[\frac{\mathrm{d}}{\mathrm{dt}}(\delta^* \boldsymbol{p}, \delta\hat{\boldsymbol{q}}) \cdot \mathbf{I}_S \cdot (\hat{\boldsymbol{p}}_g, \boldsymbol{q}_g) + (\delta^* \boldsymbol{p}, \delta\hat{\boldsymbol{q}}) \cdot \hat{\mathcal{R}}_m\right] \mathrm{d}t \tag{B.21}$$

where:

$$\hat{\mathcal{R}}_m = \left(\mathbf{X}^{-1} \cdot (\boldsymbol{w}_n - \hat{\boldsymbol{w}}), \hat{\boldsymbol{f}} + \boldsymbol{S}_1(\hat{\boldsymbol{p}}) \cdot \hat{\boldsymbol{w}}\right) \tag{B.22}$$

The residual vector and the tangent matrix may be separated into contributions from the Hamiltonian function and the external force.

$$\hat{\mathcal{R}}_m = \hat{\mathcal{R}}_{mh} + \hat{\mathcal{R}}_{me} \qquad \hat{\mathcal{T}}_m = \hat{\mathcal{T}}_{mh} + \hat{\mathcal{T}}_{me} \tag{B.23}$$

Clearly, $\hat{\mathcal{R}}_{me} = (0, \hat{\boldsymbol{f}})$. The tangent matrix $\hat{\mathcal{T}}_{mh}$ is obtained by taking the variation of $\hat{\mathcal{R}}_{mh}$, and is given by:

$$\hat{\mathcal{T}}_{mh} = \left[\begin{array}{c|c} -\mathbf{X}^{-1} \cdot \boldsymbol{M}_6^{-1} & \mathbf{K}_6(\boldsymbol{q}, \boldsymbol{w}_n - \hat{\boldsymbol{w}}) \\ & -\mathbf{X}^{-1} \cdot \left(\boldsymbol{S}_3(\boldsymbol{w}_n) - \boldsymbol{S}_2^t(\hat{\boldsymbol{w}}) - \boldsymbol{M}_6^{-1} \cdot \boldsymbol{S}_2^t(\hat{\boldsymbol{p}})\right) \cdot \mathbf{X} \\ \hline \boldsymbol{S}_1(\hat{\boldsymbol{p}}) \cdot \boldsymbol{M}_6^{-1} - \boldsymbol{S}_1(\hat{\boldsymbol{w}}) & \boldsymbol{S}_1(\hat{\boldsymbol{p}}) \cdot \left(\boldsymbol{S}_2^t(\hat{\boldsymbol{w}}) - \boldsymbol{M}_6^{-1} \cdot \boldsymbol{S}_2^t(\hat{\boldsymbol{p}})\right) \cdot \mathbf{X} \end{array}\right] \tag{B.24}$$

Both $\hat{\mathcal{R}}_{mh}$ and $\hat{\mathcal{T}}_{mh}$ are evaluated at the given state $(\hat{\boldsymbol{p}}_g, \boldsymbol{q}_g)$. The linear operators $\boldsymbol{S}_1$,$\boldsymbol{S}_2$ and $\boldsymbol{S}_3$ are as defined previously and the operator $\mathbf{K}_6(\boldsymbol{q}, \boldsymbol{z})$, applied to an arbitrary vector $\boldsymbol{z} = (\boldsymbol{z}_L, \boldsymbol{z}_A)$ is given by:

$$\mathbf{K}_6(\boldsymbol{q}, \boldsymbol{z}) = \begin{bmatrix} 0 & 0 \\ 0 & \mathbf{K}(\boldsymbol{r}, \boldsymbol{z}_A) \end{bmatrix} \tag{B.25}$$

The full expression for $\mathbf{K}(\boldsymbol{r}, \boldsymbol{z}_A)$ is given in Appendix A.

Mixed Form - Symmetric Approach

Now consider the tangent map given by equation Eq.(3.42) in order to find the expressions for the residual vector $\mathcal{R}_m$ and the tangent matrix $\mathcal{T}_m$. Again the vector $\mathcal{R}_m$ and the matrix $\mathcal{T}_m$ have contributions due to the Hamiltonian function as well as the external force i.e.:

$$\mathcal{R}_m = \mathcal{R}_{mh} + \mathcal{R}_{me} \qquad \mathcal{T}_m = \mathcal{T}_{mh} + \mathcal{T}_{me} \tag{B.26}$$

Since the expressions for $\mathcal{R}_{me}$ and for $\mathcal{T}_{me}$ depend on the specific nature of the external forces, only the expressions for $\mathcal{R}_{mh}$ and for $\mathcal{T}_{mh}$ are developed here.

Starting from Eq.(3.37), the Hamiltonian function may be expressed as:

$$H(\boldsymbol{p}, \boldsymbol{q}, t) = \tfrac{1}{2}\hat{\boldsymbol{p}} \cdot \boldsymbol{M}_6^{-1} \cdot \hat{\boldsymbol{p}} - \hat{\boldsymbol{p}} \cdot \boldsymbol{w}_n \tag{B.27}$$

Using the relationship between $\hat{\boldsymbol{p}}$ and $\boldsymbol{p}$, leads to:

$$\delta\hat{\boldsymbol{p}} = \mathbf{X}^{-t} \cdot \delta\boldsymbol{p} + \delta\mathbf{X}^{-t} \cdot \boldsymbol{p} = \mathbf{X}^{-t}(\delta\boldsymbol{p} - \delta\mathbf{X}^{t} \cdot \hat{\boldsymbol{p}}) \tag{B.28}$$

which may be written as:

$$(\delta\hat{\boldsymbol{p}}, \delta\hat{\boldsymbol{q}}) = \boldsymbol{Z} \cdot (\delta\boldsymbol{p}, \delta\boldsymbol{q}) \qquad \boldsymbol{Z} = \begin{bmatrix} \mathbf{X}^{-t} & \mathbf{X}^{-t} \cdot \mathbf{H}_6(\boldsymbol{q}, \hat{\boldsymbol{p}}) \\ 0 & \mathbf{X} \end{bmatrix} \tag{B.29}$$

Then the virtual change of the Hamiltonian function can be stated equivalently as;

$$\delta H = (\delta\hat{\boldsymbol{p}}, \delta\hat{\boldsymbol{q}}) \cdot \hat{\mathcal{R}}_{mh} = (\delta\boldsymbol{p}, \delta\boldsymbol{q}) \cdot \mathcal{R}_{mh} \tag{B.30}$$

and the vectors $\hat{\mathcal{R}}_{mh}$ and $\mathcal{R}_{mh}$ can be seen to be related by: $\hat{\mathcal{R}}_{mh} = \boldsymbol{Z}^t \cdot \mathcal{R}_{mh}$.

The linearization of the virtual change of the Hamiltonian can then be written as:

$$\begin{aligned} \mathrm{d}\delta H &= (\delta\hat{\boldsymbol{p}}, \delta\hat{\boldsymbol{q}}) \cdot \hat{\mathcal{T}}_{mh} \cdot (\mathrm{d}\hat{\boldsymbol{p}}, \mathrm{d}\hat{\boldsymbol{q}}) + (\mathrm{d}\delta\hat{\boldsymbol{p}}, \mathrm{d}\delta\hat{\boldsymbol{q}}) \cdot \hat{\mathcal{R}}_{mh} \\ &= (\delta\boldsymbol{p}, \delta\boldsymbol{q}) \cdot \mathcal{T}_{mh} \cdot (\mathrm{d}\boldsymbol{p}, \mathrm{d}\boldsymbol{q}) \end{aligned} \tag{B.31}$$

where $(\mathrm{d}\hat{\boldsymbol{p}}, \mathrm{d}\hat{\boldsymbol{q}}) = \boldsymbol{Z} \cdot (\mathrm{d}\boldsymbol{p}, \mathrm{d}\boldsymbol{q})$. By comparison, then:

$$\mathcal{T}_{mh} = \boldsymbol{Z}^t \cdot \hat{\mathcal{T}}_{mh} \cdot \boldsymbol{Z} + \left(\frac{\partial(\boldsymbol{Z}^t \cdot \hat{\mathcal{R}}_{mh})}{\partial \boldsymbol{p}}, \frac{\partial(\boldsymbol{Z}^t \cdot \hat{\mathcal{R}}_{mh})}{\partial \boldsymbol{q}} \right) \tag{B.32}$$

In the last expression $\hat{\mathcal{R}}_{mh}$ is the value of the residual evaluated at the given state $(\hat{\boldsymbol{p}}_g, \hat{\boldsymbol{q}}_g)$, and is considered constant. The definitions of $\hat{\mathcal{R}}_{mh}$ and $\hat{\mathcal{T}}_{mh}$, are not the same as in the previous section, but are consistent with the notation that $\hat{()}$ indicates test functions wich are variations of $\hat{\boldsymbol{p}}$ and $\hat{\boldsymbol{q}}$.

The expressions for $\hat{\mathcal{R}}_{mh}$ and for $\hat{\mathcal{T}}_{mh}$, are now developed. The virtual change of the Hamiltonian function is expressed by:

$$\delta H = \delta^o \hat{\boldsymbol{p}} \cdot (\hat{\boldsymbol{w}} - \boldsymbol{w}_n) - \delta^o \boldsymbol{w}_n \cdot \hat{\boldsymbol{p}} \tag{B.33}$$

where $\hat{\boldsymbol{w}} = \boldsymbol{M}_6^{-1} \cdot \hat{\boldsymbol{p}}$. Since it is known that:

$$\delta^o \hat{\boldsymbol{p}} = \delta \hat{\boldsymbol{p}} - \boldsymbol{S}_2^t(\hat{\boldsymbol{p}}) \cdot \delta \hat{\boldsymbol{q}} \qquad \delta^o \boldsymbol{w}_n = -\boldsymbol{S}_1^t(\boldsymbol{w}_n) \cdot \delta \hat{\boldsymbol{q}} \tag{B.34}$$

Eq.(B.33) can be rewritten as:

$$\delta H = \delta \hat{\boldsymbol{p}} \cdot (\hat{\boldsymbol{w}} - \boldsymbol{w}_n) - \delta \hat{\boldsymbol{q}} \cdot [\boldsymbol{S}_3(\hat{\boldsymbol{p}}) \cdot \boldsymbol{w}_n - \boldsymbol{S}_2(\hat{\boldsymbol{p}}) \cdot \hat{\boldsymbol{w}}] \tag{B.35}$$

then the vector $\mathcal{R}_{mh}$ has the following expression:

$$\mathcal{R}_{mh} = (\hat{\boldsymbol{w}} - \boldsymbol{w}_n, \boldsymbol{S}_3(\hat{\boldsymbol{p}}) \cdot \boldsymbol{w}_n - \boldsymbol{S}_2(\hat{\boldsymbol{p}}) \cdot \hat{\boldsymbol{w}}) \tag{B.36}$$

From this, it is straightforward to find the expression of the tangent matrix $\hat{\mathcal{T}}_{mh}$, which has the form:

$$\hat{\mathcal{T}}_{mh} = \left[\begin{array}{c|c} \boldsymbol{M}_6^{-1} & \begin{array}{c} \boldsymbol{S}_2^t(\hat{\boldsymbol{w}}) - \boldsymbol{S}_3^t(\boldsymbol{w}_n) \\ -\boldsymbol{M}_6^{-1} \cdot \boldsymbol{S}_2^t(\hat{\boldsymbol{p}}) \end{array} \\ \hline \begin{array}{c} \boldsymbol{S}_2(\hat{\boldsymbol{w}}) - \boldsymbol{S}_3(\boldsymbol{w}_n) \\ -\boldsymbol{S}_2(\hat{\boldsymbol{p}}) \cdot \boldsymbol{M}_6^{-1} \end{array} & \begin{array}{c} \boldsymbol{S}_2(\hat{\boldsymbol{p}}) \cdot \boldsymbol{M}_6^{-1} \cdot \boldsymbol{S}_2^t(\hat{\boldsymbol{p}}) - \\ \boldsymbol{S}_2(\hat{\boldsymbol{p}}) \cdot \boldsymbol{S}_2^t(\hat{\boldsymbol{w}}) + \boldsymbol{S}_3(\hat{\boldsymbol{p}}) \cdot \boldsymbol{S}_3^t(\boldsymbol{w}_n) \end{array} \end{array}\right] \tag{B.37}$$

In order to compute the terms $(\mathrm{d}\delta\hat{\boldsymbol{p}}, \mathrm{d}\delta\hat{\boldsymbol{q}}) \cdot \hat{\mathcal{R}}_{mh}$ recall the expressions for $\delta\boldsymbol{\Gamma}^{-1}$ and $\mathrm{d}\delta\boldsymbol{\Gamma}^{-1}$ that are computed in Appendix A. Specifically:

$$\delta\boldsymbol{\Gamma}^{-1} \cdot \boldsymbol{b} = \mathbf{K}(\boldsymbol{r}, \boldsymbol{b}) \cdot \delta\boldsymbol{r} \tag{B.38}$$

and:

$$\boldsymbol{c} \cdot \mathrm{d}\delta\boldsymbol{\Gamma}^{-1} \cdot \boldsymbol{b} = \mathrm{d}\boldsymbol{r}^t \cdot \mathbf{L}(\boldsymbol{c}, \boldsymbol{r}, \boldsymbol{b}) \cdot \delta\boldsymbol{r} \tag{B.39}$$

The map $\mathbf{K}_6(\boldsymbol{q}, \boldsymbol{z})$ is defined in the previous section. In a similar way $\mathbf{L}_6(\boldsymbol{x}, \boldsymbol{q}, \boldsymbol{z})$, is defined, considering two general six dimensional vector $\boldsymbol{x}$ and $\boldsymbol{z}$), to be;

$$\mathbf{K}_6(q,z)=\begin{bmatrix}0 & 0\\ 0 & \mathbf{K}(r,z_A)\end{bmatrix}\qquad \mathbf{L}_6(x,q,z)=\begin{bmatrix}0 & 0\\ 0 & \mathbf{L}(x_A,r,z_A)\end{bmatrix}\tag{B.40}$$

With the use of these definitions the last term in Eq.(B.32) can be rewritten as:

$$\left(\frac{\partial(Z^t\cdot\mathcal{R}_{mh})}{\partial p},\frac{\partial(Z^t\cdot\mathcal{R}_{mh})}{\partial q}\right)=$$

$$\left[\begin{array}{c|c}0 & \mathbf{K}_6(q,\hat{w}-w_n)\\ \hline \mathbf{K}_6^t(q,\hat{w}-w_n) & \begin{array}{c}\mathbf{L}_6(\mathbf{X}^t\cdot\hat{p},q,\hat{w}-w_n)+\\ \mathbf{H}_6(q,\hat{p})\cdot(S_3(\hat{p})\cdot w_n-S_2(\hat{p})\cdot\hat{w})\end{array}\end{array}\right]\tag{B.41}$$

Even if the programming of the tangent matrix can be optimized, the fully symmetric mixed method requires a great deal of computations.

Three Field Form

The linearization of the three field principle Eq.(3.46) is much more straightforward. For convenience the three field form is recalled here:

$$\begin{aligned}\int_{t_1}^{t_2}[\delta\hat{q}\cdot\left(\hat{f}-\mathbf{S}_1(w)\cdot\frac{\delta\hat{\mathcal{L}}}{\delta w}\right)-\delta^*w\cdot\left(\hat{p}-\frac{\delta\hat{\mathcal{L}}}{\delta w}\right)-\delta^*\hat{p}\cdot\mathbf{X}^{-1}\cdot(w-w_n)\\ +\frac{\mathrm{d}}{\mathrm{dt}}(\delta\hat{q})\cdot\hat{p}-\frac{\mathrm{d}}{\mathrm{dt}}(\delta^*p)\cdot q]\mathrm{d}t=(\delta\hat{q}\cdot\hat{p}_b-\delta^*\hat{p}\cdot q_b)|_{t_1}^{t_2}\end{aligned}\tag{B.42}$$

Grouping the test functions into a single vector, Eq.(B.42) may be rewritten as:

$$\begin{aligned}\int_{t_1}^{t_2}[(\delta\hat{q},\delta^*w,\delta^*\hat{p})\cdot\left(\hat{f}-\mathbf{S}_1(w)\cdot\frac{\delta\hat{\mathcal{L}}}{\delta w},-\hat{p}+\frac{\delta\hat{\mathcal{L}}}{\delta w},-\mathbf{X}^{-1}\cdot(w-w_n)\right)\mathrm{d}t\\ +\int_{t_1}^{t_2}(\frac{\mathrm{d}}{\mathrm{dt}}\delta^*p,\frac{\mathrm{d}}{\mathrm{dt}}\delta\hat{q})\cdot\mathbf{I}_S\cdot(\hat{p},q)\mathrm{d}t=(\delta\hat{q}\cdot\hat{p}_b-\delta^*\hat{p}\cdot q_b)|_{t_1}^{t_2}\end{aligned}\tag{B.43}$$

The linearization is then given by:

$$\int_{t_1}^{t_2}\left[\frac{\mathrm{d}}{\mathrm{dt}}(\delta^*\boldsymbol{p},\delta\hat{\boldsymbol{q}})\cdot\mathbf{I}_S\cdot(\mathrm{d}\hat{\boldsymbol{p}},\mathrm{d}\hat{\boldsymbol{q}})\mathrm{d}t+\int_{t_1}^{t_2}(\delta\hat{\boldsymbol{q}},\delta^*\boldsymbol{w},\delta^*\boldsymbol{p})\cdot\hat{\mathcal{T}}_3\cdot(\mathrm{d}\boldsymbol{q},\mathrm{d}\boldsymbol{w},\mathrm{d}\hat{\boldsymbol{p}})\right]\mathrm{d}t$$

$$=(\delta^*\boldsymbol{p},\delta\hat{\boldsymbol{q}})\cdot\mathbf{I}_S\cdot(\hat{\boldsymbol{p}}_b,\boldsymbol{q}_b)|_{t_1}^{t_2}-\int_{t_1}^{t_2}\frac{\mathrm{d}}{\mathrm{dt}}(\delta^*\boldsymbol{p},\delta\hat{\boldsymbol{q}})\cdot\mathbf{I}_S\cdot(\hat{\boldsymbol{p}}_g,\boldsymbol{q}_g)\mathrm{d}t \tag{B.44}$$

$$+\int_{t_1}^{t_2}(\delta\hat{\boldsymbol{q}},\delta^*\boldsymbol{w},\delta^*\boldsymbol{p})\cdot\hat{\mathcal{R}}_3\mathrm{d}t$$

where:

$$\hat{\mathcal{R}}_3=\left(\hat{\boldsymbol{f}}-\boldsymbol{S}_1(\boldsymbol{w})\cdot\frac{\delta\hat{\mathcal{L}}}{\delta\boldsymbol{w}},-\hat{\boldsymbol{p}}+\frac{\delta\hat{\mathcal{L}}}{\delta\boldsymbol{w}},-\mathbf{X}^{-1}\cdot(\boldsymbol{w}-\boldsymbol{w}_n)\right) \tag{B.45}$$

Once more, it is a simple matter to separate the contribution from the external force. The variation of the residual, neglecting the external force terms leads to the tangent matrix for the three field approach.

$$\hat{\mathcal{T}}_3=\left[\begin{array}{c|c|c}\boldsymbol{S}_1(\boldsymbol{w})\cdot\dfrac{\delta^2\hat{\mathcal{L}}}{\delta\boldsymbol{w}\delta\boldsymbol{q}} & \boldsymbol{S}_1(\boldsymbol{M}_6\cdot\boldsymbol{w})-\boldsymbol{S}_1(\boldsymbol{w})\cdot\boldsymbol{M}_6 & 0\\ \hline \dfrac{\delta^2\hat{\mathcal{L}}}{\delta\boldsymbol{w}\delta\boldsymbol{q}} & \boldsymbol{M}_6 & -\boldsymbol{I}_6\\ \hline \mathbf{K}_6(\boldsymbol{q},\boldsymbol{w}-\boldsymbol{w}_n)-\boldsymbol{S}_3(\boldsymbol{w}_n)\cdot\mathbf{X} & -\mathbf{X}^{-1} & 0\end{array}\right] \tag{B.46}$$

The first and second partial derivative of $\hat{\mathcal{L}}$ are given by:

$$\frac{\partial\hat{\mathcal{L}}}{\partial\boldsymbol{w}}=\boldsymbol{M}_6\cdot\boldsymbol{w}$$

$$\frac{\partial^2\hat{\mathcal{L}}}{\partial\boldsymbol{w}\partial\boldsymbol{q}}=[\boldsymbol{S}_2^t(\boldsymbol{M}_6\cdot\boldsymbol{w})-\boldsymbol{M}_6\cdot\boldsymbol{S}_2(\boldsymbol{w})]\cdot\mathbf{X} \tag{B.47}$$

and the partial derivative of $\boldsymbol{w}_n$ with respect to $\boldsymbol{q}$ is $\dfrac{\partial\boldsymbol{w}_n}{\partial\boldsymbol{q}}=\boldsymbol{S}_3^t(\boldsymbol{w}_n)\cdot\mathbf{X}$. The simplicity of this tangent matrix, combined with the fact that for initial value problems symmetry of the tangent matrix is not easily exploited, makes this a an attractive formulation, with the obvious drawback of increased degrees of freedom.

Table1 Eigenvalues for Vertical Top - Exact Integration

Eigenvalues for Exact Integration						
	Two Nodes		Three Nodes		Four Nodes	
Δt	Real	Imag	Real	Imag	Real	Imag
0.02	1.6031E-02	1.6663	2.7599E-04	1.6666	1.7240E-05	1.6666
0.04	3.2027E-02	1.6654	1.1032E-03	1.6666	4.1751E-05	1.6666
0.06	4.7952E-02	1.6638	2.4795E-03	1.6666	1.4113E-04	1.6666
0.08	6.3772E-02	1.6617	4.4010E-03	1.6666	3.3443E-04	1.6666
0.10	7.9453E-02	1.6590	6.8623E-03	1.6665	6.5150E-04	1.6666
0.12	9.4963E-02	1.6557	9.8564E-03	1.6664	1.1222E-03	1.6666
0.14	0.1102	1.6518	1.3374E-02	1.6663	1.7753E-03	1.6666
0.16	0.1253	1.6474	1.7404E-02	1.6661	2.6385E-03	1.6666
0.18	0.1401	1.6424	2.1934E-02	1.6658	3.7381E-03	1.6666
0.20	0.1546	1.6370	2.6949E-02	1.6653	5.0991E-03	1.6666

Table 2 Eigenvalues for Vertical Top - Under Integration

Eigenvalues for Reduced Integration						
	Two Nodes		Three Nodes		Four Nodes	
Δt	Real	Imag	Real	Imag	Real	Imag
0.02	2.3881E-05	1.6665	2.3261E-05	1.6666	1.6713E-05	1.6666
0.04	2.3211E-05	1.6660	1.0527E-05	1.6666	1.3681E-05	1.6666
0.06	1.6634E-05	1.6652	1.3681E-05	1.6666	7.9443E-06	1.6666
0.08	1.0443E-05	1.6642	7.7153E-06	1.6666	8.0284E-06	1.6666
0.10	1.2153E-05	1.6628	8.0605E-06	1.6666	7.6044E-06	1.6666
0.12	1.3460E-05	1.6611	8.0266E-06	1.6666	7.4198E-06	1.6666
0.14	7.2016E-06	1.6591	7.7597E-06	1.6665	8.3770E-06	1.6666
0.16	7.5157E-06	1.6568	7.4664E-06	1.6664	6.2104E-06	1.6666
0.18	7.6967E-06	1.6543	7.4116E-06	1.6663	6.1258E-06	1.6666
0.20	7.7657E-06	1.6514	7.8648E-06	1.6662	6.0095E-06	1.6666

Figure 1: Absolute Error 2 Noded Elements

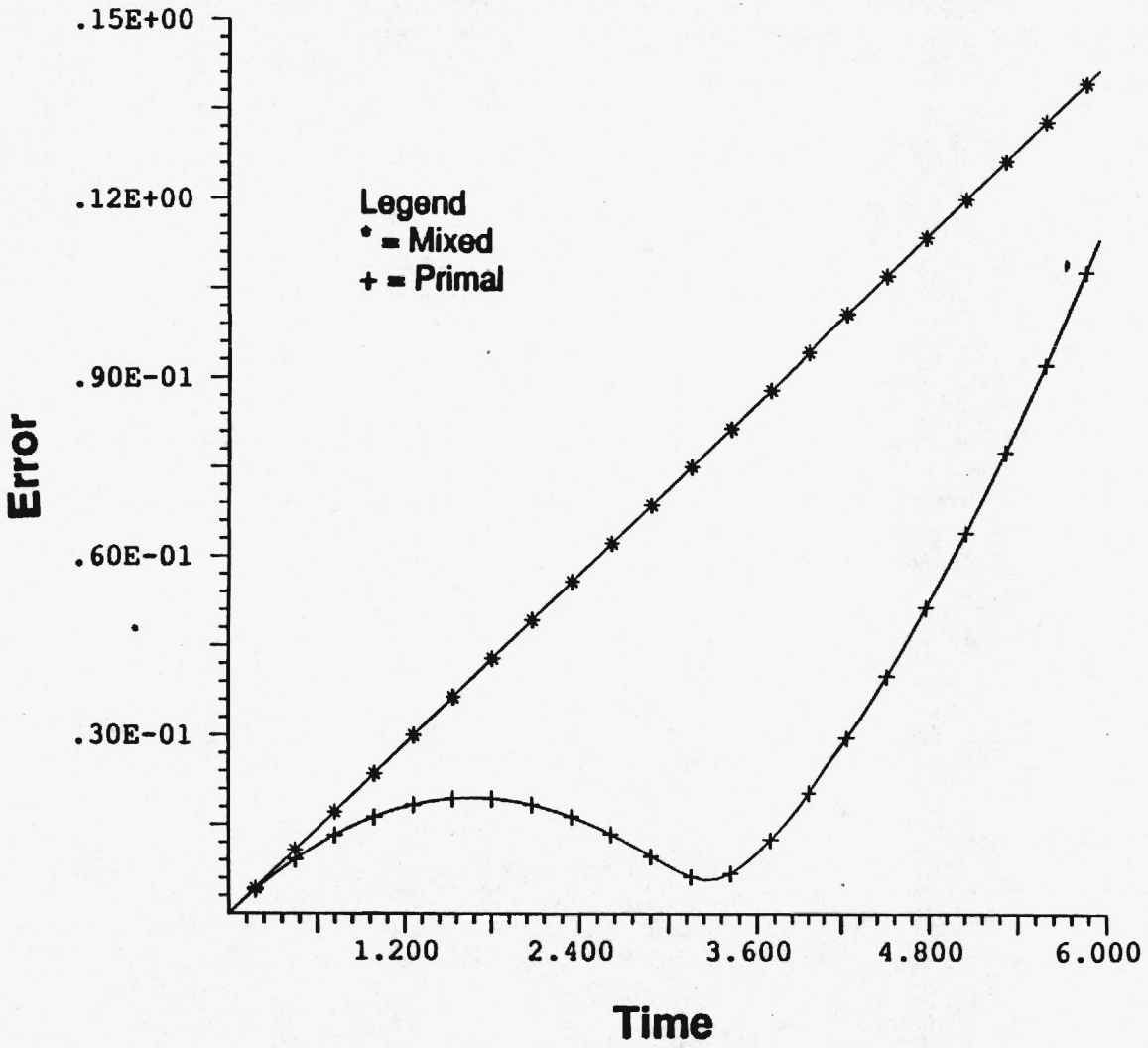

Figure 2: Absolute Error 3 Noded Elements

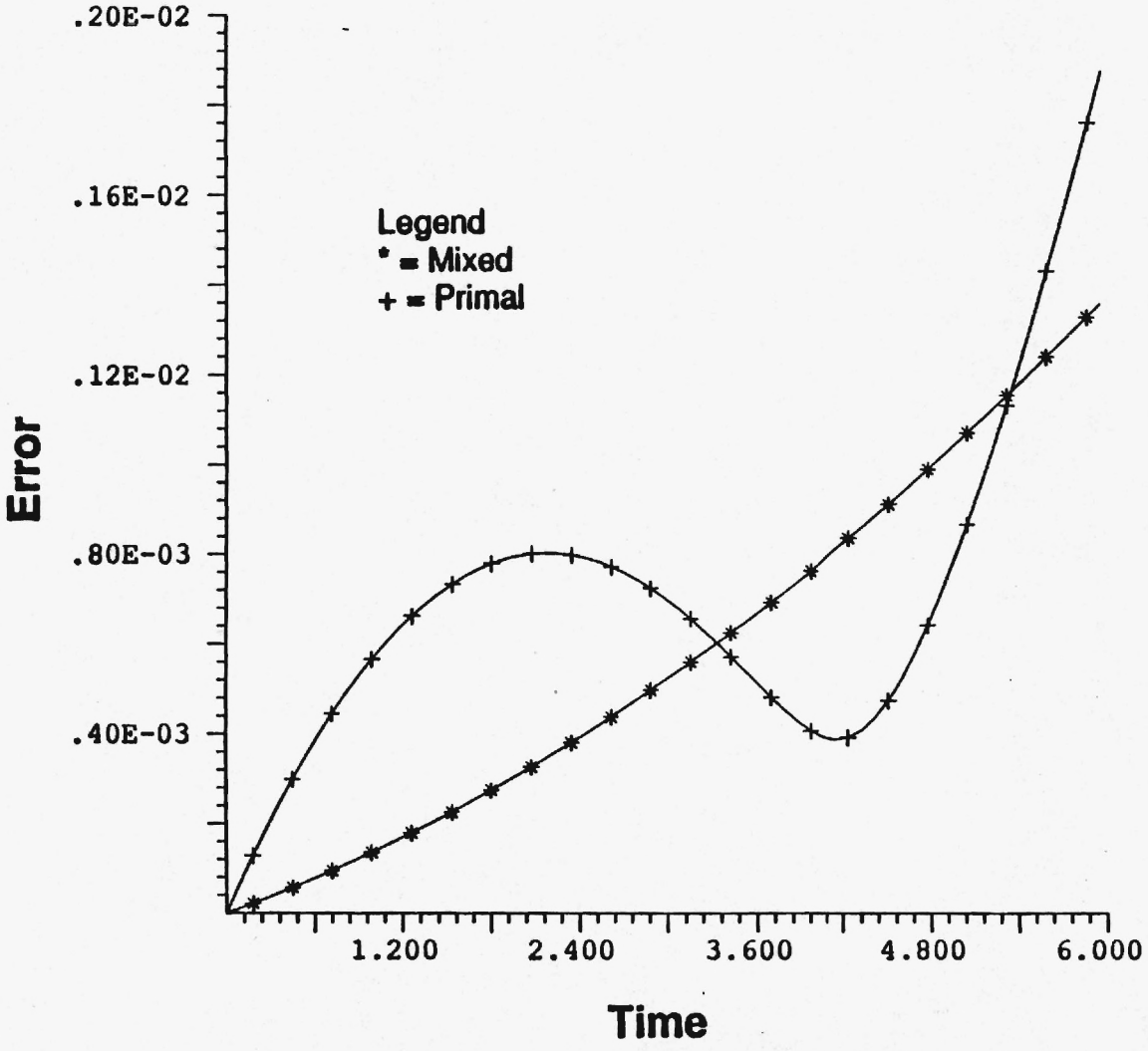

Figure 3: Absolute Error 4 Noded Elements

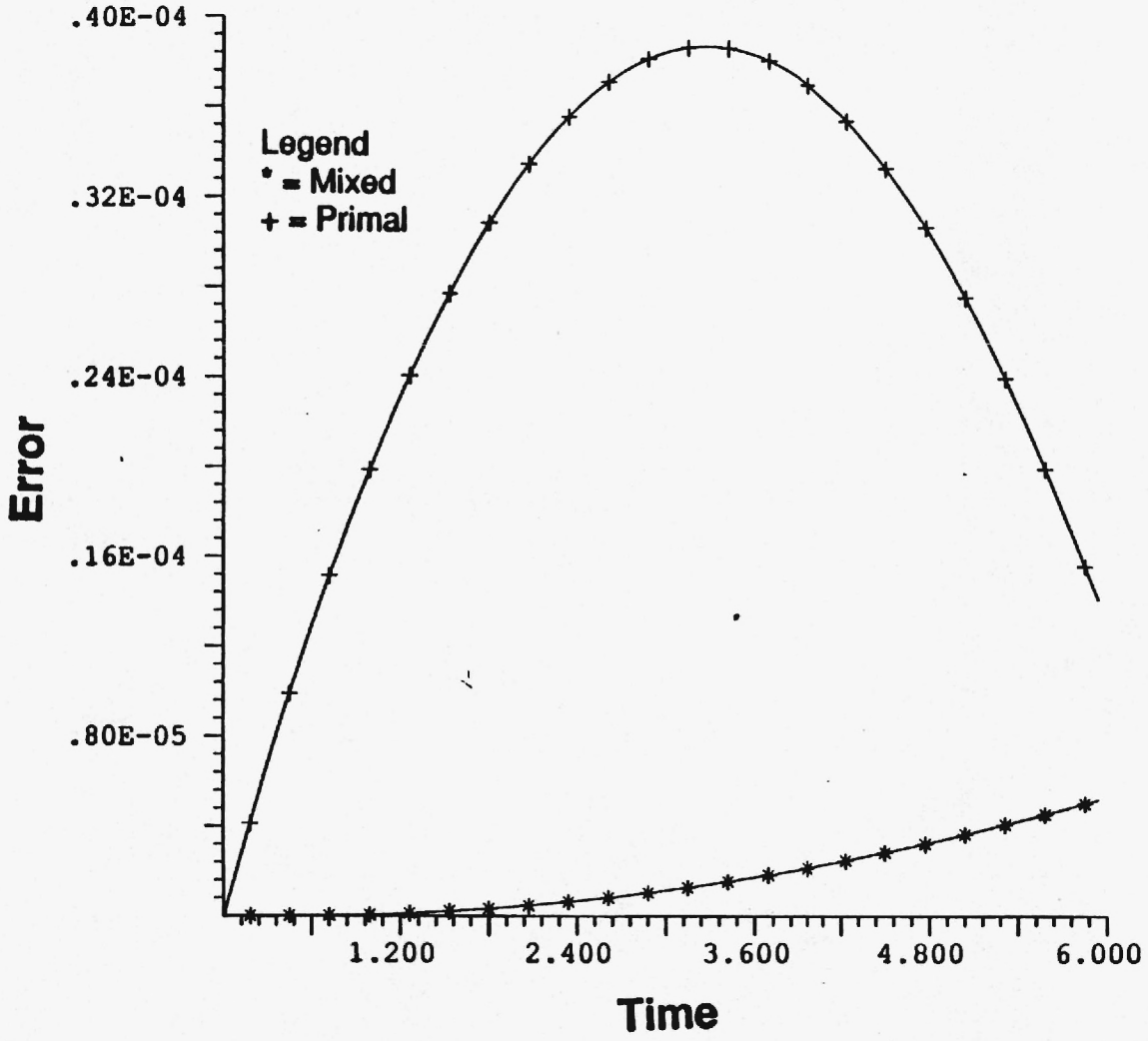

Figure 4: Absolute Error 4 Noded Elements

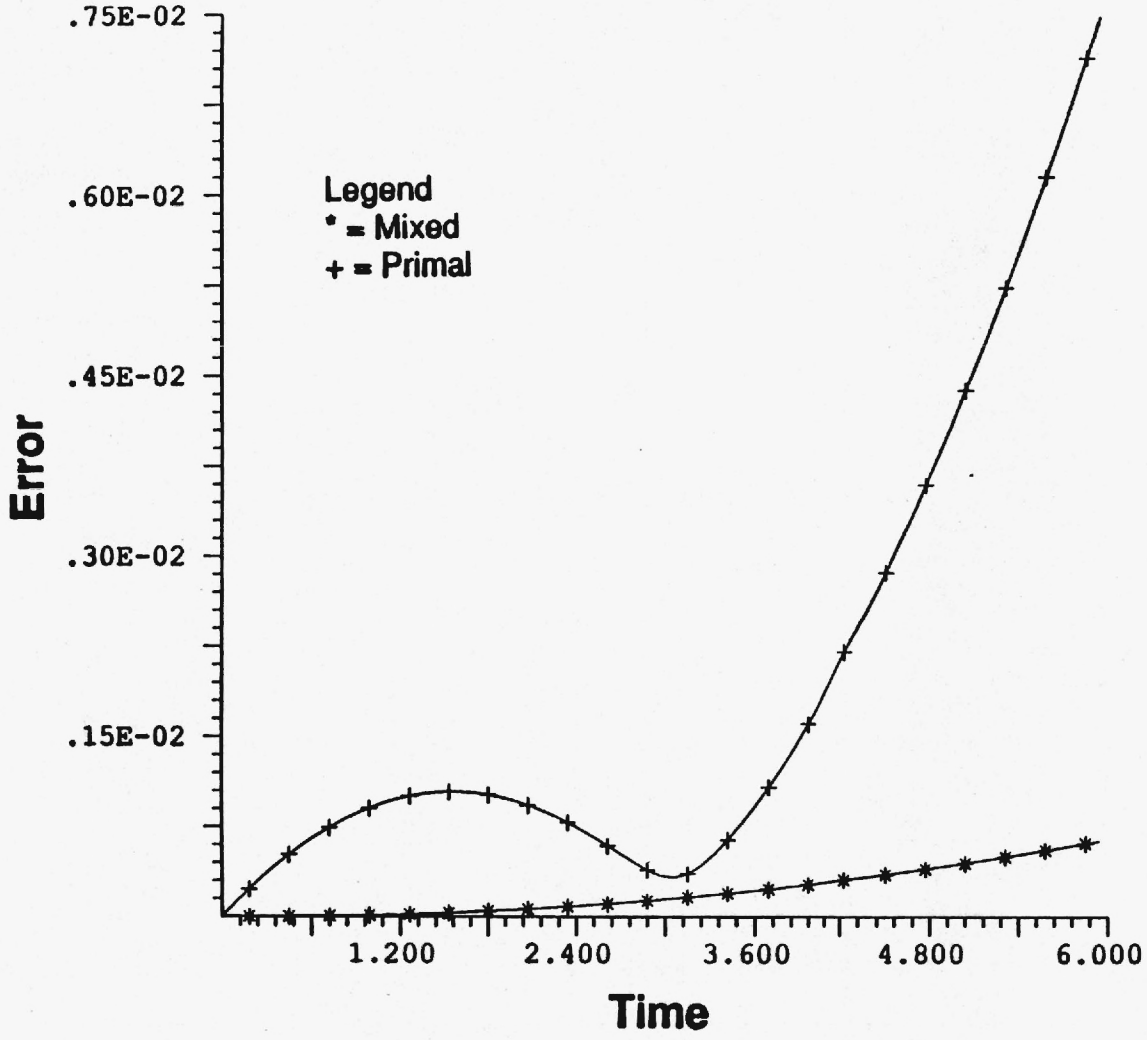

Figure 5: Absolute Error 4 Noded Elements

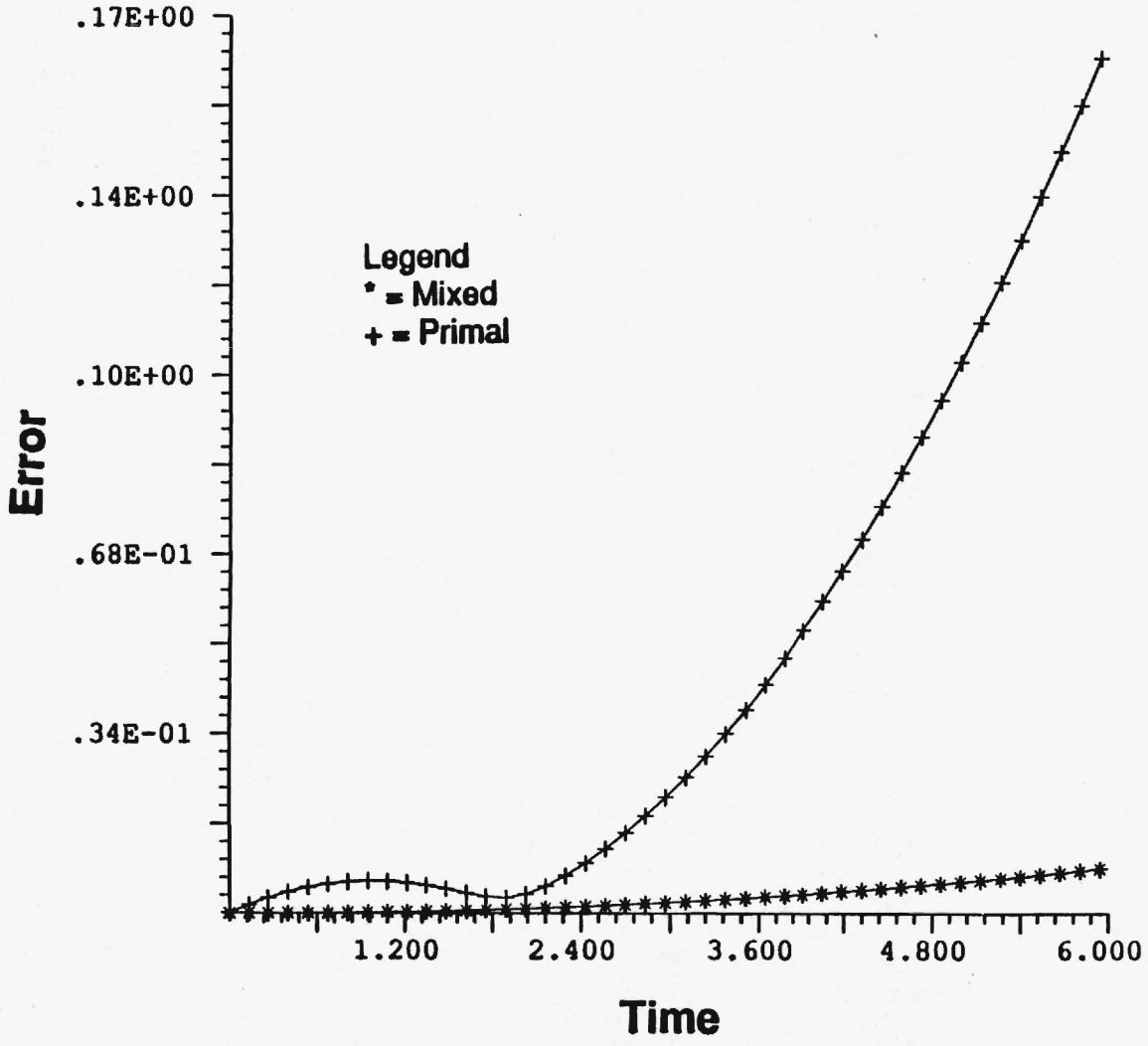

TIME FINITE ELEMENT METHODS FOR LARGE ROTATIONAL DYNAMICS OF MULTIBODY SYSTEMS

F. J. Mello M. Borri S. N. Atluri

Center for Computational Mechanics

School of Civil Engineering

Georgia Institute of Technology

Atlanta, GA 30332

ABSTRACT

Weak formulations in Analytical Dynamics are developed, paralleling the variational methods in elastostatics, and including a fundamental yet novel approach for treating constraints (both holonomic and nonholonomic). A general three field approach is presented, in which the momentum balance conditions, the compatibility conditions between displacement and velocity, the constitutive relations and the displacement and momentum boundary conditions are all enforced in weak form. A primal, or kinematic formulation is developed from the general form by enforcing the compatibility conditions and displacement boundary conditions *a priori*. The conditonal stability of the kinematic formulation is the counterpart of the locking phenomenon in elastostatics and may be avoided, either by reduced order integration, or by utilizing a mixed formulation. Toward this end, a two field mixed formulation

is presented, which follows from the general form, when the constitutive relations are satisfied *a priori*. A general set of the constraint equations are introduced into the kinematic and mixed formulations, using a specific choice of multipliers, which results in modified variational principles. Several simple examples concerning rigid body dynamics are presented.

NOMENCLATURE

Most of the symbols use in this paper are defined in context and discussed in more detail in our previous work [1,2]. A brief summary is given here.

$\boldsymbol{f}$	—	generalized external force
H	—	Hamiltonian
$\mathcal{L}$	—	Lagrangian
$\boldsymbol{p}$	—	generalized momentum
$\boldsymbol{q}$	—	generalized coordiantes
$\boldsymbol{R}$	—	rotation tensor
$\boldsymbol{v}$	—	generalized velocity
$\boldsymbol{x}$	—	mass center position coordinates
$\boldsymbol{\theta}_\delta$	—	virtual rotation, $\boldsymbol{\theta}_\delta \times \boldsymbol{I} = \delta \boldsymbol{R} \cdot \boldsymbol{R}^t$
$\boldsymbol{\theta}_\mathrm{d}$	—	incremental rotation, $\boldsymbol{\theta}_\mathrm{d} \times \boldsymbol{I} = \mathrm{d}\boldsymbol{R} \cdot \boldsymbol{R}^t$
$\boldsymbol{\mu}$	—	constraint multipliers
$\boldsymbol{\omega}$	—	angular velocity, $\boldsymbol{\omega} \times \boldsymbol{I} = \dot{\boldsymbol{R}} \cdot \boldsymbol{R}^t$

Subscripts on these symbols indicate an association with a particular body, or identify boundary quatities.

INTRODUCTION

Recently there has been a renewed interest in the study of multibody dynamics and its application to a wide variety of engineering problems. The nonlinear equations of motion, in explicit form are quite complex, due to the expression for absolute

acceleration. These complexities are avoided, if a weak formulation is employed. The priciple of virtual work, or Hamilton's principle, is one such weak formulation. There has been much discussion in the literature [3,4,5], concerning Hamilton's principle as a starting point for the numerical solution of dynamics problems. Much of this discussion involves the conditions under which Hamilton's principle may be stated as the stationarity condition of a scalar functional. Due to the unsymmetric character of initial value problems, the governing equations are not expressible as such a condition. This fact in no way deminishes the usefullness of variational approaches for initial value problems. In fact, drawing on the mature literature concerning variational methods in solid mechanics, very general weak forms can be developed for dynamic systems, the most general being analogous to a Hu - Washizu type formulation. The principle of virtual work is obtainable from the general weak form by satisfying displacement compatibility and the displacement boundary conditions *a priori*. A Hamiltonian, or complementary energy approach, is obtained by satisfying the constitutive relations between momentum and velocity *a priori*.

In two previous papers [1,2], simple, single rigid body problems were used to demonstrate the validity of the primal and mixed formulations, for both holonomic and nonholonomic constraints. These example problems, which have either exact solutions, or well known behavior, have shown the primal and mixed forms to be accurate numerical methods. In this paper, the highlights of the previous work will be briefly sketched out. We will then discuss the linearization of three common constraints, which may be used to construct multibody systems.

The formation and assembly of the tangent matrices and residual vectors for each body may be carried out without regard for the adjacent bodies, or the characteristics of any joints. In this sense, the multibody problem is no more difficult than the

single body case. The expressions for constraint residual vectors and tangent matices developed here are combined with those developed in [1], for unconstrained rigid bodies and several multibody examples are solved. We will assess the behavior of the method by considering the two bar system shown in Figure 1. Bar 1 is connected by means of a spherical joint to the fixed datum. Bar 2 is connected to bar 1 by one of the three joint types (spherical, universal or revolute). The results for this simple system, can be judged intuitively.

Finally, the two dimesional case of a fifteen bar linkage, treated by Kamman and Huston [6], is cosidered for comparison.

One practical complication of multibody problems, as compared with the single body case, is the data structure. In the multibody dynamics literature, there are many references to the Wittenberg - Roberson formalism [7]. The idea of a directed graph, or node to datum array, is an important part of this formalism, since it defines the path from any given body in the system to the reference body. Clearly, this is central to formulating equations of motion in relative joint coordinates. In the relative joint coordinate approach, the position of a body is described in terms of the position of its master (the previous body in the node to datum array). The position of the slave body is completely described, relative to its master, by n coordinates, where n is the number of degrees of freedom allowed by the connection between the bodies. This process results in the minimum number of equations, but is not well suited for systems with closed loops. Relative joint coordinates are typically applied to systems with open chain, or tree configurations. Formulating equations of motion for closed loop systems by relative joint coordinates, requires releasing a sufficient number of connections, in order to form a tree configuration, and then imposing the loop closure conditions as constraints.

The approach taken here accounts for all constraints by the use of multipliers. Six degrees of freedom are added to the number of global degrees of freedom for each body of the system. Treating the constraints individually, their tangent matrices and residual vectors may be calculated and assembled. For each joint, there is a multiplier corresponding to each constrained degree of freedom. Consequently, the system of equations which must be solved is much larger than in the relative joint coordinate approach. The anticipated benefit of this method is, that in a parallel computing environment, all of the matrix formation and assembly for the bodies, and the connections, may be done concurrently. The resulting system of equations is highly structured and very sparse. A diagram showing this structure is presented in Figure 2. This system may then be solved using techniques which exploit the structure and sparsity, or various coordinate reduction techniques may be applied to the assembled system of equations [8-12].

WEAK FORMULATIONS IN ANALYTICAL DYNAMICS

Let us consider a dynamical system with generalized coordinates $\boldsymbol{q}$, acted upon by a generalized external load $\boldsymbol{f}$. We denote the Lagrangian of the system by $\mathcal{L}$, regarded as a function of the coordinates, $\boldsymbol{q}$, the velocities $\boldsymbol{v}$ and time t.

The equations of motion:

$$\boldsymbol{f} + \frac{\partial \mathcal{L}}{\partial \boldsymbol{q}} - \dot{\boldsymbol{p}} = 0 \tag{2.1}$$

the conditions of compatibility and the constitutive relations:

$$\boldsymbol{v} = \dot{\boldsymbol{q}} \qquad\qquad \boldsymbol{p} = \frac{\partial \mathcal{L}}{\partial v} \tag{2.2}$$

the displacement and momentum boundary conditions:

$$q(t_k) = q_k \qquad p(t_k) = p_k \qquad k = 1,2 \tag{2.3}$$

can be combined in the following weak form:

$$\begin{aligned}\int_{t_1}^{t_2} \left\{ \left(f + \frac{\partial \mathcal{L}}{\partial q} - \dot{p} \right) \cdot \delta q - \left(v - \dot{q} \right) \cdot \delta p - \left(p - \frac{\partial \mathcal{L}}{\partial v} \right) \cdot \delta v \right\} \mathrm{d}t = \\ [(p(t_2) - p_2) \cdot \delta q(t_2) - (q(t_2) - q_2) \cdot \delta p(t_2)] - \\ [(p(t_1) - p_1) \cdot \delta q(t_1) - (q(t_1) - q_1) \cdot \delta p(t_1)]\end{aligned} \tag{2.4}$$

which has no subsidiary conditions. Integrating by parts, the terms explicitly involving time derivatives, Eq.(2.4) may be simplified as:

$$\int_{t_1}^{t_2} \left\{ \delta \left(\mathcal{L} - p \cdot v \right) + f \cdot \delta q + \delta \dot{q} \cdot p - \delta \dot{p} \cdot q \right\} \mathrm{d}t = \left[p_b \cdot \delta q - q_b \cdot \delta p \right]_{t_1}^{t_2} \tag{2.5}$$

where $b = 1$ for $t = t_1$ and $b = 2$ for $t = t_2$. This result is analogous to the Hu-Washizu (general 3 field) form [13]. Each of the variables, q, v, and p, appear as independent fields and have no continuity requirements at the time boundaries. The test functions δp and δq, however must be differentiable on the interval and continuous at the boundary.

The Principle of Virtual Work is obtained from the three field form when the compatibility conditions and displacement boundary conditions are satisfied *a priori*. Moreover, the momentum field may be eliminated from the domain integral assuming the compatibility conditions are also satisfied for the test functions, i.e.: $\delta v = \delta \dot{q}$. In this way we obtain:

$$\int_{t_1}^{t_2} (\delta \mathcal{L} + f \cdot \delta q) \mathrm{d}t = p_b \cdot \delta q \Big|_{t_1}^{t_2} \tag{2.6}$$

This expression corresponds to Hamilton's principle in configuration space, having only one independent field in the domain (q). Equation (2.6) is referred to as the

primal, or kinematic form of Hamilton's principle, and has been successfully applied to mechanical systems and periodic problems [14,15].

As with the locking phenomenon, which is well known in elasto-statics of volumetrically rigid media or shear rigid thin plates, typical of kinematic formulations, the kinematic form of Hamilton's principle is conditionally stable [2]. We can avoid the resulting restriction on the time step, either through selective reduced integration, or by utilizing a mixed formulation. In fact, if we choose to satisfy the constitutive relations *a priori*, we may eliminate the velocity as a function of the momentum, and a two field mixed form is obtained. This is accomplished through a Legendre transformation, introducing the Hamiltonian function, $H(\boldsymbol{p},\boldsymbol{q},t) = \boldsymbol{p}\cdot\boldsymbol{v} - \mathcal{L}(\boldsymbol{v},\boldsymbol{q},t)$, in which $\boldsymbol{v} = \boldsymbol{v}(\boldsymbol{p},\boldsymbol{q},t)$ is understood. Then the two field mixed form involving $\boldsymbol{p}$ and $\boldsymbol{q}$ may be written as:

$$\int_{t_1}^{t_2} \left\{ -\delta H + \boldsymbol{f}\cdot\delta\boldsymbol{q} + \delta\,\dot{\boldsymbol{q}}\cdot\boldsymbol{p} - \delta\,\dot{\boldsymbol{p}}\cdot\boldsymbol{q} \right\} \mathrm{d}t = \left[\boldsymbol{p}_b\cdot\delta\boldsymbol{q} - \boldsymbol{q}_b\cdot\delta\boldsymbol{p}\right]_{t_1}^{t_2} \tag{2.7}$$

In this form $\boldsymbol{p}$ and $\boldsymbol{q}$ are treated as coordinates in the phase space, and are not required to be differentiable. It is important to note that since the test and the trial functions have different continuity requirements, the test functions $\delta\boldsymbol{p}$ and $\delta\boldsymbol{q}$ are properly understood to be weighting functions, independent of the variations of $\boldsymbol{p}$ and $\boldsymbol{q}$. The numerical implementation of this mixed form is unconditionally stable. The stability behavior of the primal and mixed forms is illustrated in a previous paper [2].

WEAK FORM OF CONSTRAINTS

For the purposes of illustration, we consider only the kinematic and two field mixed forms, and the class of constraints which can be expressed as:

$$\boldsymbol{\psi}(\dot{\boldsymbol{q}},\boldsymbol{q},t) = \mathbf{A}(\boldsymbol{q},t)\cdot\dot{\boldsymbol{q}} + \boldsymbol{a}(\boldsymbol{q},t) = 0 \tag{3.1}$$

If calculating the work of constraint forces is to be avoided, the following constraint on the virtual displacements must be enforced.

$$\mathbf{A} \cdot \delta \boldsymbol{q} = 0 \tag{3.2}$$

Equation (3.1) can be either nonholomonic, or the time derivative of a holonomic constraint. In order to enforce Eq.(3.8) and Eq.(3.9), we cast them in weak form, with a convenient choice of test functions. Let $\boldsymbol{\mu}$ be the Lagrange multipliers. We then weight Eq.(3.8) with the variation $\delta\boldsymbol{\mu}$ and Eq.(3.9) with the time derivative $\dot{\boldsymbol{\mu}}$, obtaining:

$$\int_{t_1}^{t_2} \left(\delta \boldsymbol{\mu} \cdot \boldsymbol{\psi} - \dot{\boldsymbol{\mu}} \cdot \frac{\partial \boldsymbol{\psi}}{\partial \dot{\boldsymbol{q}}} \cdot \delta \boldsymbol{q} \right) \mathrm{d}t = 0 \tag{3.3}$$

The benefit of this form is that it allows an integration by parts that reduces the continuity requirements for the Lagrangian multipliers. Combining Eq.(3.10) with the kinematic form, Eq.(2.6), we obtain a modified form:

$$\int_{t_1}^{t_2} (\delta \bar{\mathcal{L}} + \delta \boldsymbol{q} \cdot \bar{\boldsymbol{f}}) \mathrm{d}t = \delta \boldsymbol{q} \cdot \bar{\boldsymbol{p}}_b |_{t_1}^{t_2} \tag{3.4}$$

where:

$$\bar{\mathcal{L}} = \mathcal{L} + \boldsymbol{\mu} \cdot \boldsymbol{\psi} \qquad \bar{\boldsymbol{p}} = \boldsymbol{p} + \boldsymbol{\mu} \cdot \frac{\partial \boldsymbol{\psi}}{\partial \dot{\boldsymbol{q}}} \qquad \bar{\boldsymbol{f}} = \boldsymbol{f} + \boldsymbol{f}_c \tag{3.5}$$

and $\boldsymbol{f}_c = \boldsymbol{\mu} \cdot \left(\frac{\mathrm{d}}{\mathrm{d}t} \frac{\partial \boldsymbol{\psi}}{\partial \dot{\boldsymbol{q}}} - \frac{\partial \boldsymbol{\psi}}{\partial \boldsymbol{q}} \right)$. The Eq.(3.12) is the modified Hamilton's principle for the constrained systems and $\bar{\mathcal{L}}$, $\bar{\boldsymbol{p}}$, $\bar{\boldsymbol{f}}$ are respectively the modified Lagrangian function, the modified generalized momenta and the external forces modified by the reactions due to the nonholonomic constraints [9]. The constraint reactions, $\boldsymbol{f}_c$, are just the weighted integrability conditions of the constraint equations.

It is interesting to note that $\bar{\boldsymbol{p}}$ are the generalized momenta associated with the modified Lagrangian. In fact, it can easily be seen that $\bar{\boldsymbol{p}} = \dfrac{\partial \bar{\mathcal{L}}}{\partial \dot{\boldsymbol{q}}}$. We can then define the modified Hamiltonian function as, $\bar{H} = \bar{\boldsymbol{p}} \cdot \dot{\boldsymbol{q}} - \bar{\mathcal{L}}$ and obtain a mixed form,

following the procedure discussed in the preceding section:

$$\int_{t_1}^{t_2}(-\delta\bar{H}+\delta\boldsymbol{q}\cdot\bar{\boldsymbol{f}}+\delta\dot{\boldsymbol{q}}\cdot\bar{\boldsymbol{p}}-\delta\dot{\bar{\boldsymbol{p}}}\cdot\boldsymbol{q})\mathrm{d}t=(\delta\boldsymbol{q}\cdot\bar{\boldsymbol{p}}_b-\delta\bar{p}\cdot q_b)|_{t_1}^{t_2} \tag{3.6}$$

The modified momenta $\bar{\boldsymbol{p}}$, the generalized coordinates $\boldsymbol{q}$, and the multipliers $\boldsymbol{\mu}$, are the independent fields in this formulation. The true momenta may be recovered from the modified momenta by a projection.

In the numerical examples that follow, we will make use of three common constraint types; the spherical, universal and revolute joints. These are shown in Figures 3, 4 and 5, respectively.

Spherical Joint

The spherical joint constraint is closely related to the suspension point constraint for the top, which was considered in [2]. The difference is, that the connection point of the spherical joint is not fixed. Figure 3 shows a spherical joint. The location of the connection point, relative to the mass centers of the two connected bodies, is described by position vectors $\boldsymbol{\rho}_1$ and $\boldsymbol{\rho}_2$, respectively. The constraint, which must be satisfied in order for the joint to stay connected, is:

$$\dot{\boldsymbol{x}}_1-\boldsymbol{\rho}_1\times\boldsymbol{\omega}_1=\dot{\boldsymbol{x}}_2-\boldsymbol{\rho}_2\times\boldsymbol{\omega}_2 \tag{3.7}$$

The constraint on virtual displacement is then :

$$\delta\boldsymbol{x}_1-\boldsymbol{\rho}_1\times\boldsymbol{\theta}_{\delta 1}=\delta\boldsymbol{x}_2-\boldsymbol{\rho}_2\times\boldsymbol{\theta}_{\delta 2} \tag{3.8}$$

Following the procedure outline above, the residual vector and tangent matrix for the constraint are calculated. The combined weak form for each side of the constraint equation is:

$$\int_{t_1}^{t_2}\delta\boldsymbol{\mu}\cdot\left(\dot{\boldsymbol{x}}-\boldsymbol{\rho}\times\boldsymbol{\omega}\right)-\dot{\boldsymbol{\mu}}\cdot(\delta\boldsymbol{x}-\boldsymbol{\rho}\times\boldsymbol{\theta}_\delta)\,\mathrm{d}t \tag{3.9}$$

Subscripts are omitted, but it is understood this expression must be evaluated for each of the bodies attached at the joint. The difference in these results is the residual vector. Integrating by parts the term involving $\dot{\boldsymbol{\mu}}$, leads to:

$$\int_{t_1}^{t_2} \delta\boldsymbol{\mu} \cdot \left(\dot{\boldsymbol{x}} - \boldsymbol{\rho} \times \boldsymbol{\omega}\right) + \boldsymbol{\mu} \cdot \left(\delta\, \dot{\boldsymbol{x}} - \boldsymbol{\rho} \times \dot{\boldsymbol{\theta}}_\delta - \dot{\boldsymbol{\rho}} \times \boldsymbol{\theta}_\delta\right) \mathrm{d}t = \boldsymbol{\mu} \cdot (\delta \boldsymbol{x} - \boldsymbol{\rho} \times \boldsymbol{\theta}_\delta) \Big|_{t_1}^{t_2} \tag{3.10}$$

The terms under the integral in Eq.(3.10) constitute the residual vector.

$$\left\{\left(\dot{\boldsymbol{x}} - \boldsymbol{\rho} \times \boldsymbol{\omega}\right), \boldsymbol{\mu}, (\boldsymbol{\rho} \times \boldsymbol{\mu}), 0, \left(\dot{\boldsymbol{\rho}} \times \boldsymbol{\mu}\right)\right\} \tag{3.11}$$

where the organization of the test functions is $(\delta\boldsymbol{\mu}, \delta\dot{\boldsymbol{x}}, \dot{\boldsymbol{\theta}}_\delta, \delta\boldsymbol{x}, \boldsymbol{\theta}_\delta)$. It should be noted that the test functions are expressed in "quasi-coordinates". Since the incremental solution process must use true coordinates for the trial functions, the associated tangent matrix will be unsymmetric. The linearization process is more easily accomplished by using "quasi-coordinates" and later tranforming the matrix to involve true coordinates, as discussed in [1,2].

The tangent matrix for this constraint is obtained by linearizing the residual vector. The following identities are discussed in Appendix A of [1], and are repeated here for convenience.

$$\mathrm{d}\boldsymbol{\rho} = \boldsymbol{\theta}_\mathrm{d} \times \boldsymbol{\rho} = -\boldsymbol{\rho} \times \boldsymbol{\theta}_\mathrm{d} \tag{3.12}$$

$$\dot{\boldsymbol{\rho}} = \boldsymbol{\omega} \times \boldsymbol{\rho} \tag{3.13}$$

$$\mathrm{d}\,\dot{\boldsymbol{\rho}} = \dot{\boldsymbol{\theta}}_\mathrm{d} \times \boldsymbol{\rho} + \boldsymbol{\theta}_\mathrm{d} \times \dot{\boldsymbol{\rho}} = -\boldsymbol{\rho} \times \dot{\boldsymbol{\theta}}_\mathrm{d} - \dot{\boldsymbol{\rho}} \times \boldsymbol{\theta}_\mathrm{d} \tag{3.14}$$

$$\mathrm{d}\boldsymbol{\omega} = \dot{\boldsymbol{\theta}}_\mathrm{d} - \boldsymbol{\omega} \times \boldsymbol{\theta}_\mathrm{d} \tag{3.15}$$

With these relations in mind, we may perform the linearization. Linearizing the first group of terms in Eq.(3.11), corresponding to the test functions $\delta\boldsymbol{\mu}$, leads to:

$$\delta\boldsymbol{\mu} \cdot \left(\mathrm{d}\,\dot{\boldsymbol{x}} - \mathrm{d}\boldsymbol{\rho} \times \boldsymbol{\omega} - \boldsymbol{\rho} \times \mathrm{d}\boldsymbol{\omega}\right) \tag{3.16}$$

which, in view of the above identities, simplifies to:

$$\delta\mu \cdot [\boldsymbol{I}, (\rho \times \boldsymbol{I}), (\rho \times \omega) \times \boldsymbol{I}] \cdot \left\{ \begin{array}{c} \mathrm{d}\,\dot{\boldsymbol{x}} \\ \dot{\theta}_{\mathrm{d}} \\ \theta_{\mathrm{d}} \end{array} \right\} \tag{3.17}$$

Similarly, the second group of terms in the residual vector, corresponding to the test functions $\delta\,\dot{\boldsymbol{x}}$, lead to:

$$\delta\,\dot{\boldsymbol{x}} \cdot \boldsymbol{I} \cdot \mathrm{d}\mu \tag{3.18}$$

The terms involving the test functions $\dot{\theta}_{\delta}$ linearize as:

$$\dot{\theta}_{\delta} \cdot (\mathrm{d}\rho \times \mu + \rho \times \mathrm{d}\mu) \tag{3.19}$$

which reduces to:

$$\dot{\theta}_{\delta} \cdot [\rho \times \boldsymbol{I}, \mu \times \rho \times \boldsymbol{I}] \cdot \left\{ \begin{array}{c} \mathrm{d}\mu \\ \theta_{\mathrm{d}} \end{array} \right\} \tag{3.20}$$

Finally, the last group of terms in the residual vector leads to:

$$\theta_{\delta} \cdot \left(\mathrm{d}\,\dot{\rho} \times \mu + \dot{\rho} \times \mathrm{d}\mu\right) \tag{3.21}$$

which may be written as:

$$\theta_{\delta} \cdot \left[\dot{\rho} \times \boldsymbol{I}, \mu \times \rho \times \dot{\theta}_{\mathrm{d}}, \mu \times \dot{\rho} \times \boldsymbol{I}\right] \cdot \left\{ \begin{array}{c} \mathrm{d}\mu \\ \dot{\theta}_{\mathrm{d}} \\ \theta_{\mathrm{d}} \end{array} \right\} \tag{3.22}$$

Combining these relations provides the tangent matrix for the constraint.

$$\mathcal{T} = \begin{bmatrix} 0 & \boldsymbol{I} & -\rho \times \boldsymbol{I} & 0 & -\dot{\rho} \times \boldsymbol{I} \\ \boldsymbol{I} & 0 & 0 & 0 & 0 \\ \rho \times \boldsymbol{I} & 0 & 0 & 0 & \mu \times \rho \times \boldsymbol{I} \\ 0 & 0 & 0 & 0 & 0 \\ \dot{\rho} \times \boldsymbol{I} & 0 & \mu \times \rho \times \boldsymbol{I} & 0 & \mu \times \dot{\rho} \times \boldsymbol{I} \end{bmatrix} \tag{3.23}$$

Lastly, this tangent matrix must be transformed so that the linearization involves increments of true coordinates. This transformation is discussed in [2] and is not repeated here.

The spherical joint forms the basis for the other two joints considered below.

Universal Joint

Next, the universal joint depicted in Figure 4 is considered. The joint consists of a spherical joint, with the additional constraint that the unit vectors $\boldsymbol{i}$ and $\boldsymbol{j}$, shown in the figure, remain perpendicular throughout the motion. These vectors are fixed in bodies 1 and 2, respectively. This constraint can be written concisely as:

$$(\boldsymbol{R}_1 \cdot \boldsymbol{i}) \cdot (\boldsymbol{R}_2 \cdot \boldsymbol{j}) = 0 \tag{3.24}$$

where $\boldsymbol{R}_1$ and $\boldsymbol{R}_2$, denote the rotations of bodies 1 and 2, respectively. Using the definitions of the angular velocities of bodies 1 and 2, this constraint may be expressed in differential form as:

$$[(\boldsymbol{\omega}_1 \times \boldsymbol{I}) \cdot \boldsymbol{R}_1 \cdot \boldsymbol{i}] \cdot [\boldsymbol{R}_2 \cdot \boldsymbol{j}] + [\boldsymbol{R}_1 \cdot \boldsymbol{i}] \cdot [(\boldsymbol{\omega}_2 \times \boldsymbol{I}) \cdot \boldsymbol{R}_2 \cdot \boldsymbol{j}] = 0 \tag{3.25}$$

Letting $\boldsymbol{i}' = \boldsymbol{R}_1 \cdot \boldsymbol{i}$ and $\boldsymbol{j}' = \boldsymbol{R}_2 \cdot \boldsymbol{j}$, Eq.(3.32) takes on the simpler form:

$$(\boldsymbol{i}' \times \boldsymbol{j}') \cdot \boldsymbol{\omega}_1 - (\boldsymbol{i}' \times \boldsymbol{j}') \cdot \boldsymbol{\omega}_2 = 0 \tag{3.26}$$

The constraint on virtual displacements is then:

$$(\boldsymbol{i}' \times \boldsymbol{j}') \cdot \boldsymbol{\theta}_{\delta 1} - (\boldsymbol{i}' \times \boldsymbol{j}') \cdot \boldsymbol{\theta}_{\delta 2} = 0 \tag{3.27}$$

Again, the constraint Eq.(3.33) is weighted with the variation of the multiplier $\delta\mu$, while Eq.(3.34) is weighted with the time derivative $\dot{\mu}$. Combining these weak forms and performing the integration by parts, leads to:

$$\begin{aligned} \int_{t_1}^{t_2} \delta\mu \cdot \boldsymbol{A} \cdot (\boldsymbol{\omega}_1, \boldsymbol{\omega}_2) + \frac{\mathrm{d}}{\mathrm{dt}}(\boldsymbol{\theta}_{\delta 1}, \boldsymbol{\theta}_{\delta 2}) \cdot \boldsymbol{A}^t \cdot \mu + (\boldsymbol{\theta}_{\delta 1}, \boldsymbol{\theta}_{\delta 2}) \cdot \dot{\boldsymbol{A}}^t \cdot \mu \, \mathrm{d}t \\ = (\boldsymbol{\theta}_{\delta 1}, \boldsymbol{\theta}_{\delta 2}) \cdot \boldsymbol{A}^t \cdot \mu \, |_{t_1}^{t_2} \end{aligned} \tag{3.28}$$

where $A = (i' \times j', -i' \times j')$.

If the test functions are arranged as $(\delta\mu,\ \dot{\theta}_{\delta 1},\ \theta_{\delta 1},\ \dot{\theta}_{\delta 2},\ \theta_{\delta 2}\ )$, then the residual vector may be written as:

$$\left\{ \begin{array}{c} (i' \times j') \cdot \omega_1 - (i' \times j') \cdot \omega_2 \\ (i' \times j')\mu \\ ((\omega_1 \times i') \times j' + i' \times \omega_2 \times j')\,\mu \\ -(i' \times j')\mu \\ ((\omega_2 \times j') \times i' + j' \times \omega_1 \times i')\,\mu \end{array} \right\} \tag{3.29}$$

The fact that i is fixed with respect to body 1, and j is fixed relative to body 2, has been used to express $\dot{i}' = \omega_1 \times i'$ and $\dot{j}' = \omega_2 \times j'$. Similarly, the virtual changes in i' and j', are given as $\delta i' = \theta_{\delta 1} \times i'$ and $\delta j' = \theta_{\delta 2} \times j'$, respectively. The linearization of this residual vector is tedious, but straightforward. The resulting tangent matrix may be verified to be:

$$\left[\begin{array}{c|c|c|c|c} 0 & \mu(j' \times i' \times I) & 0 & -\mu(i' \times j' \times I) & i' \times j' \\ \hline \mu(j' \times i' \times I) & C_1 & -\mu(i' \times j' \times I) & C_2 & C_3 \\ \hline 0 & -\mu(j' \times i' \times I) & 0 & \mu(i' \times j' \times I) & -i' \times j' \\ \hline -\mu(j' \times i' \times I) & -C_1 & \mu(i' \times j' \times I) & -C_2 & C_4 \\ \hline i' \times j' & C_5 & -i' \times j' & C_6 & 0 \end{array} \right] \tag{3.30}$$

where:

$$C_1 = \left[\begin{array}{c} j' \times \omega_1 \times i' \times I \\ -j' \times i' \times \omega_1 \times I \\ +(\omega_2 \times j') \times i' \times I \end{array} \right] \tag{3.31}$$

$$C_2 = \begin{bmatrix} -i' \times \omega_2 \times j' \times I \\ +i \times j' \times \omega_2 \times I \\ -(\omega_1 \times i') \times j' \times I \end{bmatrix} \tag{3.32}$$

$$C_3 = \begin{bmatrix} (\omega_1 \times i') \times j' + \\ i' \times \omega_2 \times j' \end{bmatrix} \qquad C_4 = \begin{bmatrix} (\omega_2 \times j') \times i' + \\ j' \times \omega_1 \times i' \end{bmatrix} \tag{3.33}$$

$$C_5 = \begin{bmatrix} j' \times i' \times (\omega_1 - \omega_2) \\ +\omega_1 \times i' \times j' \end{bmatrix} \qquad C_6 = \begin{bmatrix} i' \times j' \times (\omega_2 - \omega_1) \\ +\omega_2 \times j' \times i' \end{bmatrix} \tag{3.34}$$

Revolute Joint

The last joint type which will be considered here is the revolute joint, depicted in Figure 5. The constraint provided by this joint is that the relative rotation between body 1 and body 2 must be about the axis of the joint. In order to describe the constraint, the vectors i, j and k shown in Figure 5, are defined as follows. The vector i is fixed in body 1, and is the unit vector normal to the plane defined by the hinge axis and the center of mass of body 1. Vector j is then defined to be a unit vector normal to the plane of the hinge axis and i, and is fixed in body 1. The unit vector along the axis of the hinge is k, but will be associated with body 2. The revolute joint constraint may then be expressed as a sperical joint, with the additional constraints that:

$$k \cdot i = 0 \qquad \text{and} \qquad k \cdot j = 0 \tag{3.35}$$

In differential form, these two constraint equations are:

$$\begin{aligned} (\omega_2 \times k) \cdot i + k \cdot (\omega_1 \times i) = 0 \\ (\omega_2 \times k) \cdot i + k \cdot (\omega_1 \times i) = 0 \end{aligned} \tag{3.36}$$

which, in matrix form, appears as:

$$\begin{bmatrix} i \times k & -i \times k \\ j \times k & -j \times k \end{bmatrix} \cdot \begin{Bmatrix} \omega_1 \\ \omega_2 \end{Bmatrix} = 0 \tag{3.37}$$

The matrix in Eq.(3.44) is the A matrix of Eq.(3.8), for this constraint. The weak form of the constraint, after carrying out the integration by parts, is then:

$$\begin{aligned} &\int_{t_1}^{t_2} \delta\mu \cdot \mathbf{A} \cdot (\omega_1, \omega_2) + \mu \cdot \dot{\mathbf{A}} \cdot (\theta_{\delta 1}, \theta_{\delta 2}) + \mu \cdot \mathbf{A} \cdot (\dot{\theta}_{\delta 1}, \dot{\theta}_{\delta 2})\, \mathrm{d}t \\ &\qquad = (\theta_{\delta 1}, \theta_{\delta 2}) \cdot \mathbf{A}^t \cdot \mu \Big|_{t_1}^{t_2} \end{aligned} \tag{3.38}$$

where the matrix $\dot{\mathbf{A}}$ is given by:

$$\dot{\mathbf{A}} = \begin{bmatrix} (\omega_1 \times i) \times k + i \times \omega_2 \times k & -(\omega_1 \times i) \times k - i \times \omega_2 \times k \\ (\omega_1 \times j) \times k + j \times \omega_2 \times k & -(\omega_1 \times j) \times k - j \times \omega_2 \times k \end{bmatrix} \tag{3.39}$$

The residual vector, in this case, may then be written as:

$$\begin{Bmatrix} \mu_1(i \times k) + \mu_2(j \times k) \\ \mu_1(k \times i \times (\omega_1 - \omega_2)) + \mu_2(k \times j \times (\omega_1 - \omega_2)) \\ -\mu_1(i \times k) - \mu_2(j \times k) \\ -\mu_1(k \times i \times (\omega_1 - \omega_2)) - \mu_2(k \times j \times (\omega_1 - \omega_2)) \\ (i \times k) \cdot (\omega_1 - \omega_2) \\ (j \times k) \cdot (\omega_1 - \omega_2) \end{Bmatrix} \tag{3.40}$$

The organization of the test functionsm is; $\dot{\theta}_{\delta 1}$, $\theta_{\delta 1}$, $\dot{\theta}_{\delta 2}$, $\theta_{\delta 2}$ and $\delta\mu$. Again, linearization of this residual vector leads to the tangent matrix for the revolute joint.

$$
\begin{bmatrix}
0 & \mathcal{D}_1 & 0 & -\mathcal{D}_2 & \begin{bmatrix} i \times k \\ j \times k \end{bmatrix}^t \\
\mathcal{D}_1 & \mathcal{D}_3 & -\mathcal{D}_1 & \mathcal{D}_4 & \begin{bmatrix} k \times i \times (\omega_1 - \omega_2) \\ k \times j \times (\omega_1 - \omega_2) \end{bmatrix}^t \\
0 & -\mathcal{D}_1 & 0 & \mathcal{D}_2 & -\begin{bmatrix} i \times k \\ j \times k \end{bmatrix}^t \\
-\mathcal{D}_1 & -\mathcal{D}_3 & \mathcal{D}_1 & -\mathcal{D}_4 & -\begin{bmatrix} k \times i \times (\omega_1 - \omega_2) \\ k \times j \times (\omega_1 - \omega_2) \end{bmatrix}^t \\
\begin{bmatrix} i \times k \\ j \times k \end{bmatrix} & \mathcal{D}_5 & -\begin{bmatrix} i \times k \\ j \times k \end{bmatrix} & \mathcal{D}_6 & 0
\end{bmatrix} \tag{3.41}
$$

where the submatrices $\mathcal{D}_1$, $\mathcal{D}_2$, $\mathcal{D}_3$ $\mathcal{D}_4$, $\mathcal{D}_5$, $\mathcal{D}_6$ are given by:

$$
\mathcal{D}_1 = \begin{bmatrix} \mu_1(k \times i \times I) \\ +\mu_2(k \times j \times I) \end{bmatrix} \qquad \mathcal{D}_2 = \begin{bmatrix} \mu_1(i \times k \times I) \\ +\mu_2(j \times k \times I) \end{bmatrix} \tag{3.42}
$$

$$
\mathcal{D}_3 = \begin{bmatrix} \mu_1(k \times (\omega_1 - \omega_2) \times i \times I - k \times i \times \omega_1 \times I) \\ +\mu_2(k \times (\omega_1 - \omega_2) \times j \times I - k \times j \times \omega_1 \times I) \end{bmatrix} \tag{3.43}
$$

$$
\mathcal{D}_4 = \begin{bmatrix} \mu_1((i \times (\omega_1 - \omega_2)) \times k \times I + k \times i \times \omega_2 \times I) \\ +\mu_2((j \times (\omega_1 - \omega_2) \times k \times I + k \times j \times \omega_2 \times I) \end{bmatrix} \tag{3.44}
$$

$$
\mathcal{D}_5 = \begin{bmatrix} k \times i \times (\omega_1 - \omega_2) \\ +\omega_1 \times i \times k \\ \\ k \times j \times (\omega_1 - \omega_2) \\ +\omega_1 \times j \times k \end{bmatrix} \qquad \mathcal{D}_6 = -\begin{bmatrix} i \times k \times (\omega_1 - \omega_2) \\ -\omega_2 \times i \times k \\ \\ j \times k \times (\omega_1 - \omega_2) \\ -\omega_2 \times j \times k \end{bmatrix} \tag{3.45}
$$

NUMERICAL EXAMPLES

The primal and mixed forms, for holonomic and nonholonomic constraints, have been verified in our previous work [1,2]. Here, we consider several simple numerical examples to illustrate the extension of the approach to multibody systems. Each of the three joints considered in the previous section is verified by a simple two body problem. As an additional check, the degenerate case of a planar linkage is compared with the results presented by Kamman and Huston [6].

For the spherical joint, the procedure for establishing constraint equations is to form and assemble the residual vector and tangent matrix for the first body connected at the joint. Then, the residual vector and tangent matrix are calculated for the second body, and assembled with the opposite sign. So, for each node of the time element, there is a three by twelve constraint matrix, which couples the degrees of freedom of the connected bodies. To test the joint element, the two bar example of Figure 1 has been run, with the problem definition given as:

- Both bars start in a position aligned with the negative y axis.
- The initial velocities are given, in body fixed coordinates, as $\boldsymbol{v}_1 = (2,0,0)$, $\boldsymbol{\omega}_1 = (0,0,4)$ and $\boldsymbol{v}_2 = (6,0,0)$, $\boldsymbol{\omega}_2 = (0,0,4)$.
- The only external force acting on the bars is gravity.

Results for this case are presented in Figures 6, 7 and 8. This problem and the other multibody examples presented, use a three noded primal time finite element. The XY displacement is shown in Figure 6, while the YZ and XZ displacement curves are plotted in Figures 7 and 8, respectively.

As a further check that the program is predicting correct behavior, the same problem was repeated, with the exception that bar 2 was given a high angular velocity, along its axis. Figures 9, 10 and 11 show, respectively, the XY, YZ and XZ displacement for this case. As expected, bar 2 remains very nearly horizontal throughout the motion.

The universal joint has been tested by solving a similar problem. In this case, bar 1 is started in the vertical position, while bar 2 is started in a horizontal position. This example is started with the following initial conditions:

- Bar 1 is aligned with the negative z axis, bar 2 is alligned with the negative y axis.
- The initial velocities are given, in body fixed coordinates, as $\boldsymbol{v}_1 = (0,0,0)$, $\boldsymbol{\omega}_1 = (0,6,0)$ and $\boldsymbol{v}_2 = (3,0,0)$, $\boldsymbol{\omega}_2 = (0,0,6)$.
- The only external force acting on the bars is gravity.

In this situation, one would expect bar 2 to be thrown outward, away from the axis of rotation tending to straighten the linkage. As the bars become more nearly straight, a whirling type motion would result. This is, in fact, the behavior which is observed in the simulation (see Figures 12, 13 and 14).

The revolute joint has been verified in a similar fashion, but the results are not included here. The behavior of the revolute joint is most easily seen by animating the solution.

Finally, we consider the fifteen bar linkage presented by Kamman and Huston [6]. Equations of motion, developed using Kane's method, are used in their simulation. Since this problem is planar, it does not demonstrate the accuracy of a three

dimensional multibody program. However, it does show that the implementation degenerates correctly to the two dimensional case.

The original configuration of the linkage is shown in Figure 15. The linkage consists of fifteen identical bars, connected by spherical joints. Points B and C are released, and the linkage is allowed to fall. The shape of the chain is calculated for times between 0 and 1 second. The input data for this problem are as follows:

$$\begin{array}{lcll} M & = & .4565 \text{ slugs} & = \text{Mass} \\ L & = & 1.0\text{ft.} & = \text{Length} \\ I_t & = & .0308\text{slug} - \text{ft}^2 & = \text{Transverse Inertia} \\ I_a & = & .0001\text{slug} - \text{ft}^2 & = \text{Axial Inertia} \end{array} \tag{3.46}$$

Here, the axial inertia is simply set to any nonzero number. The linkage falls, as shown in Figure 16, and the center link reaches a low point at t=.47 seconds. At this point, the motion reflects and the center bar starts to move upward. The plot of the motion from t=.47 seconds until t=1 second is shown in Figure 17. Figure 18, shows a plot of the vertical displacement of the center bar vs. time. This clearly shows, the reflection point at t=.47, and another point at t=.69, where the bar stops moving up and begins to fall again. These results agree very well with those presented by Kamman and Huston [6].

CONCLUSIONS

Kinematic and mixed forms for dynamics, derived form a very general framework are presented. Multibody simulations are carried out using finite elements in the time domain. A new approach for incorporating constraints is shown to be an effective and general method of enforcing interbody connections.

The intuitive results obtained for the three dimensional motion of the two bar system, coupled with the results for the planar linkage, verify the presented procedures.

ACKNOWLEDGEMENTS

The authors gratefully acknowledge the support of the Air Force Office of Scientific Research.

REFERENCES

1. M. Borri, F. J. Mello and S. N. Atluri. "Variational Approaches for Dynamics and Time - Finite - Elements: Numerical Studies", Computational Mechanics, to appear

2. M. Borri, F. J. Mello and S. N. Atluri. "Primal and Mixed Forms of Hamilton's Principle for Constrained Rigid Body Systems: Numerical Studies", Computational Mechanics, to appear.

3. C. D. Bailey. "Application of Hamilton's Law to Forced, Damped, Stationary Systems", Journal of Sound and Vibration, Vol. 75, pp. 117-126, 1981.

4. M. Baruch and R. Riff. "Hamilton's Principle, Hamilton's Law, 6^n correct formulations", AIAA Journal, Vol. 21, pp. 687-692, 1982.

5. T. E. Simkins. "Finite Element for Initial Value Problems in Dynamics", AIAA Journal, Vol. 13, pp. 1154-1157, 1981.

6. J. W. Kamman and R. L. Huston. "Dynamics of Constrained Multibody Systems", Journal of Applied Mechanics, Vol. 51, pp. 899-903, 1984.

7. J. Wittenburg. "Dynamics of Multibody Systems", International Union of Theoretical and Applied Mechanics, pp. 197-207, 1980.

8. A. J. Kurdila. "Concurrent Multiprocessors in Computational Mechanics for Constrained Dynamical Systems", Ph.D. thesis, Georgia Institute of Technology, Dec. 1988.

9. P. E. Nikravesh and E. J. Haug. "Generalized Coordinate Partioning for Analysis of Mechanical Systems with Nonholonomic Constraints", Journal of Mechanisms, Transmissions, and Automation in Design, September 1983, Vol. 105, pp. 379-384.

10. R. A. Wehage and E. J. Haug. "Generalized Coordinate Partitioning for Dimension Reduction in Analysis of Constrained Dynamic Systems", Journal of Mechanical Design, Vol. 104, pp. 247-255, 1982.

11. R. P. Singh and P. W. Likins. "Singular Value Decomposition for Constrained Dynamical Systems", Journal of Applied Mechanics, Vol. 52, pp. 943-948, 1985.

12. F. M. L. Amirouche and T. Jai. "Automatic Elimination of the Undetermined Multipliers in Kane's Equations Using a Pseudo Uptriangular Decomposition (PUTD) Method", Computers and Structures, Vol. 27, No. 2, pp 203-210, 1987.

13. K. Washizu. *Variational Methods in Elasticity and Plasticity*, third edition, Pergamon 1980.

14. M. Borri, G. L. Ghiringhelli, M. Lanz, P. Mantegazza and T. Merlini. "Dynamic Response of Mechanical Systems by a Weak Hamilton's Formulation", Computers & Structures, Vol. 20, pp. 495-508, 1985.

15. M. Borri, M. Lanz and P. Mantegazza. "Helicopter Rotor Dynamics by Finite Element Time Discretization", L'Aerotecnica Missili e Spazio, Vol. 60, pp. 193-200, 1981.

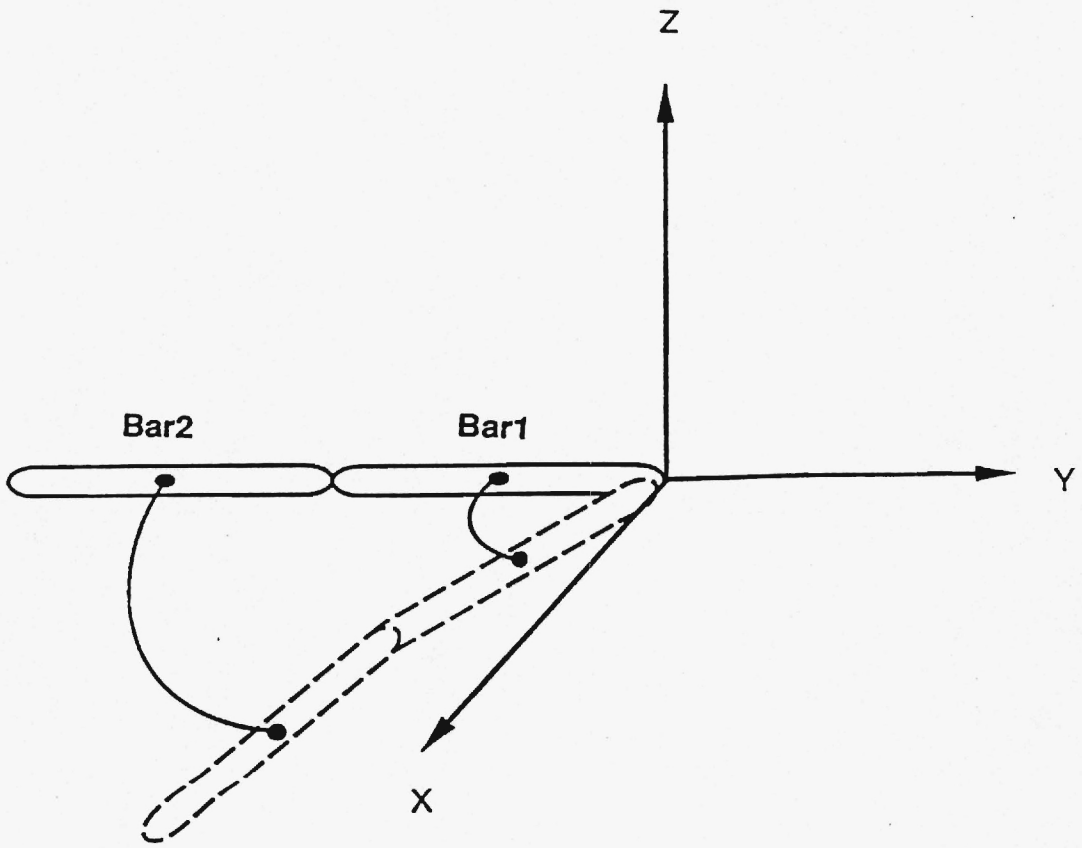

Figure 1: Two Bar Test Problem

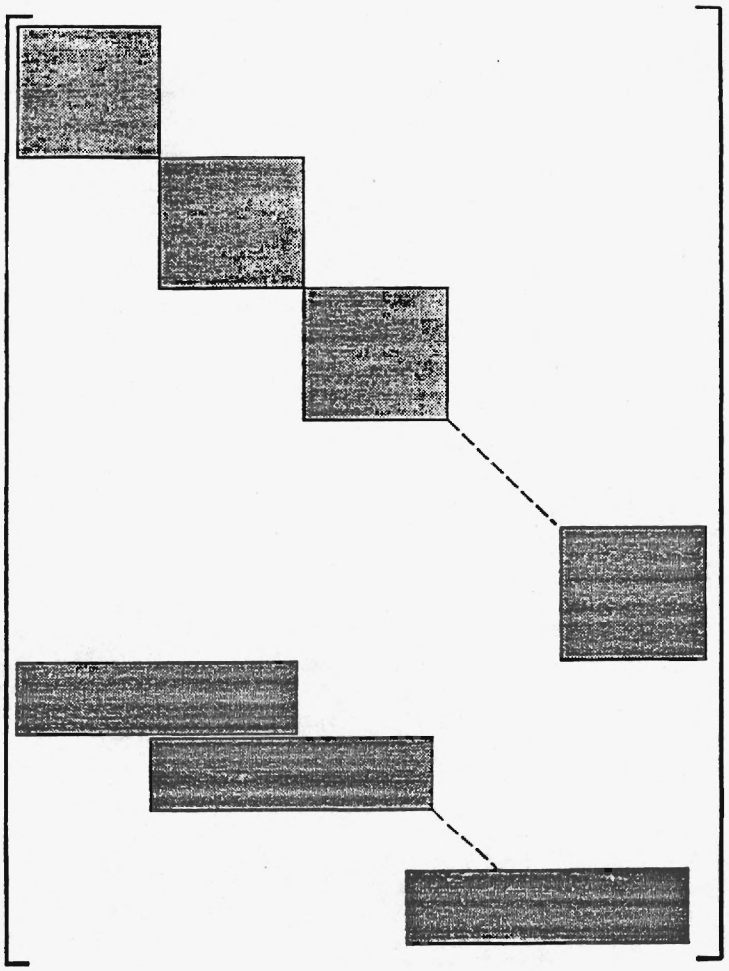

Figure 2: Sparse Matrix Structure for Multibody Problems

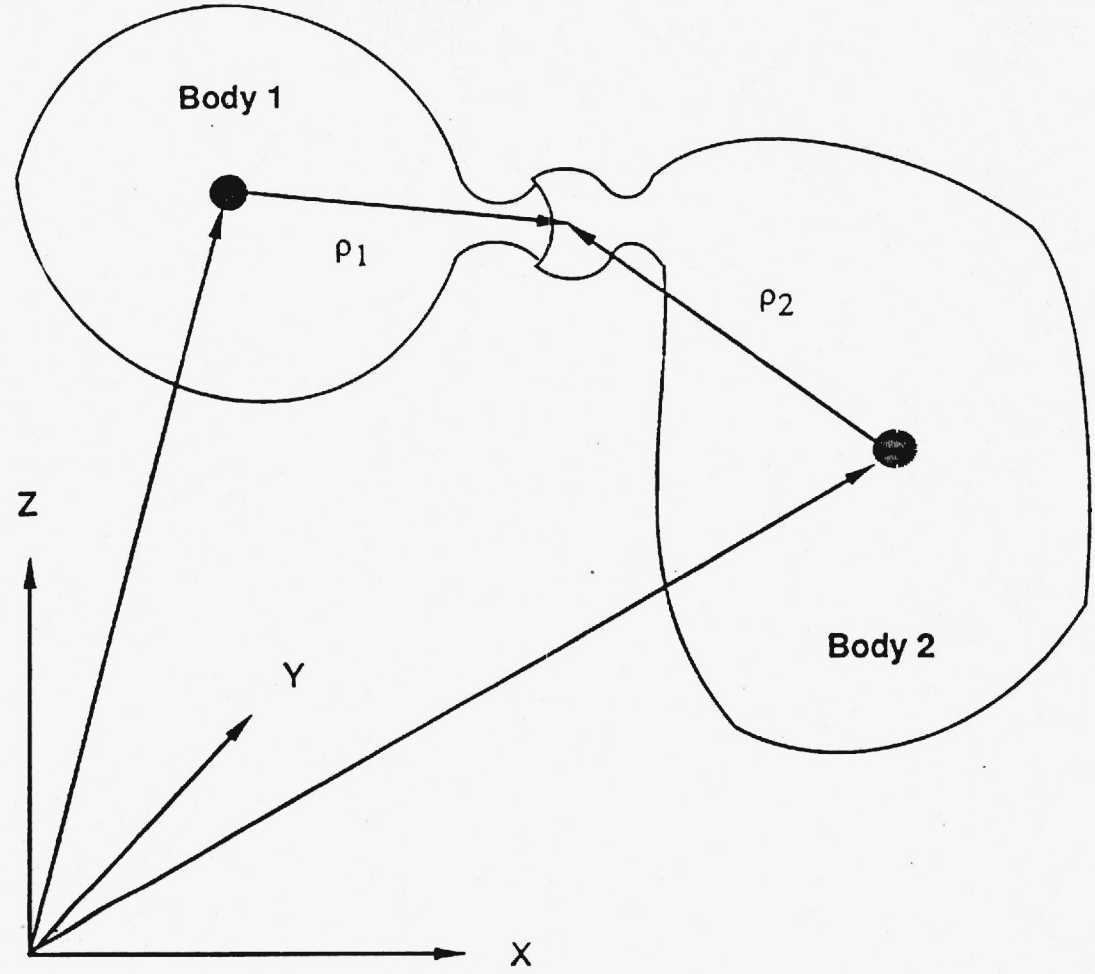

Figure 3: Spherical Joint

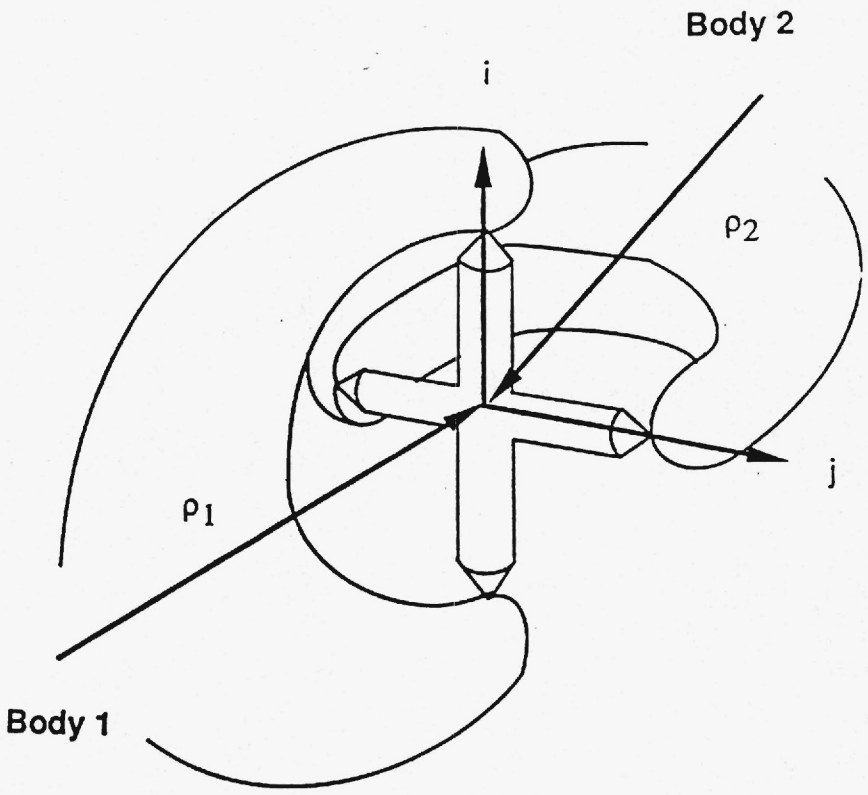

Figure 4: Universal Joint

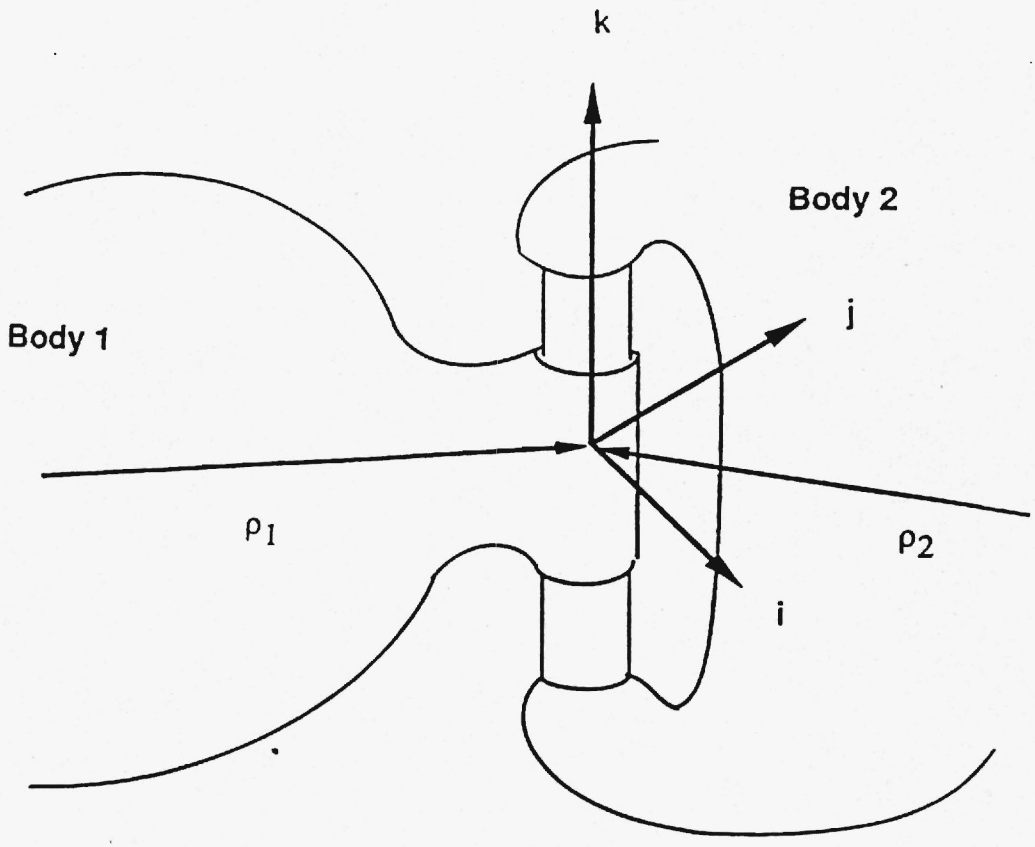

Figure 5: Revolute Joint

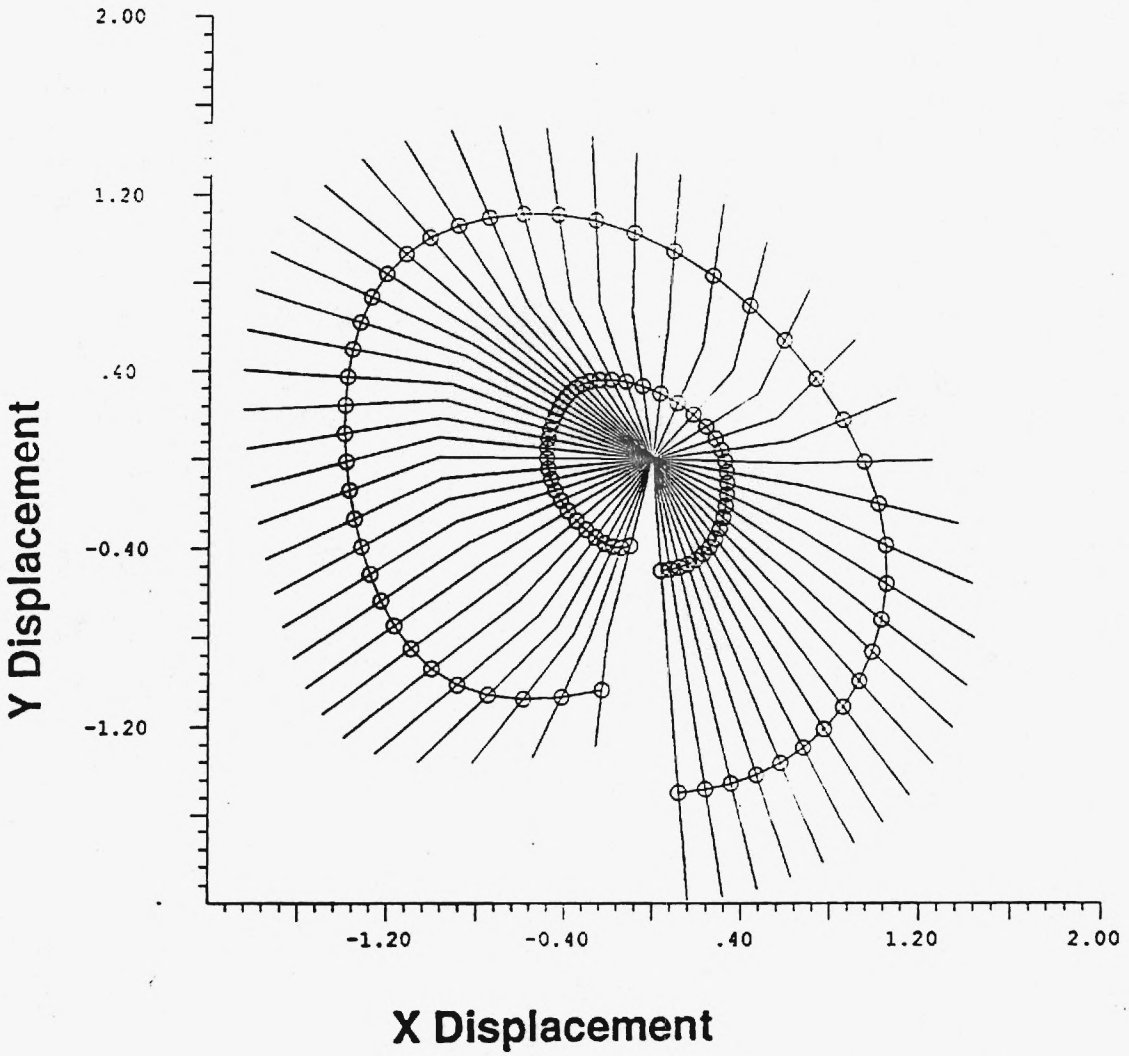

Figure 6: XY Displacement - Spherical Joint Case 1

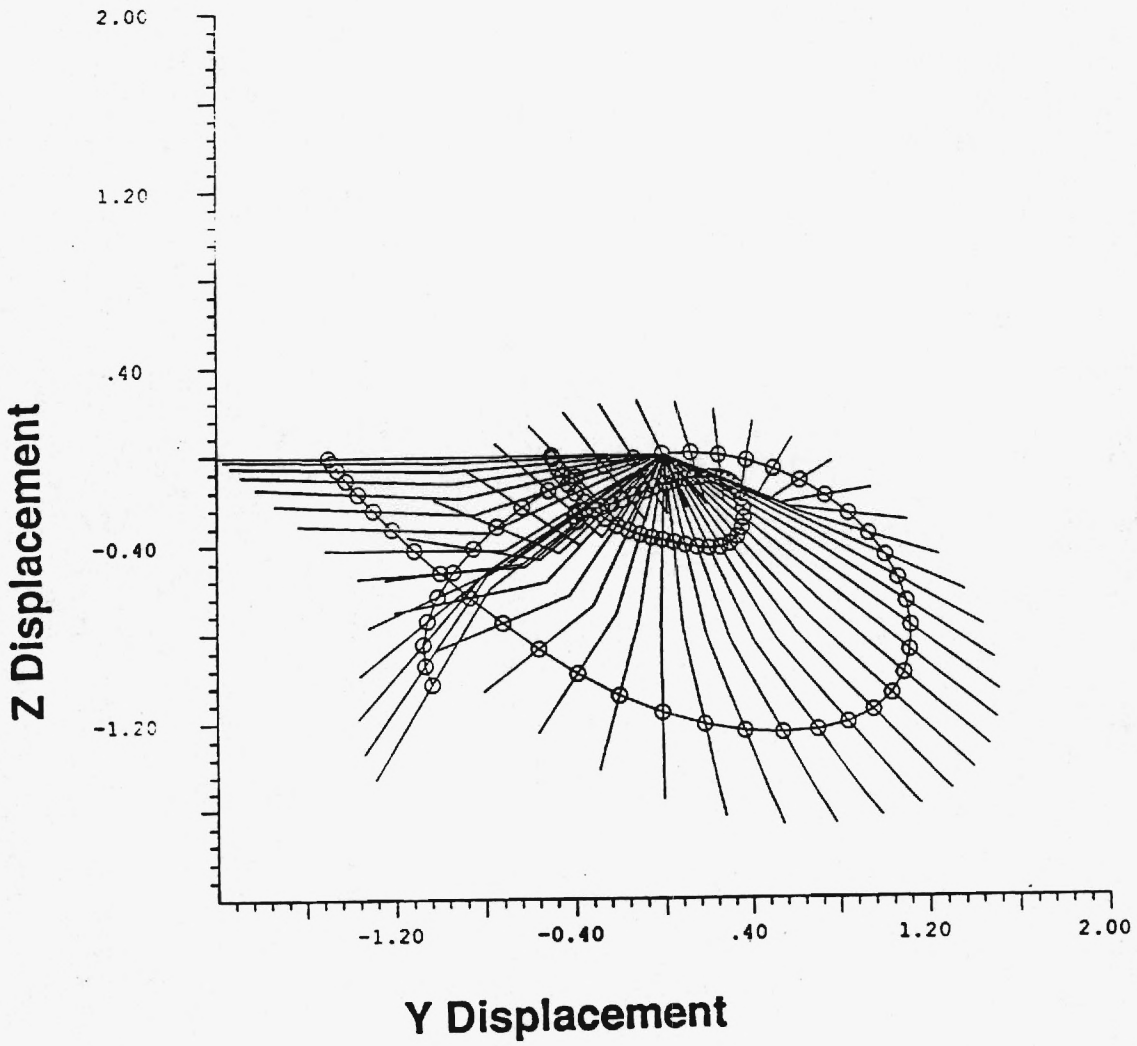

Figure 7: YZ Displacement - Spherical Joint Case 1

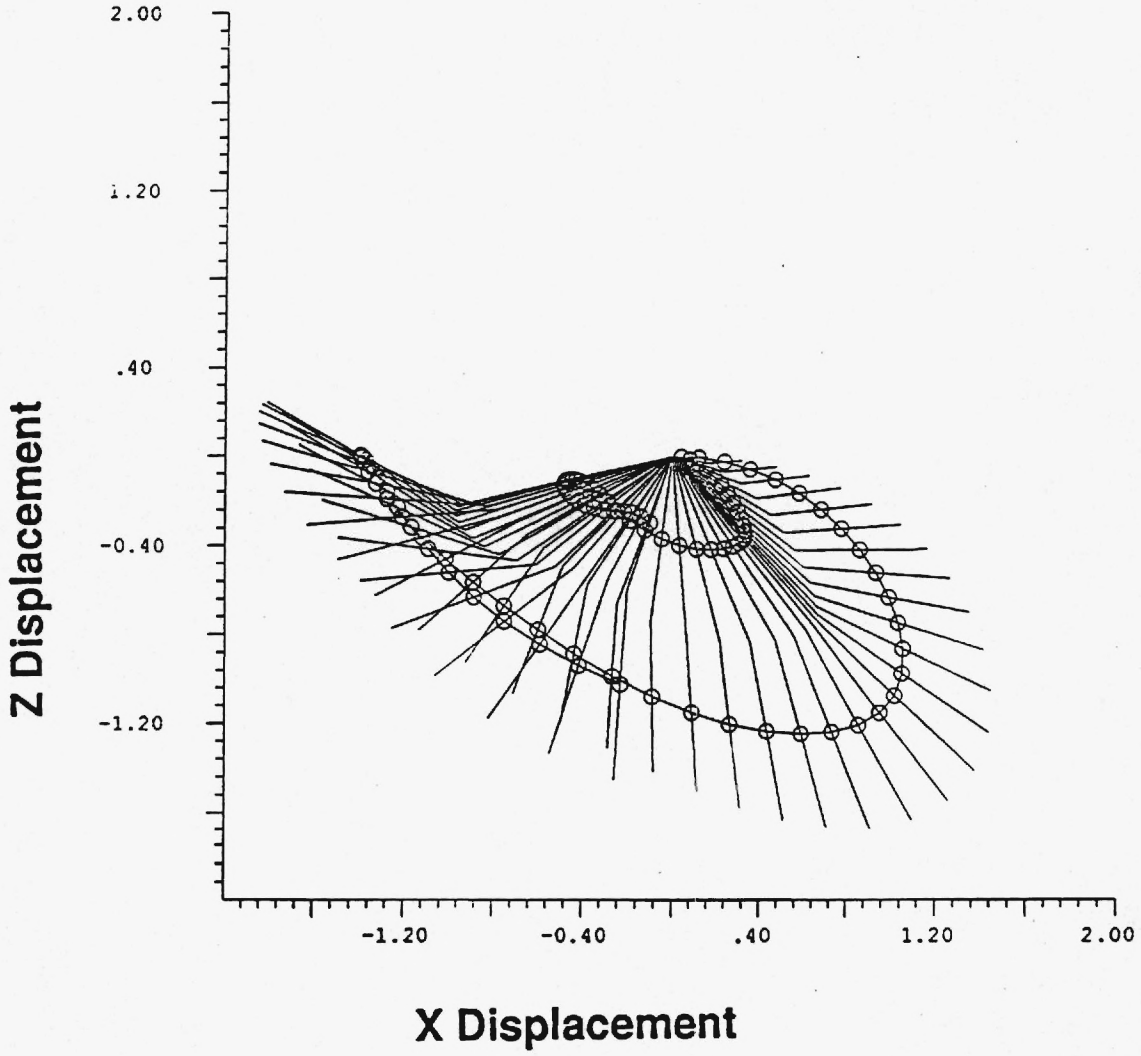

Figure 8: XZ Displacement - Spherical Joint Case 1

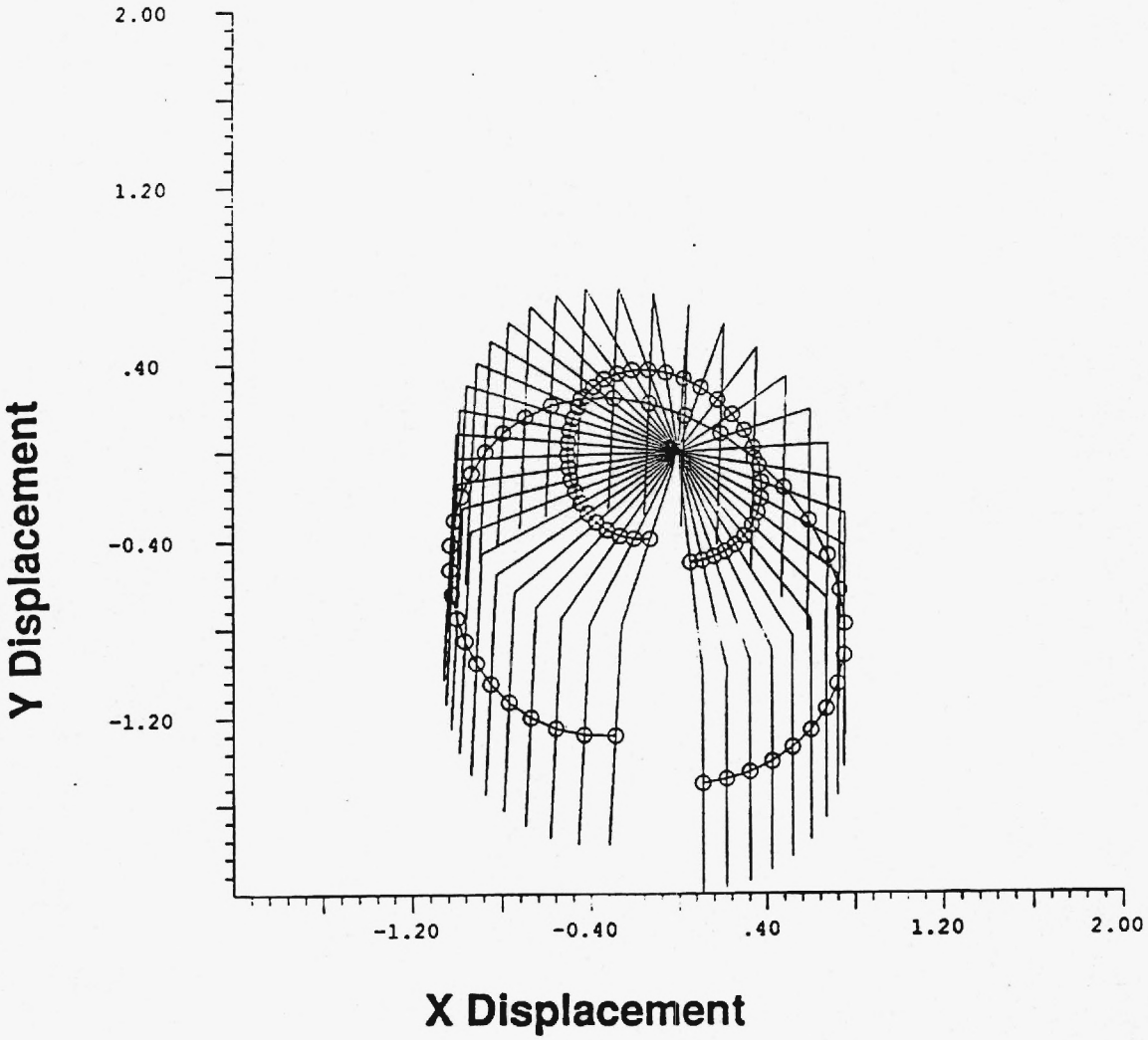

Figure 9: XY Displacement - Spherical Joint Case 2

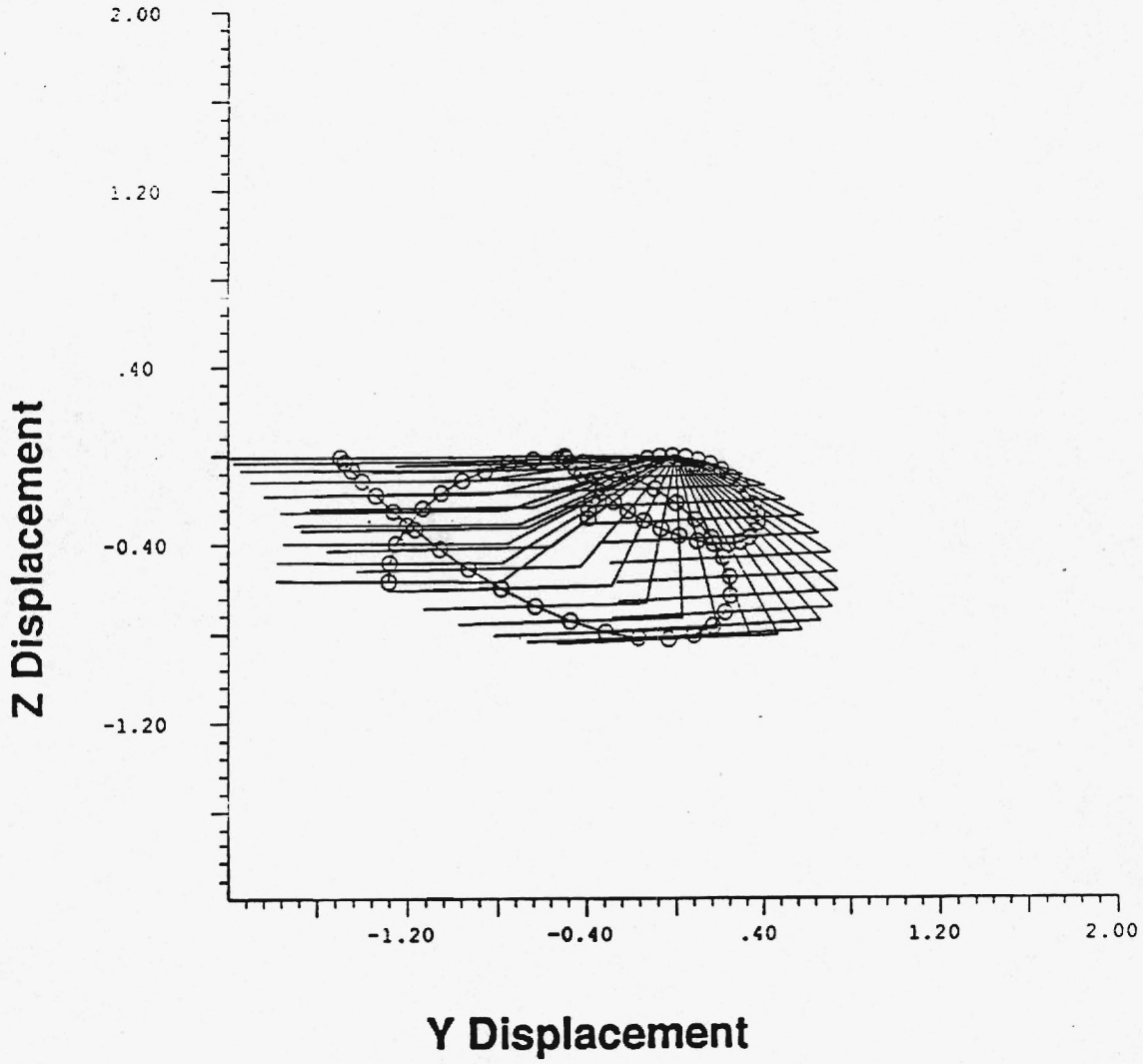

Figure 10: YZ Displacement - Spherical Joint Case 2

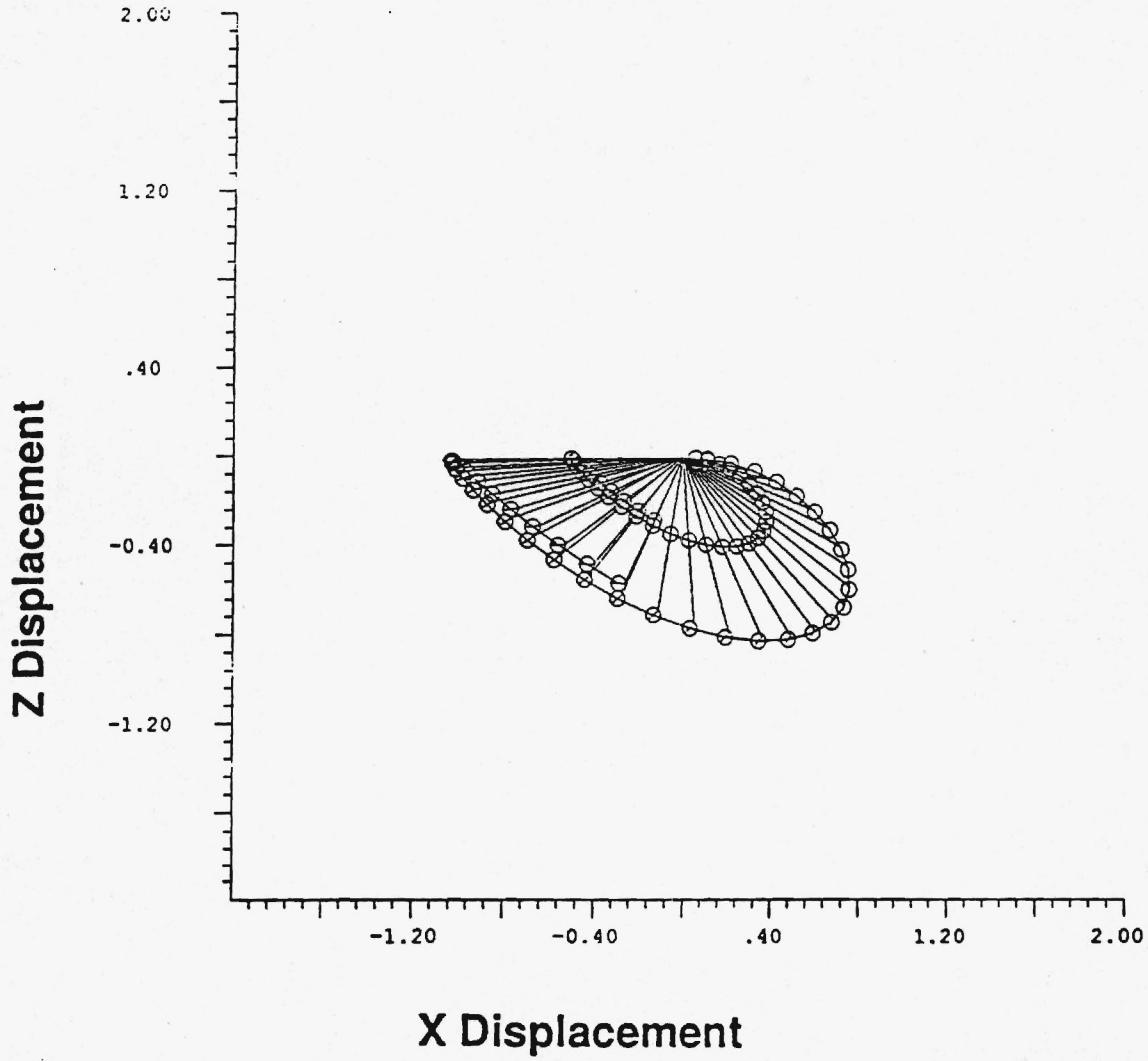

Figure 11: XZ Displacement - Spherical Joint Case 2

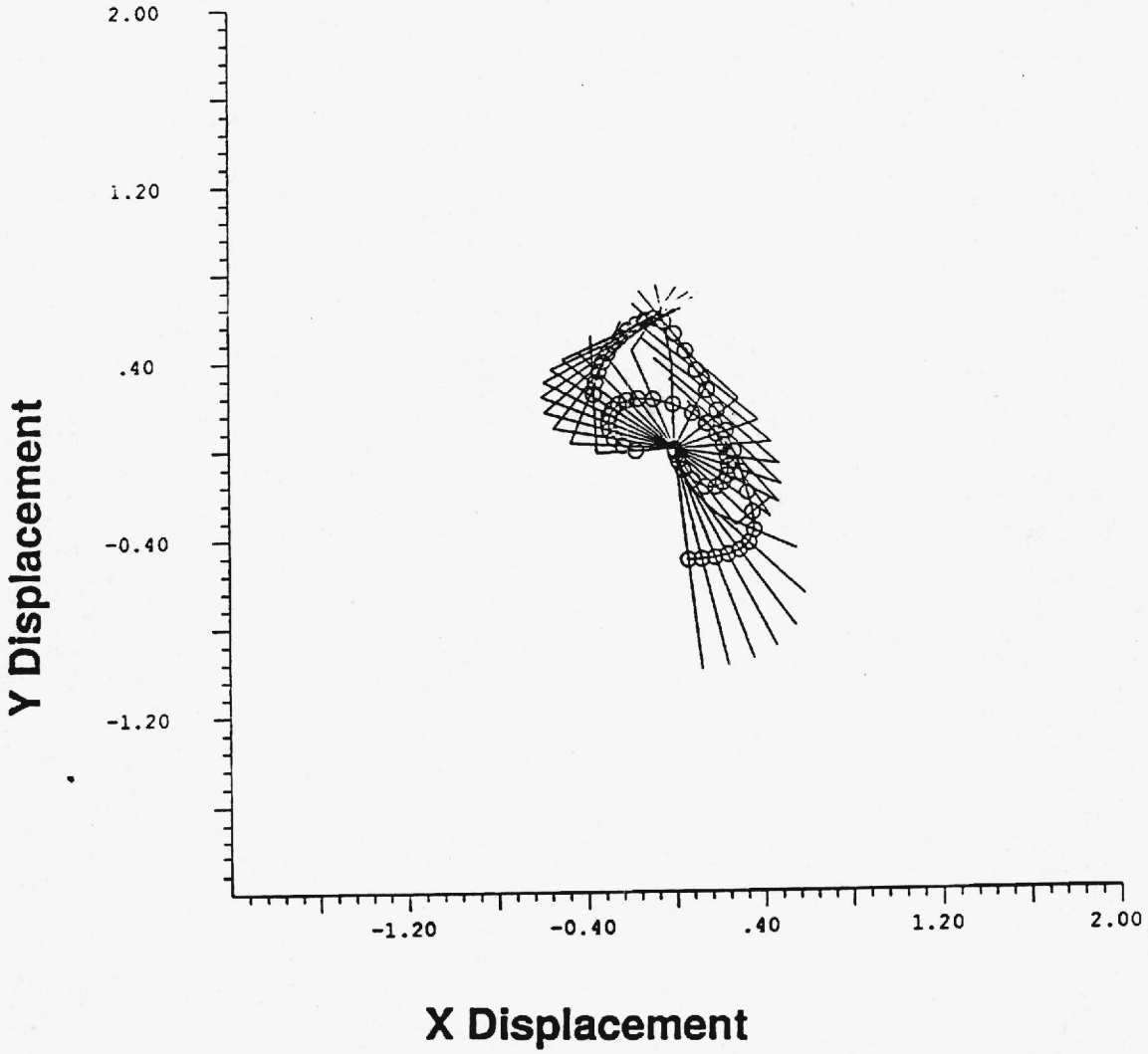

Figure 12: XY Displacement - Universal Joint

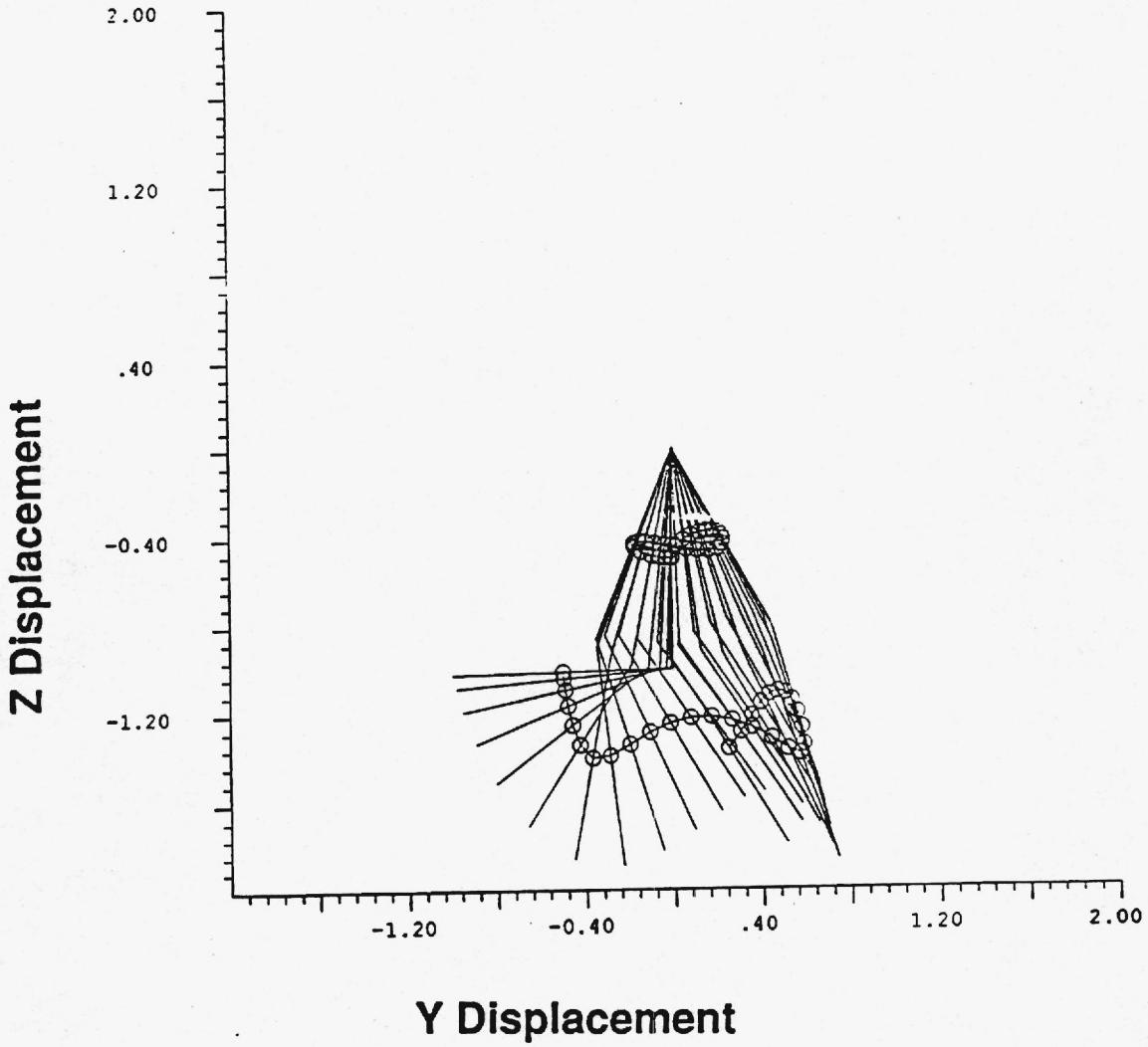

Figure 13: YZ Displacement - Universal Joint

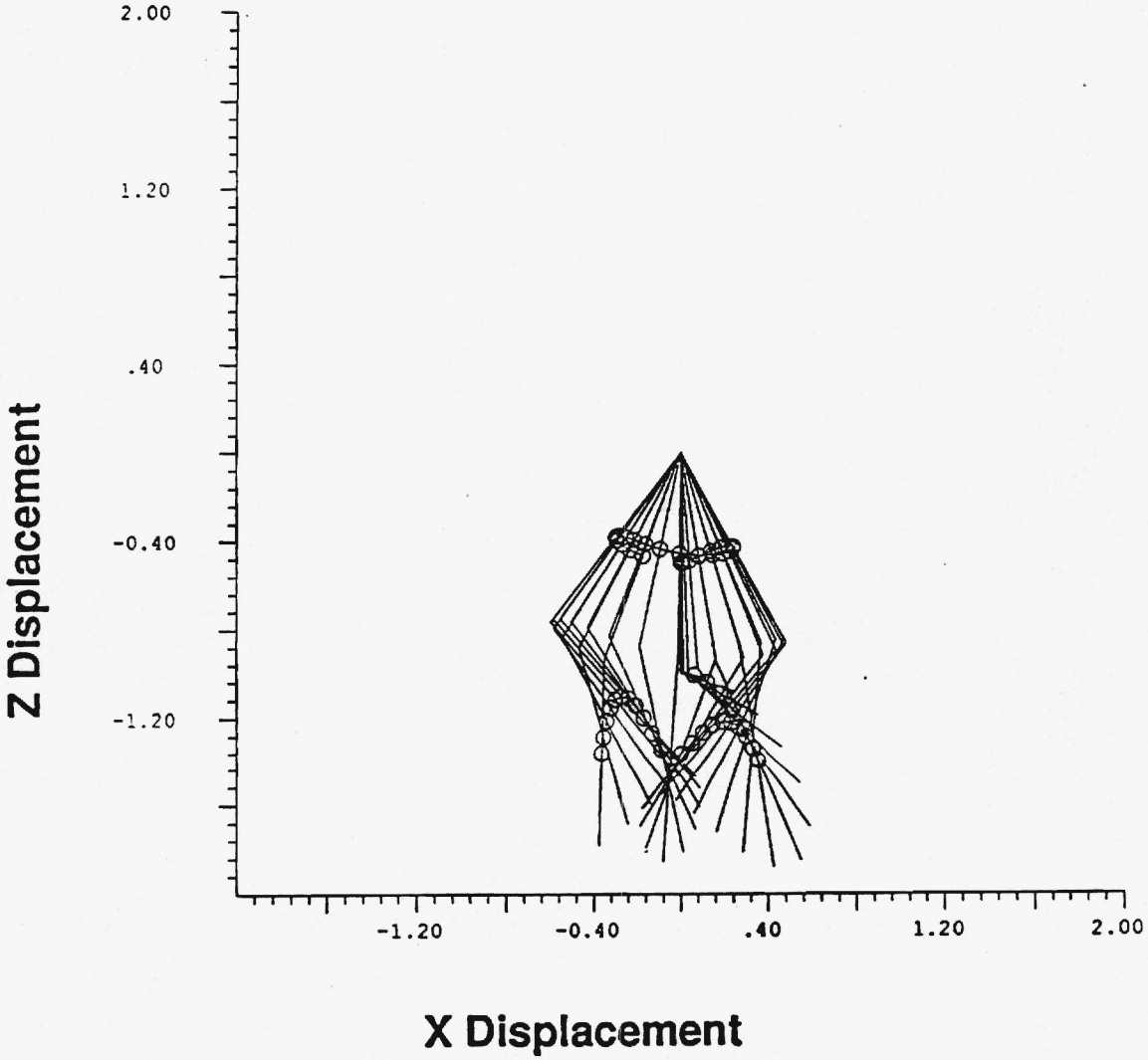

Figure 14: XZ Displacement - Universal Joint

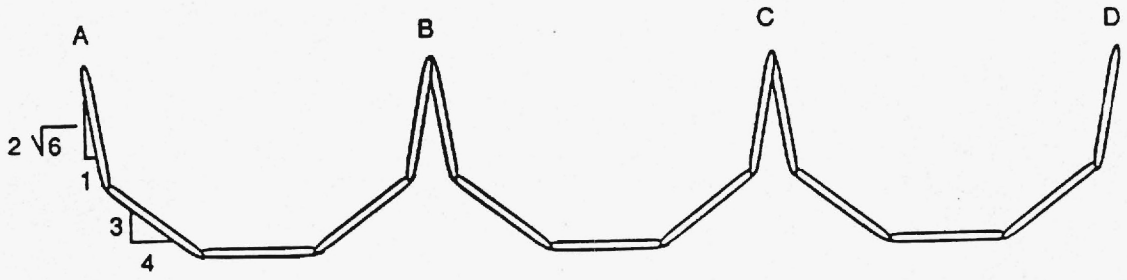

Figure 15: Fifteen Bar Linkage

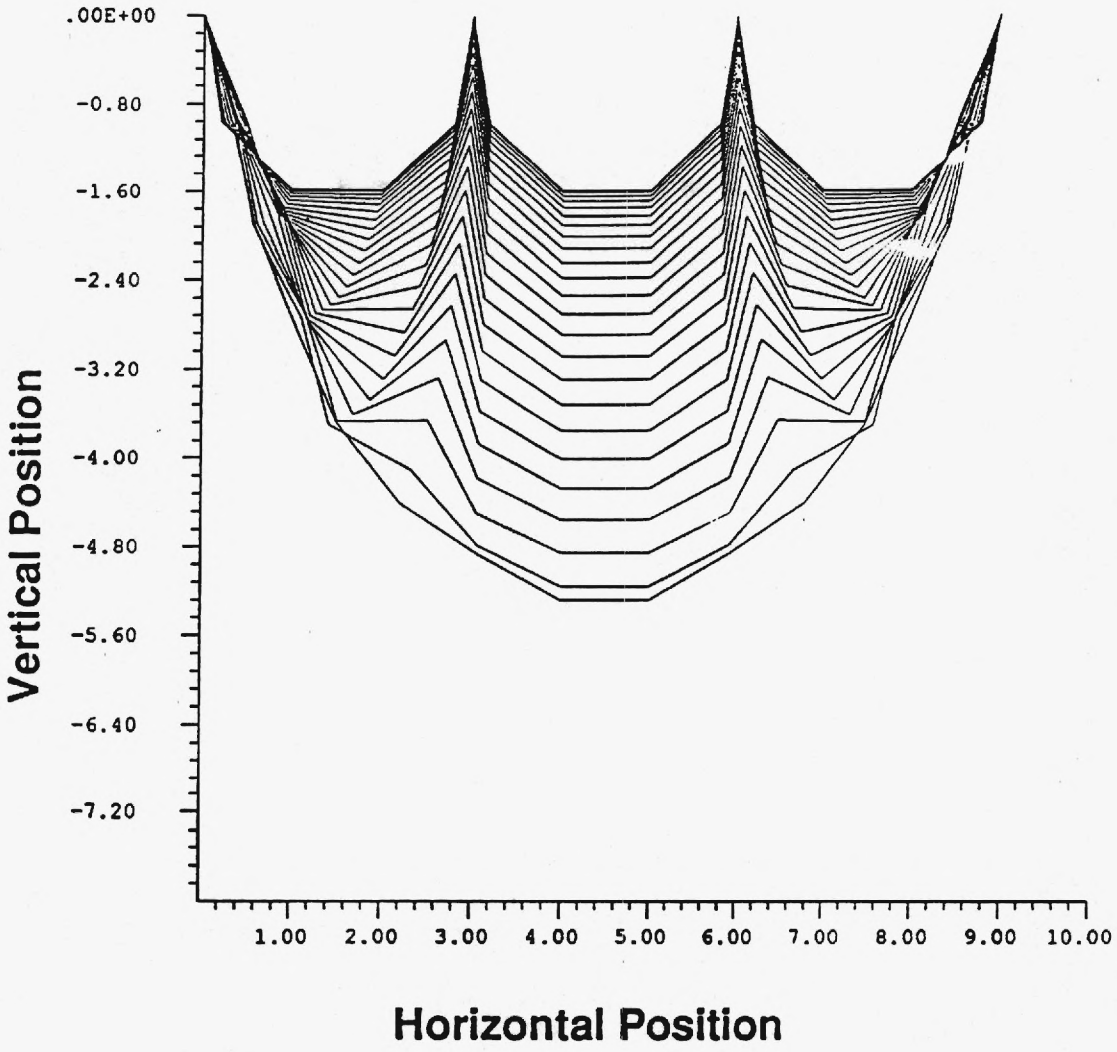

Figure 16: Linkage Profile - Falling

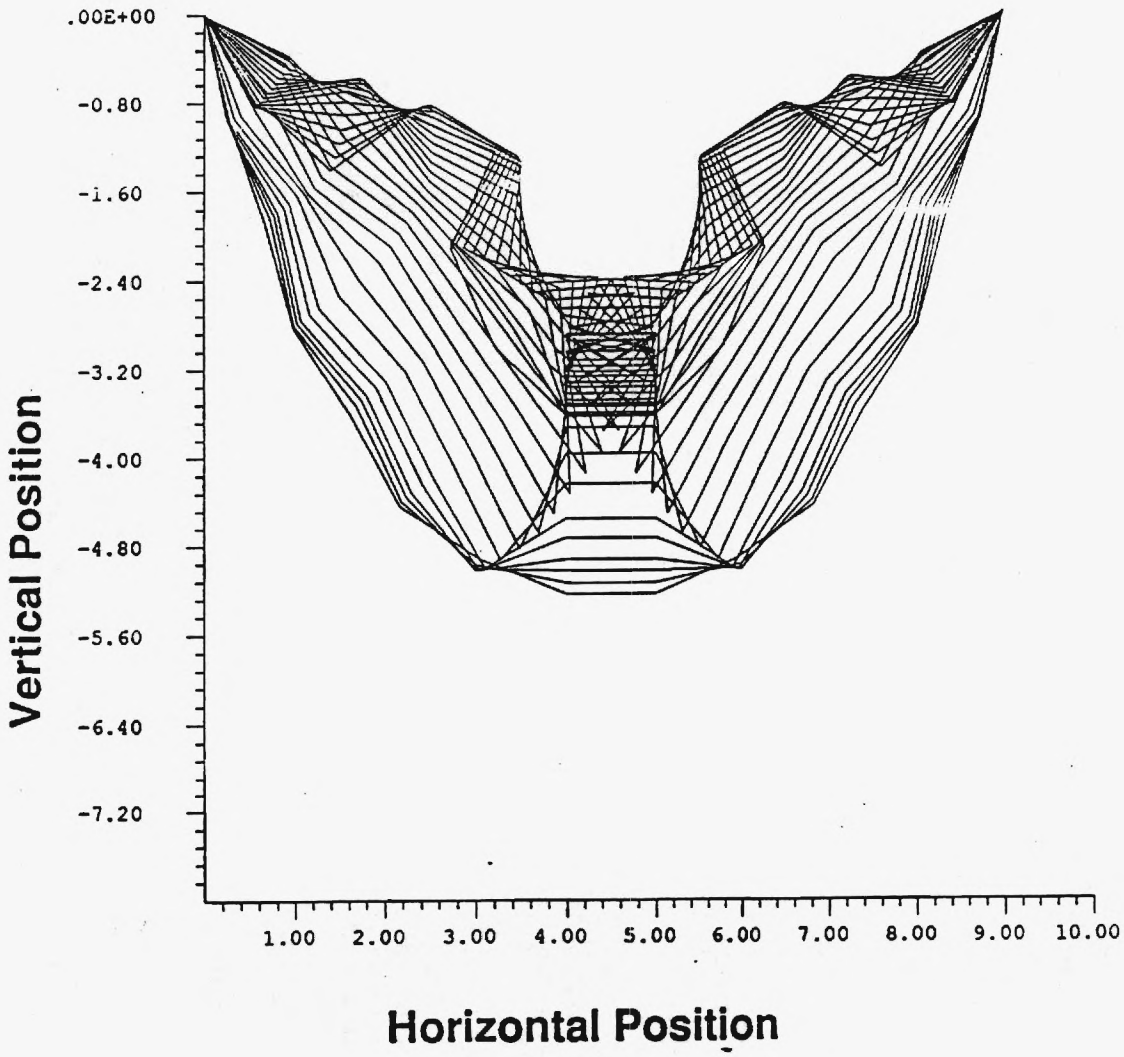

Figure 17: Linkage Profile - Rebounding

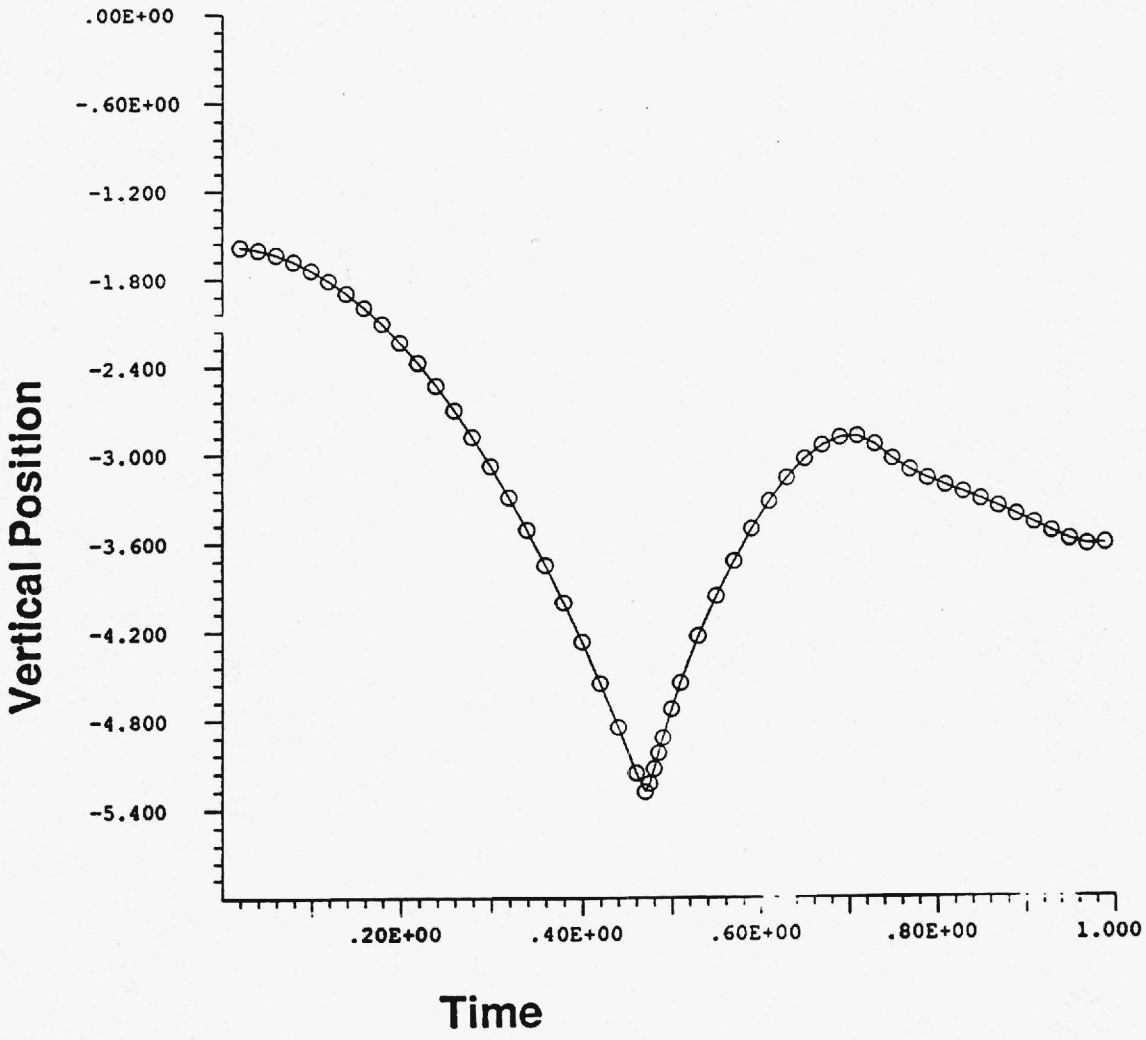

Figure 18: Vertical Displacement of Center Link